

ReWind

Regenerative Wind Farming - Final Report

Design Synthesis Exercise DSE-06

Delft University of Technology



This page is intentionally left blank.

ReWind

Regenerative Wind Farming - Final Report

by

DSE-06

Student Name	Student Number
Alessandro Carraro	5523524
Kilian Rave	5310644
Jordi Salvador Masip	5533449
Noah Schotmeijer	5546230
Marcos Garcia Bravo	5490650
Matin Shams	5208076
Valentin Le Bailly de Tillegem	5532671
Mark Nibbelke	5454174
Frederick Dequae	5228921
Tiago Domingues Coelho	5448433

Tutor: Prof. C. Simão Ferreira
Project Coaches: Dr. U. Fechner
W. E. Dyer
Duration: April, 2024 - June, 2024
Faculty: Faculty of Aerospace Engineering, Delft

Executive Summary

Since the final decades of the twentieth century, society has become increasingly aware of the climatological impact of relying on fossil fuels as the cornerstone of the world's energy supply. In response, there has been a committed effort to reduce this impact and address climate change. The global shift from fossil fuels to renewable energy sources is a crucial endeavor to combat environmental degradation. However, as societies electrify, driven by technological advancements and the pursuit of cleaner energy, the demand for electricity is rising sharply. This means that energy suppliers are now not only tasked with transitioning to renewable energy sources but must also ensure these sources can meet the growing energy demands. This dual challenge necessitates innovative energy solutions.

In order to limit the impact of climate change, the Dutch government has set out to achieve a drastic 95% reduction of greenhouse gasses by 2050¹. Offshore wind energy will play a pivotal role in achieving this target, but its capacity, however, will need to be increased greatly. The current 4.5 [GW] installed offshore wind energy capacity represents a mere 3.3 % of the total energy demand in the Netherlands². However, this relatively low capacity is expected to increase rapidly with the construction of new offshore wind farms, aiming to reach 21 [GW] by 2030 and meet 16% of the total Dutch energy demand².

The planned growth of offshore wind energy in the North Sea faces numerous technical challenges, with limited available space being the most critical. Not only do wind turbines individually impact each other negatively through rotor wakes, wind farms also further slow down the atmospheric boundary layer. Much like a dense forest, wind farms create combined wakes from each turbine, slowing down the local airflow. The larger and more densely packed the wind farm, the more pronounced these effects become. Consequently, downstream turbines receive significantly less clean airflow, leading to lower capacity factors. This phenomenon, as illustrated in Figure 1, obtained from dozens of reference wind farms, indicates that simply installing more capacity without further innovations is not a viable option to meet energy goals, as it would drastically decrease overall wind farm efficiency. Wind farm efficiency is defined as the average capacity factors of all turbines in the wind farm divided by the capacity factor of a single turbine experiencing clean airflow.

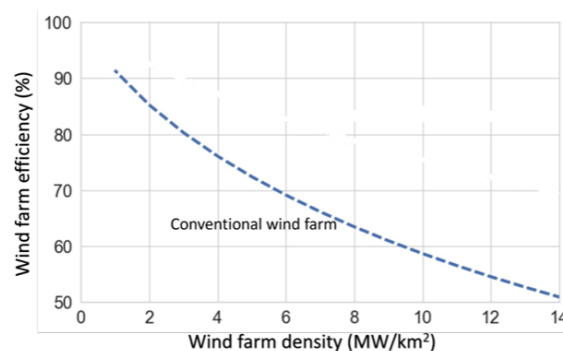


Figure 1: Wind farm efficiency and power density relation [1].

The ReWind concept aims to minimize this effect by proposing a new and innovative turbine design utilizing regenerative wind farming strategies to minimize wind farm losses. This new design should be able to meet the Dutch wind energy goals and be competitive within the wind energy market. Reducing the Levelized Cost of Energy (LCoE) by 45%, improving CO₂ emissions, improving material use and overall life cycle performance compared to the current Dutch proposed North Sea program. To address this issue, an innovative system will be implemented to re-energize the low-level atmosphere. The underlying idea is to deflect the flow at sea level, with low energy, upwards and get high energy flow at higher altitudes to come down. This would allow the creation of high-density wind farms places close to each other, each of them receiving clean and undisturbed flow from the wind farms upwind [1]. This project aims at developing a new generation of wind farms, starting with a 6 [GW] sized wind farm that uses multi-rotor wind turbine units of 30 [MW] each and implements very promising systems to actively re-energize the flow. Alongside these revolutionary aspects, the design of said

¹<https://www.government.nl/topics/climate-change/climate-policy> [Accessed 19-06-2024]

²<https://www.government.nl/topics/renewable-energy/offshore-wind-energy> [Accessed 19-06-2024]

wind farm also aims at reaching a 40% lower environmental impact as well as a 45% lower cost of energy.

The Active Flow Control (AFC) will consist of multiple wings designed to deflect the wake. By generating large vortices on the sides, these wings can mix the lower-energy wake flow—slowed down by the rotors—with higher-velocity, higher-energy winds found at greater altitudes. This results in more efficient energy capture. Furthermore, the multi-rotor concept is advantageous due to its scalability. As single-rotor turbines increase in size to generate more energy, with the largest currently producing about 15 MW, their blades and generators also become larger and more complex. This leads to higher costs and greater installation challenges. In contrast, the multi-rotor approach uses multiple smaller components, which helps to keep costs down while still generating lots of energy.

Figure 2 presents the Wind Farm Capacity Factor vs the Wind Farm Wind Factor for a whole range of currently operating wind farms [1]. The green star shows the optimistic planned Dutch North Sea program, where it can be noted that the performance is above the theoretical limit for wind farms. This clearly indicates that the North Sea program, as it is, is unfeasible [1]. The blue star represents the actual expected performance for the North Sea program based on current wind farm data and a theoretically established limit. As can be noted, this difference is very significant and shows the unrealistically high expectations from the Dutch North Sea program. The ReWind concept aim is denoted by the orange star in Figure 2. While this aim may seem trivial because existing wind farms already operate at these wind farm capacities and factors, these wind farms show very low power densities and installed capacities. The strength of the ReWind farm stems from the aim of combining high wind farm capacities and low wind farm factors along with high power densities above 10 [MW/km²] and high installed capacities. By doing so, the ReWind farm will be supplying significantly more energy and aiding with the Dutch energy transiting goals.

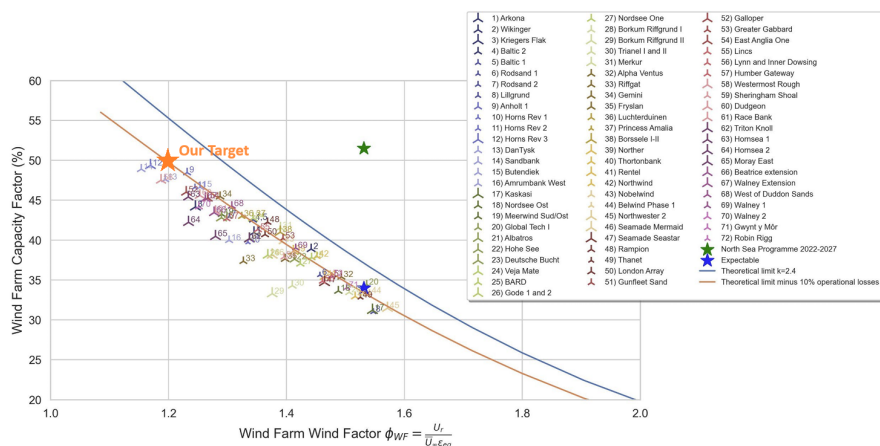


Figure 2: Analysis of the Dutch wind energy goals [1].

This report aims at presenting the ReWind conceptual design by looking at the wind farm aspect and the single turbine simultaneously. This executive summary covers an overview of the financial aspect of such project, how sustainability was implemented in this design and a description of the final conceptual design. Alongside these topics, some of the manufacturing and operational aspects will be discussed shortly.

Farm location & Layout

The Lagelander wind energy area, situated in Dutch territorial waters approximately 33 to 75 km off the coast near Texel, has been selected due to its sufficient size (600 km²) to accommodate a wind farm with a minimum rated power of 6 GW and a power density of 10 MW/km².

Wind data from the ERA5 Database provides comprehensive information on wind speeds and prevailing directions. Using a power law, wind speeds at various heights have been extrapolated, with an average speed of 9.25 m/s recorded at the expected hub height of 150 m. The predominant southwest wind direction, depicted in a wind rose plot, guides the optimal layout strategy for turbine placement within the farm.

Additionally, wave data from ERA5³ is utilised to assess mean wave heights and periods, influencing the design parameters for the monopile foundations. The water depth analysis reveals depths ranging from 10 to 20 m at the chosen site, informing the design of robust foundations capable of withstanding varying seabed conditions.

The optimised wind farm layout is proposed based on the collected data, aiming to achieve maximum energy density while ensuring efficient turbine spacing and alignment with prevailing wind patterns. This integrated approach ensures that the wind farm is designed to harness optimal wind resources and withstand environmental conditions in Dutch North Sea waters.

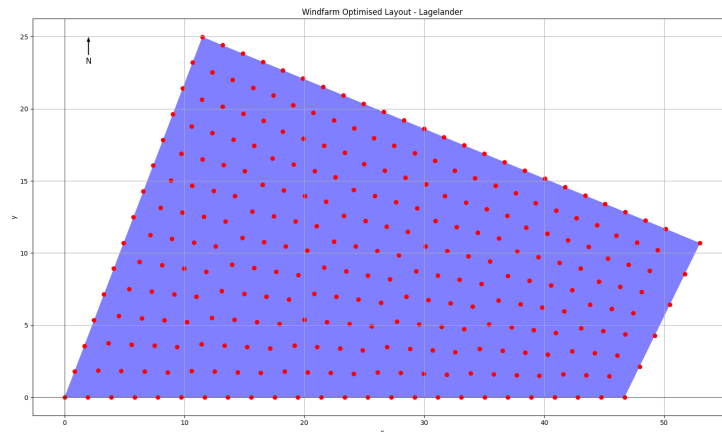


Figure 3: *Wind farm layout*

Design

For the detailed design of the ReWind turbine, the system has been divided into different subsections. Each subsection's specific design will be detailed below.

Rotor Design

ReWind's design incorporates 34 rotors arranged in a honeycomb structure to maximize space efficiency and performance, as can be seen in Figure 5. This configuration balances mass, manufacturability, and maintainability. The rotors are sized to achieve optimal performance while minimizing weight and load impacts. Using the International Energy Agency (IEA) 15 MW reference wind turbine as a benchmark, the combined swept area of the 34 rotors is matched to that of a single large turbine, resulting in a rotor radius of approximately 29 meters. This approach ensures a good performance at both high and low wind speeds.

Airfoil design is critical for maximizing lift and minimizing drag. ReWind utilizes airfoils developed by the U.S. National Renewable Energy Laboratory (NREL), specifically the S818, S816, and S817 models, which are suited for turbines around 1 MW per rotor. These airfoils are chosen for their high performance at various sections of the blade, ensuring structural integrity and aerodynamic efficiency.

To achieve maximum power generation, the blade geometry is optimized using the Blade Element Momentum (BEM) model. This model iterates between aerodynamic forces and momentum conservation to refine the axial and tangential forces on each blade element. Adjustments to the chord length and twist angle of the blades are made to enhance the overall performance, resulting in a rotor radius of 28.93 meters and a mechanical power coefficient (CP) of 0.49, slightly higher than the reference turbine.

The optimized rotor design features a maximum chord of 3.3 [m] and a root twist angle of -9.9 degrees, providing a balanced and efficient structure. The system operates at a tip speed ratio (TSR) of 8, with a rated wind speed of 10.59 [m/s] and a rotational speed of 28 [rpm]. Each rotor delivers a rated power of 882 [kW], contributing to a highly efficient and powerful wind energy solution.

³<https://cds.climate.copernicus.eu/cdsapp#!/dataset/reanalysis-era5-single-levels?tab=form> [Accessed 24-06-2024]

Active Flow Control

Wake losses are becoming a more pressing problem for larger and denser wind farms. The deceleration of the flow by the upwind turbines decreases downwind turbine energy production and overall wind farm capacity factor. Resulting in less energy produced and more variability of the power delivered. To tackle this problem, ReWind will use an innovative process of wind farming. By entraining high momentum flow from the upper layers of the atmosphere, the wake of the turbines can be effectively re-energized, and the adverse effects of wake interference can be mitigated. This process of momentum entraining can be achieved via vertical fluxes created by high-lift systems.

ReWind utilizes downforce-generating multi-element wings to re-energize the wake of the turbine, hereby allowing for closer spacing of turbines and, thus, higher wind farm energy density and capacity factor. The wings are designed to create a downforce of more than 1.3 times the amount of thrust provided by the rotors in order to re-energize the velocity of the wake by 95.7%. At rated speed, the Active Flow Control system produces a total of 6.5 [MN] of downforce. The downforce is produced by three three-element wings spaced along the height of the turbine, which are able to retract during severe weather conditions in order to reduce the load on the structure.

The three-element wing is designed with the same NACA 4418 airfoil shape for each element to keep the manufacturing simple and uniform. The chord of the complete wing is 50 [m], with a total span of 277, 241, and 241 [m] for the top, middle, and lower wing, respectively. The bottom and middle wing are slightly smaller because they cannot traverse the tower while the top wing can simply run across this tower without inhibiting any maintenance operations. To facilitate easier assembly and transportation, the span of the wing is split up into sections of 27.38 [m]. The three-element wing is designed to achieve a maximum lift coefficient of 3.381 and a minimum lift coefficient in a retracted state of 0.345. The designed shape for this wing is presented in Figure 4.



Figure 4: 3-element NACA 4418 wing configuration

Structure

The Structure consists of a truss carrying the rotor nacelle assemblies and AFC, which is itself supported by a combined monopile and tower. To provide yaw capability, the structure includes two yaw bearings, as shown in Figure 5. To size the structure, several static design load cases were introduced, which are representative of the operational envelope of each turbine unit, including rated power production and parking during storm conditions. In these cases, the structure is loaded primarily by the aerodynamic forces of the AFC devices, the aerodynamic drag, rotor thrust, and weight forces.

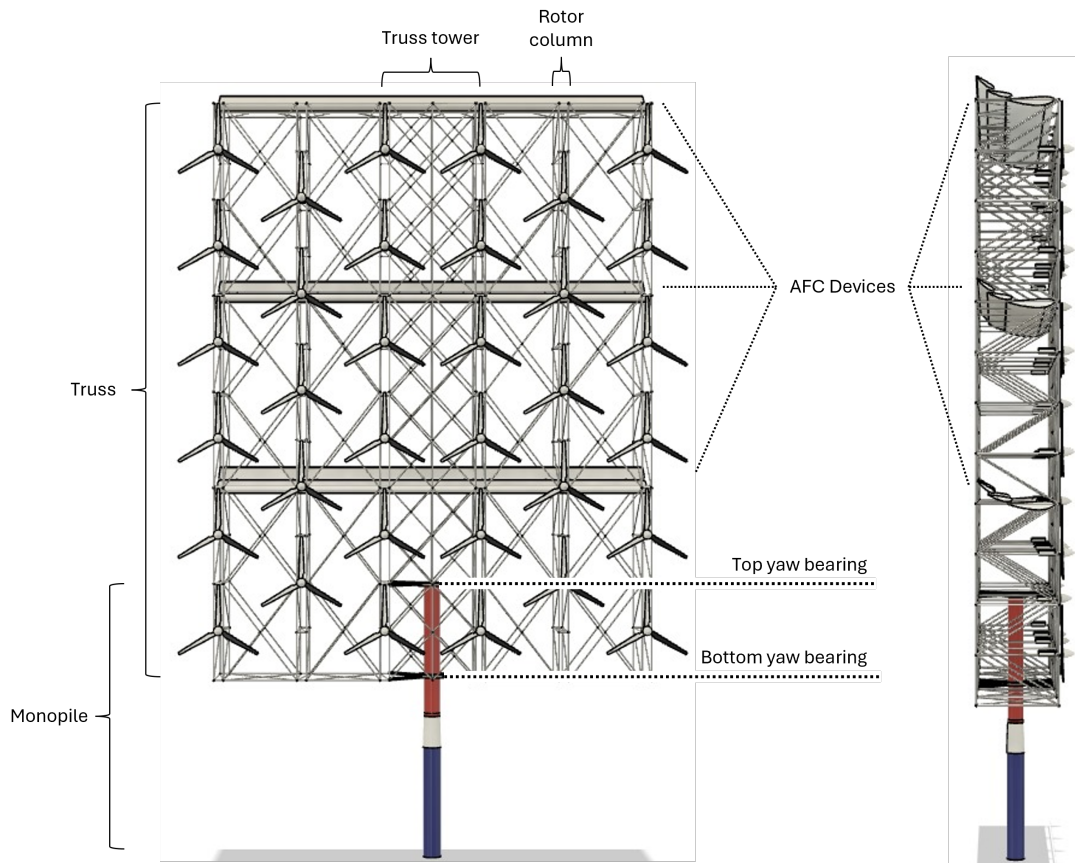


Figure 5: Overview of the structural configuration and subsystem integration of a single turbine unit.

The truss structure is designed using thin-walled cylindrical members and a column-based geometry, which allows the rotors to be arranged in an area-efficient honeycomb packing, as shown in Figure 5. A truss tower is used to provide rigidity whilst still allowing the wings of the AFC devices to pass through the structure with minimal interruption. Additionally, it allows for the installation of a central elevator system, which enables easy access to various installed components during maintenance operations. The truss geometry, consisting of six repeated layers having the same topology, is designed with assembly and manufacturability in mind. To this end, manufacturability bounds are also imposed on the member wall-thickness ratio and minimum diameter. The design of the truss follows the design standards set in IEC 61400-1 and considers both local and global failure of the members. An iterative method was applied to size the geometry of each member for the considered failure mode, which ensures the results are representative of the structural requirements necessary to withstand the considered load cases.

The monopile transfers the loads applied to the truss to the sea floor, and was determined to be the most suited foundation type on the basis of water depth and ability to provide yaw capabilities. The monopile is designed to withstand both the loads applied by the truss structure, as well as the distributed wave and current loads it experiences underwater. Its design considers yield failure, and both local and global buckling modes.

Yaw & Pitch

The pitch and yaw systems of the ReWind wind turbine are integral to optimizing the operational efficiency and safety of the turbines. This system is designed to alter blade pitch both to maximize power output during optimal wind conditions and to feather the blades during storms to reduce loads and potential damage. Such automatic adjustments help maintain the turbines within safe operational limits, thereby enhancing reliability and extending the lifespan of the components. For stakeholders, this automated pitch control translates into consistent power efficiency, reduced maintenance costs, and improved return on investment due to the increased durability and efficiency of the rotor blades.

The yaw system employs differential pitching along with six secondary electric motors rotating around two yaw bearings. Differential pitching involves adjusting rotor pitches asymmetrically to create varied aerodynamic

forces, generating rotational moments around the central tower. This method is fast and convenient, reducing costs due to the smaller motor size and lower maintenance requirements.

The operational envelope for differential pitching shows that its effectiveness decreases for yaw misalignments greater than 45 [deg] at rated wind speeds but can correct up to 70 [deg] of misalignment at speeds near cutoff. This broad operational range makes the yaw system effective in nearly every condition. For situations such as restarts after a storm or post-maintenance, six motors will be employed. Six TK-3080 motors were selected for their high torque and low rotational speed capabilities, achieving the required 5 [MNm] torque for large yaw angles. These motors will be installed in the emerged section of the monopile, with gear ratios enhancing their torque output.

Drivetrain

The drivetrain design within the ReWind wind turbines is a critical component for converting the mechanical rotational energy captured from the wind into electrical energy. This modular drivetrain system is built around a torsionally stiff bedplate and includes a main bearing that greatly improves torque isolation. The design features a 900 [kW] Indar DFIG generator to produce electricity and a Gamesa G5X gearbox is used to increase rotational speed of the shaft.

The modular nature of the drivetrain allows for easy maintenance and quick replacement of components, which is crucial for minimizing operational disruptions and maintaining consistent energy production. This reliability directly translates into better financial performance and a lower risk profile for investors. Furthermore, the advanced technology used in the gearbox and generator ensures efficient energy conversion, thereby maximizing the output and overall efficiency of the wind turbines. This efficiency not only leads to higher returns on investment but also contributes to the overall sustainability of the wind farm by ensuring that each turbine operates at its optimal capacity with minimal waste.

Production & Installation

The ReWind wind farm concept, designed to withstand the harsh North Sea conditions, involves the following key components:

- **Monopile Foundation:** Manufactured from steel sheets, welded to form robust cylinders. Companies like Sif Offshore Foundations are potential suppliers.
- **Truss Structure:** Made of 1,353 steel members, cut and formed into shape. Standardizing member types can simplify manufacturing. Potential suppliers include Tata Steel and Kersten.
- **Active Flow Control System:** Steel components manufactured using similar techniques to the monopile. Tata Steel, Kersten, and 3D Metal Forming are suitable suppliers.
- **Rotor Blades:** Produced using resin infusion techniques for high precision. Manufacturing in-house ensures quality and innovation.
- **Standard Components:** Off-the-shelf parts like generators and transformers from companies like Indar, Gamesa, Hitachi Energy, and ABB.

The wind turbine structures will be fully assembled at onshore facilities in the port of Rotterdam to simplify and expedite the offshore installation process as well as keep the costs for specialized vessels with large cranes to a minimum. The companies mentioned previously were chosen both for their expertise and their proximity to the assembly location. This close proximity ensures that transportation emissions will be minimized. The assembly begins with the construction of the entire wind turbine structure onshore, followed by its transportation using a skid way to move the fully built structure from the construction site onto the vessel for offshore installation.

The superstructure assembly involves stacking horizontal layers. Initially, low-level modules containing RNA platforms are assembled and reinforced. These modules are then aligned and connected horizontally to form sections. A central connection module is created and integrated with the left and right sections of RNA platforms. All layers are subsequently stacked and bolted together to complete the superstructure. During this process, AFC wings are attached within the superstructure, and additional reinforcement is added for structural integrity.

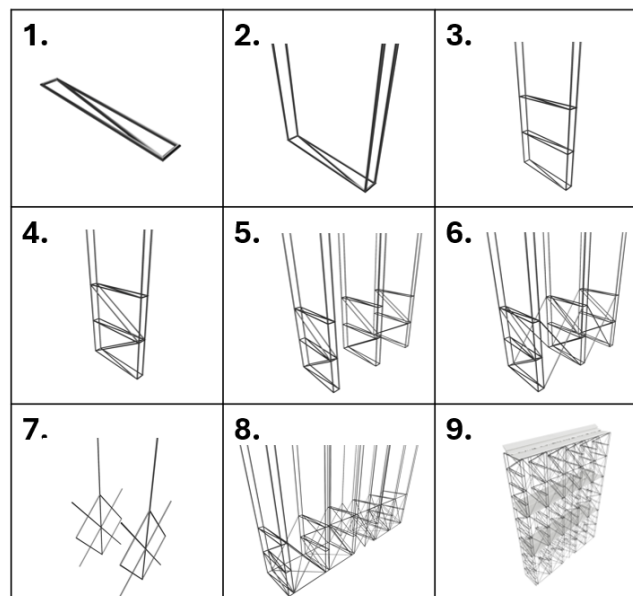


Figure 6: Assembly plan

The integration of the monopile-superstructure interface and RNA involves connecting a specially designed interface for load transfer and stability to the superstructure. All RNA components are then installed using on-shore facilities, which saves time and resources. The completed structure, including all RNAs and the monopile interface, will be ready for efficient offshore installation. This approach ensures precise assembly, optimal use of resources, and a streamlined installation process.

The installation of the ReWind Turbine involves two main phases: foundation installation and array installation. Foundation installation begins with the monopile, yaw bearing, and yaw motors. The monopile, measuring 90.32 [m], is first installed into the seabed using a specialized vessel like the DEME Orion. This vessel, equipped with a 5000-metric-ton crane, ensures precise positioning of the monopile and uses hydraulic or vibratory hammers to drive it securely into the seabed. Yaw motors are then inserted and pinned inside the monopile, followed by the installation of the yaw bearing at sea level, securing the upper monopile section above it.

For the array installation, a float-over technique is employed. Integrated topsides are prepared onshore and transferred onto a transportation barge, which is then positioned near the monopile using mooring lines and fenders. During the mating stage, the barge approaches the monopile while Deck Support Units assist in load transfer. The topsides' superstructure-monopile interface aligns and connects with the monopile using tide and ballast systems or hydraulic jacks for precise placement. After load transfer, the barge is ballasted down for clearance before departure.

Decommissioning strategies are crucial after the wind turbine's operational lifetime of 25 years. The process begins with evaluating options like repowering or refurbishment to enhance efficiency before considering dismantling. Decommissioning methods prioritize minimal on-water disassembly to reduce environmental risks, preferring float-over deinstallation for efficient removal and potential repowering of the existing monopile. Options for foundation dismantling include full removal to optimize future turbine deployment space, and utilizing innovative pump systems for minimal seabed disruption. Electrical substations and subsea cables are dismantled with similar environmental considerations, balancing operational needs with marine habitat preservation.

Operations

In the operational phase of the ReWind wind farm, a sophisticated array of sensors plays a pivotal role in optimizing turbine performance and maintaining structural integrity. These sensors enable dynamic adjustments based on real-time environmental data, ensuring maximum energy capture and minimizing mechanical stress. The collected data is processed through a detailed data handling system, which channels information from the sensors to the turbine's main controller. This system fine-tunes operational parameters such as blade pitch and rotor yaw, enhancing efficiency and output. Additionally, a robust communication infrastructure ensures seamless data transfer between individual turbines and the central control system, employing fiber-optic networks for rapid and reliable data synchronization across the farm.

The operational lifecycle of each turbine is delineated into phases of parking, start-up, power generation, and braking, managed to adapt swiftly to changing wind conditions. During the start-up phase, turbines transition from dormancy to active power generation as wind speeds surpass operational thresholds, carefully monitored to mitigate component stress. The implementation of Maximum Power Point Tracking (MPPT) strategies, particularly the Power Signal Feedback (PSF) method, ensures each turbine consistently operates at peak efficiency. This method proves advantageous in its robustness and adaptability, facilitating scalable energy optimization across varying wind conditions.

Particular attention is given to operations during storm conditions, where turbines face higher wind speeds and potential structural impacts. Strategies are employed to gradually reduce turbine operations as conditions intensify, including strategic yaw adjustments and blade pitching to reduce the effective surface area against high winds. This proactive management not only protects the turbines from potential damage but also maintains a stable and efficient operational state, thereby prolonging the infrastructure's lifespan and ensuring sustained energy production during adverse weather conditions. These operational protocols underscore ReWind's commitment to maximizing energy output while ensuring the durability and safety of its wind farm through advanced technological integration and strategic operational planning.

RAMS

The Reliability, Availability, Maintenance and Safety (RAMS) analysis for ReWind's wind turbine project is critical to assess its feasibility and operational efficiency. RAMS factors significantly impact the project's success, with Operations and Maintenance (O&M) costs accounting for up to 34% of the total Levelized Cost of Energy (LCoE) over the turbine's lifespan [2]. The key findings from this analysis are as follows:

- **Accessibility of the Site:** The turbine design includes horizontal platforms, an elevator system, and auxiliary pulley hoists for safe and efficient maintenance access. Crew Transfer Vessels (CTVs) stationed at the port of Den Helder ensure prompt and cost-effective transportation for maintenance crews, enhancing operational uptime.
- **Safety:** Strict safety protocols during maintenance operations include selectively shutting down adjacent rotors and complete turbine shutdowns for major component replacements, ensuring operational integrity and worker safety.
- **Maintenance Strategy:** ReWind adopts an opportunistic maintenance strategy combining preventive and condition-based approaches to optimize maintenance intervals and minimize operational risks while maximizing turbine longevity and performance.
- **Actual Availability:** Taking into account component failure rates, site accessibility and safety measures, the actual availability of ReWind's wind turbine project is estimated at 95.38%, demonstrating its reliability and efficiency in sustainable energy generation.

Cost Analysis

ReWind aims to significantly reduce the cost of energy compared to conventional wind energy systems. In the energy market, the cost of energy is measured by the Levelized Cost of Energy (LCoE) in [€/MWh]. This metric takes into account initial capital cost, operation cost, maintenance cost, financing, project lifespan and total energy output. Thus, it is very relevant to measure the economic viability and competitiveness of ReWind.

The LCoE of the ReWind project was calculated from scaling and adapting the cost model for a conventional wind farm from Catapult [3]. The following LCoE-driving modifications are applied to move from the Catapult wind farm LCoE to the ReWind wind farm LCoE. First, the rated power of the turbine is increased from 10 [MW] to 30 [MW]. Secondly, the LCoE is adapted for a higher power density and a different location. Subsequently, wake losses are accounted for. Finally, the LCoE is changed for a multi-rotor turbine including Active Flow Control (AFC) devices.

Completing these steps, ReWind has an estimated LCoE of 40.70 [€/MWh], which is 39% lower than current technology high energy density wind farms, which have an LCoE of 66.25 [€/MWh]. The LCoE is broken down into its constituents in Figure 7. ReWind provides reduced Capital- and Operational Expenditures compared to existing wind farms at 2,556.40 [€/kW] and 27.40 [€/kW/yr], respectively.

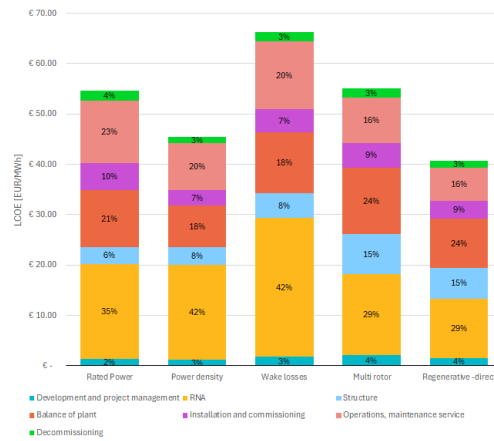


Figure 7: LCoE breakdown into its components of each step

Furthermore, next to the LCoE, the Return On Investment (ROI) and Net Present Value (NPV) will be determined for the ReWind wind farm, as these values give a good indication of the profitability of this project for potential investors. Following the calculations, it is concluded that ReWind is very attractive as an investment opportunity due to its high annual ROI between 7.77% and 10.20% compared to conventional wind farms and a NPV in the range of 15,697,000,000 - 29,171,000,000 [€]. Overall, ReWind proves to be economically very exciting due to lower cost and higher returns than conventional systems.

Sustainability

ReWind aims to reduce its carbon footprint compared to industry standards significantly. The project targets a 32% reduction in CO₂ emissions per megawatt-hour [MWh], achieving an estimated emission rate of 7.49 [kgCO₂/MWh]. This reduction is achieved through innovative design choices and efficient operational practices.

Key phases analyzed include material extraction, production, transportation, operations, and end-of-life considerations. During material extraction, approximately 6.3 megatons of CO₂ were emitted, with 18.3 million [MWh] of energy consumed. Production processes contributed 2.98 million tonnes of CO₂ emissions and consumed 14.4 million [MWh]. Transportation logistics accounted for 9,734.3 tonnes of CO₂ emissions.

Throughout its 25-year operational lifespan, ReWind expects to emit 2.18 megatons of CO₂ and consume 7.96 million [MWh] during operations. However, effective decommissioning practices are projected to save 6.10 megatons of CO₂ and 17.5 million [MWh] of energy through recycling efforts.

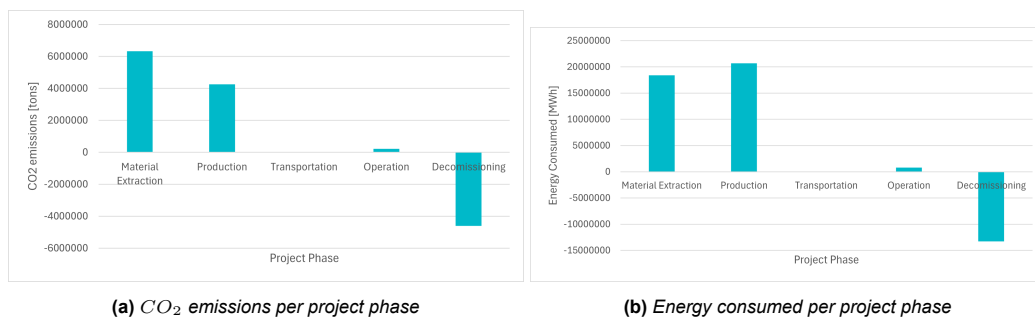


Figure 8: Life Cycle Analysis of the different project phases

Based on the LCA, incorporating energy storage systems will become essential for grid stability. Assuming industry-standard emissions and energy consumption for producing batteries (27,500 [kgCO₂] emitted and 42.5 [MWh] consumed per [MWh] of storage [4, 5]), the additional emissions and energy consumed during the wind farm's lifetime due to the storage system amount to approximately 19.23 [kgCO₂/MWh] and 0.03 [MWhconsumed/MWhproduced].

Therefore, the overall emissions for the wind farm, including the storage system, are estimated at 25.52 [kgCO₂/MWh], with an additional energy consumption of 0.057 [MWhconsumed/MWhproduced]. In comparison, existing wind farms with storage systems would emit around 32.5 [kgCO₂/MWh].

Compliance

The ReWind project was initiated by a set of initial requirements set by the stakeholders. These initial requirements were further translated into detailed and specific mission, system, and subsystem requirements. However, ultimately, it is the stakeholder requirements that need to be met, as they most accurately reflect the customer's wishes. In Table 1, the most important stakeholder requirements are shown, along with the achieved performance of the ReWind concept. Based on this performance, the cells are colored green if the requirement is met and red if it is not. Clearly, the ReWind project meets the large majority of the stakeholder requirements, as it achieves the desired power density and annual energy efficiency (AEP) combined with the necessary large size of the wind farm. However, the requirement focusing on the LCOE is not met. The ReWind concept has a 39% better LCOE compared to industry standards, not the required 45% lower LCOE. Finally, the ReWind shows a 32 % lower carbon footprint than current standards.

Table 1: Main stakeholder requirement compliance

ID	Requirement	ReWind performance
REQ-STK-CUS-01	The farm shall have a rated power of 6 GW	The wind farm has a rated power of 8.69 [GW]. (section 4.5)
REQ-STK-CUS-02	The farm shall have a rated power density of 10 [MW/km ²]	The wind farm power density is 10.36 [MW/km ²]. (section 4.5)
REQ-STK-CUS-03	The wind farm efficiency of the entire wind farm shall exceed 80%	The ReWind concept achieves a wind farm efficiency of 84.5 %. (section 5.3)
REQ-STK-CUS-04	The LCOE of the wind farm shall be 45% lower than current industry standards, estimated to be 68 [€/MWh] for the Netherlands	The ReWind wind farm achieves an LCOE of 40.7 [€/MWh], or 39 % lower than industry standards. (section 10.2)
REQ-STK-CUS-06	The wind farm shall have a 40% lower carbon footprint than current standards, estimated to be 11 [g/kWh]	For each kWh produced, the Rewind system emits only 7.48 [g] of CO ₂ or 32% lower. (subsection 13.1.6)

Future Design

This report outlines the conceptual design of the ReWind wind farm, but this is not the concluding phase of the project. Based on the results obtained in the conceptual design phase, a future design logic is outlined, which covers the final detailed design and qualification, manufacturing, assembly and installation, operation and sustainment, and decommissioning.

Performance analysis

With the complete ReWind wind farm design finished and the associated cost and sustainability analysis completed, the overall performance can be compared with a 30MW turbine reference wind farm to show overall competitiveness within the wind energy market. Each important parameter is tabulated in Table 2, and its relative performance is shown.

Table 2: Performance Analysis of the wind farm

Parameter	Value	Units	Improvement/Reduction
Wind Farm Rated Power	8.812	[GW]	
Wind Farm Capacity Factor	47.5 %	-	+35%
Wind Farm efficiency	84.5 %	-	+47%
Power density	10.36	[MW/km ²]	
LCOE	40.7	[€/MWh]	-40%
CO ₂ emitted	7.48	[kgCO ₂ /MWh]	-32%
Energy Density	41202	[MWh/km ² /year]	+34%
Steel Use	3.2163	[kg/MWh]	+91%
Glass Fiber Use	0.0812	[kg/MWh]	-58%
Rare Earth Metal Use	0.01	[g/MWh]	-99%
Wind Turbine Mass	11003	[tonnes]	
Wind Turbine Rated Power	30.6	[MW]	

Contents

1	Introduction	1
2	Market analysis	2
2.1	Current market size	2
2.2	Competition	3
2.3	Market gap and SWOT analysis	4
2.3.1	Market Gap	4
2.3.2	SWOT analysis	6
2.4	Stakeholder identification	7
3	Functional Analysis	9
3.1	Functional Flow	9
3.2	Functional Breakdown	9
3.3	Diagrams	9
4	Site Measurements	12
4.1	Farm Location	12
4.2	Wind Data	12
4.3	Wave Data	13
4.4	Water Depth	14
4.5	Layout of Wind Farm	14
5	Detailed design	15
5.1	Rotor Design	15
5.1.1	Number of Rotors	15
5.1.2	Rotor Dimension	15
5.1.3	Airfoil Selection	16
5.1.4	Blade Element Momentum model	16
5.1.5	Blade Geometry Optimization	17
5.2	Active Flow Control design	18
5.2.1	AFC Sizing	18
5.2.2	Airfoil Selection and Design	21
5.2.3	AFC Overview	23
5.2.4	AFC Mass Estimation	24
5.3	Annual Energy Production	25
5.4	Structural Design	25
5.4.1	Load Cases	25
5.4.2	Truss Model Description	26
5.4.3	Truss Element Design	28
5.4.4	Load Application	29
5.4.5	Space Frame Sizing	30
5.4.6	Foundation Trade-Off	33
5.4.7	Monopile Sizing	35
5.4.8	Load identification and boundary conditions	35
5.4.9	Limitations	39
5.5	Control Systems	40
5.5.1	Yaw	40
5.5.2	Pitch	43
5.6	Drivetrain Design	46
5.6.1	Generator	47
5.6.2	Gearbox	48
6	Verification & Validation	50
6.1	BEM Model	50
6.2	Yaw System Simulation	50
6.3	Truss Structural Model	51
6.4	Monopile sizing model	52
6.5	Product	53

7	Production, Assembly and Installation	55
7.1	Production	55
7.2	Installation Method Trade-off	56
7.2.1	On site assembly of substructures built onshore	57
7.2.2	Full onshore construction with float over installation on site	58
7.3	Assembly	58
7.3.1	Assembly of the low level modules	59
7.3.2	Assembly of central connection section	59
7.3.3	Assembly of RNA layer	60
7.3.4	Complete assembly of the superstructure	60
7.3.5	Integration of monopile-superstructure interface and RNA	61
7.4	Transport & Installation	61
7.4.1	Monopile & Bearing Installation	61
7.4.2	Float-Over Topside Installation	62
7.4.3	End of Life	63
8	Operations	65
8.1	Data Sensors	65
8.2	Data Handling Block Diagram / HW-SW	66
8.3	Communication Block Diagram	66
8.4	Operation Phases	67
8.5	Power Generation Control Strategy	69
8.6	Active Flow Control Operations	70
8.7	Storm Condition	70
9	Reliability, Availability, Maintainability and Safety	72
9.1	Reliability	72
9.1.1	Failure Rate Modeling	75
9.2	Accessibility of the Site	77
9.3	Safety	78
9.4	Maintenance Strategy	78
9.5	Actual Accessibility	79
10	Cost Breakdown and Analysis	80
10.1	Methodology	80
10.1.1	Rated Power	81
10.1.2	Power Density and Location	81
10.1.3	Wake Losses	83
10.1.4	Energy Storage	83
10.1.5	Multi-rotor	85
10.1.6	Wake Re-energization	86
10.2	Results	87
10.3	Return on Investment	89
11	Sensitivity Analysis	91
11.1	Parameters of interest	91
11.2	Results	91
11.3	Conclusions	93
12	Budget Breakdown	94
13	Sustainable Development Strategy	97
13.1	Life Cycle Analysis	97
13.1.1	Extracting materials	97
13.1.2	Production	98
13.1.3	Transportation	99
13.1.4	Operations	99
13.1.5	End Of Life	100
13.1.6	LCA conclusion	100
13.1.7	Storage system	100
13.2	Materials used over the lifetime	100
13.3	Measures to Improve the environmental impact	101
13.4	Bird Fatalities	101
13.5	Reduced Sea Routes and Fishing Areas	101

13.6 Marine Biodiversity	101
13.7 Thermal Pollution and Corrosion	102
13.8 Acoustic Pollution	102
13.9 Magnetism Effects	102
14 Risk Assessment	103
14.1 Risk Management Table	103
14.2 Risk Map	107
15 Final Design	108
15.1 Subsystem Overview	108
15.2 Performance Analysis	110
15.3 Final Design Summary	110
16 Requirement compliance	112
16.1 Subsystem compliance	112
16.2 System compliance	113
16.3 Mission compliance	115
16.4 Stakeholder compliance	116
16.5 Future compliance	116
17 Future Design	118
17.1 Future Design and Development Logic	118
17.1.1 Final Design and Qualification	118
17.1.2 Manufacturing	119
17.1.3 Assembly, Integration and Testing	119
17.1.4 Operations and Sustainment	119
17.1.5 Decommissioning	119
17.2 Future Design Gantt Chart	119
18 Conclusion	123
References	125

Acronyms

AC Alternating Current.

AEP Annual Energy Production.

AFC Active Flow Control.

BEM Blade Element Momentum.

BPA Bidirectional Power Actuator.

CDF Cumulative Distribution Function.

CFD Computational Fluid Dynamics.

CTV Crew Transfer Vessel.

DC Direct Current.

DFIG Doubly Fed Induction Generator.

DLC Design Load Case.

DOF Degrees of Freedom.

DtS Distance to Shore.

DTU Technical University of Denmark.

ECMWF European Centre for Medium-Range
Weather Forecasts.

EOL End Of Life.

EOM Equations Of Motion.

EZK Ministry of Economic Affairs and Climate Policy.

FBS Functional Breakdown Structure.

FFD Functional Flow Diagram.

FY Fiscal Year.

GBS Gravity Based Structure.

HAWT Horizontal Axis Wind Turbine.

HCS Hill Climb Search.

HLD High Lift Device.

HVDC High Voltage Direct Current.

IEA International Energy Agency.

IEC International Electrotechnical Commission.

IGBT Insulated-Gate Bipolar Transistor.

INC Incremental Conductance.

JUV Jack Up Vessel.

LCA Life Cycle Analysis.

LCoE Levelized Cost of Energy.

MPC Model Predictive Control.

MPPT Maximum Power Point Tracking.

MRS Multi Rotor System.

NPV Net Present Value.

NREL National Renewable Energy Laboratory.

O&M Operations and Maintenance.

ONU Optical Network Unit.

ORB Optimum Relation Base.

OTC Optimal Torque Control.

PAL Pressure Accumulator Link.

PC Pitch Controller.

PID Proportional, Integral, Derivative.

PMF Probability Mass Function.

PMSG Permanent Magnet Synchronous Generator.

PSF Power Signal Feedback.

RAMS Reliability, Availability, Maintenance and
Safety.

RNA Rotor Nacelle Assembly.

ROI Return On Investment.

RPA Rotary Power Actuator.

RTM Resin Transfer Molding.

RTU Remote Terminal Unit.

SCADA Supervisory Control and Data Acquisition.

SOV Service Operation Vessel.

SRT Single Rotor Turbine.

SWOT Strengths, Weaknesses, Opportunities and
Threats.

TSR Tip Speed Ratio.

V&V Verification and Validation.

VARTM Vacuum Assisted Resin Transfer Molding.

WD Water Depth.

WTC Wind Turbine Controller.

1. Introduction

The North Sea Programme, implemented by the Dutch government, aims to enhance offshore wind energy production to meet rising energy demands and environmental goals¹. However, this ambitious initiative faces inherent problems, particularly concerning the scalability of wind farms, which cause increasingly high energy losses. Furthermore, the total wind farm area required for a significant reduction of carbon emissions comes with logistical and environmental challenges, including space constraints and potential disruptions to marine ecosystems. Additionally, the recyclability of wind turbines presents a critical issue. As wind turbines are up-scaled to meet these energy goals, the use of rare earth metals in turbine construction becomes increasingly problematic. These metals are not only difficult to recycle but also pose environmental and ethical concerns due to their mining and processing impacts. Thus, while the North Sea Programme strives for a sustainable energy future, it must navigate significant obstacles in scalability and material sustainability.

To address the aforementioned problems, this report explores the implementation of multi-rotor wind turbine systems as a viable solution. Multi-rotor systems consist of several smaller rotors mounted on a single truss structure, capable of achieving larger unit capacities than traditional single-rotor turbines due to easier scalability, making them a cost-effective alternative. Furthermore, the simpler design of these systems enhances manufacturability, streamlining production processes.

The truss structure present in multi-rotor systems also allows for the installation of high-lift devices, which can be adapted to change the properties of the wake of the turbine. This process effectively consists of creating vertical momentum fluxes in the wake of the turbine which reenergize the lower atmospheric boundary layer, increasing the wind speed. This highly increases the efficiency of the downstream turbines and, as a result, the entire wind farm. Consequently, turbines can be packed more closely together, increasing wind energy density and optimizing the efficiency of wind farms.

This report is the culmination of a ten-week design synthesis of a multi-rotor Horizontal Axis Wind Turbine (HAWT) system. ReWind intends to combine and apply the solutions mentioned above and offer a promising pathway to overcoming the challenges faced by the North Sea Programme, advancing towards more sustainable wind energy solutions. This final design report is the conclusion of a trilogy of deliverables made up of the Baseline and Midterm reports, where other elements of the ReWind project such as the subsystem trade-off, and subsystem requirements can be found.

Firstly, the wind energy market will be studied in chapter 2, where a market gap is found and the stakeholders are identified. Thereafter, the relationships between systems of the wind turbine is depicted in chapter 3 through the use of a functional flow and a breakdown diagram. After this, the wind farm site is chosen and all the data is extracted and presented under chapter 4. Finally, under chapter 5 the final design of the wind turbine system is defined and presented. In addition, the verification and validation is performed under chapter 6 to ensure a correct design has been calculated and chosen.

Once the design has been introduced, the report delves into more detailed aspects. In effect, the production, assembly and installation of the wind turbine is presented in chapter 7 and the operative aspects of the system under chapter 8. Additionally, chapter 9 defines and measures the availability and maintenance of the wind turbine. Following this, the costs will be established in chapter 10. This cost analysis is verified with a sensitivity analysis in chapter 11. Hereafter, in chapter 12, the mass and cost budget will be broken down into components. Subsequently, in chapter 13 an extensive analysis of the carbon footprint of the entire life cycle of the system is performed, from design phase, operations to end of life. In addition, the impact the wind farm can have on maritime life and its surrounding environment is also defined and attenuated.

Moreover, chapter 14 presents an overview of the potential technical risks that come with the ReWind project, as well as different strategies to mitigate the defined risks. Then, chapter 15 summarizes the design giving the key performance, and operational parameters and, chapter 16 evaluates whether all of the previously defined requirements have been met, or otherwise certify that the adjustments have been negotiated with the client. Finally, chapter 17 defines the next steps to be taken in the design, operation and decommissioning processes of the wind turbine. These steps are meant to be taken after this report to outline the future of the ReWind project.

¹<https://english.rvo.nl/news/netherlands-exceeds-2023-offshore-wind-target> [Accessed 07-06-2024]

2. Market analysis

This chapter analyzes the offshore wind energy market. It begins by defining the market and examining the current market size, detailed in section 2.1. A comparison with competitors is explored in section 2.2 to underline the competitive landscape and cost dynamics. Finally, and most importantly, this chapter presents the market gap that this project can fill and extrapolates the strengths and weaknesses of this project, detailed in section 2.3.

2.1. Current market size

Wind energy production is separated into two categories: land-based and offshore. This project, ReWind, will focus on offshore wind farms. Typically, offshore projects exhibit higher complexity due to additional technological and logistical challenges, as well as extra environmental regulations.

The total global installed capacity of offshore wind energy as of 2022 is 59 [GW] [6]. As can be seen under Figure 2.1a, during 2022, the largest increase in installed capacity was seen in China, followed by the European continent. Furthermore, the wind energy market is expected to grow exponentially over the coming years, with many more projects planned and under development with a highly optimistic market that does not predict these numbers to slow down. Figure 2.1b shows the developments in the wind energy market, indicating that this sector is projected to exceed 426 [GW] of total capacity in the coming years. In addition, The Netherlands aims to achieve 21 [GW] by 2030 and a capacity of 70 [GW] by 2050¹.

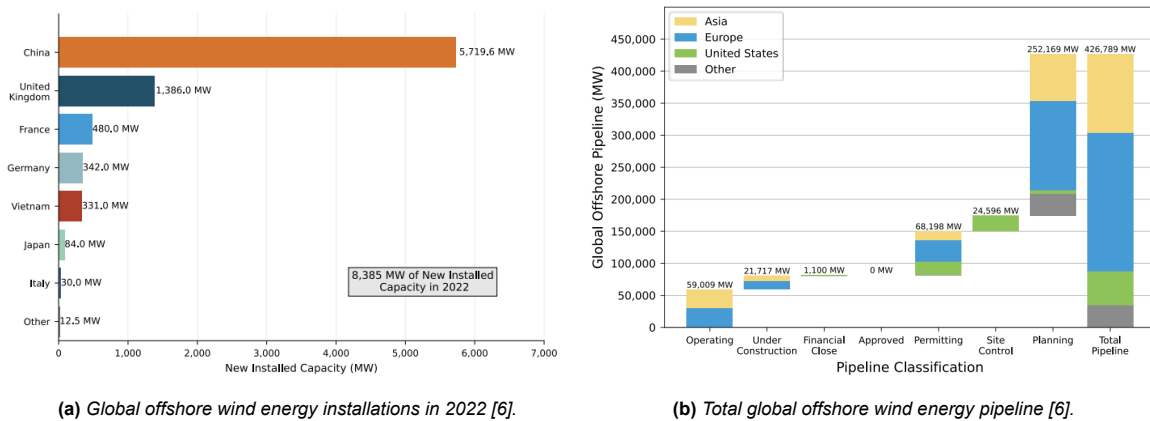


Figure 2.1: Current global offshore wind energy situation

Moreover, this vast development in wind energy technology naturally leads to an increase in the learning rate as the technology matures, which in turn decreases the Levelized Cost of Energy (LCoE). The LCoE is crucial for stakeholders as it determines the break-even point and evaluates the cost-effectiveness of the deployed wind farms. It is an all-encompassing metric that takes into account the initial capital costs, ongoing operations and maintenance costs, the cost of financing, the project lifespan, and the total energy output. Therefore, it is a useful measure to compare the viability of this project with respect to the current market.

Levelized Cost of Energy (LCoE) is measured in €/MWh and can be calculated using Equation 2.1 [7]:

$$LCOE = \frac{CapEx \cdot FCR + OpEx}{\left(\frac{AEP_{net}}{1000}\right)}, \quad (2.1)$$

where FCR represents the fixed charge rate [%], $CapEx$ the capital expenditures [€/kW], AEP_{net} the net average annual energy production [MWh/MW/yr] and $OpEx$ the operational expenditures [€/kW/yr].

On average, the LCoE of offshore wind ranges between 50 - 65 [€/MWh]². This translates to an average LCoE range of 53.5 - 69.55 [€/MWh] in the 2024 Fiscal Year (FY) accounting for inflation. This value can be used as a

¹<https://english.rvo.nl/news/netherlands-exceeds-2023-offshore-wind-target> [Accessed 28-05-2024]

²<https://windeurope.org/policy/topics/economics/> [Accessed 18-06-2024]

benchmark to compare with this project's design. A more accurate estimate of the LCoE of the ReWind project, as well as for a conventional wind farm will be presented in chapter 10. From these values, the economic performance of ReWind will be determined.

2.2. Competition

The main competitors of wind energy as a renewable energy source are nuclear power, solar energy and geothermal energy. While nuclear power is a highly established technology, solar and geothermal energy is continuously evolving and improving in efficiency. This section analyses these alternatives and compares them to wind energy.

Nuclear Power

Nuclear power can be regarded as a form of renewable energy; however, its fuel, enriched Uranium, is not as it is finite and very scarce. Nonetheless, this is a highly efficient energy source that does not release any greenhouse gases nor pollute the air. However, the byproduct of nuclear power is radioactive, which makes it its main drawback. This radioactive waste is long-lasting and must be disposed of with care, a task regulated by the government. In figure Figure 2.2, it is possible to see the comparison of nuclear energy with other non-renewable energy sources. Here, the LCoE of nuclear energy is calculated to be between 27-32 [€/MWh] for already operating power plants and 131-206 [€/MWh] for a new build [8].

Solar Energy

Solar is a highly promising energy source that has become highly commercial in the last 10 years, mainly due to the tremendous increase in learning rate. Consequently, the efficiency of commercial solar cells has increased rapidly, standing around 23% efficiency currently [9]. In addition, the large resources invested in research and development of new solar cell technologies have led to countless promising improvements that can soon be implemented in commercial solar modules.

Finally, all relevant aspects of this energy source lead to the summarised figure Figure 2.2, where it can be seen that the LCoE of solar energy is calculated to be between 22-89 [€/MWh] [8].

Geothermal Energy

Geothermal is also one of the most widely used renewable energy sources in the Netherlands. Here, the high thermal potential stored within the Earth's crust is used to generate energy. According to estimations, around a quarter of the Dutch energy demands could be met using geothermal³. Thus, at the moment, the LCoE of this renewable energy source is situated between 57-95 [€/MWh] as depicted in Figure 2.2 [8].

Units	Solar PV								
	Nuclear (Operating)		Utility-Scale		Utility Scale + Storage		Geothermal		
	Low Case	High Case	Low Case	High Case	Low Case	High Case	Low Case	High Case	
Net Facility Output	MW	2,200		150		100		250	
Total Capital Costs ⁽¹⁾	\$/kW	\$0.00		\$700 - \$1,400		\$1,075 - \$1,600		\$4,700 - \$6,075	
Fixed O&M	\$/kW-yr	\$97.25 - \$120.00		\$7.00 - \$14.00		\$20.00 - \$45.00		\$14.00 - \$15.25	
Variable O&M	\$/MWh	\$3.05 - \$3.55		—		—		\$8.75 - \$24.00	
Heat Rate	Btu/kWh	10,400		—		—		—	
Capacity Factor	%	95% - 90%		30% - 15%		27% - 20%		90% - 80%	
Fuel Price	\$/MMBTU	\$0.79		—		—		—	
Construction Time	Months	69		9		9		36	
Facility Life	Years	40		30		30		25	
Levelized Cost of Energy	\$/MWh	\$29 - \$34		\$24 - \$96		\$46 - \$102		\$61 - \$102	

Figure 2.2: Levelized cost of Energy comparison for other different energy sources [8] (edited).

Lastly, the evolution of the levelized costs of energy for various energy sources currently available in the market are shown in Figure 2.3. In this graph, it is possible to see the rapid evolution of solar energy between 2009 and 2015. These technological achievements have made both solar and wind energy competitive and relatively

³<https://geothermie.nl/en/> [Accessed 28-05-2024]

cheap in comparison with other non-renewable energy sources. It is also important to note that in this graph, nuclear energy is shown for new-build nuclear projects.

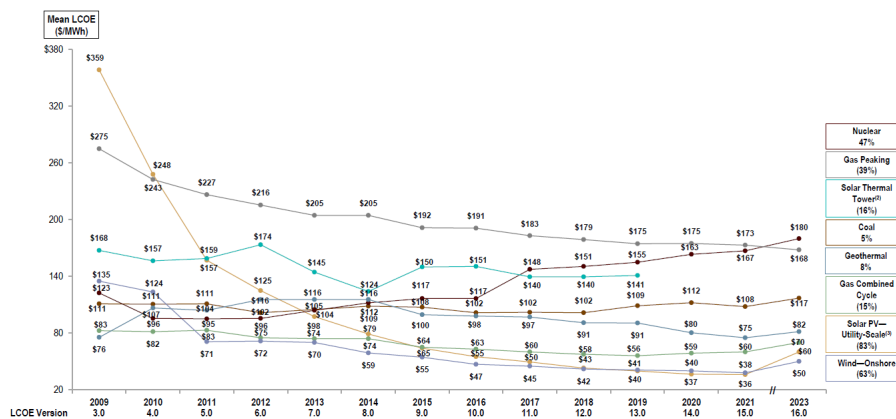


Figure 2.3: Evolution of the Levelized cost of Energy comparison for multiple energy sources [8].

Consequently, from this analysis it can be concluded that wind energy presents a viable and promising opportunity in the renewable energy market. Wind energy displays LCoE values lower than most of its competitors, values which are predicted to continue decreasing as the technology matures further in the years to come.

2.3. Market gap and SWOT analysis

This section aims to identify the market gap that can be filled by the ReWind concept. Furthermore, the Strengths, Weaknesses, Opportunities and Threats (SWOT) with respect to the current market is determined and presented. Finally, all stakeholders are identified and illustrated in a stakeholder map.

2.3.1. Market Gap

Based on the previous market size examination and competitor evaluation, it was determined that the market gap for this project stems from the Dutch energy goals to reach a climate-neutral energy supply by 2050⁴. Wind energy is expected to have a large contribution to this goal. Thus, the government has set the target for an offshore wind capacity of 21 [GW], supplying 16% of the total Dutch energy needs.

This planned growth comes with numerous technical challenges, the most critical being the limited available space in the North Sea. This issue is further complicated by the wake effects of wind turbines. As wind passes through a wind turbine, a wake is formed which negatively impacts the power produced by turbines downstream. Over the past decades, much research has gone into limiting the effects of single-rotor wakes. However, less attention has been dedicated to the effects of wind farm wakes. Much like a forest, wind farms affect the atmospheric boundary layer through the combined wakes of each tree or turbine, slowing down the flow locally. The bigger and more densely packed the forest or wind farm, the more noticeable these effects are. As a result, wind turbines positioned downstream in a wind farm receive much lower clean flow, leading to lower capacity factors, which relates the power production to the installed power, and poor wind farm efficiencies.

The relation between power density and wind farm efficiency, obtained from dozens of reference wind farms, is plotted in Figure 2.4, where it is clear that wind farm efficiency reduces as the wind farm density increases. Wind farm efficiency is defined as the average capacity factors of all turbines in the wind farm divided by the capacity factor of a single turbine experiencing fully clean airflow. As mentioned before, this decrease in efficiency is a direct result of the 'forest effect' of the wind farm, which is further exacerbated if the number of trees or turbines increases per unit area.

⁴<https://english.rvo.nl/news/netherlands-exceeds-2023-offshore-wind-target> [Accessed 07-06-2024]

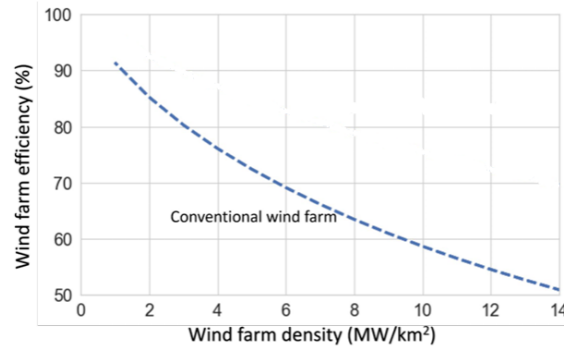


Figure 2.4: Wind farm efficiency and power density relation [1].

Consequently, with current turbine designs and the associated wind farm efficiency and energy density relation, it will be impossible to realise the highly optimistic energy goals of the Dutch government. This premise has been pointed out by Prof. Carlos Ferreira in Figure 2.5, which plots the wind farm capacity factor (average capacity factor of all turbines in the wind farm) against the wind farm factor for a broad selection of current operational wind farms. The wind farm factor is defined as:

$$\phi_{WF} = \frac{U_r}{\bar{U}_\infty \epsilon_{eq}}, \tag{2.2}$$

where U_r is the rated wind speed, \bar{U}_∞ is the wind speed and ϵ_{eq} is a correction factor. The blue line indicates the maximum theoretical achievable capacity factor, while the orange line takes into account 10% operational losses [1].

In order to produce the largest amount of energy possible, it is necessary to optimize both the installed capacity and the wind farm capacity factor while minimizing the used area, aiming for high power density. The orange star indicates the target of the proposed conceptual design for ReWind’s farm. Although several wind farms currently achieve capacity factors and wind farm wind factors similar to the ReWind target, they typically have very low power densities (around 3-5 [MW/km²]) and low installed capacities (around 200-400 [MW]), which explains their high capacity factors [1]. The challenge remains to achieve these high figures with a power density of 10 [MW/km²] and a large farm size on the order of 6 [GW].

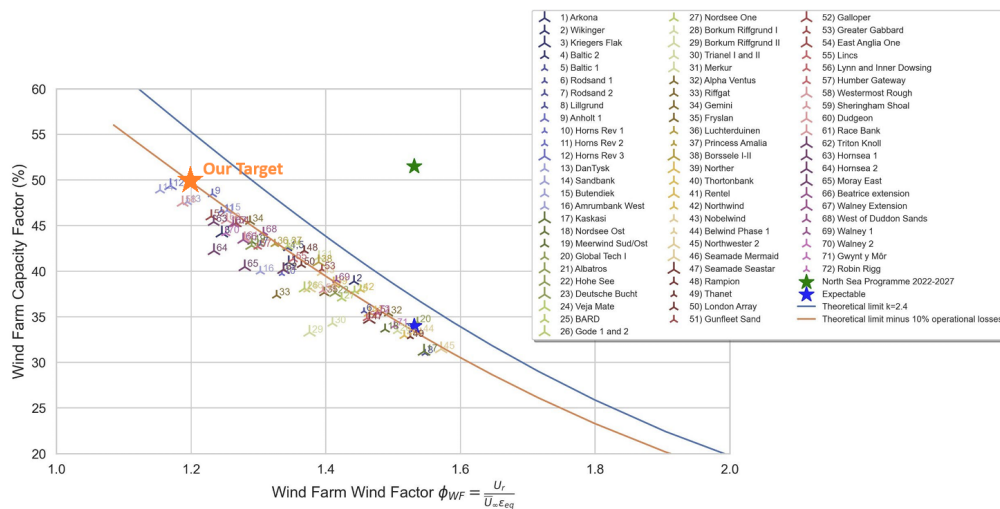


Figure 2.5: Analysis of the Dutch wind energy goals [1].

To move along the orange curve, wind farms can alter their wind farm wind factor by making specific changes. However, some parameters, such as the free-stream wind speed, can not be changed and reducing the rated wind speed would lead to very low power production values, which is not desired. This leaves the option to

increase the ϵ parameter. This can be achieved by modifying the atmospheric boundary, resulting in a lower wind farm wind factor, which subsequently leads to a lower potential wind farm capacity factor.

The reason why wind farms using current wind turbine designs remain relatively small is due to low wind farm capacity factors, which worsen as you scale up. Furthermore, another negative consequence of this low capacity factor is that losses in efficiency are mainly incurred at low wind speeds, as is shown in Figure 2.6. At high wind speeds, above rated wind speed, turbines inside the wind farm still produce close to rated power. However, at low wind speeds, the wake effects are more noticeable.

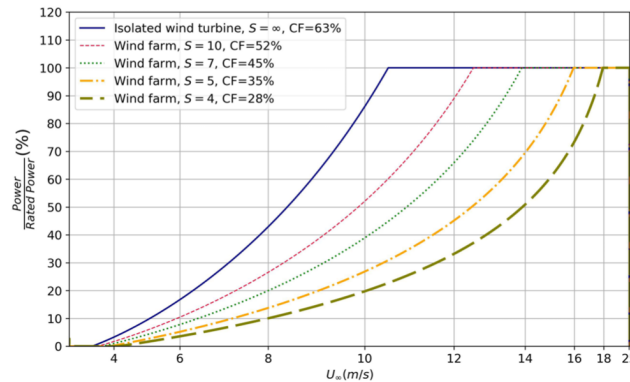


Figure 2.6: Low wind speeds incurred losses [1].

During times of low wind speed, wind farms can provide a lower amount of power to the grid. Since the demand for electricity remains constant, a lower supply results in an increase in the price of energy. This means that losses at low wind are even more detrimental to the economic feasibility of wind energy, as you cannot provide energy when its price is highest, which is the case for current wind turbine designs. This increased volatility in energy production brings additional technical challenges and costs. TenneT, the main Dutch grid operator, predicts that the Netherlands will need around 9 [GW] of large-scale battery capacity by 2030 to maintain grid stability⁵, up from the 200 [MW] of available storage at the end of 2023⁶. This significant increase is mainly due to the greater volatility of renewable energy sources compared to more stable options like nuclear power. The cost of this extra storage is also high and varies by the type of storage used. For instance, pumped hydropower costs about \$60/kWh, whereas lithium-ion batteries currently cost around \$300/kWh⁷; although this number is expected to decrease considerably in the following years due to rapid advancements in this field. However, the flat landscape of the Netherlands naturally limits the feasibility of large-scale hydropower storage, leaving the more expensive lithium-ion battery solution as one of the main options. Therefore, it is crucial to reduce the variability of power generation in future wind energy designs, a feature ReWind aims to address.

After this extensive analysis, the market gap for the ReWind project can be identified. ReWind aims to create a large-scale, high-power offshore wind farm with a high Wind Farm Capacity Factor to help meet the Dutch energy transition goals.

2.3.2. SWOT analysis

The ReWind concept has been designed to address the market gap identified in subsection 2.3.1. To evaluate this project, a Strengths, Weaknesses, Opportunities and Threats (SWOT) analysis can be conducted, examining the strengths, weaknesses, opportunities, and threats based on current market conditions and gaps.

Strengths

- **High Power density:** The implementation of the Active Flow Control (AFC) system guarantees higher wind speeds for downwind turbines, meaning a higher power density can be achieved without compromising the wind farm capacity factor.
- **Cost efficiency:** The improved efficiency of the wind farm, particularly noticeable at low wind speeds, improves cost efficiency. This will lead to a lower Levelized Cost of Energy (LCoE) for the proposed

⁵https://tennet-drupal.s3.eu-central-1.amazonaws.com/default/2023-06/TenneT_s_position_large_BESS_-_Public_Info_-_update.pdf [Accessed 07-06-2024]

⁶<https://green-giraffe.com/publication/blog-post/whats-in-store-for-dutch-batteries/> [Accessed 07-06-2024]

⁷<https://energypost.eu/batteries-made-of-super-hot-sand-for-long-duration-grid-storage-at-4-to-10-per-kwh/> [Accessed 07-06-2024]

ReWind design.

- **Manufacturability:** The ReWind design employs a multi-rotor concept, capturing significant energy with a large swept area while maintaining a small blade radius. A larger blade radius would result in a more complex and heavier structure, complicating manufacturing. The large number of rotors also allows standardization options in the production of the blades.
- **Material Efficiency:** The multi-rotor concept allows for more efficient use of materials. Smaller generators are simpler and require less material to be made. Additionally, smaller blades are less complex and use materials more efficiently.
- **Environmental Benefits:** The ReWind concept's higher power density means less maritime area is disturbed while still producing more energy than currently operational wind farms.

Weaknesses

- **High Capital cost:** A 30 [MW] wind turbine is a very large and expensive structure. The substantial capital investment required may limit the pool of potential customers who have the necessary resources to purchase a ReWind turbine.
- **Infrastructure needs:** The large scale of the wind farm necessitates complex supporting infrastructure. Additionally, the capacity of the cabling required to transport the generated energy to the grid is significant, further increasing infrastructure demands.

Opportunities

- **Market Growth:** The market for offshore wind energy is rapidly expanding. With its exceptional efficiency, the ReWind concept has the potential to become the preferred choice for consumers seeking high-energy production.
- **Technological Leadership:** By swiftly advancing the development of the ReWind concept, it could set a new industry standard and secure a significant market share.
- **Sustainability goals:** The Dutch government's wind energy goals are unattainable with current wind turbine designs. A revolutionary new design, such as the ReWind concept, could address these challenges and meet the ambitious sustainability targets.
- **New emerging markets:** Many countries beyond the Netherlands face limited maritime space for wind farms. The ReWind concept, which allows for high energy-density farms, could provide an ideal solution for these markets.

Threats

- **Competitive technologies:** The energy supply market, particularly offshore wind energy, is highly competitive and dominated by a few large turbine manufacturers, as discussed in chapter 2. Entering this market may be challenging. Additionally, significant technological advancements in alternative energy sources such as solar, nuclear, or geothermal energy could potentially diminish the appeal of wind energy solutions.
- **Regulatory changes:** While unlikely, potential regulatory changes could favour other renewable energy sources over offshore wind energy, leading to reduced attention and public funding for wind energy projects. However, the trend over the past decade has shown a strong promotion of offshore wind energy.

2.4. Stakeholder identification

This final section contains an interest-influence graph/stakeholder map, presented in Figure 2.7. Here, the different stakeholders of the project are identified and classified according to their predicted interest and influence on the design of this wind turbine.

The key stakeholders are identified based on their potential influence on the project. All stakeholders who can significantly delay or hinder this project's development are labelled "key" stakeholders. In effect, it can be seen, from Figure 2.7 that the customer and the Dutch energy companies are identified as the most important stakeholders due to their close relation to the outcome of this project. Furthermore, the Ministry of Economic Affairs and Climate Policy (EZK), the investors and the suppliers/contractors are also predicted to have a lot of power on this project as their decisions can highly influence its outcome. Key stakeholders will naturally be given a lot more attention during the design process.

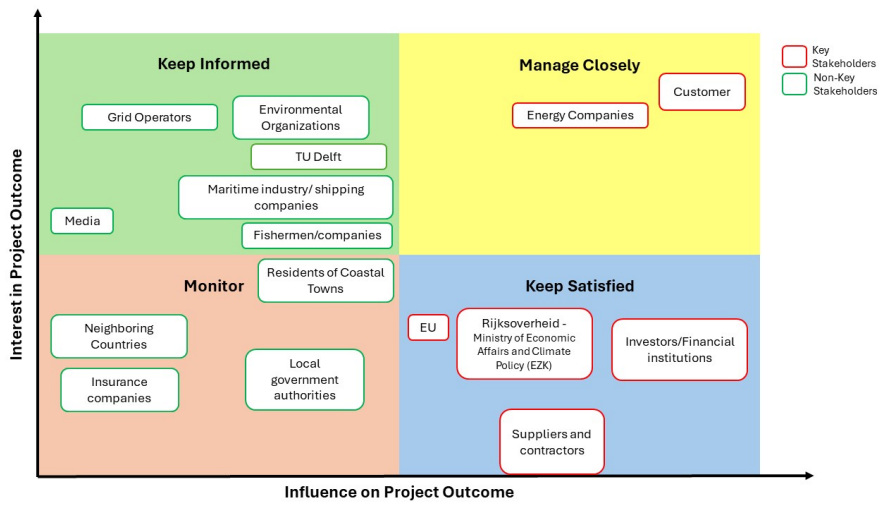


Figure 2.7: Interest-influence graph of different stakeholders of the project

3. Functional Analysis

A functional analysis is performed to better understand how systems function, their flow, and interactions. It consists of two main parts. The functional flow diagram shows how systems work together, illustrating their flow and interactions. Meanwhile, the functional breakdown structure organizes the functions of each system individually.

3.1. Functional Flow

The Functional Flow Diagram (FFD) provides a representation of the sequential flow of processes, interactions and inter-dependencies within the system. It illustrates how various actions and functions interact with each other to achieve specific objectives. By mapping out these flows, the diagram offers insights into the overall functionality and structure of the system. The FFD can be seen in Figure 3.1. The functions are divided into design, manufacturing, operations and End Of Life (EOL). From this set of functions, the most critical is operation; which includes start-up, data collection, power generation, shutdown procedure, sending power to grid and maintenance. Indeed, operations are specified the deepest, as it is the most crucial phase of ReWind's project. The wind farm should be designed to perform a series of functions; such as being able to yaw, extract wind energy and transform it into electricity, actively control the flow, provide power to turbine electronics, and transform the electricity to the grid standards. As a result, different subsystems must be developed to address these functions, with each function specified within its respective cell. The functions within operations are not directly connected to the EOL, as they will be repeated continuously until the end of the farm's operational life.

3.2. Functional Breakdown

The Functional Breakdown Structure (FBS) provides a hierarchical representation of the system's functions, organizing them into manageable and logically structured components. It serves as a useful tool to identify dependencies and ensure the complete coverage of system functionalities. This breakdown is shown in Figure 3.2. Note that the functions in the design function are high level, the reader is invited to review the work breakdown to get more detailed insights into this stage of the mission. The breakdown further specifies the functions, especially, the types of Non-destructive testing to be performed, and the different sub-assemblies to be manufactured.

3.3. Diagrams

The aforementioned diagrams are presented below:

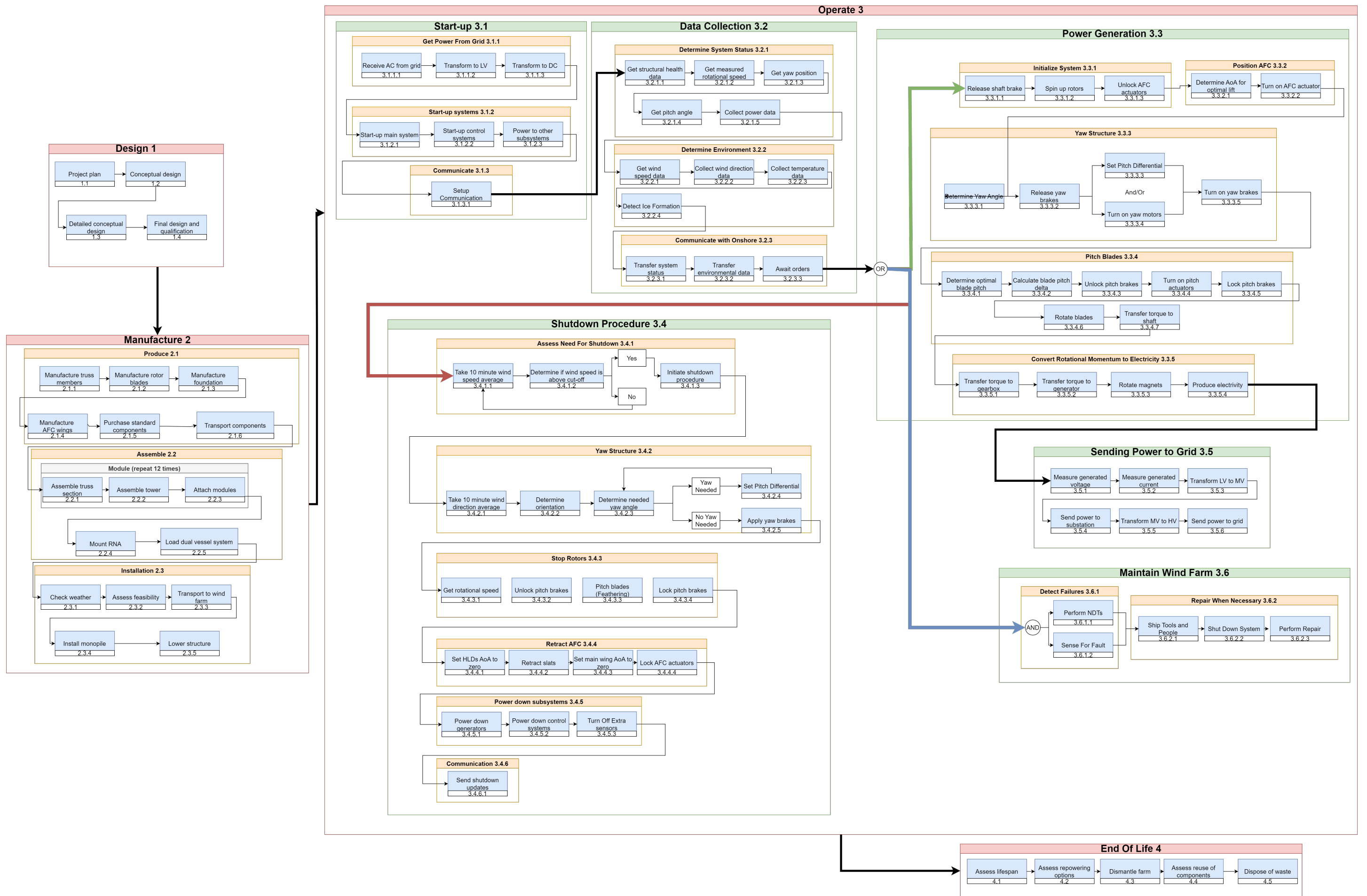


Figure 3.1: Functional Flow Diagram

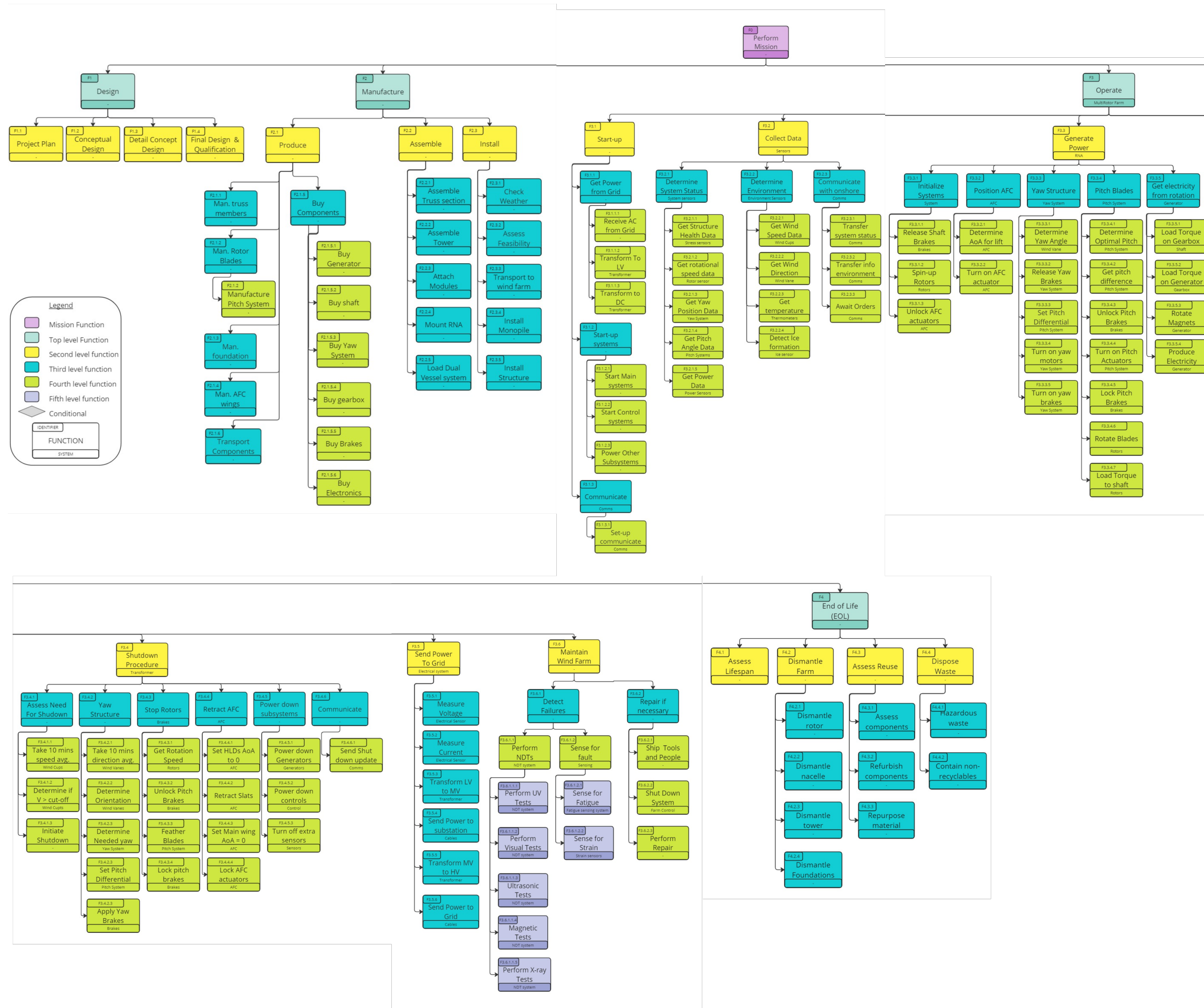


Figure 3.2: Functional Breakdown Structure.

4. Site Measurements

In this chapter, the exact location of the wind farm will be identified. Selecting this site will enable the collection of wind and wave measurement data, as well as the ocean depth for which the turbines have to be designed for. This data will provide a representative example of the wind conditions that can be expected in Dutch North Sea territorial waters, facilitating more detailed sizing and design of the rest of the project.

4.1. Farm Location

As per REQ-STK-CUS-01, the wind farm needs to have a rated power of at least 6 [GW], while REQ-STK-CUS-02 specifies a rated power density of at least 10 [MW/km²]. These two numbers lead to a size of about 600 [km²] required to construct the wind farm. Through the overview of wind farm locations available on the website 4C Offshore¹, only the Lagelander wind farm development zone shows a size close to or larger than 600 [km²]. The Lagelander development zone is located in Dutch territorial waters (REQ-STK-CUS-05), approximately between 33 and 75 km off the coast of the Dutch coast, close to the island of Texel². The location can also be seen in Figure 4.1 highlighted in orange.



Figure 4.1: Lagelander wind energy area

4.2. Wind Data

The wind data for the Lagelander wind Farm site has been obtained from the ERA5 Database³. ERA5 is a database created by the European Centre for Medium-Range Weather Forecasts (ECMWF). The ECMWF is an organization known for medium-range weather forecasts, providing accurate and reliable weather predictions. ERA5 combines computer model data with observations from around the world to create a consistent and complete dataset, using methods similar to those used in weather forecasting.

For the ReWind project, which is still in the conceptual design phase, the accuracy provided by ERA5 is sufficient. This design is required to work in the entire Dutch North Sea territorial waters, and ERA5's detailed and consistent data gives the necessary information about the wind and wave conditions in this area to support this early-stage design. Naturally during further design phases, long term on-site measurements will need to be carried out, this will be discussed further in chapter 17.

The wind speed data was collected for a height of 10 meters above sea level, for the year 2023. Naturally, the wind speeds at a height of 10 [m] differ from those at higher altitudes [10]. Therefore, the velocity of the wind at a given altitude, h , can be calculated based on the wind velocity at 10 [m], v_{10} , using the wind profile power law [11], as seen in Equation 4.1:

$$v(h) = v_{10} \cdot \left(\frac{h}{h_{10}} \right)^a. \quad (4.1)$$

A Hellman coefficient, a , of 0.06 is used, which corresponds to unstable atmospheric conditions above an open water surface [11]. These unstable conditions are characteristic of the North Sea [12], where the wind farm is intended to be built. Consequently, the average wind speeds at heights between 0 and 400 [m] can be calculated, as illustrated in Figure 4.2a. This range of heights has been considered as it covers the entire height of the turbine.

Furthermore, the wind speeds recorded throughout the year, have been extrapolated to a height of 150 [m], since this is the expected average hub height. To enhance readability, only the daily, monthly, and yearly averages are presented in Figure 4.2b. The yearly average wind speed at 150 [m] altitude is found to be 9.25 [m/s]. However, the data reveals a clear seasonal pattern: wind speeds are higher during the winter months and slightly lower in the summer. This variation is due to several factors. For instance, during winter increased

¹<https://map.4coffshore.com/offshorewind/> [Accessed 30-05-2024]

²<https://windopzee.nl/imagemaps/kaart-waar-wanneer/lagelander/> [Accessed 30-05-2024]

³<https://cds.climate.copernicus.eu/cdsapp#!/dataset/reanalysis-era5-single-levels?tab=overview> [Accessed 30-05-2024]

storm activity and cold air moving over warm water create unstable conditions. These conditions lead to greater air mixing, resulting in higher wind speeds [13].

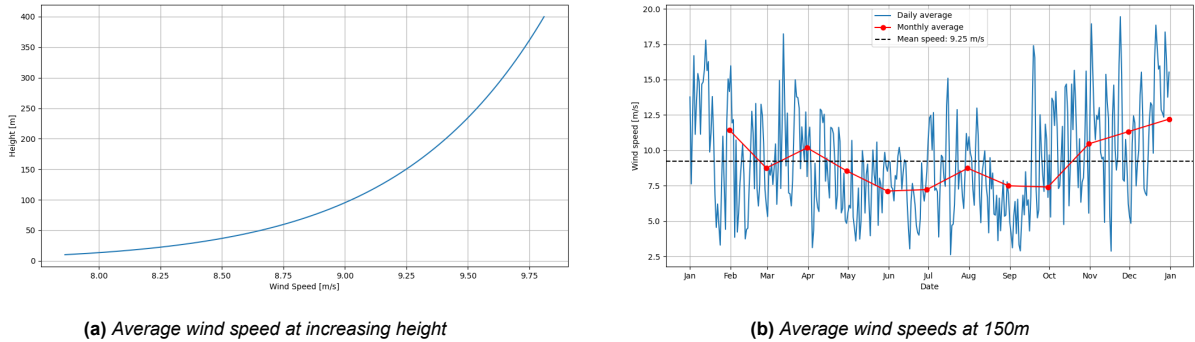


Figure 4.2: Average Wind Speeds in 2023

To decide the optimal direction for building the wind farm, it is important to know the prevailing wind direction. A wind frequency rose, depicting the wind’s origin, is shown in Figure 4.3. In this plot, 0 degrees corresponds to the northern direction. Figure 4.3 clearly indicates that the dominant incoming wind direction is from the southwest. Different angles of the wind as a function of height have been neglected due to the Coriolis force at this stage of the design. It has been assumed that the wind direction remains constant for each height.

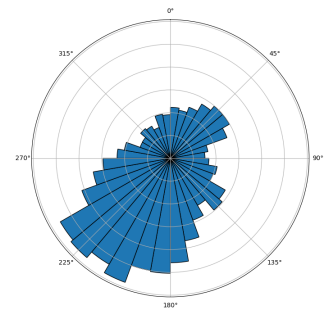


Figure 4.3: Wind speed direction

4.3. Wave Data

The wave data for the Lagelander wind farm site has also been sourced from the ERA5 database, similarly to the data collected in section 4.2. This data is important for the design and sizing on the monopile. The ERA5 data includes the mean wave period, the combined height of wind waves and swell, and the Stokes drift velocity. However, to maintain conciseness, not all data is displayed in this section.

The Stokes drift velocity is the average velocity of a particle, as it moves along with the fluid, in this case the seawater. The Stokes drift can be used to determine the wavelength through means of Equation 4.2. In this equation, T is the wave period, λ is the wavelength, \bar{u}_S is the Stokes drift velocity, a is the amplitude and z is the vertical coordinate, in this case set to 0, as only the particles at the surface are of interest.

$$\bar{u}_S \approx \omega k a^2 e^{2kz} = \frac{4\pi^2 a^2}{\lambda T} e^{4\pi z/\lambda}. \tag{4.2}$$

In Figure 4.4, the daily, monthly and yearly mean wave height is displayed throughout the year. This data is needed for the sizing of the monopile, as will be detailed in subsection 5.4.7. Much the same as in Figure 4.2b, the wave height is larger during the winter period of the year.

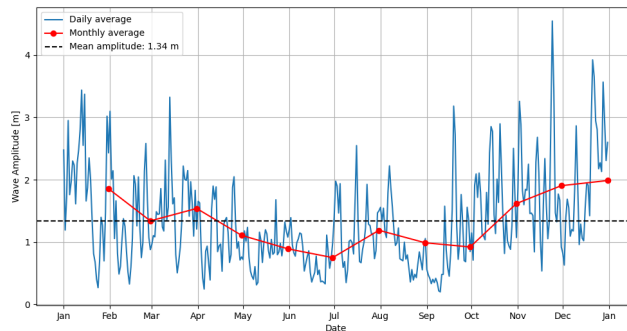


Figure 4.4: Wave amplitude

4.4. Water Depth

In order to size the dimensions of the monopile of the wind turbine, it is necessary to know the depth of the water at the location where the wind farm will be built. Figure 4.5 shows the water depth of the North Sea in Dutch territorial waters [14]. The proposed farm location is shown by the red outline. The legend shows that at this location, the water depth ranges from 10-20 [m]. Therefore, to ensure that every wind turbine can be installed in this area, a conservative assumption will be made, where a water depth of 20 [m] will be considered for the design of the wind turbine. This is the worst case scenario and will ensure that even if the water depth is smaller, the turbine can still withstand the relevant loading.

4.5. Layout of Wind Farm

After having selected the desired site for the wind farm, an optimisation strategy is applied in order to ensure the required wind farm energy density of at least 10 [MW/km²] is achieved (REQ-STK-CUS-02). Considering the selected site, Lagelander constitutes a total area of 850.28 [km²]. Thus, filling this area with turbines with a rated power of 30 [MW], a total of 288 turbines are necessary to attain the aforementioned requirement. Thus, an optimization is performed to achieve the minimum distance between turbines in order to fit 288 in the designated site.

Furthermore, as seen under section 4.2 the dominant wind direction is predicted to be from the southwest. Thus, the lower-left vertex of the parallelogram delineated by the site will be taken as the reference point where the best wind conditions are expected and thus where the turbines will be placed from. Furthermore, according to Yong et. al. placing the different wind turbines in a parallelogram shape proves to achieve the best performance when compared to other optimisation strategies [15].

Finally, by applying the method provided by Yong et. al., and the measured wind data, a layout is plotted for the wind farm as presented under Figure 4.6. Each red dot signifies a turbine, while the purple area depicts the Lagelander area. This is achieved by applying a distance between turbines of 1.9 [km] with 288 turbines being plotted, attaining an energy density of 10.36 [MW/km²], meeting REQ-STK-CUS-02.

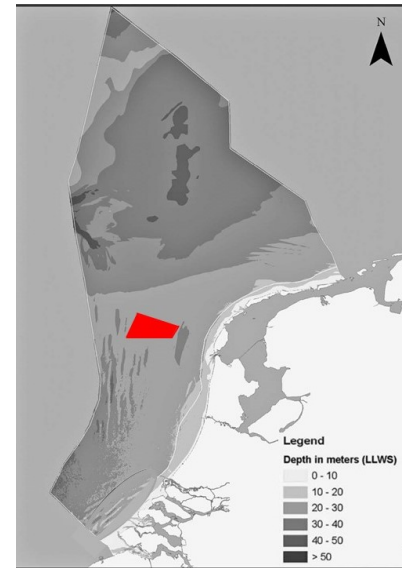


Figure 4.5: Water depth in Dutch territorial waters [14]

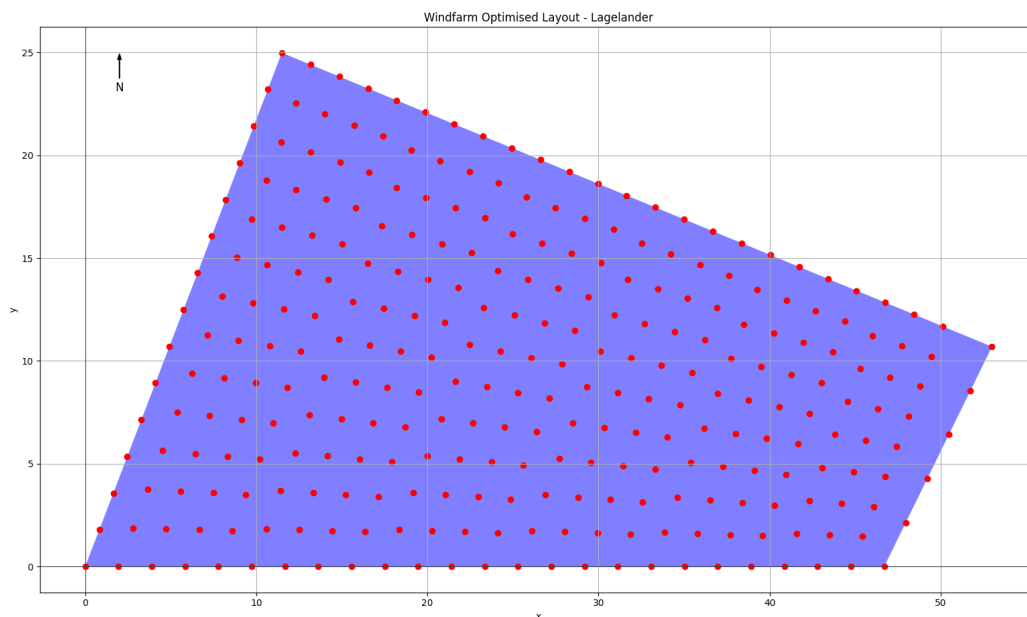


Figure 4.6: Optimised layout of the wind farm at the Lagelander site.

5. Detailed design

The design of the ReWind turbine will be elaborated upon in this chapter. First, the design of the rotor will be explained in section 5.1. Following, the Active Flow Control will be sized in section 5.2. With the rotors and AFC sized, the Annual Energy Production can be estimated in section 5.3. Using the loads of the rotors and AFC, the structure will be designed in section 5.4. Knowing the dimensions and inertia of the structure, the yaw and pitch control can be designed in section 5.5. Finally, the drivetrain will be sized in section 5.6.

5.1. Rotor Design

This section will cover the design of ReWind’s rotor subsystem. First, the number of rotors will be determined based on both aerodynamic performance and structural considerations. This number will then facilitate the determination of an initial rotor diameter and the corresponding rated wind speed. Finally, by selecting appropriate airfoils and using a Blade Element Momentum model, the blade geometry will be optimized.

5.1.1. Number of Rotors

As detailed in the midterm report [16], the number of rotors was determined to be approximately 33. As illustrated in Figure 5.1, the rotor radius decreases with the square root of the number of rotors. This relationship indicates that there is an optimal number of rotors, beyond which the challenges of manufacturing and maintenance outweigh the benefits of further reducing the rotor radius.

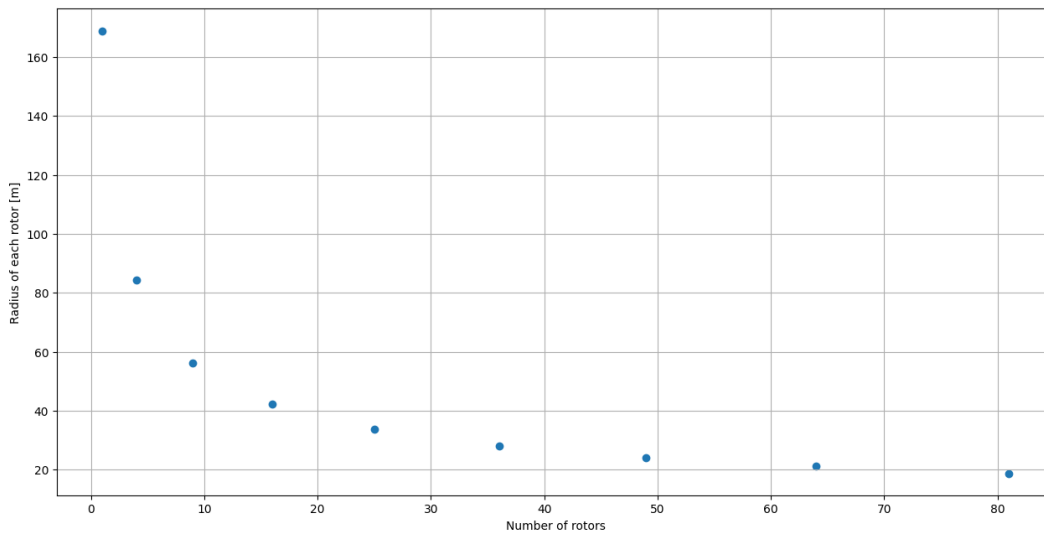


Figure 5.1: Individual rotor radius with number of rotors

However, the exact number of rotors is closely tied to the design of the supporting structure. The rotors are installed using a honeycomb structure, which significantly reduces the area required for rotor placement [17]. Ultimately, 34 rotors were chosen, enabling a honeycomb configuration with 17 rotors on each side of the central structure, as illustrated in Figure 15.1. The decisions regarding the supporting structure itself will be detailed in section 5.4.

5.1.2. Rotor Dimension

The sizing of the rotors is of great importance, as it directly impacts the efficiency of the turbine and, by extension, the wind farm. Choosing a rotor radius that is too large would result in excessive weight and very high loads at high wind speeds, while a rotor that is too small would perform poorly at low wind speeds. Therefore, an initial estimation is obtained using the International Energy Agency (IEA) 15 MW reference wind turbine.

The IEA reference wind turbine [18] is a conceptual 15 MW turbine designed through a collaboration among multiple partners, including the National Renewable Energy Laboratory (NREL) and the Technical University of Denmark (DTU).

To size the rotors, the swept area of the combination of the 34 wind turbines is set equal to the swept area of the IEA wind turbine, ensuring the same power density (W/m^2). This approach ensures that the design will perform well and be versatile enough to be deployed in other locations in the North Sea.

With a blade radius of 120 m, the IEA turbine has a swept area of 45238.9 m². For 34 rotors, this would imply a radius of 29.1 m.

The rated wind speed was assumed to be the same as in the IEA reference turbine analysis, 10.59 [m/s].

5.1.3. Airfoil Selection

The airfoils of wind turbines are specifically designed to have a high value of $\frac{C_l}{C_d}$ at an angle below $C_{l_{max}}$. The airfoil at the root section of the blades should have a large thickness, due to structural demands, which decreases for the mid section and tip section [19]. Specifically for Wind Turbines, the U.S. National Renewable Energy Laboratory designed airfoils for different rated powers. For large wind turbines, around the order of 1 MW, which is close to ReWind's rated power per rotor, the airfoils S818, S816 and S817 are used [20]. This paper also specified the blade section that should contain each airfoil, and the design Reynolds number. However, the Reynolds number was re-estimated with an assumed chord of 2 m, and a tangential speed of 80m/s (Tip Speed Ratio (TSR) is 8, and an approximate wind speed of 10 m/s). That way, the C_l - C_d polars of the root section, mid section and tip section were obtained using the method described in subsection 5.2.2.

5.1.4. Blade Element Momentum model

Now that the rotors have been sized and given cross-sections, a Blade Element Momentum (BEM) model will be used to optimize their size and geometry.

The Blade Element Momentum (BEM) theory is a fundamental approach used to predict the performance of wind turbines and propellers. It combines the momentum theory and blade element theory to model the forces acting on each segment of a rotor blade. This model was used to iterate between the momentum theory and blade element forces to converge to an induction factor, which then gives the Thrust Coefficient and Power coefficient of the rotors. [21]

This BEM model takes as inputs the free stream velocity of the wind, the rotational speed of the rotors, the radius of the rotors, the chord and twist distribution and the airfoils of every section of the blades. Then, each blade is divided longitudinally into small elements. Each element has a specific chord length and twist angle. For every blade element, the iteration begins by assuming initial axial and tangential induction factors, a and a' , which determine the tangential and axial speed at the rotors, as seen in Equation 5.1 and Equation 5.2.

$$V_{axial} = U_{inf} * (1 - a) \quad (5.1)$$

$$V_{tangential} = \omega * R * (1 + a') \quad (5.2)$$

These induction factors are a measure on the effect of the rotor on the wind velocity.

With the information given so far, for every blade element, the Lift and Drag can be calculated, which then are translated into an axial and a tangential force. Then, from the axial force, the Thrust coefficient produced by a single blade element:

$$CT = \frac{F_{axial}}{1/2 \cdot \rho \cdot U_{\infty}^2 \cdot Area} \quad (5.3)$$

The *Area* is the area of the streamtube, which is the area that the blade element sweeps in one revolution.

From this CT, according to momentum conservation laws, the induction factor a can be calculated as in Equation 5.4. However, it is necessary to apply the glauert's correction for induction factors larger than 0.326, where Equation 5.5 applies [19].

$$CT = 4a \cdot (1 - a) \quad (5.4)$$

$$CT = 1.816 - 4(\sqrt{1.816 - 1}) \cdot (1 - a) \quad (5.5)$$

The tangential induction is also calculated as in Equation 5.6, which will increase the tangential velocities at the blades.

$$a' = \frac{F_{tan} \cdot NBlades}{2 \cdot \pi \cdot U_{inf} \cdot (1 - a) \cdot \omega \cdot 2(r_R \cdot Radius)^2} \quad (5.6)$$

Here, r_R is the normalized radius of the centroid of the blade element analysed in the current iteration.

With the new axial and tangential inductions, the new velocities are calculated, and the described iteration is repeated until converged to a final induction and forces on that blade element. This is repeated for every blade element, to get a distribution of the axial and tangential forces throughout the blades.

The final CT is given by the sum of the CT for each blade element, given by Equation 5.3, multiplying F_{axial} by the number of blades, and the Area is now the total swept area of the rotor. To calculate the final CP, Equation 5.7 is used:

$$CP = \sum_{i=1}^n \frac{F_{tan} * V_{tan,i}}{1/2 \cdot U_{\infty}^3 * Area}, \quad (5.7)$$

where $Area$ is the total swept area of the rotor.

A correction that was applied to this BEM model, was the Prandtl tip-root correction [19]. This correction is applied because tip vortices at the blades create an asymptotic induction field, for which the balance of momentum approach is no longer valid. Thus the correction is applied as shown in Equation 5.8, Equation 5.9, Equation 5.10 and Equation 5.11 are used.

$$f_{tip(\mu)} = \frac{2}{\pi} \arccos \left(e^{\left(-\frac{B}{2} \left(\frac{1-\mu}{\mu} \right) \sqrt{1 + \frac{\lambda^2 \mu^2}{(1-a)^2}} \right)} \right) \quad (5.8)$$

$$f_{root(\mu)} = \frac{2}{\pi} \arccos \left(e^{\left(-\frac{B}{2} \left(\frac{\mu - \mu_{root}}{\mu} \right) \sqrt{1 + \frac{\lambda^2 \mu^2}{(1-a)^2}} \right)} \right) \quad (5.9)$$

where μ_{root} is the location of the root vortex, and μ_{tip} for the tip.

$$f_{total(\mu)} = f_{tip(\mu)} * f_{root(\mu)} \quad (5.10)$$

and then the induction is corrected by:

$$a = \frac{a}{f_{total}} \quad (5.11)$$

5.1.5. Blade Geometry Optimization

Now that a model has been created to estimate CP and CT based on blade geometry, the latter can be optimized to obtain maximum power generated.

For starters, the radius of the rotor can be re-calculated based on the actual CP value, obtained from the BEM model. This radius is re-inputed in the BEM to re-calculate CP. This process is an iteration that converges into a final radius and CP value. The radius was then 28.93, with a CP of 0.49, slightly higher than the 15 MW reference turbine at 0.489.

Then, the chord and twist distribution can also be optimized. Indeed, as mentioned in subsection 5.1.4, the blade geometry, which includes the chord and twist of each element determines the Lift and Drag in each element, which affect CP and CT. This means that there can be an optimal chord and twist distribution that will get the highest CP. The optimal root and tip chord were determined, as well as the root and tip twist distribution. The geometry of the blade and their properties are presented in Table 5.1.

Table 5.1: Rotor Geometry

Description	Value	Units
Rotor radius	28.93	m
Max chord	3.3	m
Tip chord	1.6	m
Root twist	-9.9	deg
Tip twist	-3.22	deg
TSR	8	-
Rated Wind Speed	10.59	m/s
Rotational Speed	28	rpm
Mechanical Power Coefficient CP	0.49	-
Thrust Coefficient CT	0.82	-
Number of Rotors	34	-
Rated Power per Rotor	882	kW

5.2. Active Flow Control design

The wake of the rotors will be re-energized using the Active Flow Control (AFC) system to facilitate higher energy density. The trade-off performed in the Baseline report shows that the AFC subsystem consists of multiple retractable multi-element wings. This design allows for high performance during normal operating conditions but can limit the loads on the structure during a storm. This section will detail the sizing of the AFC in subsection 5.2.1, specific airfoil selection in subsection 5.2.2 and concludes with a summary of all the important parameters of the final AFC design in subsection 5.2.3

5.2.1. AFC Sizing

From [22], it has been shown that introducing large-scale vortical structures in the wake of the turbine can effectively entrain high momentum flow from the upper layers of the atmospheric boundary layer and re-energize the wake of the turbine, leading to overall significant increases in wind farm efficiency. To achieve these large-scale vertical structures, circulation needs to be produced by creating "lift" in the downward direction. This is the main purpose of the multi-element wings that form the AFC.

In order to get an understanding of the sizing of the wings to recover and re-energize the wake of the turbine effectively, the total lift that needs to be produced by the AFC needs to be estimated. Studies show that for effective entrainment of high momentum flow, the required lift can be related to the thrust by the relation in Equation 5.12.

$$L = 1.3 \cdot T \quad (5.12)$$

From this relation, the necessary lift produced by the AFC follows. The system, operating at full power, will have a thrust of 5 MN. Hence, the AFC will be designed to produce 6.5 MN of lift.

Given that this is a significant amount of lift to produce for a single wing and the fact that the wake recovery improves significantly when increasing the number of wings to at least two [23], supports the choice of using multiple wings for the AFC.

To improve simplicity and keep the manufacturing costs low, it was decided that all wings should have the same lift coefficient in isolation. Using this fact, Equation 5.13 can be derived in order to estimate the appropriate lift coefficient (C_L) for each wing.

$$C_l = \frac{2.6T}{\rho bcnV^2} \quad (5.13)$$

Where b is the span of the wing, c is the cord, n is the number of wings, and V is the incoming velocity of the flow. Equation 5.13 is over-simplified and makes use of several assumptions. Namely, it assumes that the incoming flow has the same velocity for each wing and the wings produce the same amount of lift in isolation as they produce when placed together. This is not representative of reality, since there will be a difference in incoming flow velocity due to changes in altitude. Furthermore, placing the wings too close to each other will have a negative impact on the lift produced per wing due to interference effects.

To account for this, there will be an interference factor, f , included, as well as a different velocity and span for each wing. The lift coefficient can now be calculated with Equation 5.14.

$$C_l = \frac{2.6T}{\rho c \sum_{i=1}^n b_i f_i V_i^2} \quad (5.14)$$

Where b_i is the span of wing i , f_i is the interference factor of wing i , and V_i is the velocity at wing i . The determination of the velocities and interference factors will be explained in Equation 5.2.1 and Figure 5.2.1, respectively.

Velocity Profile

Due to the large height of the turbine, the velocity experienced by the AFC will change according to its placement. To account for the varying velocity profile over the system, the wind velocity power law is used [11], as presented in Equation 4.1. Furthermore, accounting for the induction factor behind the rotor of 0.71, where an extra margin of 0.02 is used to encapsulate the effect of the interference of the truss structure, resulting in a total induction factor of 0.69. Calculating the velocity change over the height of the system with and without the induction factor results in Figure 5.2.

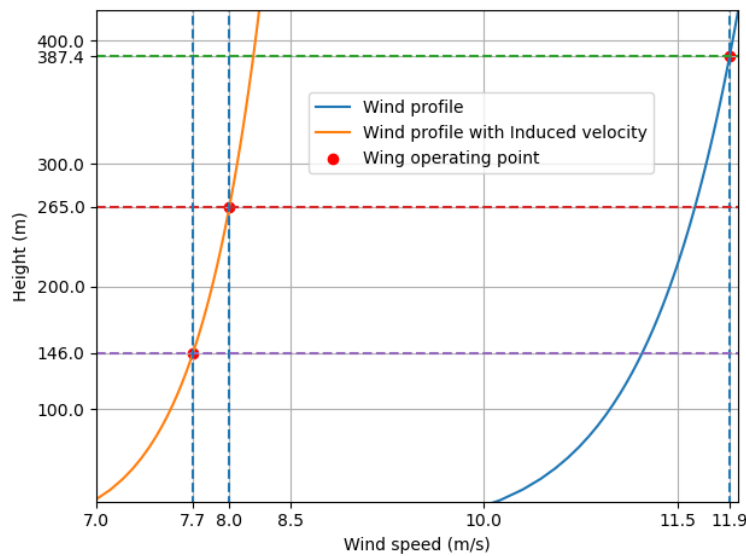


Figure 5.2: Wind profiles with and without induced velocity.

In this case, the assumption is made that the bottom rotor is operating at rated velocity, and therefore, the turbine is producing maximum thrust. This is a worst-case assumption, requiring the AFC to produce the maximum amount of lift, therefore ensuring that under these circumstances, the AFC meets the required performance.

From Figure 5.2, the experienced velocity of each wing of the AFC can be determined. A discretionary number of 3 wings was chosen, this is not expected to be the optimal number of wings, but will have sufficient performance in the current stage. Now, using the current choice of using three wings, one placed on top of the structure and two behind it, at an arbitrary height, results in the following incoming flow velocity per wing. Since the top wing is not placed behind the rotors, it encounters a higher incoming flow velocity of 11.9 [m/s]. For the two wings below it, which are placed behind the rotors, the induction factor needs to be taken into account, resulting in a middle wing and bottom wing velocity of 8.0 [m/s] and 7.7 [m/s], respectively. These velocities allow for a more accurate calculation of the total lift produced by the AFC.

Wing Interactions

Furthermore, two main interactions must be accounted for when estimating the lift produced by the AFC: the effect of stacking the wings on top of each other and the effect of the sea level on the wings or the "ground effect".

The effect of wings interacting with each other can be estimated using thin airfoil theory. To take care of the effect, the wings are modelled using a circulation, Γ , at the quarter cord. Then, a no penetration condition is applied at the three-quarters cord point. Doing this for all wings Equation 5.15 can be derived.

$$\begin{bmatrix} \frac{c}{4\pi\|r_{1,1}\|^2} & \frac{c}{4\pi\|r_{1,2}\|^2} & \cdots & \frac{c}{4\pi\|r_{1,n}\|^2} \\ \frac{c}{4\pi\|r_{2,1}\|^2} & \frac{c}{4\pi\|r_{2,2}\|^2} & \cdots & \frac{c}{4\pi\|r_{2,n}\|^2} \\ \vdots & \vdots & \ddots & \vdots \\ \frac{c}{4\pi\|r_{n,1}\|^2} & \frac{c}{4\pi\|r_{n,2}\|^2} & \cdots & \frac{c}{4\pi\|r_{n,n}\|^2} \end{bmatrix} \begin{bmatrix} \Gamma_1 \\ \Gamma_2 \\ \vdots \\ \Gamma_n \end{bmatrix} = \alpha \begin{bmatrix} V_1 \\ V_2 \\ \vdots \\ V_n \end{bmatrix} \quad (5.15)$$

Where $r_{i,j}$ is the vector from the quarter cord point of wing i to the three-quarters cord point of wing j .

Another effect to take into account is the ground effect. This is modelled by mirroring the points of circulation around the plane of the sea level and setting their strength to the opposite of their corresponding vortex above. Including this effect, Equation 5.15 can be expanded into Equation 5.16.

$$\begin{bmatrix} \frac{c}{4\pi\|r_{1,1}\|^2} - \frac{c}{4\pi\|r_{1,2n}\|^2} & \frac{c}{4\pi\|r_{1,2}\|^2} - \frac{c}{4\pi\|r_{1,2n-1}\|^2} & \cdots & \frac{c}{4\pi\|r_{1,n}\|^2} - \frac{c}{4\pi\|r_{1,n+1}\|^2} \\ \frac{c}{4\pi\|r_{2,1}\|^2} - \frac{c}{4\pi\|r_{2,2n}\|^2} & \frac{c}{4\pi\|r_{2,2}\|^2} - \frac{c}{4\pi\|r_{2,2n-1}\|^2} & \cdots & \frac{c}{4\pi\|r_{2,n}\|^2} - \frac{c}{4\pi\|r_{2,n+1}\|^2} \\ \vdots & \vdots & \ddots & \vdots \\ \frac{c}{4\pi\|r_{n,1}\|^2} - \frac{c}{4\pi\|r_{n,2n}\|^2} & \frac{c}{4\pi\|r_{n,2}\|^2} - \frac{c}{4\pi\|r_{n,2n-1}\|^2} & \cdots & \frac{c}{4\pi\|r_{n,n}\|^2} - \frac{c}{4\pi\|r_{n,n+1}\|^2} \end{bmatrix} \begin{bmatrix} \Gamma_1 \\ \Gamma_2 \\ \vdots \\ \Gamma_n \end{bmatrix} = \alpha \begin{bmatrix} V_1 \\ V_2 \\ \vdots \\ V_n \end{bmatrix} \quad (5.16)$$

Note that the wings must be sorted in descending order of height.

From this, the C_l of the wings can be calculated using the Kutta-Joukowski theorem as shown in Equation 5.17 [24].

$$L' = \rho_\infty V_\infty \Gamma \quad (5.17)$$

Using the equation above, Equation 5.18 can be derived.

$$\begin{bmatrix} C_{l1} \\ C_{l2} \\ \vdots \\ C_{ln} \end{bmatrix} = \frac{2\alpha}{c} \begin{bmatrix} \frac{c}{4\pi\|r_{1,1}\|^2} - \frac{c}{4\pi\|r_{1,2n}\|^2} & \frac{c}{4\pi\|r_{1,2}\|^2} - \frac{c}{4\pi\|r_{1,2n-1}\|^2} & \cdots & \frac{c}{4\pi\|r_{1,n}\|^2} - \frac{c}{4\pi\|r_{1,n+1}\|^2} \\ \frac{c}{4\pi\|r_{2,1}\|^2} - \frac{c}{4\pi\|r_{2,2n}\|^2} & \frac{c}{4\pi\|r_{2,2}\|^2} - \frac{c}{4\pi\|r_{2,2n-1}\|^2} & \cdots & \frac{c}{4\pi\|r_{2,n}\|^2} - \frac{c}{4\pi\|r_{2,n+1}\|^2} \\ \vdots & \vdots & \ddots & \vdots \\ \frac{c}{4\pi\|r_{n,1}\|^2} - \frac{c}{4\pi\|r_{n,2n}\|^2} & \frac{c}{4\pi\|r_{n,2}\|^2} - \frac{c}{4\pi\|r_{n,2n-1}\|^2} & \cdots & \frac{c}{4\pi\|r_{n,n}\|^2} - \frac{c}{4\pi\|r_{n,n+1}\|^2} \end{bmatrix}^{-1} \vec{1} \quad (5.18)$$

Comparing this to regular thin airfoils, which have a C_l of $2\pi\alpha$ [24], a correction factor f can be identified Equation 5.19.

$$\begin{bmatrix} f_1 \\ f_2 \\ \vdots \\ f_n \end{bmatrix} = \frac{1}{\pi c} \begin{bmatrix} \frac{c}{4\pi\|r_{1,1}\|^2} - \frac{c}{4\pi\|r_{1,2n}\|^2} & \frac{c}{4\pi\|r_{1,2}\|^2} - \frac{c}{4\pi\|r_{1,2n-1}\|^2} & \cdots & \frac{c}{4\pi\|r_{1,n}\|^2} - \frac{c}{4\pi\|r_{1,n+1}\|^2} \\ \frac{c}{4\pi\|r_{2,1}\|^2} - \frac{c}{4\pi\|r_{2,2n}\|^2} & \frac{c}{4\pi\|r_{2,2}\|^2} - \frac{c}{4\pi\|r_{2,2n-1}\|^2} & \cdots & \frac{c}{4\pi\|r_{2,n}\|^2} - \frac{c}{4\pi\|r_{2,n+1}\|^2} \\ \vdots & \vdots & \ddots & \vdots \\ \frac{c}{4\pi\|r_{n,1}\|^2} - \frac{c}{4\pi\|r_{n,2n}\|^2} & \frac{c}{4\pi\|r_{n,2}\|^2} - \frac{c}{4\pi\|r_{n,2n-1}\|^2} & \cdots & \frac{c}{4\pi\|r_{n,n}\|^2} - \frac{c}{4\pi\|r_{n,n+1}\|^2} \end{bmatrix}^{-1} \vec{1} \quad (5.19)$$

Sizing Results

With the velocity profile and wing interactions determined, Equation 5.14 can be used to get an estimate of the dimensions of the AFC and the required lift coefficient per wing.

To accurately size the AFC system, it is important to consider the structural dimensions of the turbine. Because the AFC will be placed within the structure, there are certain sizing limitations it must adhere to. It was found that a chord length of 50 [m] is the maximum structurally achievable chord. Furthermore, it has been determined that, given this chord length, the structure can support three wings while ensuring adequate spacing to keep the wing interference to a minimum. Subsequently, placing a wing on top of the structure allows for a maximum span of 277 [m] while avoiding rotor induction. For the lower wings, the span is reduced to 241 meters to facilitate the placement of the nacelles. These design choices, along with other important decisions and the results of the sizing process, are shown in Table 5.2.

Table 5.2: Sizing parameters and results for the Active Flow Control.

Variable	Value	Unit
Thrust	5	[MN]
Lift	6.5	[MN]
ρ	1.225	[kg/m ³]
Number of Wings	3	[-]
Chord	50	[m]
Span (b_1, b_2, b_3)	277, 241, 241	[m]
Heights (h_1, h_2, h_3)	387.4, 265, 146	[m]
Velocities (V_1, V_2, V_3)	11.9, 8.0, 7.7	[m/s]
Interference Factors (f_1, f_2, f_3)	0.957, 0.928, 0.963	[-]
C_l	3.22	[-]

5.2.2. Airfoil Selection and Design

In order to select the appropriate airfoil to fulfil all the functions of the AFC, certain considerations have to be taken into account. Since the performance of the AFC depends on the amount of lift and circulation it can create, which is directly related to the lift coefficient according to Equation 5.17, the main function of the airfoil is to create a high lift coefficient (C_L). Furthermore, the AFC needs to be able to retract during storm conditions to reduce the amount of loading on the structure. This will allow the complete AFC to have essentially the same performance as a single-element airfoil at zero angle of attack. This leads to the importance of a relatively low C_L at an angle of attack of zero. Furthermore, due to varying wind speeds and, therefore, varying Reynolds numbers, it is desired that the selected airfoil has a constant performance over the wide range of Reynolds numbers encountered. Furthermore, it is preferred that after the maximum lift coefficient is reached, there isn't a large sudden decrease in C_L , but a more gradual slope. Finally, a very important aspect of the AFC is to have a high performance when extended in a multi-element wing configuration. This means that the airfoil also has to be well suited for a multi-element wing, where generally a high camber is preferred.

From these considerations, a small selection of airfoils was made, which could be traded off. From the NACA Airfoil library [25], the following airfoils were selected: NACA 0012, NACA 2412, NACA 4412 and NACA 4418. The NACA 0012 option was chosen due to its zero lift coefficient at zero angle of attack. The NACA 4412/18 were considered due to their high C_{Lmax} , and the NACA 2412 was selected due to its combination of relatively high C_{Lmax} and relatively low zero angle of attack C_L .

Comparing the following airfoils with the XFLR5¹ software at a Reynolds number of 20 million results in the following lift polar, see Figure 5.3.

¹<http://www.xflr5.tech/xflr5.htm> [Accessed 06-06-2024]

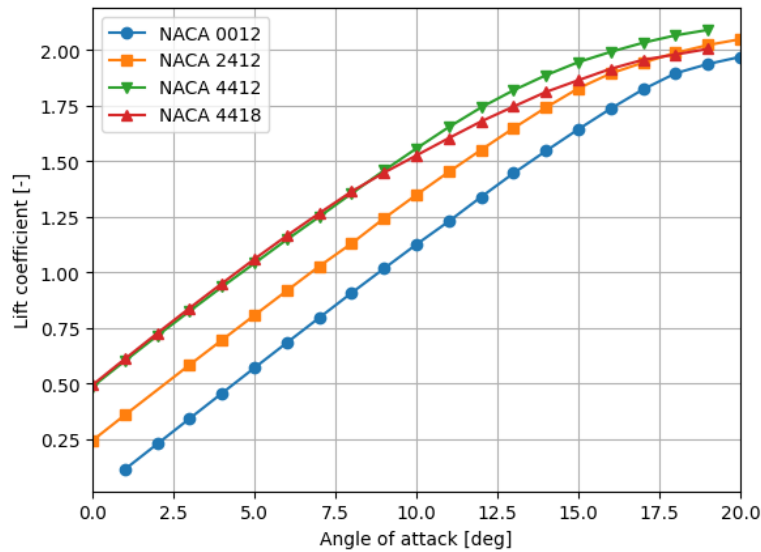


Figure 5.3: C_L vs α for different airfoils

From this figure, it follows that the NACA 4412 figure obtains the highest C_{Lmax} by a slight margin, followed by the NACA 2412 and 4418 airfoil. The NACA 0012 has, as expected, zero C_L at zero angle of attack, but suffers from a lower C_{Lmax} .

Now, the performance of each airfoil when configured in a multi-element wing design needs to be assessed. Since the NACA 0012 is a straight, symmetric airfoil with no camber, it performs subpar in a multi-element airfoil configuration and therefore is omitted for this design. Configuring the remaining airfoils in the following 3-element wing configuration, as visualised in Figure 5.4, Figure 5.5 and Figure 5.6, Results in the following lift polars, see Figure 5.7.



Figure 5.4: NACA 4418 3-element airfoil configuration

Figure 5.5: NACA 2412 3-element airfoil configuration

Figure 5.6: NACA 4412 3-element airfoil configuration

This analysis is performed with the JavaFoil² software, where it must be noted that this software is based on a higher-order panel method and does not model laminar separation bubbles and turbulent flow separation. Furthermore, beyond stall, the results become very inaccurate [26] and, therefore, this region will not be considered for this analysis. For the examination of multi-element airfoils, it is important that the outlines between elements never intersect and that the gaps between elements are not too small. Keeping these considerations in mind and using the Eppler stall model, which is preferred for multi-element-airfoils [26], this analysis is deemed sufficient to find the most suitable airfoil option and get a rough understanding of its performance characteristics.

²<https://www.mh-aerotoools.de/airfoils/javafoil.htm> [Accessed 06-06-2024]

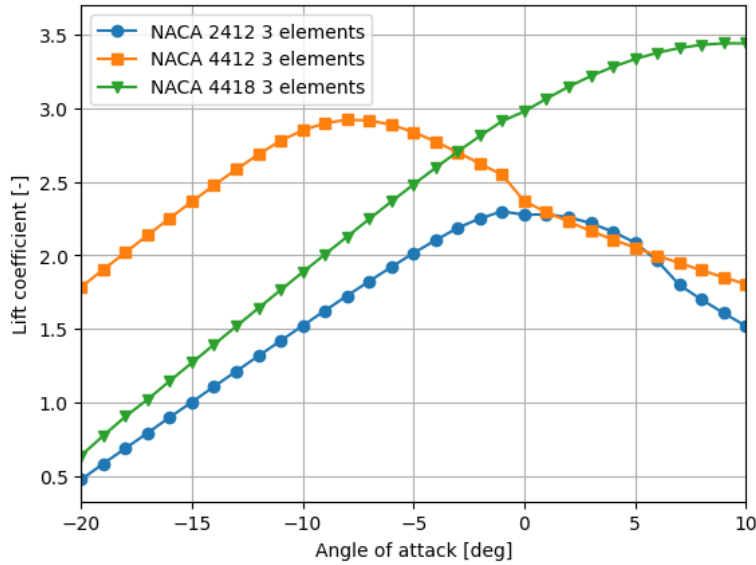


Figure 5.7: C_L vs α for 3-element configurations

From these figures, it can be observed that the NACA 4418 3-element configuration performs the best with a C_{Lmax} of 3.381. Therefore, this configuration was chosen for this design and will be used for the wings of the AFC. With the airfoil in place, the option of using a 2-element or 4-element configuration was also analysed, but it was quickly observed that the increased complexity of using a 4-element design outweighs the marginal increase of C_{Lmax} to 3.4. The 2-element configuration decreases the performance significantly to a C_{Lmax} of 2.5, which does not meet the required C_L of the AFC, as determined in Equation 5.2.1, and therefore is omitted. Therefore, the NACA 4418 3-element airfoil, as configured in Figure 5.4, is the chosen option to be used for the AFC, with a C_{Lmax} of 3.381.

It should be noted that the selection process for the airfoil and multi-element wing configuration was not a thorough and systematic trade-off. For this design, achieving a C_L higher than 3.22 was found sufficient, as per the calculations done in subsection 5.2.1. Therefore, it was decided not to invest significant effort and resources in optimizing the airfoil and multi-element wing configuration. Instead, a less rigid trade-off approach, relying more on engineering judgment and arbitrary choices, was adopted to achieve a result that was deemed sufficient for the purposes of this design. This area may benefit from significant improvement, as the performance of the AFC is closely related to the C_L of the selected multi-element airfoil. Furthermore, it has been speculated that lift coefficients up to 5 are achievable for a multi-element airfoil in this particular application, given that many constraints applicable to conventional aircraft, such as the Reynolds and Mach number, do not apply here. This increase might lead to significant improvements in the AFC and is an interesting point of focus for further designs.

5.2.3. AFC Overview

From the sizing results in subsection 5.2.1 and the selected airfoil in subsection 5.2.2, the performance can be estimated.

For drag calculations, a parabolic lift-drag polar was assumed as in Equation 5.20 [24].

$$C_D = C_{d_0} + \frac{C_l^2}{\pi A e} \quad (5.20)$$

Where C_{d_0} is the zero-lift drag coefficient as computed using JavaFoil, A is the aspect ratio of the wing, and e is the Oswald efficiency factor that relates to the ellipticalness of the lift distribution. Since the wing is not tapered or swept, the e was assumed to be relatively low at 0.6. With a C_l of 3.22, C_{d_0} of 0.03648 and C_m of -0.501 the loads can be computed as tabulated in Table 5.3. Note that the wing is oriented such that it produces upwash, explaining the flipped signs of the lift and moment produced.

Table 5.3: Active Flow Control Loading during Nominal Operation Conditions.

Wing	Lift [MN]	Drag [kN]	Moment [MNm]
Wing 1	-3.70	863	28.8
Wing 2	-1.42	368	11.1
Wing 3	-1.37	368	10.7
Total	-6.5	1599	50.6

For the structure to survive storms on the North Sea, it must be able to carry the loads from the AFC at 65 [m/s] [REQ-SYS-08] in case the turbine is unable to yaw. During the storm, the rotors will be turned off, and the induction effect of the rotors is thus not present, and each wing will see the same velocity. The interference effects do have to be taken into account however. If the AFC were to not retract and yaw during storms, it would create loads unfeasible to carry by the structure; it must thus contract. It was found using JavaFoil analysis that the lift coefficient at the retracted position is reduced to 0.345, the C_{d_0} to 0.01015 and the moment coefficient to -0.051. The loads during the storm are presented in Table 5.4.

Table 5.4: Active Flow Control Loading during Storm Conditions.

Wing	Lift [MN]	Drag [kN]	Moment [MNm]
Wing 1	-11.8	706	87.5
Wing 2	-10.0	620	73.8
Wing 3	-10.4	670	76.6
Total	-32.2	1996	237.8

5.2.4. AFC Mass Estimation

Finally, it needs to be ensured that the AFC is able to withstand the aerodynamic loading it creates. From this, a rough estimation of the AFC mass can be made.

To determine the mass of the system, the simplified case will be analysed, where the wing is assumed to be a single-element airfoil wing of type NACA 4418, with a chord of 50 [m]. This wing will be assembled and supported by the structure every 27.38 [m], which will essentially function as the span of this wing. Furthermore, for the purposes of this design, it was assumed that the majority of the wing mass consists of its spars, which are the main load-carrying members. Additionally, the wings will be sized for bending, which was determined to be the most critical loading case.

The loads, presented in subsection 5.2.3, show that the most critical loading is experienced during storm conditions, where the maximum wing loading occurs on the bottom wing with a loading of -43,2 [kN/m]. It is assumed that this load will be carried by an "n" number of spars. The maximum stress in the spar occurs in the middle of the spar and is described by Equation 5.21.

$$\sigma = \frac{M\gamma \cdot y}{I} = \frac{1.7 \frac{wL^2}{8} \frac{H}{2}}{\frac{n}{12} tH^3} = \frac{51}{40} \frac{wL^2}{ntH^2} \quad (5.21)$$

Where w is the wing loading, L the section length, n the number of spars, t the thickness of the spars and H the height of the spars.

During storms, the wing loading is -43.2 [kN/m]. With a safety factor of 1.7, an average spar height of 6 [m], spar thickness of 1.7 [mm], 2 spars and a section length of 27.38 [m], a maximum bending stress of 337 [MPa] is reached. This is below the yield stress of S355 steel at 340 [MPa] [27], and the spars can thus carry the most critical loads.

From these dimensions, the total mass of the spars can be calculated using Equation 5.22.

$$m = \rho n t H \sum_{i=1}^3 b_i \quad (5.22)$$

Where ρ is the density of S355 steel at 7800 [kg/m³] [27] and b_i the span of wing i . Filling in the numbers gives a total mass of 121 [t]. To account for the mass of other parts of the AFC system, such as the ribs and retraction

mechanisms, an uncertainty of 70% was applied, resulting in a total estimated mass of the AFC system of 205.7 [t].

5.3. Annual Energy Production

With the integration of the Active Flow Control (AFC) device, the wake of each turbine is regenerated, minimizing the reduction in flow speed. This enhancement increases the wind farm's capacity factor, defined as the energy produced divided by the energy installed. Consequently, the Annual Energy Production (AEP) efficiency is boosted. This section calculates the new AEP resulting from these improvements.

To quantify the regeneration of the wind produced by the wings, Figure 5.8 shows the cubed velocity ratio behind each turbine depending on the number of wings.

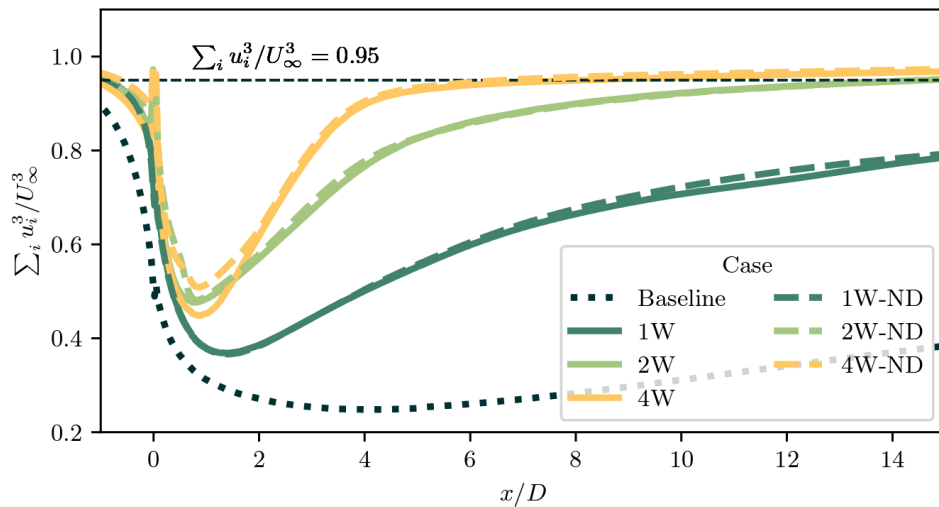


Figure 5.8: Velocity Recovery behind each turbine [23]

Here x/D , is the distance behind the unit normalized by the multi-rotor unit's width. For ReWind's case, as the wind farm has a spacing of 1900 m, with a width of 278 m, x/D results in 6.83. Interpolating between the 2 and 4 wings, the ratio of the cubed velocities is 0.928, which is a velocity ratio of 0.975.

Additionally, it was assumed that the velocity decreases equally behind each turbine, meaning that behind the first turbine, the velocity is 0.975; behind the second turbine, it becomes 0.975^2 ; behind the third, 0.975^3 , etc. This is a rough assumption, as the interaction between wakes and AFC devices is not considered and might be a topic for further improvement in future design, as these assumptions have a large impact on the design as a whole.

The velocity measurements were taken throughout the whole year, as explained in chapter 4, and the wind direction was assumed to be along 225 degrees. This means that the number of turbines behind each other varies between 6 and 15.

Then, given the power curve of each rotor, the local velocity at each individual rotor of the wind farm, and the actual availability of the wind farm of 0.923 found in section 9.1, the energy produced in a year can be calculated, which divided by the possible energy produced yields to a capacity factor of 47.5%. The annual energy production was found to be 84.5%.

5.4. Structural Design

The design of the structure for the multi-rotor wind turbine is a crucial component in ensuring structural integrity and optimal performance. This section delves into the engineering and optimization processes involved in creating the structure, which acts as the main supporting structure for the multiple rotors and the Active Flow Control (AFC) devices. First, the different load cases will be considered. Then the structure will be sized. After which the foundation will be designed.

5.4.1. Load Cases

According to IEC 61400-1 standard [28], a Design Load Case (DLC) is categorized by their analysis type: ultimate loading or fatigue loading. These DLCs encompass various conditions that could potentially be critical

for turbine operation [28]. Given that the objective of the conceptual design is primarily to demonstrate the feasibility of the proposed ReWind design, the scope of these DLCs was limited at this stage of the design. To that end, three static (ultimate load) DLCs are considered, which are described in Table 5.5. These are considered the most critical cases that can be quantified at this stage of the design process and collectively represent the operational envelope of each turbine unit. Naturally, in the further design stages, the complete set of DLCs prescribed in [28] will have to be evaluated.

Table 5.5: Description of the design load cases considered.

Identifier	Description	Wind speed [m/s]
DLC-1	Rated windspeed: the thrust force is maximal, and the structure is loaded by drag forces and the aerodynamic loads of the AFC corresponding to rated thrust.	10.59
DLC-2	Cutoff wind speed: the wind turbine operates at the transition point between the operating and parked states. The higher wind speed increases the structural drag, but reduced the rotor thrust (the power remains constant). Furthermore, the AFC aerodynamic forces are kept the same with respect to DLC-1 by manipulating the AFC actuators.	25
DLC-3	Inoperative storm condition: The wind speed reaches levels well above the cut-off speed and the turbine has been yawed to a parked position such that the wind hits the structure from its shortest side. Here, it is assumed that the yaw alignment is exact within the operating margin of $\pm 5^\circ$, such that it can be assumed that the AFC aerodynamic loads are negligible. Additionally, the rotors are parked and do not contribute to the loading of the structure.	66

In this preliminary structural sizing, both the monopile and truss will be sized on the basis of the aforementioned design load cases. To then demonstrate feasibility of the designed structure, several characteristics will be used as metrics: the total mass of the truss and monopile, the maximum required truss member diameter, and monopile diameter. If these fall within financial, manufacturing and installation limits, then it can be concluded that the concept is feasible, and can be carried into the next design phase.

5.4.2. Truss Model Description

The truss analysis model determines the deflections and internal loading states of each member given a set of prescribed loads and boundary conditions. The following assumptions are made:

- A-S01: Each truss member carries only axial loads.
- A-S02: The mass of each member is lumped in its nodes.
- A-S03: Each member fails due to either ultimate stress or column buckling.
- A-S04: At the connecting boundary nodes, the connection is pinned.
- A-S05: Each member is thin walled, such that the diameter to thickness ratio, $D/t \geq 10$.
- A-S06 Linear analysis: the displacements are infinitesimal, the equilibrium is well-posed with respect to the unloaded configuration, and the elasticity is independent of the local stress state.

Static Model

Let the structure be discretized by N nodes, connected by k unique finite elements representing the truss members. The global displacements, $\mathbf{U}(z, y, z) := [U_1 V_1 W_1 \cdots U_N V_N W_N]^T \in \mathbb{R}^{3N}$, measured in a global coordinate system x, y, z are a function of the displacements of all N nodes. The problem formulation is then as follows: given the geometry of the structure, the applied loads, imposed boundary conditions, and assumed constitutive stress-strain relation, find the the nodal displacements and corresponding stresses and strains, ε and σ .

For element $m \in \{0, 1, \dots, k-1\}$, the (actual) displacement is approximated by interpolating a vector $\tilde{\mathbf{u}}^{(m)} \in \mathbb{R}^2$ containing the local element degrees of freedom. The equivalent three-dimensional global displacements, $\mathbf{u}^{(m)} \in \mathbb{R}^6$, are obtained by applying a transformation matrix $\mathbb{T}^{(m)}$ [29]:

$$\tilde{\mathbf{u}}^{(m)} = \mathbb{T}^{(m)} \mathbf{u}^{(m)} \quad (5.23)$$

where the entries of $\mathbb{T}^{(m)}$ are the direction cosines between the global and local coordinate directions. The actual element strains, $\varepsilon^{(m)}$, corresponding to $\tilde{\mathbf{u}}$ are then given by,

$$\varepsilon^{(m)} = \tilde{\mathbb{B}}^{(m)} \tilde{\mathbf{u}}^{(m)}, \quad (5.24)$$

where $\mathbb{B}^{(m)}$ is the local strain-displacement matrix. Since linear displacements have been assumed, the entries of $\mathbb{B}^{(m)}$ are given by differentiating the matrix of linear basis functions along the member axis [30]:

$$\tilde{\mathbb{B}}^{(m)} = \frac{1}{l_m} \begin{bmatrix} -1 & 1 \end{bmatrix}, \quad (5.25)$$

where l_m is the element length. Using the local strain, the actual stresses, $\boldsymbol{\sigma}^{(m)}$, in each finite element are given by the (linear) constitutive law [29]:

$$\boldsymbol{\sigma}^{(m)} = \mathbb{C}^{(m)} \boldsymbol{\varepsilon}^{(m)} = E_m \boldsymbol{\varepsilon}^{(m)}, \quad (5.26)$$

Where $\mathbb{C}^{(m)}$ is the elasticity matrix corresponding to element m , and it has been assumed that the element initial stresses are zero. Since members only deform axially, the matrix $\mathbb{C}^{(m)}$ reduces to a scalar E_m , the modulus of elasticity of the m^{th} element. The equilibrium equations describing the nodal displacements of the structure can be derived by requiring that the total internal virtual work of the structure must equal the total external virtual work. Considering only point loads applied to the discrete nodes, this produces an expression of the form [29]:

$$\sum_{m=0}^{k-1} \int_{V^{(m)}} \bar{\boldsymbol{\varepsilon}}^{(m)T} \boldsymbol{\sigma}^{(m)} dV^{(m)} = \sum_{i=0}^{N-1} \bar{\mathbf{u}}^{iT} \mathbf{R}_C^i, \quad (5.27)$$

Where $\bar{\boldsymbol{\varepsilon}}^{(m)}$ are the virtual strains corresponding to the virtual displacements $\bar{\mathbf{u}}^{(m)}$, and \mathbf{R}_C^i is the point force on the i^{th} node. Applying the same assumptions to the virtual displacements and strains, namely $\bar{\boldsymbol{\varepsilon}} = \tilde{\mathbb{B}}^{(m)} \bar{\mathbf{u}}$ and corresponding linear displacements, the matrix formulation can be derived by substituting in (5.27):

$$\sum_m \int_{V^{(m)}} \bar{\mathbf{u}}^{(m)T} \tilde{\mathbb{B}}^{(m)T} E_m \tilde{\mathbb{B}}^{(m)} \mathbf{u}^{(m)} dV^{(m)} = \sum_i \bar{\mathbf{u}}^{iT} \mathbf{R}_C^i. \quad (5.28)$$

Then, expressing the left expansion in terms of the virtual and real displacements, $\bar{\mathbf{u}}^{(m)}$ and $\mathbf{u}^{(m)}$, in global coordinates,

$$\sum_m \bar{\mathbf{u}}^{(m)T} \mathbb{T}^{(m)T} \left[\int_{V^{(m)}} \tilde{\mathbb{B}}^{(m)T} E_m \tilde{\mathbb{B}}^{(m)} dV^{(m)} \right] \mathbb{T}^{(m)} \mathbf{u}^{(m)} = \sum_m \bar{\mathbf{u}}^{(m)T} \mathbb{K}^{(m)} \mathbf{u}^{(m)}, \quad (5.29)$$

it becomes apparent that $\mathbb{K}^{(m)} = \mathbb{T}^{(m)T} \tilde{\mathbb{K}}^{(m)} \mathbb{T}^{(m)}$, with $\tilde{\mathbb{K}}^{(m)}$ being the element stiffness matrix in local coordinates. The element stiffness matrices (with respect to the element degrees of freedom), are thus constructed by first finding the matrices $\tilde{\mathbb{K}}^{(m)}$ in local coordinates, and then using the transformation rule defined by (5.29) [30, 31]:

$$\tilde{\mathbb{K}}^{(m)} = \int_{V^{(m)}} \tilde{\mathbb{B}}^{(m)T} E_m \tilde{\mathbb{B}}^{(m)} dV^{(m)} = \frac{E_m}{l_m^2} \int_{V^{(m)}} \begin{bmatrix} -1 \\ 1 \end{bmatrix} \begin{bmatrix} -1 & 1 \end{bmatrix} dV^{(m)} = \frac{E_m A_m}{l_m} \begin{bmatrix} 1 & -1 \\ -1 & 1 \end{bmatrix}, \quad (5.30)$$

since $\int_{V^{(m)}} dV^{(m)} = l_m A_m$, and where A_m is the cross-sectional area of the m^{th} element. Letting each virtual displacement equal a unit displacement (requiring that (5.27) holds for arbitrary virtual displacements), the expansion in (5.29) defines an assembled system in terms of the global vector of unknown displacements $\mathbf{U} \in \mathbb{R}^{3N}$:

$$\mathbb{K} \mathbf{U} = \mathbf{R}, \quad (5.31)$$

in which the left-multiplied identity matrices have been omitted. The assembled system (5.31) can be decomposed into [29]:

$$\begin{bmatrix} \mathbb{K}_{aa} & \mathbb{K}_{ab} \\ \mathbb{K}_{ba} & \mathbb{K}_{bb} \end{bmatrix} \begin{bmatrix} \mathbf{U}_a \\ \mathbf{U}_b \end{bmatrix} = \begin{bmatrix} \mathbf{R}_a \\ \mathbf{R}_b \end{bmatrix}, \quad (5.32)$$

where \mathbf{U}_a are the unknown degrees of freedom, and \mathbf{U}_b are those which have been prescribed on the boundaries. (5.32) can be solved for \mathbf{U}_a , after which the reaction forces, \mathbf{R}_r can be found [29]:

$$\begin{aligned} \mathbb{K}_{aa} \mathbf{U}_a &= \mathbf{R}_a - \mathbb{K}_{ab} \mathbf{U}_b, \\ \mathbf{R}_b &= \mathbf{R}_C^b + \mathbf{R}_r \\ \mathbf{R}_r &= \mathbb{K}_{bb} \mathbf{U}_b - \mathbf{R}_C^b. \end{aligned} \quad (5.33)$$

Dynamic Model

As per A-S02, the member masses are lumped in their respective nodes. Subsequently, the local element mass matrix is given by the following approximation [31]:

$$\tilde{\mathbb{M}}^{(m)} = \frac{\rho_m A_m l_m}{2} \begin{bmatrix} 1 & 0 \\ 0 & 1 \end{bmatrix} \quad (5.34)$$

where ρ_m is the member density. In a similar fashion to (5.29), the global mass matrix, \mathbb{M} , is assembled by first computing $\mathbb{M}^{(m)} = \mathbb{T}^{(m)T} \tilde{\mathbb{M}}^{(m)} \mathbb{T}^{(m)}$, and then performing a direct summation over the global degrees of freedom. With the global mass and stiffness matrices, the non-dynamic problem can be formulated in matrix form as follows [29]:

$$\begin{bmatrix} \mathbb{M}_{aa} & \mathbb{M}_{ab} \\ \mathbb{M}_{ba} & \mathbb{M}_{bb} \end{bmatrix} \begin{bmatrix} \ddot{\mathbf{U}}_a \\ \ddot{\mathbf{U}}_b \end{bmatrix} + \begin{bmatrix} \mathbb{K}_{aa} & \mathbb{K}_{ab} \\ \mathbb{K}_{ba} & \mathbb{K}_{bb} \end{bmatrix} \begin{bmatrix} \mathbf{U}_a \\ \mathbf{U}_b \end{bmatrix} = \begin{bmatrix} \mathbf{R}_a \\ \mathbf{R}_b \end{bmatrix}, \quad (5.35)$$

for which the eigenvalue problem is given by:

$$\left| \frac{1}{\omega^2} \mathbb{I}_a - (\mathbb{K}_{aa})^{-1} \mathbb{M}_{aa} \right| = 0, \quad (5.36)$$

where \mathbb{I}_a is the identity matrix compatible with the dimension of the unconstrained problem. Thus the eigenvalues, $\lambda = 1/\omega^2$, of (5.35) are the eigenvalues of the matrix $(\mathbb{K}_{aa})^{-1} \mathbb{M}_{aa}$.

5.4.3. Truss Element Design

A simple cube-based truss design was introduced, taking inspiration from the hexagonal packing of the rotors. For the preliminary sizing, each cube element has been over-dimensioned, such that at a later stage possible redundant members can be identified and removed. To improve the ease of manufacturing, the truss is designed with repeating layers, as shown in Figure 5.9.

Additionally, the maximum length of each member was limited by splitting the structure into various different columns so as to limit the error in assuming members only carry axial forces. Additionally, the narrow rotor columns allow the drive-trains to be easily mounted in their respective positions, and a direct load path is provided for the thrust and weight forces. The support columns are unobstructed in the xz -planes, so as to provide free space for mounting of the AFC wings and their high lift devices.

Using a honeycomb packing of the rotors, this truss design requires 12 layers, such that the rotor and drive train assemblies can be placed in an alternating fashion in each rotor column. The total structure is depicted in Figure 5.9. The attachment points to the transition piece structure are modelled as pinned connections at the base of the truss tower, and at the tower corners one layer up the truss.

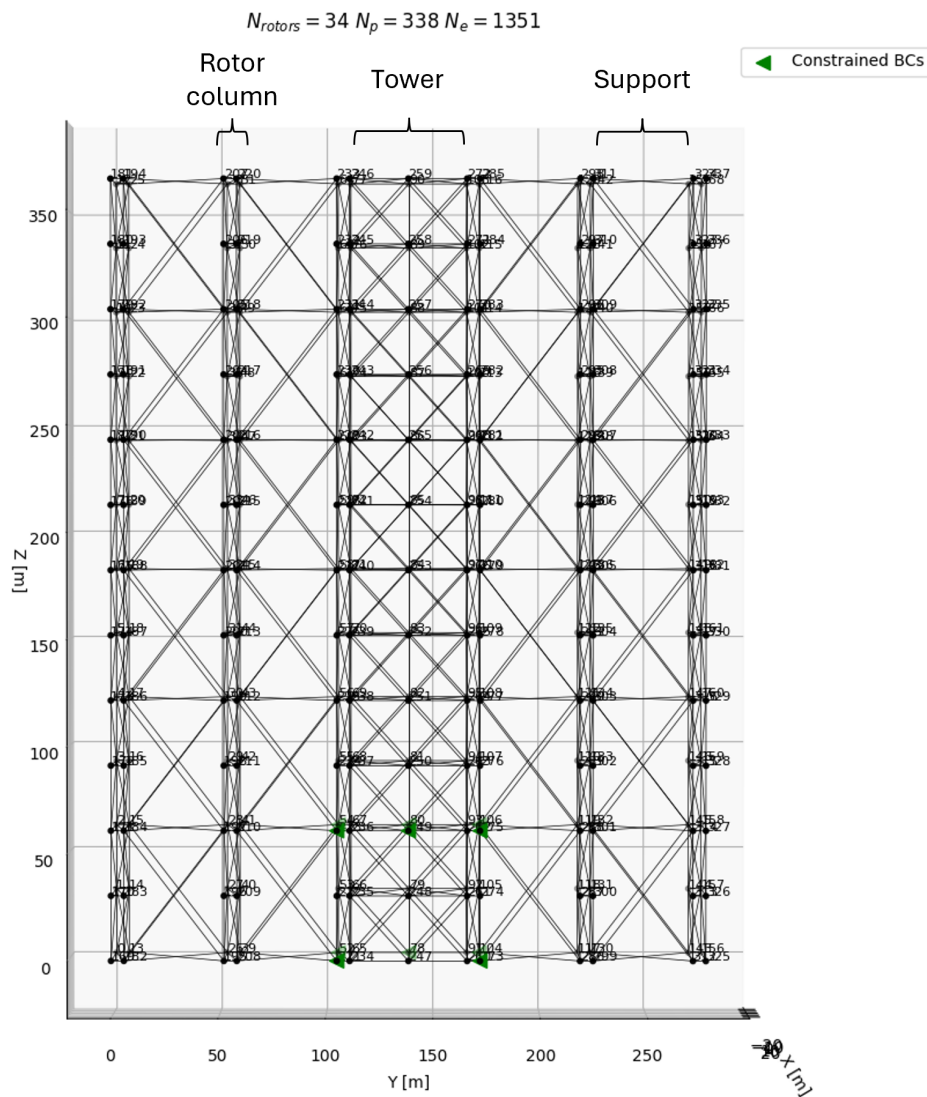


Figure 5.9: Final truss structure, including central truss tower.

Each layer is kept identical to increase the manufacturability of the truss. To ensure symmetry of the structure about the xz -plane, this would only require a half-rotation about the z -axis of one half of the cube elements with respect to the other. The cube-based option shows lower joint complexity, with a maximum of 8 truss members joined at a single connection joint. Furthermore, all truss members are oriented at 0, 45 or 90 degrees with respect to the horizontal plane, making this option viable to manufacture. Therefore, the cube based elements were deemed feasible, and will be used in the ReWind conceptual design.

5.4.4. Load Application

The drag force of the space frame is estimated using the projected area of the truss structure perpendicular to the wind. Since the diameter of the members is small relative to their spacing (see Figure 5.10), it is assumed that bars positioned behind the first perpendicular plane experience no shielding [32]. Thus the loading on the front face is assumed to be applied identically to each parallel plane of the structure. This is a conservative assumption, since there are also members in planes parallel to the wind direction which provide more shielding than depicted in Figure 5.10.

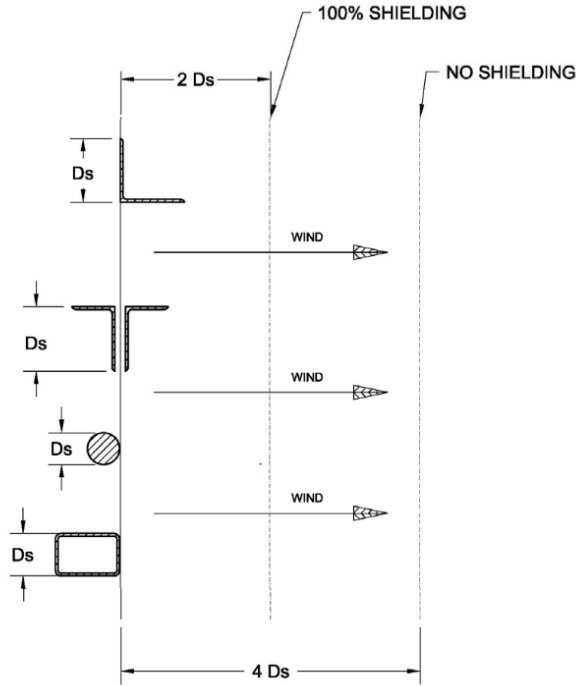


Figure 5.10: Shielding rule used based on the bar diameter to spacing ratio [32].

The drag and lift forces of the AFC is distributed evenly across the planes of the truss structure on which the wings are mounted. Since the exact attachment of the AFC devices to the structure is still to be determined in further detailed design, the aerodynamic moment has at this stage been neglected. Additionally, no dynamic load cases have been considered at this stage, as a result of which no inertial loads are applied.

The thrust produced by the rotor for optimal power production is a function of the wind speed. Depending on the wind speed appearing in each specific DLC, the rotor thrust is recalculated and inserted in the model, being distributed over the mounting nodes for the rotor-nacelle assemblies. Estimations of the weights of the nacelle, rotor and the structure itself are taken into account. The weight of each rotor nacelle assembly is applied on the same mounting nodes where the thrust force is applied. The initial weight of the AFC system was assumed to be around 200 [t] (see subsection 5.2.4), which has been considered negligible compared to the significant lift produced and was therefore neglected in this analysis.

5.4.5. Space Frame Sizing

This subsection focuses on methodology used for final truss sizing and the results of different load cases.

Method

In the structural design of the space frame, the member material is assumed to be S355 steel, the properties of which are given in Table 5.6. This material choice aligns with industry standards for off-shore structures [33, 34]. Additionally, each member is assumed to be thin walled, and with a circular cross-section. Since the goal of this analysis is to assess feasibility of designing the structure, a detailed material and section property trade-off has not been considered, and is instead deemed relevant for a further, more detailed design phase.

Table 5.6: Assumed material properties (S355 steel) [27]

Property	Value	Unit
Young's Modulus (E)	190	GPa
Yield stress (σ_y)	340	MPa
Density (ρ)	7800	kg/m ³

As per A-S01 and A-S03, three failure modes are considered: yield failure in tension, yield failure in compression, and Euler buckling in each truss member. A manufacturability constraint is introduced by assuming a constant ratio of wall thickness to member diameter, $r_t := t/D$, $D := 2R$. Given an assumed r_t , the sizing diameter for yield stress, $D_{i,\sigma}$, of the i^{th} member, $i \in [0, k - 1]$, is given by:

$$D_{i,\sigma} = \sqrt{\frac{|F_{bar,i}| \gamma_M}{\sigma_{y,i} \pi r_t}}, \quad (5.37)$$

where $F_{bar,i}$ is the internal axial force, $\sigma_{y,i}$ is the yield stress, and $\gamma_M = 1.2$ is the material safety factor [35]. Then, if the internal force is compressive, the critical Euler buckling load, N_{cr} , is given by [35]:

$$N_{cr} = \pi^2 \frac{EI_b}{l_k^2}, \quad (5.38)$$

where $I_b \approx \frac{\pi}{8} D^3 t$, and it has been assumed that both ends of each member are free to rotate such that the characteristic length $l_k = l_i$. From this, the sizing diameter for Euler buckling, $D_{i,buckling}$, can be obtained as

follows [35]:

$$D_{i,buckling} = \left(\frac{8|F_{bar,i}|\gamma_{M,buckling}l_i^2}{\pi^3 E_i r_t} \right)^{1/4}, \quad F_{bar,i} < 0. \quad (5.39)$$

where $\gamma_{M,buckling} = 1.3$ is the buckling safety factor. The sizing diameter of each bar is then the diameter resulting from the most critical failure mode:

$$D_i = \max \{D_{i,\sigma}, D_{i,buckling}\}, \quad (5.40)$$

which in turn determines the wall thicknesses, $t_i = r_t D_i$.

Results per Load Case

In the analysis, a wall thickness ratio of $r_t = 1/120$ has been assumed in accordance with [35]. Then, the analysis is performed by re-sizing the member diameters such that each satisfies (5.37) and (5.39). Because a change in the cross sectional area changes both the mass of the members and the drag force they experience, this process is repeated iteratively until the diameters of all members in the space frame converge to within a prescribed tolerance of the desired values. This ensures the space frame is sized exactly for a given load case, allowing an accurate mass estimate to be obtained. The mass of each member is determined using the converged cross-sectional area and material density, ρ ,

$$m_i = l_i A_i \rho_i, \quad (5.41)$$

where the member density has been assumed to be homogeneous, and from A-S02, the area is approximated by $A_i \approx \pi D_i^2 r_t$. This process is first performed for each load case separately. The space frame mass and maximum member diameter for each load case are tabulated in Table 5.7, where a minimum member diameter of $D_{i,min} = 0.36$ m has been assumed such that members which are not load bearing in a given load case do not vanish, and such that the minimum thickness $t_{min} = r_t D_{min} = 3$ mm. In this analysis, the purpose is primarily to establish the bounds on the required member diameters, and the mass of the structure. Since the loading prescribed by DLC-3 is asymmetric, the structure is first loaded by drag from one side (the asymmetric entry in Table 5.7), after which it is loaded from the opposite direction. The two resulting structures are then intersected to find a geometry which can sustain loading from both sides in storm conditions (the symmetric entry in Table 5.7)

Table 5.7: Sizing results for the three design load cases.

Load Case	V [m/s]	$\sum m_i$ [t]	$D_{i,max}$ [m]	I_{zz} [kgm ²]	$(f_{\lambda,1}, \dots, f_{\lambda,5})$ [Hz]
DLC-1	$V_r = 10.59$	2683.79	1.51	1.92e+10	(0.45,0.51,0.95,1.08,1.16)
DLC-2	$V_{co} = 25$	2691.53	1.47	1.91e+10	(0.46,0.52,0.95,1.10,1.17)
DLC-3 (asymmetric)	$V_{storm} = 66$	3013.69	1.77	2.24E+10	(-)
DLC-3 (symmetric)	$V_{storm} = 66$	4188.26	1.77	3.10E+10	(0.44,0.52,1.04,1.12,1.20)

Additionally, Table 5.7 provides the first five natural frequencies of the sized structures, and their moments of inertia about the yawing axis. Magnified deformations of the structure under DLC-1 and DLC-3 are shown in Figure 5.11. From Table 5.7, it becomes apparent that the storm case, DLC-3, is limiting both in terms of space frame mass and maximum required member diameter. However, the mass is significantly higher, and may suggest inefficiencies in the base truss design for this specific load case. Thus, a further analysis is suggested, such that load paths can be optimised, and the criticality of the load case itself can be assessed. For instance, for loading with a 50 year occurrence, it may be more feasible to allow some local (but non-catastrophic) failure of the truss elements most heavily loaded, accounting for maintenance of the structure afterwards. Additionally, the properties presented in Table 5.7 reflect structures where each member has a unique optimised geometry. These unique bar diameters (since with a constant r_t the diameter fully determines the section geometry) must still be distributed into a pre-determined number of bins, such that the manufacturability of the truss is viable. However, with the number of uncertainties and remaining opportunities for optimisation at this stage in the design process, this member sorting was deemed premature, and the corresponding increase in mass with respect to Table 5.7 which would result from this would not necessarily be more representative. Instead, the current results primarily provide a theoretical sizing of the truss, as is sufficient to determine the feasibility of its design.

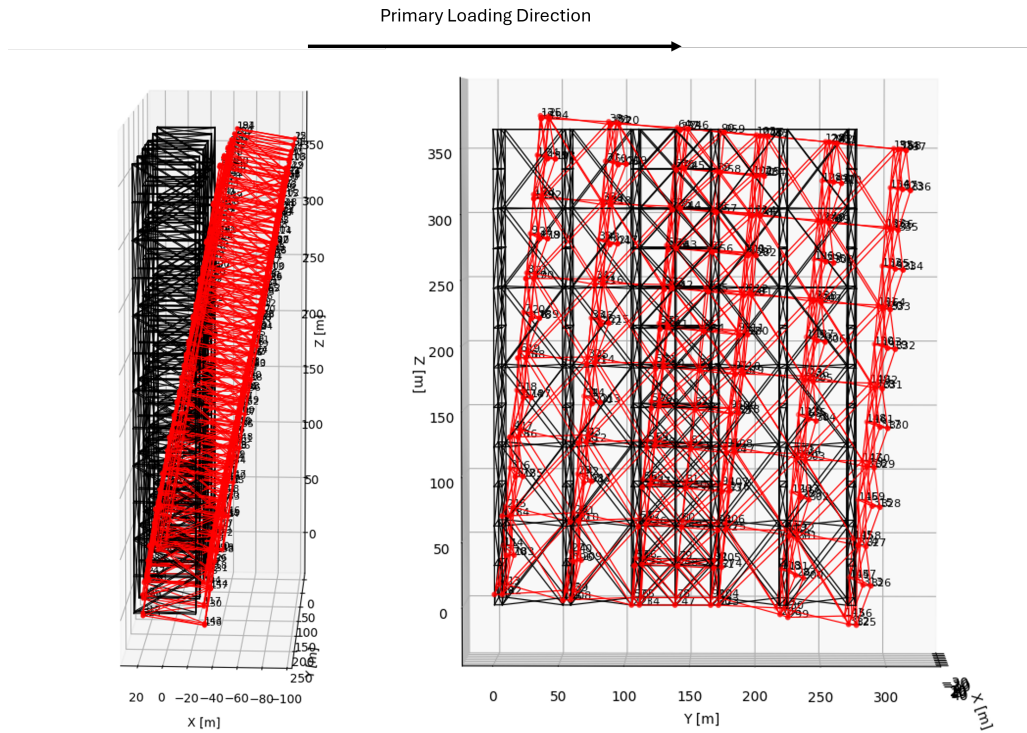


Figure 5.11: Magnified deformations (red) of the truss under DLC-1 (left) and DLC-3 (right) with respect to the unloaded structure (black).

Final Truss Sizing

A combined mass estimate is obtained by intersecting the maxima of the sets of bar masses for each load case given in Table 5.7, which results in a structural mass estimate of $M = 4315$ [t], and a corresponding structural moment of inertia of $2.71 \cdot 10^{10}$ kgm^2 . Again, this could potentially be reduced at a later stage by optimising the truss design for the asymmetric load case in DLC-3.

Table 5.8: Final truss sizing characteristics

Quantity	Value	Unit
r_t	1/120	[-]
$D_{i,max}$	1.77	[m]
$D_{i,min}$	0.36	[m]
$\sum_i m_i$	4315.21	[t]
$(f_{\lambda,1}, \dots, f_{\lambda,5})$	(0.46, 0.54, 1.07, 1.15, 1.21)	[Hz]
I_{zz}	$3.16E+10$	[kgm^2]
N_e	1351	[-]

For the dynamic analysis, the modal frequencies given in Table 5.8 are compared against possible excitation frequencies. Firstly, the frequency of the constant hub rotation rate is $P_1 = 0.466$ Hz, which falls within $\pm 10\%$ of $f_{\lambda,2}$. The second excitation frequency lies at $P_2 = N_b P_1 = 1.398$ Hz, where N_b is the number of blades [36], which again lies within $\pm 10\%$ of $f_{\lambda,5} = 1.07$ Hz. Thus, in the current configuration, resonance is expected in the truss structure. There are several possible solutions to this issues which can be explored in further design:

- **Augmentation of the natural frequencies:** Increasing the structure mass would increase its natural frequencies, but at the same time would increase the truss costs, and the loads on the monopile. Thus, this is not effective as a primary solution. Similarly, increasing the stiffness of the structure would increase the natural frequencies, for instance by modifying the wall thickness ratio, adding additional members, or the member material.
- **Damping:** A second solution involves the use of damping, either in the form of damping materials, or the implementation of active or passive damping systems. In the latter case, a tuned-mass damper could be used to shift the natural frequencies away from the current resonant frequencies.

- **Isolation:** The excitation sources can be isolated from the structure by making use of isolating mounts, for instance at the connection points between the rotor nacelles and the structure.

5.4.6. Foundation Trade-Off

This section evaluates different types of foundations suitable for the design of an offshore wind farm. The selection of foundations is critical due to varying environmental conditions and operational requirements. Based on this evaluation, foundation sizing will be addressed in the subsequent section. The trade-off follows the methodology described in the Midterm Report [16]. Therefore, this section focuses on the choice of criteria and their scoring.

Monopiles are one of the most common foundation types used in offshore wind farms. They consist of a single, large-diameter steel tube driven into the seabed. This simplicity makes them relatively cost-effective and easy to install. Monopiles are particularly suitable for shallow waters, up to 30 meters deep [14]. Given the site's water depth of approximately 20 meters, monopiles appear to be a strong contender due to their straightforward installation process and proven stability in similar environments. Jacket foundations, on the other hand, are lattice structures anchored to the seabed with piles at each corner. These foundations are designed for deeper waters, typically beyond 30 meters [14]. They offer robustness and the ability to support larger turbines, but their installation is more complex and costly compared to monopiles [14]. Jackets are favored in environments where deeper waters require a more stable and resilient structure. Gravity Based Structure (GBS) rely on their weight to remain stable on the seabed. Typically constructed from concrete, GBS foundations are suitable for shallow to moderate depths, up to 25 meters [14]. Their heavy construction ensures high stability, but they require extensive seabed preparation and are logistically challenging to transport due to their weight. However, their cost-effectiveness and stability make them a viable option for sites with suitable seabed conditions [14]. Floating foundations represent the most flexible solution, as they are anchored to the seabed using mooring lines and can be deployed in very deep waters, greater than 50 meters [14]. These foundations are less dependent on water depth, providing a versatile option for various site conditions. However, they are significantly more expensive and involve complex installation and maintenance processes as well as complicated load transfers to the turbine. Despite their adaptability, the high costs and operational complexities often limit their use to specific deep-water locations [14].

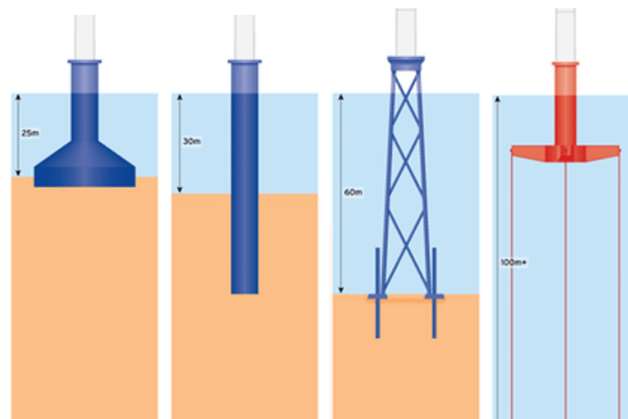


Figure 5.12: Types of Foundations [37]

Trade-off Criteria

According to the aforementioned description of the different types of foundation the following criteria deemed most effective.

- **Water depth (0.25):** The water depth at the site, approximately 20 meters, significantly influences the choice of foundation. It is essential to ensure that the foundation can support the structure at this depth.
- **Rated power (0.2):** This criterion assesses whether the foundation can support turbines capable of producing higher power outputs, which is crucial for scaling the wind farm efficiently.
- **Subsystem Integration (0.35):** This criterion evaluates the compatibility of the foundation with various subsystems, particularly the yaw system, which is critical for optimal turbine performance.
- **Cost (0.2):** The cost-effectiveness of the foundation, measured in million € per MW of power produced, is crucial for economic feasibility.

Trade-off Results

The results of the performed trade-off are tabulated below in Table 5.9. The monopile received the highest total score and is thus the winner of the trade-off.

Table 5.9: Foundation trade-off

Option \ Criteria	Water depth (0.25)	Rated power (0.2)	Subsystem Integration (0.35)	Cost (0.2)	Total
Monopile	Suitable for 0-30m [14] 5	Frequency of use for installed turbines [38] 5	Single conventional bearing 5	1.17 M€/MW 2	4.4
Jacket	Suitable for >30m [14] 2	Frequency of use for installed turbines [38] 4	No attachment for bearing 1	0.93 M€/MW 3	2.25
GBS	Suitable for 0-25m [14] 5	Frequency of use for installed turbines [38] 1	Single conventional bearing 5	0.68 M€/MW 4	4
Floating	Suitable for >50m [14] 1	Frequency of use for installed turbines [38] 2	Higher yaw error due to coupling motion between turbine and platform [39] 2	8 times more expensive than non-floating foundation [38] 1	1.55

Scoring

Below, the scoring of the different categories will be elaborated upon.

Water depth (0.25): Monopiles score the highest in this criterion with a score of 5, as they are ideally suited for water depths up to 30 meters. GBS also scores a 5, being appropriate for depths up to 25 meters. In contrast, jackets score lower with a 2, as they are designed for deeper waters, making them less suitable for this site. Floating foundations score the lowest with a 1, as they are intended for depths greater than 50 meters, making them the least compatible with the site's conditions [14].

Rated power (0.2): Monopiles again score the highest with a 5, demonstrating their capacity to handle high power outputs effectively. Jackets score a 4, indicating moderate suitability for high power outputs. GBS scores a 1, reflecting its limited effectiveness for high power outputs due to its heavy structure. Floating foundations score a 2, as they can support high power turbines but at a higher complexity and cost. The scoring for this specific criterion is strongly based on the frequency of use for the existing operating wind turbine with power outputs close to ReWind [38].

Subsystem Integration (0.35): Monopiles and GBS score the highest with a 5, offering seamless integration with conventional bearing systems. Jackets score a 1, as they lack attachment for bearing, complicating subsystem integration. Floating foundations score a 2, due to higher errors arising from the coupling motion between the turbine and platform [39].

Cost (0.2): GBS foundations score the highest with a 5, being the most cost-effective at 0.68 M€/MW. Monopiles score a 2, with a cost of 1.17 M€/MW. Jackets score a 1, with a moderate expense of 0.93 M€/MW. Floating foundations score the lowest with a 1, as they are significantly more expensive, being eight times more costly than non-floating foundations. The cost evaluations for each foundation type were derived using specific formulas that account for the Water Depth (WD) and Distance to Shore (DtS) [38]. The formulas used are as follows:

- Monopile Foundation Cost:

$$\text{Monopile foundation cost} \left[\frac{\$}{\text{MW}} \right] = 986.059 \times \exp(0.0182 \times \text{WD}) \quad (5.42)$$

- Gravity-Based Foundation Cost:

$$\text{Gravity-based foundation cost} \left[\frac{\$}{\text{MW}} \right] = 278.34 \times \text{DtS} + 814,403.8 \quad (5.43)$$

- Jacket Foundation Cost:

$$\text{Jacket foundation cost} \left[\frac{\$}{\text{MW}} \right] = 459.72 \times \text{DtS} + 1,104,771 \quad (5.44)$$

Monopiles, with their suitability for water depths up to 30 meters, ease of installation, and strong support for high power outputs, emerge as a leading option. They achieve a high total score of 4.4, reflecting their balance of technical feasibility, cost-effectiveness, and integration efficiency.

5.4.7. Monopile Sizing

The monopile's primary function is transferring all the loads from the truss into the seabed. Additionally, it is also supposed to provide clearance above the waves to make sure none of the blades or drivetrains get submerged. Consequently, sizing the monopile plays a paramount role in the structural integrity of the entire turbine. To accomplish this task, the different failure modes of the monopile will first be identified. Subsequently, the different applied loads and the internal loads they induce will be covered before outlining the strategy used to size the monopile.

Failure modes

In this conceptual design stage, the monopile could initially be modelled as a straight, hollow, thin-walled cylinder. Thin-walled signifies essentially the assumption that the skin is too thin to bear any shear forces, this assumption is usually only valid for thickness-to-diameter ratio's higher than 10 ($\frac{D}{t} > 10$). With this assumption in mind, the following failure cases can be identified:

- Endurance failure: the internal normal stress inside a member must not exceed the endurance stress of the material in order to prevent any sort of plastic deformation. The endurance stress is the stress at which the material can be cyclically loaded without showing any sign of fatigue.
- Local buckling failure: Since the radius of this monopile is so large, a very localized buckling of the skin can be considered.
- Global buckling: The monopile could potentially also fail in a way similar to Euler-Bernoulli beam buckling.
- Resonant frequencies: Indirectly, loads applied periodically at certain frequencies can lead the entire monopile to resonate and amplify said loads until failure occurs. Therefore, finding these eigenfrequencies by performing a modal analysis of the monopile is essential to avoid resonant failures.

All the aforementioned failure modes were analysed simultaneously such that the monopile had enough structural integrity to cope with all the failures modes at any given location along the length of the monopile.

5.4.8. Load identification and boundary conditions

Identifying the loads applied onto the monopile is crucial in order to size it properly. Furthermore, one must also clearly define what section of the monopile will be examined in the subsequent analysis.

Sections: Figure 5.13 gives a representation of the three sections of the monopile. Colours were added to this render in order to further emphasize the difference between the sections. The different sections from the top down are: a first emerged section with height 25 [m] that provides clearance from the waves (red), subsequently a submerged part of 20 [m] at most depending on the water depth (white) and lastly a part that is buried in the seabed (blue) over a length of roughly 70 [m] or 6 diameters [40].

In the subsequent analysis, only the upper two sections of the monopile will be considered for sizing. This can be justified by the assumption that the soil will heavily unload the monopile right at the start of the lower blue section in Figure 5.13. This assumption comes with the benefit of heavily simplifying the model by considering the monopile to be pinned at the seabed, however it is quite non-conservative. One could assume that the internal shear force could be transferred uniformly to the soil, leading to a uniform decrease in shear with depth and thus a constant internal bending moment with depth. To mitigate the possible consequences of this assumption a safety factor of 1.35 was applied to all the applied loads [35].

Applied loads: The loads applied to the monopile can be divided in two main components. Firstly, all the loads from the truss structure must be transferred to the red section in Figure 5.13 through the truss-monopile interface. These loads can be modelled as compressive forces along the axis of the monopile, shear forces transverse to its axis and equivalent point moments as follows:

- Compressive forces:
 - Weight of the truss structure



Figure 5.13: Representation of the sized monopile with additional colours to improve contrast

- Weight of the Rotor Nacelle Assembly (RNA)
- Weight of the AFC
- Downforce of the AFC
- Shear forces:
 - Thrust of the rotors
 - Drag of the truss
 - Drag of the AFC
- Point moments:
 - Equivalent moment of the thrust
 - Equivalent moment of the AFC drag
 - Equivalent moment of the truss drag

Point moments are necessary to implement at the junction between the monopile and the tower since the thrust and the drag of the AFC are applied at roughly half the height of the truss structure.

Secondly, the monopile itself also experiences external forces coming from the environment, namely: the drag of the emerged section of the monopile and the force exerted by the waves on the submerged section. The former was neglected due to its small magnitude compared to the other loads (e.g. 10^4 [N] compared to 10^7 [N] for the equivalent wave load) and the added difficulty of recomputing the drag for updated monopile diameters at every design iteration.

Consequently, the only load considered acting directly on the monopile is the distributed wave force. This assumption comes with two significant consequences. Firstly, only the submerged part of the monopile is subjected to additional loads, thus in order to ease installation the emerged section can be kept as a straight tube with its diameter corresponding to the diameter of the submerged section at the waterline. Secondly, now the loads have all been identified, the analysis only focuses on the submerged section of the monopile.

From above discussion, it becomes necessary to estimate the distributed load the waves apply on the submerged section of the monopile. This was performed using the Morison equation, which is the sum of the linear inertia forces and the drag force of the wave [41]:

$$F(t) = \frac{\pi}{4} \rho C_M D^2 \cdot \dot{u}(t) + \frac{1}{2} \rho C_D D \cdot u(t) |u(t)| \quad (5.45)$$

In this equation, ρ is the density of the sea water which was assumed to be 1029 [kg/m³]³. C_D and C_M are empirical coefficients that heavily depend on the Reynolds number and the Keulegan-Carpenter number, which in the case of ReWind can be assumed to be 0.6 and 1.7 respectively [41]. Lastly, $\dot{u}(t)$ and $u(t)$ respectively represent the acceleration and the velocity of the waves, which can be computed as a function of depth and time using the following linear wave theory [41]:

$$u(z, t) = \frac{\omega H}{2} \cdot \frac{\cosh[k(z + h)]}{\sinh(k \cdot h)} \cdot \cos(\omega t) \quad (5.46)$$

$$\dot{u}(z, t) = -\frac{\omega^2 H}{2} \cdot \frac{\cosh[k(z + h)]}{\sinh(k \cdot h)} \cdot \sin(\omega t) \quad (5.47)$$

As one can see from Equation 5.46 and Equation 5.47, the main parameters of interest are the water depth h , the wave number k and the mean wave height H . With these values in mind taken for the mean wave conditions⁴, the wave force can be plotted as a function of time and water depth using Equation 5.45. This yields a three dimensional array which gives the wave force along the submerged length of the monopile for different instants in time. The time instant which yielded the highest resultant force was then taken as the design load for the distributed wave force, which is shown in Figure 5.14.

³<https://salinity.oceansciences.org/maps-global.htm> [Accessed 31-05-2024]

⁴<https://cds.climate.copernicus.eu/cdsapp#!/dataset/reanalysis-era5-single-levels?tab=overview> [Accessed 30-05-2024]

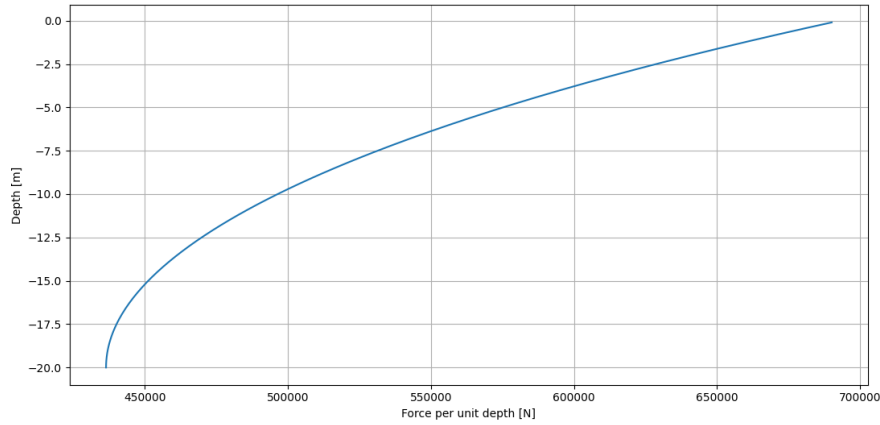


Figure 5.14: Distributed wave force applied on the monopile

Note that in order to generate Figure 5.14, the Morison model was analysed for a period of $1000s$, which is equivalent to roughly 190 complete wave oscillations. Thus the loading on the monopile was analysed for all possible loading cases during a wave oscillation.

Sizing procedure

Once load identification and application has been performed, the internal loads in the monopile can be calculated using the following methodology.

Internal Normal Force: This force increases linearly along the length of the cylinder as it simply represents the sum of the weight of all the elements supported by the monopile.

Internal Shear Force: The internal shear force in the monopile is constant across the emerged part of the monopile as was discussed in subsection 5.4.8. Subsequently, considering a worst-case scenario where the wave load acts in the same direction as the shear force from the truss, the shear force starts increasing with depth in the submerged part of the monopile with the following relation.

$$V_y(z) = V_{truss} + \int_{-w_d}^0 (w_{wave}(z) \cdot z \, dz) \quad (5.48)$$

where $w_{wave}(z)$ is the distributed wave loading and w_d the water depth.

Internal bending moment: Once the internal shear force is computed, one can easily find the internal bending moment by integrating the internal shear force along the length of the monopile and adding the equivalent point moments presented in subsection 5.4.8. This results in the following expression:

$$M_x = \int_{-w_d}^0 (V_y(z) \, dz) + M_{thrust} + M_{drag,truss} + M_{drag,AFC} \quad (5.49)$$

The internal shear force and bending moment were plotted for better visualisation in the figure below:

The internal bending moment is crucial in order to compute the normal stress within the structure. Assuming a uni-axial loading, the following formula can be used:

$$\sigma_z = \frac{M_x \cdot y}{I_{xx}} \quad (5.50)$$

where I_{xx} is the second area moment of inertia calculated about the x-axis, y the distance from the centroid along the y-axis.

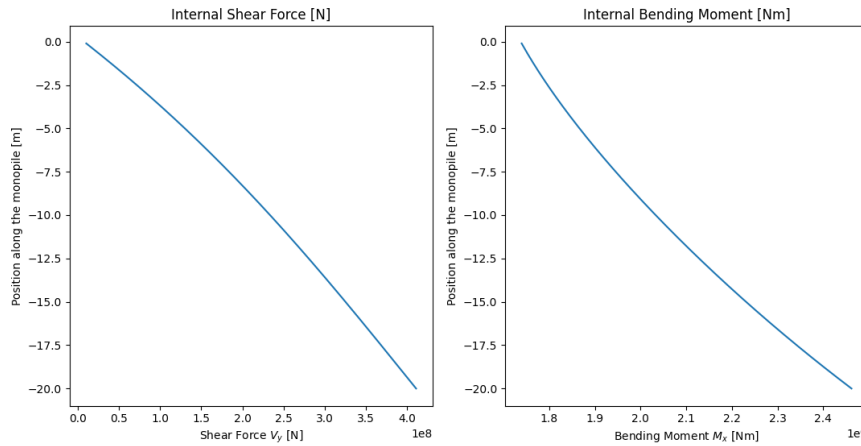


Figure 5.15: Internal shear force and bending moment along the length of the monopile, 0m stands for sea-level

Finally, the monopile can be sized. Using Equation 5.50 the internal normal stress due to bending can be computed and compared to the stress at which each of the failure modes, presented in subsection 5.4.7, occur. For each of the respective failure modes the critical stresses can be computed as follows:

- Endurance failure: The endurance stress of S355 steel is taken to be 190 [MPa] [27]
- Local buckling failure: The critical stress at which local buckling occurs can be computed using the following equation [42]:

$$\sigma_{cr} = \frac{Et_w}{0.5D\sqrt{3(1-\nu^2)}} \quad (5.51)$$

with t_w being the wall thickness, E the Young's modulus and ν a constant assumed to be 0.3 [42].

- Global buckling failure: The Euler column buckling can be modelled by the well-known Equation 5.52⁵:

$$F = \frac{\sigma_{crit} A}{\pi^2 EI} = \frac{\pi^2 EI}{(KL)^2} \quad (5.52)$$

The critical normal stress σ_{crit} can simply be computed by multiplying the force by the cross-sectional area. Also worth noting is the constant K which can be assumed to be 2 in the case of a monopile since the bottom end is assumed to be constrained in all degrees of freedom and the top is totally free.

- Resonant frequencies: The first eigenfrequency of the monopile can be estimated using the following formula [43]:

$$f_{FB} = \frac{1}{2\pi} \sqrt{\frac{3E_T I_T}{L^3 (m_{RNA} + \frac{33}{144} m'_T)}} \quad (5.53)$$

In this equation I_T is equivalent to I_{xx} . It is worth noting that m_{RNA} in this specific case also includes all the other RNA's that are supported by the monopile such as the mass of the AFC and the mass of the all the RNA's. Lastly, m'_T , represents the mass of the monopile itself.

Subsequently, a constant diameter-to-thickness ratio was set to $D/t_w = 120$ [42] and the second area moment of inertia of the monopile could be simplified using the thin-walled assumption. This yields the following expression:

$$I_{xx,thin-walled} = \pi R^3 t_w = \pi \frac{D^3}{8} t_w \quad (5.54)$$

Recalling Equation 5.50, one can easily notice that the maximum stress will occur at the maximum distance from the neutral axis, i.e. one radius away. Combining this and the simplified expression for I_{xx} , the total maximum compressive stress in the monopile is calculated as:

⁵<https://courses.ansys.com/index.php/courses/linear-column-buckling/lessons/pre-analysis-start-up-lesson-2-12/> [Accessed 30-05-2024]

$$\sigma_{total,max} = \frac{(W_{truss} + W_{RNA} + W_{AFC} + L_{AFC})}{\pi D t_w} + \frac{M_x \frac{D}{2}}{\pi \frac{D^3}{8} t_w} \quad (5.55)$$

The submerged part of the monopile is then subdivided into 200 segments of equal length for which an initial diameter of 8 [m] is chosen arbitrarily. Each segment of the monopile then goes through an iterative design process where the diameter is increased by 0.01 [m] at every iteration and the thickness ratio is kept constant. This process goes on for every segment until the applied stress including safety factors in that segment is lower than any of the calculated failure stresses computed earlier.

These iterations resulted in the following diameter and thickness distributions along the length of the monopile as shown in Figure 5.16:

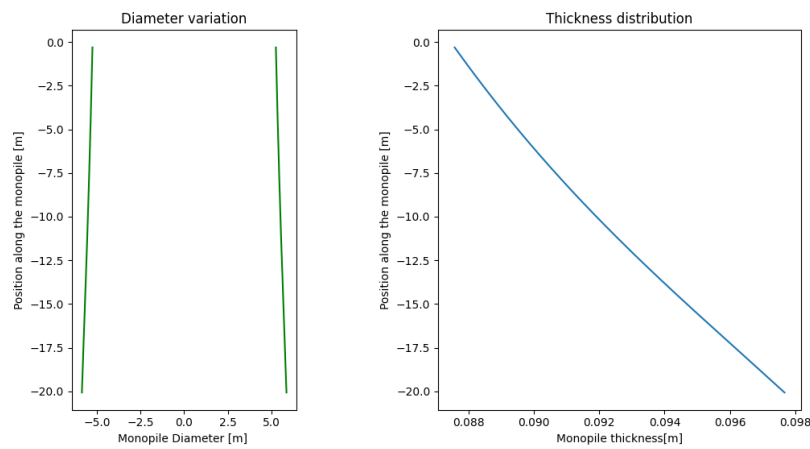


Figure 5.16: Diameter variation and thickness distribution of the submerged section of the monopile

This yields a minimum and maximum diameter of the submerged section ranging between 10.51 [m] and 11.72 [m] respectively, with for now a constant diameter-to-thickness ratio.

5.4.9. Limitations

While the current structural analysis indicates the bounds on the geometry and mass of the structure, the results are not yet conclusive and still require further analysis. As previously mentioned, modifications will have to be introduced to overcome the resonance issues identified in Figure 5.4.5. Moreover, both the truss and monopile structures have not been analysed for fatigue, and the inclusion of fatigue analysis in [44] resulted in a significant increase in mass. This would require either the analysis of a prototype model, or more likely the use of a damage accumulation model in combination with a dynamic load simulation. Moreover, the design load cases must be expanded in accordance with the cases listed in IEC 61400-1 [28], in addition to the analysis of additional test cases to give insight into how the sized structure would respond in abnormal circumstances. Finally, it is still necessary to finalise the geometry of each member in the truss. Although this will most likely increase the structure mass with respect to the current assumptions, it was determined that there still exist significant opportunities for optimisation and refinement, such as in the lack of fatigue analysis, optimisation of the truss depth ratio, member wall thickness ratio (r_t), minimum bar diameter and truss geometry, as a result of which the assignment of bar geometries was deemed premature, and the resulting increase in mass not necessarily more representative of the structural characteristics.

Additionally, another limitation should be noted with respect to the eigenfrequencies of the monopile. The original values are estimated assuming the monopile is rigidly constrained at the bottom, however in reality, the soil the monopile is installed in shows some flexibility depending on its composition. Methods exist to correct for soil effects as presented by Bakhti, et al. [43], however this would require obtaining more exact information on the soil's composition and mechanical properties which are not known at this time. Furthermore, driving the monopile into the seabed requires very large forces to be applied cyclically onto it. This further emphasizes the need to perform a fatigue analysis later as described earlier.

5.5. Control Systems

This section delves into the control systems for yaw and pitch, which are critical for enhancing the performance and efficiency of wind turbines. These systems, although they operate independently, are interconnected and work together to adapt to changing wind conditions. The yaw control system is responsible for aligning the turbine with the wind to maximize energy capture, while the pitch control system adjusts the angles of the blades to optimize power generation and safeguard the turbine during periods of high wind speeds.

5.5.1. Yaw

As determined from the trade-off analysis in the midterm report [16], the yaw system will utilize differential pitching in conjunction with a secondary electric motor. The yaw system will act upon the upper of the two yaw bearings. Even though a design utilizing two-yaw bearings is quite disruptive in the wind energy industry, it was found to present major advantages for this multi-rotor design. The first yaw bearing will be positioned at the base of the structure, 25 [m] above the waterline, while the second bearing will be positioned at a height of 60.68 [m] such that it can be connected easily to the superstructure. The main benefit of having two bearings is that it offers massively improved moment bearing capabilities compared to a single-bearing solution. This is because all the moments transferred from the superstructure into the monopile can simply be carried over as shear forces on the two bearings instead of creating a huge bending moment on one bearing. As the moment would create additional compression on one side of the bearing, adding up to the large weight of the bearing, this would result in enormous friction forces in the bearing that would need to be overcome by the yaw motors. The dual-bearing solution mitigates this friction by not only getting rid of the bending moment but also dividing the friction due to the weight of the two bearings.

Differential pitching, depicted in Figure 5.17, involves the asymmetric adjustment of rotor pitches to create varied aerodynamic forces across different sides of the array, generating rotational moments around the central tower. In this approach, rotors on one side of the array maintain regular operation, while the blades on the opposite side are pitched differently to decrease the thrust generated there. This differential pitching effectively creates a moment by reducing the aerodynamic forces on one side of the array.

For an enhanced moment effect, albeit with a reduced power output, also the other side of the array can be pitched to increase the thrust generated there. This strategy can generate a significant yawing moment, improving the system's ability to achieve the desired orientation at larger yaw angles.

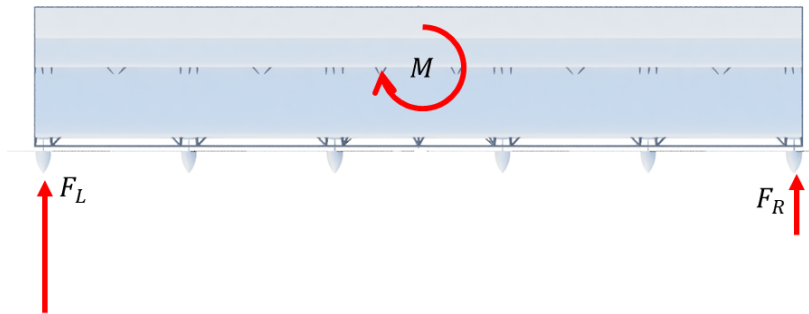


Figure 5.17: Differential thrust concept for a multirotor wind turbine

To verify adherence to requirements, analyse the operational envelope, and benchmark a control strategy, a simulation of the system dynamics was conducted. This simulation was implemented in Python. To approximate the dynamical system, the Equations Of Motion (EOM) were derived. The EOM describe the behaviour of the system over time, considering the forces and torques acting on the yaw bearing. The EOM is provided by the following expression [45]:

$$M - M_f = J\ddot{\psi} \quad (5.56)$$

Where M is the applied moment, M_f is the friction, J is the polar moment of inertia and $\ddot{\psi}$ is the second derivative of the yaw angle ψ with respect to time. The applied moment is the sum of the moment created by the thrust of each rotor at a distance from the axis of rotation which runs vertically through the monopile. The friction moment is computed using the following formula provided by the bearing manufacturer Kaydon for their TR series [46], which include bearing up to 9 metres of diameter:

$$M_f = \text{sgn}(\dot{\psi}) \frac{\mu}{2} (4.4M_k + F_a D_p + 2.2F_r D) \quad (5.57)$$

Where $\mu = 0.006$ is the friction coefficient, M_k is the tilting moment caused by the thrust being located at a height z from the bearing, F_a is the axial force, F_r is the radial force and D the bearing diameter. The radial force is the reaction force resulting from the total thrust, while the axial force results from the weight W of the structure above the bearing. The thrust of each rotor is calculated as:

$$T = qAC_T(\theta) \cos^2(\psi) \quad (5.58)$$

Where q is the dynamic pressure, A the rotor area and $C_T(\theta)$ is the thrust coefficient as a function of the pitch angle. This is provided by the BEM model in section 5.1 for a pitch angle range that goes from -10 to 10 degrees. In this range, the relationship between C_T and θ can be approximated as linear. The equations of motion for the system are highly nonlinear. This nonlinearity arises from both the applied moment M and the friction moment M_f , which include, in the terms containing the thrust, both the cosine squared term $\cos^2(\psi)$ of the yaw angle ψ and C_T which is a function of the time-dependent input θ . Let the state variables be defined as ψ and $\dot{\psi}$ the second-order non-linear differential equation can be written as a system of first-order nonlinear differential equations with the input θ .

Each rotor is positioned at varying distances from the central tower and can be pitched independently, resulting in a control system with n Degrees of Freedom (DOF). This high dimensionality, together with the inherent nonlinearities in the system dynamics, poses a substantial challenge for designing a controller which aims to achieve high yaw rates while simultaneously maximizing the power output. Advanced control techniques like Model Predictive Control (MPC) or machine learning-based optimization algorithms are typically required to address these challenges. However, the implementation of these methods is outside the scope of this design phase.

To simplify the problem, a simple concept controller is proposed. This controller divides the array into two areas, with all rotors in each area pitched at the same angle. This approach reduces the complexity of managing individual rotor pitches. The controller operates as follows: When the yaw angle error is positive, the left side of the array maintains its unaltered pitch angle θ_{opt} to maximise power, as determined by the operational strategy. In contrast, the right side changes its pitch to generate the necessary yawing moment. Conversely, if the yaw angle error is negative, the right side maintains its operational pitch, and the left side adjusts its pitch.

The pitch adjustment is calculated through a PID controller with an optimizer to fine-tune the gains and achieve required behaviors, such as minimizing the yaw rate. A gyroscope is used to measure the yaw rate, and the result is integrated to compute the yaw angle. The concept is illustrated in Figure 5.18 and does not show the side switch. Only the control loop after the switch of the side has occurred is shown, but there will be a supervisory control which reads the measured yaw and switches to the controller for the left or right side.

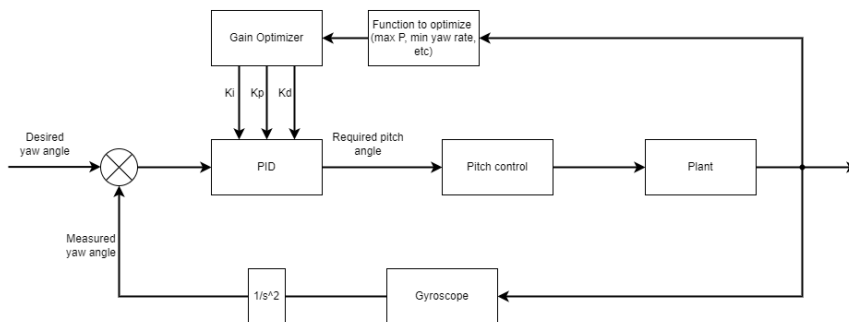
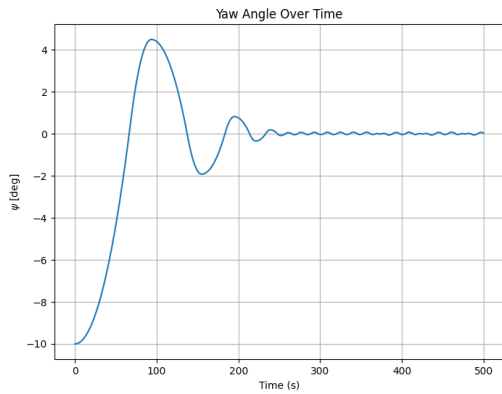


Figure 5.18: Concept controller for the left/right rotors

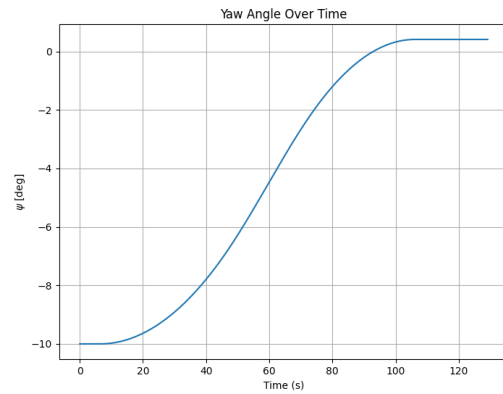
A simulation was performed to analyse the characteristics of the system. Due to time constraints, only the side-switching mechanism and a proportional gain were implemented for a proof-of-concept simulation. In Figure 5.19 the result can be observed for a misalignment angle of respectively 10 [deg] at the rated wind speed $V = 10.59$ [m/s]. Despite the lack of controller tuning, the system still manages to settle around 0 degrees over a long period, albeit exhibiting an underdamped behaviour. This underdamping results in an oscillatory behaviour where the yaw angle oscillates around the zero-degree mark before gradually stabilizing. With proper tuning of the PID controller, it should be possible to reach the desired target more quickly. Alternatively, mechanical brakes can also be employed to provide further damping.

In the second figure, the yaw angle vs time is depicted for the same initial misalignment, but with the pitch angle controlled in real time by the user via keyboard input instead of an automated controller. This approach bench-

marked the system's performance, as real-time manual control is often simpler than tuning a controller. The results demonstrate that a yaw rate of 0.3 [deg/s] can be achieved through manual intervention. The requirement REQ-SSYS-Y&P-02 specifies that the yaw rate should be at least 0.5 [deg/s]. However, this requirement is not met by the current simulation. Refining the controller and adjusting the pitch positively on the opposite side could help increase the yaw rate. However, it is unlikely to achieve the desired rate, particularly for larger yaw angles.



(a) Yaw angle vs time for initial yaw misalignment of 10 degrees at rated wind speed



(b) Yaw angle vs time for initial yaw misalignment of 10 degrees at rated wind speed controlled manually

Figure 5.19: Yaw angle vs time for initial yaw misalignment of 10 degrees at rated wind speed for different controllers

Operational diagram

The limited operational envelope presents a significant drawback to the pitching system. Differential pitching becomes ineffective at the rated wind speed for a yaw misalignment greater than 45 degrees when pitching both sides to achieve the maximum moment. To determine the effectiveness and limitations of the yaw system, the operational envelope was analyzed and plotted. This was achieved by computing the system's response for a range of yaw angles and wind speeds, utilizing the maximum available moment.

In this analysis, the limit is defined as reaching alignment within 300 seconds. This approach ignores the yaw rate but provides an estimate of when it is reasonable to use differential pitching. In Figure 5.20, the operational envelope diagram is shown. The x-axis represents the wind speeds, and the y-axis represents the initial yaw misalignment. As expected, the thrust is higher at higher speeds, allowing for greater correction. Outside this operational area, the motor must be used to achieve alignment.

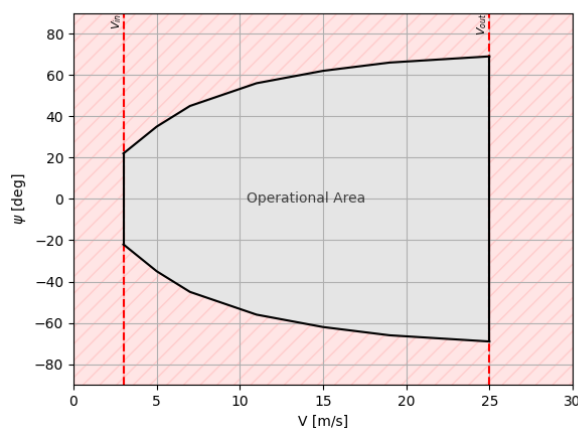


Figure 5.20: Operational Envelope for Differential Pitching

However, at low wind speeds, the impact of the limited operational envelope is less pronounced. When wind speeds are low, the direction of the wind changes slowly, reducing the likelihood of a yaw misalignment exceeding the maximum allowable for effective differential pitching. Consequently, motor usage primarily arises during

specific scenarios, such as turbine restart after maintenance. These situations can include extreme cases like wind direction shifting from the opposite direction after a prolonged period or positioning the turbine in a specific direction before a forecasted storm or above the cutoff speed.

Motor sizing

In turbine operations, the motor's torque capability directly impacts the yaw rate achievable during adjustments. High Torque motors can generate significant torque that can accelerate quickly, achieving faster yaw rates. This capability is useful to achieve swift adjustments in turbine orientation within a limited time. On the other hand, motors with limited torque offer a steady but slower acceleration over time. This approach requires more time to achieve an effective yaw rate,

In this application, the motor is utilized primarily for large yaw angles, where differential pitching alone is insufficient. In these cases, a motor providing limited torque but allowing for a gradual buildup of yaw rate is sufficient. Simulation results across various scenarios, including intense motor operations like rotating the turbine by 180 degrees while operational, indicate that 5 [MNm] of torque is adequate for achieving a 180-degree rotation within 20 minutes, whereas, for smaller rotations such as 5 degrees, it would still require approximately 120 seconds with this torque setting.

In order to reach this yaw rate, six yaw motors will be installed in the emerged section of the monopile (see subsection 5.4.7). The TK-3080 motor was selected based on its high torque, low rotational speed specification⁶ (refer to Table 5.10). This motor allows for very low rotational speeds and extremely high torques using very high currents at startup. A major drawback, however, will be the high heat losses due to the resistance of the coil windings as well as the accelerated degradation of the winding insulation.

Table 5.10: Properties of the TK-3080 motor for the desired configuration

Specification	Value	Unit	Specification	Value	Unit
Frame diameter	3080	mm	Operating voltage	425	Vac
Rated torque	287149.21	Nm	Peak power	91.035	kW
Peak torque	470799.5	Nm	max speed	2.7	rpm
Peak current	214.2	A	mass	3580	kg

As one can see in Table 5.10, each of these motors has a rated torque of roughly 287 [kNm], thus adding up to a direct combined torque 1.722 [MNm]. Reaching the 5 [MNm] torque requirement can thus simply be achieved by fixing an internal gear right below the outer section of the bearing and attaching a relatively small gear to each of the motors. The large fixed inner gear on the outer bearing ring will thus help achieve a high gear ratio, multiplying the torque of the motors.

Now that motors capable of yawing the superstructure have been identified, one faces the necessity to select a speed controller capable of delivering the high current and voltage given in Table 5.10. To accomplish this task, the Cascadia Rinehart PM150DZ was selected given its high performance at high voltage and high current as shown in Table 5.11.

Table 5.11: Properties of the Cascadia Rinehart PM150DZ [47]

Specification	Value	Unit
Maximum voltage-operating	720	V
Maximum continuous current	225	A
Peak current	300	A

5.5.2. Pitch

The pitch system of a wind turbine is a critical component responsible for adjusting the angle of the blades to optimize aerodynamic efficiency, control the rotational speed, and protect the turbine during extreme wind conditions. This section provides an overview of the pitch system operations, detailing the functionality and interaction of various components.

The necessary input sensors used to control the pitch system of the ReWind turbine are illustrated in Table 5.12. Additionally, the specific sensor that is commercially available and is able to withstand the harsh offshore environment is added between brackets.

⁶<https://www.phase.eu/fr/torque-motors/configurateur-tk/> [Accessed 12-06-2024]

Table 5.12: Overview of sensors used in pitch system

Component	Description
Wind Speed Sensor (<i>KRIWAN INT10 OF</i>)	This sensor measures the wind speed to inform the system about the current wind conditions.
Rotor Speed Sensor (<i>Leine Linde MRI2850</i>)	It measures the rotational speed of the rotor, crucial for maintaining optimal turbine operation.
Cylinder Extension Rate Sensor (<i>GBF Temposonics</i>)	Monitors how quickly the pitch cylinder is extending or retracting.
Cylinder Extension Sensor (<i>GBF Temposonics</i>)	Measures the actual position of the pitch cylinder.

At the heart of the pitch system is the Pitch Controller, which acts as the central processing unit. It receives data from all the sensors and signals mentioned in Table 5.12. The system begins with input signals, including the desired rotor speed, which is the target speed set based on optimal operating conditions, and the actual rotor speed. A control unit receives both the desired and actual rotor speeds, calculating the error between them and generating a control signal to adjust the blade pitch. The output of this controller is the desired angle of attack, the blade pitch angle needed to achieve the desired rotor speed.

This desired angle of attack is then adjusted by subtracting the inflow angle, representing the angle of the wind relative to the rotor blades, typically measured by anemometers or similar wind sensors. The result is the pitch angle command, which determines the required pitch adjustment. This command passes through a limiter to ensure it stays within the stable region (0 to 40°⁷), preventing excessive pitch changes that could destabilize the turbine or cause mechanical stress. The limited pitch command is sent to another control unit responsible for adjusting the valve position (valve command), which controls the hydraulic or electric actuators that adjust the blade pitch. The final output of this process is the valve position, dictating the precise adjustment of the blade pitch to maintain optimal rotor speed.

A critical aspect of the system is the Feedback Loop, where the cylinder extension is continuously monitored and fed back to the pitch controller. This feedback loop ensures that the desired pitch angle is accurately maintained and allows for real time adjustments to be made as necessary. A simple representation of a proposed feedback loop, simulated in MATLAB⁸, is shown in Figure 5.21 and Figure 5.22.

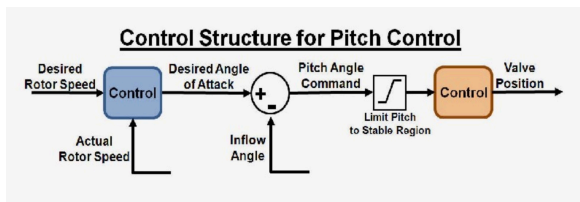


Figure 5.21: Pitch control loop [simulink MATLAB]

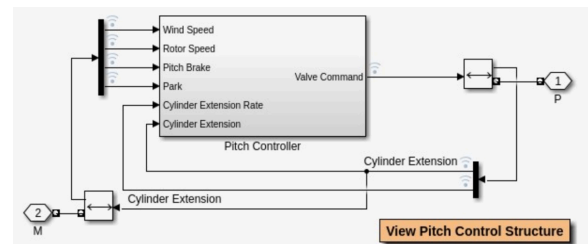


Figure 5.22: Broader picture of pitch control inputs and outputs [simulink MATLAB]

Lastly, the pitch control system is interconnected with other subsystems of the wind turbine. It works in conjunction with the yaw control system, which adjusts the turbine orientation to face the wind, and the power control system, which manages electrical output, ensuring consistent power generation. Additionally, the pitch control system integrates with the safety system, which includes mechanisms for braking and emergency shutdown, allowing rapid adjustment of blade pitch to minimize aerodynamic loads during high wind speeds or unsafe conditions. Additionally, the blades are mounted on pitch bearings and can be feathered 90 degrees for shutdown purposes⁹. Each blade has its own independent failsafe pitching mechanism capable of feathering the blade under any operating condition, similar to AN Bonus 1000/54 [48].

⁷<https://pubs.aip.org/aip/acp/article/2228/1/030005/748756/Comparative-study-Pitch-angle-variation-for-making> [Accessed 17-06-2024]

⁸<https://nl.mathworks.com/products/matlab.html> [Accessed 17-06-2024]

⁹<https://www.energy.gov/eere/articles/how-do-wind-turbines-survive-severe-storms#:~:text=Feathering%20the%20Blades,to%20ride%20out%20severe%20gusts.> [Accessed 19-06-2024]

Pitch Hydraulic Controller

As illustrated in Figure 5.23 and Figure 5.24, the pitch control system transmits control commands to the actuators, ensuring precise adjustments of the blade pitch angles. Figure 5.23 and Figure 5.24 illustrate the flow of commands from the Pitch Controller (PC) to the actuators via a series of components and linkages.

The PC processes input signals and generates control commands based on the desired pitch angle adjustments (either from the yaw system or rotor). These control commands are then transmitted to the Pressure Accumulator Link (PAL), which distributes them to the three actuators through respective linkage systems (PAL1, PAL2, and PAL3). The PAL ensures that the pressure is adequately managed and supplied to each actuator.

The linkage system, comprising linkage mechanisms (Linkage1, Linkage2, Linkage3), transmits the control commands from the PAL to the actuators. Each linkage system ensures the exact movement of the actuators based on the commands received. Each actuator (Actuator 1, Actuator 2, Actuator 3) is connected to a linkage system and consists of a Bidirectional Power Actuator (BPA) and a Rotary Power Actuator (RPA). The BPA receives commands to extend or retract, controlling the linear movement, while the RPA converts the linear motion into rotary motion to adjust the blade pitch angle. The actuators are directly connected to the rotor blades, enabling them to rotate and adjust the pitch based on the control signals.

The flow of control commands begins with the PC generating a control command based on sensor inputs and desired operating conditions. This control command (P) is sent to the PAL, which then distributes the command to the appropriate actuators via PAL1, PAL2, and PAL3. Each PAL directs the command through its respective linkage system (Linkage1, Linkage2, Linkage3) to the actuators. The BPA receives the command, causing it to either extend or retract. The RPA converts the linear motion from the BPA into rotary motion, adjusting the blade pitch [49].

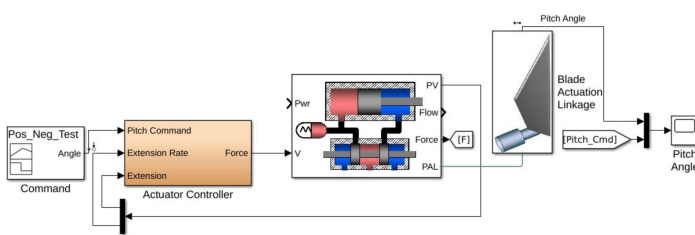


Figure 5.23: Pitch Actuator [simulink MATLAB]

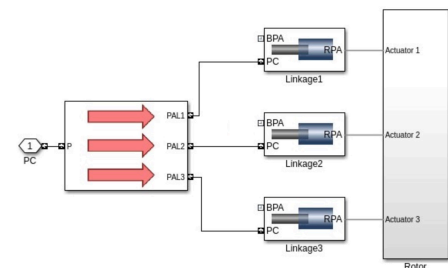


Figure 5.24: Hydraulic pitch flow [simulink MATLAB]

For wind turbines with rotor diameters like the 60m class, Hydratech Industries offers a robust hydraulic pitch system that is critical for precise blade angle control, optimizing energy production while managing structural integrity in adverse weather conditions. Their systems are engineered to withstand harsh environments, including exposure to sand, salt, and extreme temperatures. The pitch system features durable hydraulic cylinders equipped with end-cushioning and integrated length transducers for accurate blade positioning feedback. Each cylinder is designed for easy maintenance, ensuring longevity and reliability. This makes Hydratech solution ideal for large-scale turbines requiring dependable and efficient pitch control¹⁰.

Power Output Regulations

Power regulation is essential for wind turbines to limit output during high wind conditions, achieved either through stall or pitch regulation. Stall regulation uses fixed blades to reduce efficiency at high winds, providing simple and reliable power limitation, but is affected by air density and blade surface roughness. Pitch regulation, with adjustable blades, maintains constant power output by continuously adapting to wind speed and conditions, enhancing efficiency but requiring a fast-reacting and complex system. Our solution combines both methods, as seen in the AN Bonus 1000/54, leveraging stall regulation reliability and pitch regulation efficiency for consistent performance.

The adaptive stall regulation system developed for the 1 [MW] prototype AN Bonus 1000/54 [48] is a combination of the two traditional methods for power regulation. At high wind speeds, the blade pitch is continuously adjusted to match changes in wind speed with changes in pitch angle. However, contrary to normal pitch regulation, the direction of pitching at increasing wind speed is towards stall. Therefore, the power limitation as such takes

¹⁰<https://hydratech-industries.com/industries-applications/wind-power-systems/hydraulic-pitch-systems> [Accessed 19-06-2024]

place by stalling, and the blade adjustment is merely a fine-tuning of the stall process. Regulation by adaptive stall has the same advantages as pitch regulation. The maximum power output can be kept constant at high wind speeds, irrespective of the conditions, and variations in air density are automatically compensated. A small increase in aerodynamic efficiency can be achieved at partial load. Since the adaptive regulation involves stall, it retains most of the advantages of normal stall regulation. Due to the insensitivity to wind speed variations, the power output has only moderate variations under turbulent conditions [48].

5.6. Drivetrain Design

The drivetrain is the system within the wind turbine that is in charge of transforming the mechanical rotational energy of the rotor into electrical energy. From the Midterm Report [16], it was concluded that the system will feature a modular drivetrain for each rotor. This type of drivetrain attaches all of its components to a torsionally stiff bedplate and features a main bearing, which heavily improves torque isolation [50]. Furthermore, it presents massive advantages in terms of maintenance as components can easily be swapped. A simplified illustration of a typical modular drivetrain is presented in Figure 5.25.

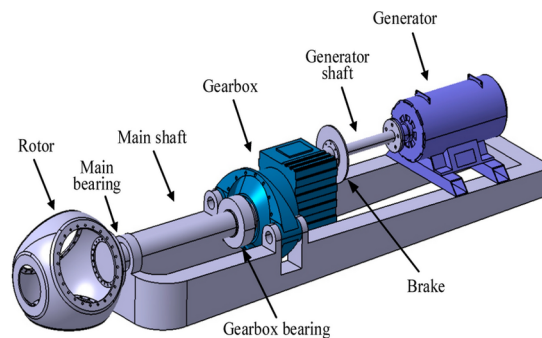


Figure 5.25: Modular Drivetrain Wind Turbine [51]

Here the main components are identified, namely:

- **Low speed (main) shaft:** It transfers the energy from the rotor to the gearbox. It is also in charge of isolating non-torsional loads from the rest of the drive train and transferring these undesirable loads to the main structure through the main bearing [50].
- **Gearbox:** Transforms the high torque, low rotational speed movement of the rotor into a more desirable low torque, high rotational speed movement for the generator.
- **Brake:** Used to bring the rotor to a complete stop when necessary. This could be for maintenance purposes, during an emergency shutdown, or when wind speeds exceed safe operational limits.
- **High speed (generator) shaft:** This shaft connects the gearbox to the generator.
- **Generator:** It transforms the mechanical energy of the transmission shaft into electrical energy to be delivered to the grid.

At this conceptual stage in the design, only the most critical components of the drivetrain will be explored in further detail, namely the gearbox and the generator. The low speed shaft, high speed shaft and brake design is out of the scope of this project and should be addressed in further detail at a later stage. However, it is worth noting that the brakes follow a fail-safe approach. This essentially means that the brakes are passively clamped using springs but, during normal operation, they are actively released using a hydraulic piston [52]. As a result, in case of a malfunction the brakes will be clamped and stop the rotor to prevent any potential damage.

As a starting point for the design of the gearbox and generator, data was collected for a number of existing turbines with similar characteristics to that of a single rotor of ReWind's multi-rotor system. The characteristics used for comparison included the rated power, rotor diameter, rated wind speed and tip speed ratio. For the initial sizing of the gearbox; gear box type, stages and ratio were considered. For the initial sizing of the generator; generator type, speed, voltage and grid connection were considered. The collected data is summarised in Table 5.13 and Table 5.14.

Table 5.13: Turbine Specifications¹¹ (Part 1)

Turbine Name	Endesa AE-59	Vestas V52	Gamesa G58	Vestas V52 (NM)	Frisia F56/850
Rated Power [kW]	800	850	850	900	850
Rotor Diameter [m]	59	52	58	52.2	56
Rated wind speed [m/s]	11	14	12.5	13	12
Tip speed ratio	6.36	6.07	7.52	7.23	6.08
Gear box type	Spur/Planetary	Spur/Planetary	Spur/Planetary	Planetary/Helical	Spur/Planetary
Gear box stages	3	3	3	3	3
Gear box ratio	66	62	62	68	68
Generator type	Synchronous	Double Fed Asyn.	<i>Asynchronous</i>	Watercooled	Synchronous
Generator speed [rpm]	1500	1620	1754	1620	2000
Voltage [V]	1000	690	690	690	690
Grid connection	IGCT	Asyncon	Thyristor	-	IGBT

Table 5.14: Turbine Specifications¹¹ (Part 2)

Turbine Name	Leitwind LTW80 850	NEG Micon NM 52/900	IWT V52	Enercon E-44	PowerWind Ltd. PW60	ReWind
Rated Power [kW]	850	900	850	900	850	883
Rotor Diameter [m]	80	52.5	52	44	60	57.86
Rated wind speed [m/s]	10	16	16	16.5	12	10.59
Tip speed ratio	8.80	3.81	5.31	4.73	6.75	8.00
Gear box type	Direct drive	Spur/Planetary	1 Planet Step/2- Step Parallel Axle	Direct drive	Spur/Planetary	Spur/Planetary
Gear box stages	-	3	3	-	3	3
Gear box ratio	-	68	-	-	54	54
Generator type	Synchronous Permanent	Asynchronous	Asynchronous	Synchronous	Asynchronous	Asynchronous
Generator speed [rpm]	20.9	1511	-	34	1400	1500
Voltage [V]	690	690	690	690	690	690
Grid connection	IGBT	Thyristor	OptiSpeed	IGBT	IGBT	IGBT

From the data represented in Table 5.13 and Table 5.14, an initial estimate of the gear box and generator types and characteristics can be made. This is presented in the last column of Table 5.14, under the name ReWind. Firstly, regarding the gearbox, a 3 stage spur/planetary gear box will be used. Furthermore, based on the rated wind speed and tip speed ratio, an initial estimate for the gear box ratio of 54 can be calculated, which is in the order of the other reference turbines. On the other hand, regarding the generator, an asynchronous Doubly Fed Induction Generator (DFIG) will be used. More specifically, an estimated generator speed of 1500 [rpm] and voltage of 690 [V] was determined, as well as having an Insulated-Gate Bipolar Transistor (IGBT) grid connection.

Using existing gear boxes and generators is generally more cost-effective and time-efficient compared to designing custom ones, as it leverages proven designs and avoids the need for extensive research and development. Additionally, these existing components often come with established supply chains and maintenance protocols, ensuring reliability and ease of replacement. Consequently, for the ReWind turbine a gear box and generator which are commercially available should be chosen. From the reference turbine data, further analysis revealed that the Gamesa G58¹² shares many similarities with the ReWind design. Consequently, the generator and gearbox from the Gamesa G58 were selected for this design. These will be explored in further detail in the following sections.

5.6.1. Generator

The Gamesa G58 features an asynchronous DFIG. Essentially, this consists of a wound rotor connected to an Alternating Current (AC) power source via slip rings and brushes, and a stator connected to the grid. The rotor windings allow for the control of both active and reactive power output, enabling variable speed operation. This capability makes DFIGs ideal for applications requiring dynamic power regulation.

DFIGs operate effectively over a wide range of wind speeds, thanks to their variable speed capability. This is achieved by controlling the rotor windings, which allows for independent regulation of active and reactive power.

¹¹<https://en.wind-turbine-models.com/turbines> [Accessed 10-06-2024]

¹²<https://en.wind-turbine-models.com/turbines/45-gamesa-g52> [Accessed 14-06-2024]

Consequently, DFIGs can maintain optimal performance even under varying wind conditions, ensuring higher energy capture and improved efficiency.

DFIGs are also known for their own reliability and durability. The technology has been extensively tested and proven in the field, with a solid track record of performance in various environmental conditions. The use of slip rings and brushes in DFIGs does introduce some mechanical complexity, but modern advancements have significantly improved their durability and maintenance requirements. Regular maintenance of these components ensures long-term reliability and minimizes downtime.

The specifications of the chosen generator, a 900 [kW] Indar DFIG, are presented in Table 5.15. Note that the rated power which can be achieved using a generator of this type goes up to 9 [MW]. However, since the ReWind multi-rotor system features 34 rotors, a rated power of 900 [kW] will suffice to meet the 30 [MW/turbine] requirement. This will result in a smaller generator that better matches the dimensions of the rotor and the selected gearbox, thereby reducing the risk of failure. This also results in a lower dry mass for the generator, as well as a lower cost. Nevertheless, at a later stage the DFIG could be oversized or even scaled up if necessary so that each turbine produces more power, thus increasing the energy density of the farm.



Figure 5.26: 900kW Indar DFIG¹³

Table 5.15: Main characteristics of the generator¹³

Main Feature	900kW Indar DFIG
Rated power range [MW]	Up to 9MW
Electrical layout	Partial Converter
Voltage [V]	690-12000
Gen frequency [Hz]	50-60
Temperature range [°C]	-30°C / +50°C
Dry mass [tons]	3.4
Cost [€]	26,500

The generator which was selected not only excels in terms of performance and reliability, but is also better than other alternatives from a sustainability perspective. DFIGs have several advantages in terms of sustainability, particularly concerning the use of materials. Unlike a Permanent Magnet Synchronous Generator (PMSG), which requires rare earth metals such as neodymium and dysprosium for their magnet, DFIGs do not rely on these materials. The extraction and processing of rare earth metals are environmentally intensive and often involve significant ecological degradation and hazardous waste production. By avoiding the use of these metals, DFIGs present a more sustainable option. Moreover, the wound rotor and stator in DFIGs are typically made from readily available materials like copper and iron, which have well-established recycling processes. This contributes to the overall sustainability of DFIG-based wind turbines, as these materials can be more easily and environmentally recycled at the end of the turbine's operational life.

Finally, another consideration is the initial cost, which is estimated to be around €26,500. DFIGs, along with their associated power electronics, can be more expensive to manufacture and install compared to simpler generator designs. However, this cost is often offset by the increased efficiency and grid support capabilities provided by DFIGs, resulting in lower operational costs over the turbine's planned lifetime of 25 years.

5.6.2. Gearbox

One of the primary functions of a gearbox in a wind turbine is to increase the rotational speed from the slow-turning blades to a speed suitable for electricity generation. Wind turbine blades typically rotate at speeds between 10 and 20 rpm. However, generators require speeds of around 1500 rpm or higher to efficiently produce electricity. The Gamesa G5X, for instance, uses a gearbox with a gear ratio of 62 to boost its output speed to 1620 [rpm], facilitating optimal generator performance¹⁴. The use of spur and planetary gears in the gearbox design is particularly advantageous. These gear systems are known for their high efficiency in power transmission and their ability to handle high power densities. This makes them ideal for applications in wind turbines where compactness and reliability are crucial. The planetary gear stages in particular help manage the high torque generated by the turbine blades, ensuring smooth and efficient power transfer to the generator [53].

¹³https://www.ingetteam.com/indar/en-us/sectors/wind-energy/p15_65_188/indar-ig-series.aspx [Accessed 11-06-2024]

¹⁴<https://www.windpowerengineering.com/how-are-gearboxes-used-in-wind-turbines/> [Accessed 14-06-2024]

In terms of sustainability, gearboxes offer significant advantages over direct-drive systems, which often rely on large amounts of rare-earth metals for their permanent magnet generators. By using a gearbox, wind turbine designs like the Gamesa G5X reduce the dependency on these rare materials, which are not only expensive but also have significant environmental impacts during mining and processing. Additionally, gearboxes are primarily made of steel and other metals, which are highly recyclable. At the end of their operational life, these materials can be recovered and reused, contributing to a circular economy. This recyclability aspect enhances the overall sustainability profile of wind turbines that employ gearboxes [54].

Gearboxes add complexity to the wind turbine system, requiring regular maintenance and sometimes costly repairs. The initial cost of a gearbox, such as the €85,000 price tag of the Gamesa G5X, reflects the significant investment needed. Additionally, gearbox failures can lead to substantial operational downtimes, as replacing a gearbox often requires cranes and other heavy equipment¹⁵.

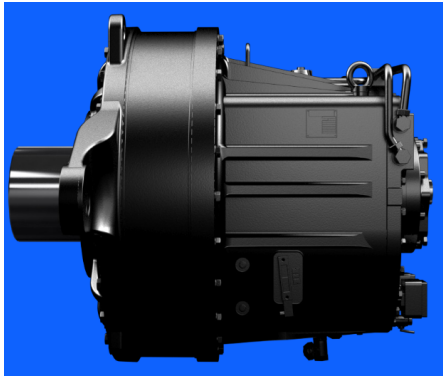


Figure 5.27: 850kW Gamesa G5X gearbox¹⁶

Table 5.16: Main characteristics of the gearbox.

Main Feature	850 kW Gamesa G5X
Rotor size [m]	52/58
Rated power [kW]	850
Gear ratio	62
Output speed [rpm]	1620
Dry mass [tons]	5.75
Cost [€]	85,000

¹⁵<https://www.energy.gov/eere/wind/articles/zeroing-no-1-cause-wind-turbine-gearbox-failures> [Accessed 11-06-2024]

¹⁶<https://www.gamesagearbox.com/gear-units/> [Accessed 11-06-2024]

6. Verification & Validation

This chapter addresses the Verification and Validation (V&V) processes for the project, covering both design and product-related V&V components. Throughout the conceptual design phase, various models have been employed to size components or predict their functionality. The Midterm report [16] proposed V&V approaches for specific models, which will be implemented accordingly. Additionally, new V&V procedures will be established and executed for newer models. After successful verification and validation of these models, the conceptual design will undergo further V&V processes as outlined in the Midterm report [16]. This step is crucial for developing a compliance matrix, which will assess the design’s alignment with customer requirements and the technical specifications derived from stakeholder needs.

The following sections outline the verification and validation procedures for the design tools, detailing the analyses conducted to ensure their accuracy and reliability.

6.1. BEM Model

Verification

In order to verify the correctness of the simulation output, the following tests are performed:

- **Sensitivity to geometry:** Different chord and twist distribution should yield suboptimal values. For example, a significantly lower pitch will result in lower CP and CT values, while a different root chord is expected to decrease CP, as the inputs are theoretically optimized.
- **Sensitivity to initial conditions:** Different initial conditions should yield different outputs, or they should not affect the outputs at all. For instance, although it may not accurately represent real-life scenarios, CP and CT values should depend on the tip speed ratio (TSR) rather than wind speed, with CP and CT values decreasing as TSR decreases.
- **Inputting nonsensical values:** Inputting nonsensical values should lead to nonsensical outputs. For example, negative wind speeds, negative chords or negative Tip Speed Ratios should raise an error in the model.
- **Unit testing:** Multiple unit tests are implemented to ensure each part works correctly in isolation.

Table 6.1: Verification compliance matrix for BEM model

	Geometry Sensitivity	Initial Conditions sensitivity	Nonsensical Values	Unit testing
BEM Model	✓	✓	✓	✓

Validation

The BEM model is widely accepted in both industry and research as a reliable estimate for the power and thrust coefficients of a rotor. In the paper by Boatto et al. [55], it was demonstrated that the BEM model, incorporating the Prandtl Root and Tip correction, achieves an accuracy of 1-5% error at 7-10 TSR when compared to an Unsteady Reynolds Averaged Navier-Stokes simulation. The airfoil polars used were obtained using XFOIL, which are considered accurate within the linear angle of attack range and below a Mach number of 0.4 [56]. Thus, the BEM model can be considered validated. Otherwise, for more accurate results, ReWind’s specific rotor geometry can be inputted into the same Reynolds Averaged Navier-Stokes simulation.

6.2. Yaw System Simulation

Verification

In order to verify the correctness of the simulation output, the same tests as in the Midterm Report [16] are performed:

- **Graphical verification** Geometry of the array is plotted to verify it is correctly implemented in the code.
- **Sensitivity to initial conditions.** When the yaw angle $\psi = 90$ [deg], no thrust is expected to be generated from the rotor and thus no yawing for differential pitching. The contrary indicates numerical errors or an incorrect modelling of the friction moment.

- **Sensitivity to inputs.** Increasing the applied moment should lead to a faster yaw rate and an increase of friction coefficient to a more damped motion. Increasing the polar moment of inertia of the system should lead to a slower yaw rate. Increasing the wind speed should increase the moment generated by the rotors and thus yaw rate
- **Numerical convergence.** To ensure the timestep is sufficiently small to avoid numerical errors, the simulation is repeated with a smaller benchmark timestep, verifying that the relative error is under 2%.
- **Unit testing.** Multiple unit tests are implemented to ensure components function correctly in isolation.

Table 6.2: Verification compliance matrix for yaw simulation tool

	Sensitivity	Numerical convergence	Unit testing	Visualization
Yaw Simulation	✓	✓	✓	✓

Validation

To validate the simulation model, real-life experiments with bearings can be conducted. Additionally, the model's application by M. Warner et al. in their published paper [45] serves as a form of independent validation, demonstrating its effectiveness in a similar simulated scenario.

The aspects of the model related to the friction moment have been directly sourced from formulas provided by the manufacturer Kaydon [46], a trusted entity in the industry. However, these formulas are for a bearing with a diameter of 8 meters, compared to the 10.59-meter bearing hypothesised in this paper. Additionally, the load range slightly differs. Therefore, a real-life experiment should be performed to confirm that the friction dynamics do not change significantly between the two bearings.

6.3. Truss Structural Model

This section focuses on the structural tool verification and validation, which evaluates the structural response of trusses to varied external loads and conditions. The model accuracy and reliability are rigorously tested, ensuring its efficacy in optimizing truss designs for enhanced performance and safety.

Verification

- **Sensitivity to changes in external loads:** Increasing the loads applied on the truss should result in increased deflections for a given geometry, or increased mass for an optimised geometry. For instance, increasing the material density should increase the compression of the structure under its own weight, and the compressive stress should accumulate towards the pinned supports. Similarly, increasing the wind speed should increase deflection due to drag, and changing the wind direction should result in an opposite deformation.
- **Verification of numerical results:** The implementation of the model was verified using a model problem, shown in Figure 6.1. This model problem was chosen because it allows the internal forces, displacements, and reaction forces to be verified in an arbitrary case wherein members are transformed, and the connectivity between members and the constrained members changes across the structure.

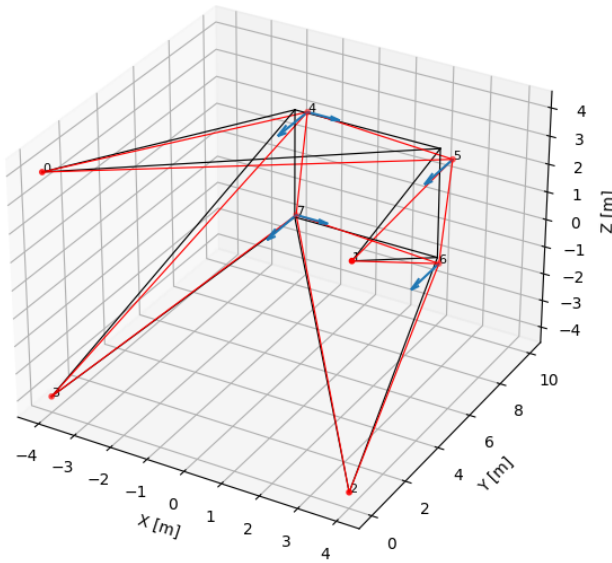


Figure 6.1: Model problem, from [30].

In some cases the errors in Table 6.3 are higher because the exact solution is only known to a certain accuracy. Moreover, the relative errors remain small in these cases. In addition to the results presented in Table 6.3, the reaction forces and internal stresses were verified using hand calculation and the further results in [30], and multiple additional verification cases from [30] have been considered in addition to the one outlined.

- **Verification of symmetry:** In problems with symmetric load cases, the deformations should be symmetric if the structure is identically symmetric.
- **Sensitivity to member properties:** Increasing the Young's modulus increases the stiffness of the structure, and should reduce the deflections relative to a structure with a lower stiffness.
- **Unit testing:** Different elements of the code are tested in isolation. For example, the stiffness, transformation, and mass matrices are verified to contain the correct entries, the node indices on which the loads are applied are verified, and the assembly of the global system. In combination with the numerical verification of the final outputs, this then provides confidence in the correct functioning of the code.

Table 6.4: Verification compliance matrix for the truss sizing model

	Sensitivity	Numerical verification	Unit testing	Symmetry
Truss Simulation	✓	✓	✓	✓

Validation

Validation of the truss sizing model would require either a comparison against a validated finite element software, or against test data for a truss model which can be modelled following the assumptions of the model. This would require the experimental problem to activate all aspects of the model, including the use of varying member properties, a mixture of boundary conditions, and varying member connectivity. The relative error between the model output and the validation data then gives an indication of how well it represents the actual behaviour of truss structures. Alternatively, the assumptions could be validated on a case-by-case basis, looking at for instance the friction of the pins in isolation.

6.4. Monopile sizing model

Verification

The verification of the monopile sizing model can be broken down into different components:

Table 6.3: Errors for the model problem [30].

Quantity	Expected	Computed	Error	Unit
$v_{4,x}$	4.3357	4.33569862	-1.4e-6	[mm]
$v_{4,y}$	-1.814	-1.8141385	-3.9e-5	[mm]
$v_{4,z}$	1.5783	1.5783313	3.1e-5	[mm]
$v_{5,x}$	4.0207	4.02069862	-1.4e-6	[mm]
$v_{5,y}$	-1.5814	-1.58135722	4.3e-5	[mm]
$v_{5,z}$	-1.6683	-1.6683313	-3.1e-5	[mm]
$v_{6,x}$	0.77404	0.77403602	-4.0e-6	[mm]
$v_{6,y}$	-0.79219	-0.79219157	-1.6e-6	[mm]
$v_{6,z}$	-1.5783	-1.5783313	-3.1e-5	[mm]
$v_{7,x}$	0.86404	0.86403602	-4.0e-6	[mm]
$v_{7,y}$	-0.97997	-0.97997285	-2.9e-6	[mm]
$v_{7,z}$	1.6683	1.6683313	3.1e-5	[mm]
p_{04}	-93.531	-9.35e+1	2.56e-4	[kN]
p_{15}	-151.99	-1.52e+2	2.54e-3	[kN]
p_{26}	-93.531	-9.35e+1	2.56e-4	[kN]
p_{37}	-35.074	-3.51e+1	-2.89e-5	[kN]
p_{05}	66.556	6.66e+1	-1.02e-4	[kN]
p_{16}	0	1.28e-14	1.28e-14	[kN]
p_{27}	-66.556	-6.66e+1	1.02e-4	[kN]
p_{34}	0	4.40e-14	4.40e-14	[kN]
p_{45}	-63	-6.30e+1	-2.13e-14	[kN]
p_{56}	-18	-18.00	-7.11e-15	[kN]
p_{67}	-18	-18.00	1.1e-14	[kN]
p_{47}	-18	-18.00	-2.84e-14	[kN]

- **Sensitivity to change in external loads:** Increasing the loads applied on the monopile should result in an increased diameter and thickness in order to withstand these increased loads. This test will be performed by multiplying the applied loads by constant factors both increasing load cases and decreasing load cases.
- **Sensitivity to diameter-to-thickness ratio:** Changing the diameter-to-thickness ratio will affect the total mass of the design. A higher thickness to diameter ratio will yield higher diameters and lower thicknesses. This combination is beneficial when carrying mostly bending loads as a large diameter will rapidly increase the area moment of inertia. Therefore higher diameter-to-thickness ratio's should lead to lower masses.
- **Inputting nonsensical values:** Unexpected or unrealistic input values should also lead to counter-intuitive values. This will be tested by inputting negative values for the initial diameter or the diameter-to-thickness ratio.
- **Unit testing:** Each of the subfunctions in the code will be tested independently in order to ensure that they yield the expected result. This will be done by inputting trivial values that allow for intuitive checks.

Table 6.5: Verification compliance matrix for the monopile sizing model

	External loads Sensitivity	Diameter-to-thickness Sensitivity	Nonsensical values	Unit testing
Monopile sizing	✓	✓	✓	✓

Validation

Validating the model used for sizing the monopile can be divided in a twofold approach. Firstly, the Morison equation and wave model are considered. Subsequently, a validation test can be proposed in order to assess whether the considered load cases on the turbine are indeed critical, i.e. if there exists no other failure mode that is more critical and was not considered in this analysis.

The wave model and the Morison equation are widely used tools for estimating the wave force on slender bodies. This model has previously been validated over the years and is widely accepted as a good preliminary predictor across the industry [57].

Moreover, the validation test for the structural load cases could be performed at the TU Delft Indoor Wave Flume facility¹. This facility allows wave to be generated on a small-scale model of the monopile. Additionally, the loads applied onto the monopile by the superstructure can be modelled by a mechanical actuator which can load the monopile in compression and bending. Alternatively, more advanced finite element simulations could be performed for the identical load cases to check whether or not the results are similar with the model used for preliminary sizing.

6.5. Product

As mentioned in chapter 17, the conceptual design will be refined and further detailed to eventually be tested and qualified. This step ensures that the product meets the requirements set forth by the customer, as outlined in [58]. The content below has been replicated from the midterm report [16].

Each requirement is assigned a verification method as well as a verification level. The four verification methods are Inspection, Analysis, Demonstration and Test, according to Gill [59]. Each verification method provides a certain level of guarantee but also comes at a certain cost. Testing yields the most reliable results but also comes at the greatest time and financial cost. Additionally, small model testing might not always be possible. Hence, analysis can be a cost-effective solution to replace testing. Therefore, the method should be chosen with careful consideration for economic efficiency, time-wise efficiency and product reliability. The verification level determines at which level the verification will be carried out [60]. The three levels were determined to be the Wind farm, the Wind turbine and specific subsystems. From an economic and efficiency point of view, verification should be carried out on the lowest level possible since this requires fewer resources. For brevity's sake, this report only showcases the requirements verified by testing, since these procedures will also represent a big chunk of the verification and validation budget. The other verification procedures are outlined in the midterm report [16].

Verification by Test

Testing being the most accurate but most expensive requirement verification method, only few requirements are planned to be tested

¹<https://www.tudelft.nl/citg/over-faculteit/afdelingen/hydraulic-engineering/sections/hydraulic-engineering-laboratory/indoor-lab-facilities> [Accessed 17-06-2024]

Table 6.6: Requirements verified by test

ID	Description	Verif. level
REQ-SYS-11	The cutoff speed shall be at least 25 [m/s]	Subsystem
REQ-SYS-12	The cut-in speed shall be at most 3 [m/s]	Subsystem
REQ-SYS-15	The power of the multi-rotor unit at low wind speeds, 6 [m/s], shall reach 20% of its rated power production (5 MW).	Wind Turbine
REQ-SYS-14	The wind farm shall be able to operate in a temperature range from -10°C to 40°C	Wind Turbine
REQ-SSYS-ROT-07	The turbine blades shall be able to withstand temperatures between -10°C and 40°C	Subsystem
REQ-SYS-07	The wind turbine shall be able to withstand a sustained wind speed of 60m/s for at least 20 seconds.	Wind Turbine
REQ-SYS-08	The wind farm shall be able to withstand a gust speed of 66m/s	Wind Turbine
REQ-MIS-04	Each multi-rotor system unit shall have active flow control mechanism to reenergize the flow	NA
REQ-SYS-26	The wind farm shall reach a total capacity factor of at least 50 %	Wind Turbine
REQ-SSYS-FDT-05	The foundation shall be resistant to corrosion	Subsystem

Table 6.7 shows the details of the test employed for each requirement, as well as the type of facility and an estimation for the budget. The budget only takes into account the renting prices for the facility, thus excludes the costs of the model and man-hours needed during the testing procedures. The Low speed wind tunnel and Icing and Heating wind tunnels were estimated to cost 750 and 1000 € per hour of use². The corrosion testing lab was assumed to cost about 500 € per day. The availability of each facility is also an important aspect. The Low speed and Icing wind tunnel can be accessed relatively easily, for example at the TU Delft facilities, while the Heating wind tunnel is slightly harder to gain access to.

Table 6.7: Testing description and budgets.

ID	Testing Facility	Testing Description	Budget
REQ-SYS-11	Low speed wind tunnel	Placement of a small-scale model inside the tunnel. The wind should be accelerated to 25 m/s. Strain gauges should be employed to make sure the structure is capable of sustaining the loads.	750 Eur.
REQ-SYS-12	Low speed wind tunnel	Placement of a small-scale model inside the tunnel. Once the wind tunnel flow is accelerated to 3 m/s, power production should be measured.	750 Eur.
REQ-SYS-15	Low speed wind tunnel	Placement of a small-scale model inside the tunnel. Once the wind tunnel flow is accelerated to 6 m/s, the produced power should be at least 20% of the rated power of the model.	1500 Eur.
REQ-SYS-14	Icing/Heated wind tunnel	Placement of a small-scale model inside the Icing tunnel. For each increment of temperature (10 degrees) and wind speed (5 m/s) the model should be operated for half an hour. Then check if no component failed.	15 000 Eur.
REQ-SSYS-ROT-07	Icing/Heated wind tunnel	Placement of a hub with blades inside the Icing tunnel. For each increment of temperature (10 degrees) and wind speed (5 m/s) the model should be operated for half an hour. Then check if no component failed.	15 000 Eur.
REQ-SYS-07	Low speed wind tunnel	Placement of a small-scale model inside the tunnel. Accelerate the flow until 60 m/s. The model should be capable of sustaining this speed for at least 20 seconds.	750 Eur.
REQ-SYS-08	Low speed wind tunnel	Placement of a small-scale model inside the tunnel. Accelerate the flow until 66m/s, then immediately slow down the flow again. Model should not have failed.	750 Eur.
REQ-MIS-02	Low speed wind tunnel	Placement of a small scale model inside the tunnel. The model should be placed on a rotating platform. The platform is rotated 360 degrees. The yawing system should be capable of keeping the rotor oriented into the wind.	1500 Eur.
REQ-SSYS-FDT-05	Corrosion testing lab	A small scale mode shall be subjected to sodium-chloride spraying. The coating needs to be assessed to determine if the foundation is corrosion resistant enough	20 000 Eur.

²https://www.aerodynamics4students.com/wind-tunnel-simulation/snr_office4.php [Accessed 27-05-2024]

7. Production, Assembly and Installation

The fast, cost effective and accurate production, assembly and installation are integral to a well performing wind farm. This chapter will discuss the production, assembly and installation in detail. In section 7.1 the manufacturing process of the turbines is illustrated. Following the manufacturing phase, section 7.2 a trade-off will be performed for the transport and installation method. In section 7.3 the assembly of the structure is detailed, followed by the transport and installation for the chosen method in section 7.4.

7.1. Production

In this section, the production plan for the ReWind concept will be presented. Given that the ReWind concept must endure the harsh North Sea conditions for over 25 years, special attention is paid to the quality of the manufactured subsystems. Additionally, due to the large scale of the wind farm project, exceeding 6 GW, supply chain reliability is also a critical consideration. The companies suggested below are examples of potential suppliers and not necessarily the final choices. Multiple other companies are available, and it may be prudent to engage several suppliers to mitigate supply chain risks.

Monopile foundation

The monopile design of the ReWind concept closely resembles existing monopile designs. However, the diameter of the ReWind monopile has been increased to 11.72 [m], somewhat larger than the conventional 8 or 9 [m]. Despite this size difference, current manufacturing techniques are sufficient for its construction.

To manufacture the monopile, steel sheets are first curved using roll bending. These curved sheets, known as 'cans,' are tack welded together to hold them in place [61]. Once properly aligned, the cans undergo circumferential welding to form a continuous, robust hollow cylinder¹. This process ensures the structural integrity required to withstand the harsh offshore environment. The manufacturing is carried out in large, specialized factories, such as those operated by Sif Offshore Foundations² in the Netherlands, which are equipped with the necessary machinery and expertise.

Truss structure

The truss structure consists of 1,353 individual truss members. In the current ReWind design, the diameter-to-thickness ratio is consistently maintained at 1:120 for all truss members. The diameters range from 0.36 [m] to 1.77 [m], with six different truss member lengths ranging from 6 [m] to 75.8 [m]. All truss members are made of steel S355³. This results in a high number of different truss member types. However, future designs could and should create member diameter 'classes' to minimize the variety of specific members. This would greatly reduce manufacturing complexity and enable standardization and mass production.

The manufacturing process for the truss structure involves three main stages: cutting, forming, and assembly. Initially, steel sheets are cut using techniques like water jets for intricate shapes and saws for straight cuts. High-pressure notches are used to punch holes where needed, for example for electrical cabling.

In the forming stage, truss members are shaped using roll bending, allowing for varying thickness and shapes. Like the foundation manufacturing, cylindrical sheets are welded together.

During the final assembly stage, traditional welding is used to join steel pieces. Each truss member will be fabricated in a specialized facility with the necessary equipment and expertise to manage the intricate production process. These facilities are also capable of applying the necessary anti corrosion coating.

The manufacturing of the truss structure will be outsourced to external parties. This is because truss members are very generic components for which existing companies already have extensive knowledge and operating facilities. For instance, Tata Steel⁴, with extensive activities in the Netherlands, could provide the steel, while

¹https://coastalvawind.com/resources/pdf/cvow_monopiles_fact_sheet_v3.pdf [Accessed 12-06-2024]

²<https://sif-group.com/en/monopiles-and-transition-pieces/> [Accessed 12-06-2024]

³https://www.joostdevree.nl/bouwkunde2/jpgs/staal_23_standarden_s355_european_standard_steel.pdf [Accessed 19-06-2024]

⁴<https://www.tatasteeleurope.com/nl/home> [Accessed 12-06-2024]

Kersten⁵, also located in the Netherlands, could handle the roll bending process. Both these companies have the expertise and capacity needed to supply the large amounts required.

Active Flow Control system

Since the Active Flow Control wings are also constructed of steel S355, similar techniques are used as in the manufacturing of monopiles and truss members. Each main AFC section has a chord of 35 [m] and a span of 277, 241 and 241 [m] for each wing, and is composed of three sheet sections: the leading edge, and the upper and lower surfaces. Naturally, the High Lift Device (HLD) sections have the same span but a shorter chord.

For each wing section, the leading edge is manufactured using a forming process. Forming processes are very cost-effective and achieve high accuracy for smaller components. Due to their larger size, the upper and lower surfaces are shaped using roll bending. Each sheet section is then assembled to create a wing section. Since the entire AFC wing is split into sections, this enables easier transportation to the assembly dock.

Much like the truss structure, the active flow control manufacturing process will be outsourced. Tata Steel can provide the steel, while Kersten can handle the sheet roll bending processes. However, due to the different technique and added complexity, the leading edge will be manufactured using 3D Metal Forming⁶, by a Dutch company based in Lelystad.

Rotor Blades

The rotor blades will be manufactured using current industry standards. As mentioned before, the relatively small size of the blades simplifies and speeds up the production process.

Wind turbine blades need to be manufactured with precision, as small imperfections can lead to the failure of other subcomponents and must be avoided at all costs, thus resin infusion is chosen. Initially, dry fibers are enclosed in molds and sealed. Resin is then injected under pressure, filling the spaces between the fibers. This process occurs through Resin Transfer Molding (RTM) or Vacuum Assisted Resin Transfer Molding (VARTM), with VARTM being the prevailing method as it only requires a one-sided mold.

After the fibers are enclosed and the resin infused, the part is cured. The cured part is then de-moulded, completing the production process. For the turbine blades, we will collaborate with specialized manufacturing firms such as Siemens Gamesa⁷, and Vestas⁸. One of the significant advantages of the multirotor system is that it uses smaller blade sizes, which are produced by multiple manufacturers. This widespread production means that we can easily secure a reliable supply of blades, reducing the risk of production delays. Additionally, the smaller blade size simplifies logistics and transportation, lowers costs, and increases flexibility in sourcing components.

Standard components

Many components used in the ReWind concept are standard parts already in use. These components can be bought off the shelf from producing companies, requiring no specific design work. This greatly reduces costs, as no additional effort is needed beyond the existing production process. The standard nature of these components also allows for relatively easy mass production. A few of the components that are bought 'off the shelf' as well as possible suppliers are:

- Generator: Indar⁹
- Converter: Hitachi Energy¹¹ or ABB¹²
- Gearbox: Gamesa¹⁰
- Transformer: Hitachi Energy¹¹ or ABB¹²

7.2. Installation Method Trade-off

Traditional single-rotor offshore wind turbines can be assembled either onshore or offshore, with the latter method often being preferred. There have been instances where wind turbines were constructed onshore and

⁵<https://www.kerstengroup.com/en> [Accessed 12-06-2024]

⁶<https://www.3dmetalforming.com/> [Accessed 12-06-2024]

⁷<https://www.siemensgamesa.com/explore/journal/recyclable-blade>

⁸<https://www.vestas.com/en/about/our-locations/production>

⁹https://www.ingeteam.com/indar/en-us/electric-generators/wind-generators/pc30_10_186/indar-dfig-series.aspx [Accessed 12-06-2024]

¹⁰<https://www.gamesagearbox.com/wp-content/uploads/2023/09/GE850PL.pdf> [Accessed 12-06-2024]

¹¹<https://www.hitachienergy.com/products-and-solutions/transformers/by-customer-segment/transformers-for-wind-power/transformers-for-wind-turbine-generators> [Accessed 12-06-2024]

¹²<https://new.abb.com/news/detail/25678/abb-wins-transformer-order-for-off-shore-wind-project-in-north-sea> [Accessed 12-06-2024]

transported to the installation location. However, this method requires large vessels and cranes, making the process inconvenient and costly.

To address these challenges, a modular approach is often adopted. The turbine is divided into its primary components: blades, hub, nacelle, and tower. Combination of these components are preassembled, and then transported and mounted offshore. This modular assembly process typically requires 2 to 6 lifts, with single-blade installation requiring the most. These offshore assemblies are often completed in less than 24 hours, providing a more efficient and streamlined installation.

While the offshore assembly approach seems naturally advantageous for single-rotor turbines, it becomes more complex and resource-intensive for multi-rotor systems. The increased size and weight of multi-rotor turbines requires the use of a larger fleet of barges and heavy-crane vessels.

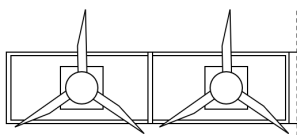
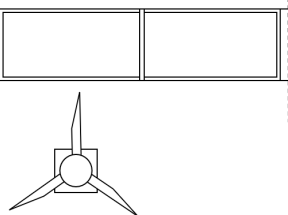
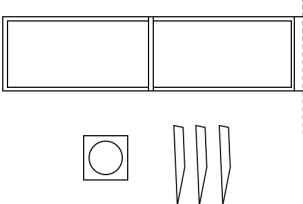
In this chapter, two approaches for the installation of the multi rotor system are compared and the most suitable option detailed. These include on site assembly with substructures built onshore, and full onshore construction with float over installation

7.2.1. On site assembly of substructures built onshore

In the first method, the truss structure is subdivided into multiple stories, which are loaded onto barges for transportation to the site. At the installation site, jack-up rigs equipped with large cranes are used. These rigs can elevate themselves above the water level, providing a stable platform for heavy lifting. The assembled rotor rows are lifted from the barges and installed onto the foundation through a coordinated effort of the cranes. Multiple configurations can be considered for this method:

1. Each floor composing the structure and the AFC is taken offshore and assembled on-site. Subsequently, the nacelles and single blades are installed
2. Each floor composing the structure and the AFC is taken offshore and assembled on-site. Subsequently, the whole nacelle and rotor assemblies are installed.
3. Each floor composing the structure and the AFC is taken offshore with the rotors and nacelles already installed

Table 7.1: Installation methods for component installation

	1	2	3
Installation method			
Number of lifts	22	22 + 34	22 + 34 · 4

Due to the height of the structure, a special fleet of boats should be used, as no vessels are currently known to be equipped to reach 300+ meters of height. Therefore, purpose-built jack-up vessels should be employed to reach a sufficient height for the large ad-hoc cranes to operate. Given the size of the farm comprising 288 turbines, the economic investment of producing an ad hoc ship, which might cost up to 1 billion dollars, excluding operations, could be diluted over time. Furthermore, an important advantage of the specialized crane is that it would significantly simplify maintenance operations. This would eliminate the need for the complex system of cranes and elevators, thus streamlining processes and potentially reducing long-term operational costs.

However a number of disadvantage arise from this modular off-shore assembly approach. Firstly, shuttling is not an option due to the high amount of materials needed. The large number of components required for the offshore assembly necessitates a continuous supply chain between the onshore staging area and the offshore installation site. This typically requires a significant number of feeder barges to transport materials back and forth. Coordinating multiple feeder barges is complex and costly, and the availability of a sufficient number of barges to meet the demand can be a limiting factor, potentially causing delays.

Secondly, the installation at sea is highly weather dependent. The unpredictability of weather conditions adds

an element of uncertainty to the project timeline, making scheduling more challenging. Each weather-related delay incurs additional costs as equipment and personnel must remain on standby until conditions improve.

Lastly, due to the height of the structure, multiple lifts of both the jack-up vessel and the crane are required to complete the installation. Each lift involves repositioning and stabilizing the vessel and crane, making the process slower than the onshore counterpart. Furthermore, the need for multiple lifts increases with the modularity of the structure, as each additional module, escalating the costs.

7.2.2. Full onshore construction with float over installation on site

For the float-over installation instead, the whole array is assembled in a port facility except for the foundation and transition piece. This assembly process may involve the use of large cranes and specialised equipment widely available in the port facilities compared to offshore. Once assembled, the structure is loaded onto two large vessels equipped with adjustable buoyancy capabilities. These vessels transport the components to the installation site. Upon arrival, the vessels position themselves over the foundation, and the turbine components are floated over and lowered into place. This method minimises the need for heavy lifting equipment at the installation site.

This solution streamlines the assembly process by allowing for more controlled and efficient construction in the port facility, where resources and equipment are more readily available. Additionally, it requires a limited fleet, as only the vessel for the foundation and the vessels for the float-over must be used. This reduction in the number of vessels needed simplifies logistics and reduces overall costs.

However, as the transport and installation require high precision, weather conditions must be extremely favorable. Adverse weather can halt the installation process for several days, during which the structure occupies space in the dock. This, coupled with the limited number of this type of vessels available, can create bottlenecks as the dock space is tied up and other assembly activities are delayed.

In the following tables a comparison between the two options is illustrated

Table 7.2: Comparison of Onshore vs. Offshore Installation methods

Criteria Option	Control over Quality (0.2)	Cost (0.3)	Logistics (0.2)	Timeliness (0.3)	Total
Onshore	High, due to controlled onshore environment 5	Potentially lower overall 4	Complex for transportation 4	Potential bottlenecks due to adverse weather 2	3.6
Offshore	Lower, due to harsh offshore conditions 2	High operational cost and specialized costly equipment 1	Complex for offshore site management 2	Potential delays due to failure in complex supply chain & weather 2	1.7

From the Table 7.2 it is evident that the float-over installation is the preferred option.

7.3. Assembly

The assembly refers to the process of creating rigid connections between the different components of the wind turbines. Considering the sheer size of these structures and the difficult nature of off-shore construction, it was decided to assemble the entirety of the structure using onshore facilities located in the port of Rotterdam. A skid way can then be used to transport the fully built structure from its construction site onto the vessel required for the float-over installation. This section will thus give a brief overview of how the superstructure is assembled, subsequently equipped with RNA's and lastly stacked on top of the superstructure-monopile interface. Figure 7.1 shows a schematic overview of the assembly process.

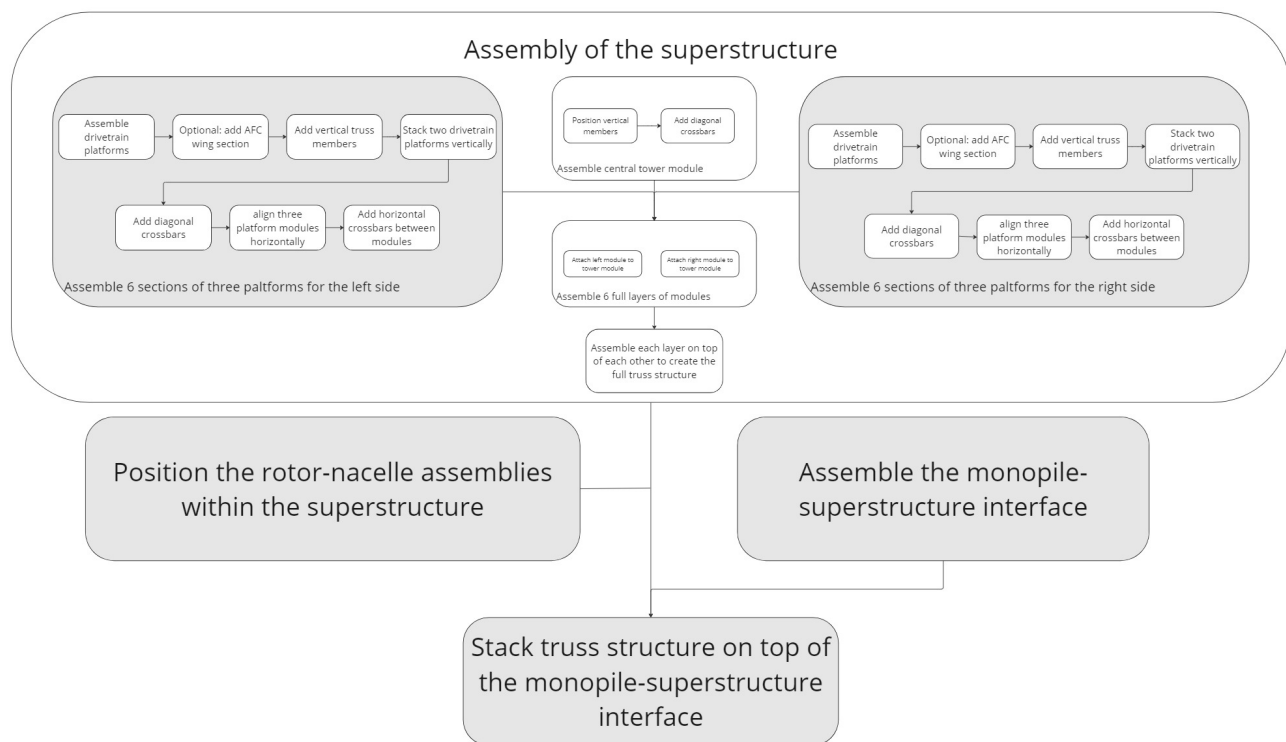


Figure 7.1: Schematic assembly procedure of a single wind turbine

This schematic shows assembly activities that can occur in parallel on the same horizontal level, these subsequently flow down towards later stages of assembly. Each of the steps of the assembly procedure will be outlined shortly. The overall idea is to assemble the superstructure by stacking horizontal layers on top of each other, then include the RNA's and lastly integrate it with the monopile adaptor.

7.3.1. Assembly of the low level modules

Firstly, the low level modules containing the RNA's shall be assembled and then horizontally stacked together into sections, as depicted in Figure 7.2. Those sections each consist of two layers of platforms capable of supporting an RNA. Therefore, the first step in assembling those modules is creating the RNA platforms, which are shown in Figure 7.2a. Subsequently, vertical truss members are added at each of the corners to allow for a vertical stack (see Figure 7.2b), please note that the vertical members are elongated due to an erroneous CAD manipulation. Once this step is performed additional RNA platforms can be stacked on top of the original one as shown in Figure 7.2c. It is worth mentioning that renders presented in Figure 7.2, are made for the lower module of the structure which needs a total of three RNA platforms other stages will only require two.

With the stack of RNA platforms in place, additional diagonal reinforcement truss members are added externally such that they can be bolted onto the main frame, as depicted in Figure 7.2d. At that point, these first four steps should have been performed three times in parallel per section, i.e. 36 times in total.

Now, it becomes possible to focus on the assembly of each section, this is firstly done by aligning three of the aforementioned modules with equal spacing horizontally as shown in Figure 7.2e. Lastly, these three modules simply get connected together using welded horizontal crossbars as shown in Figure 7.2f.

7.3.2. Assembly of central connection section

With one section on each side of the monopile a central connection module is needed to connect the left and right sections of each layer. This is performed by welding diagonal truss members to a vertical truss member that is specifically designed to provide the main load path for all compressive loads. It is worth noting that the diagonal members are located out of plane with respect to the vertical truss members of the central connection section and of each of the side sections as they will have to be connected to the latter. A representation of this central connection module is given in Figure 7.3a, note that once again the vertical truss member is much longer than what it should be in real life due to a CAD manipulation error.

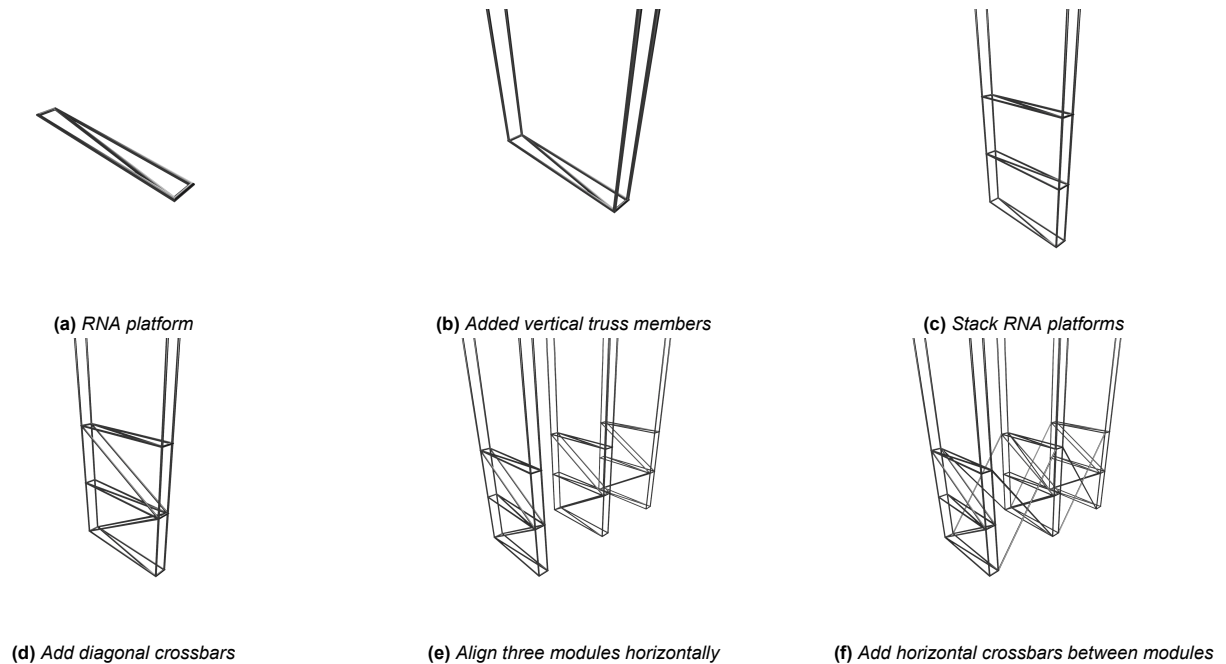


Figure 7.2: Assembly sequence of the single layer sections

7.3.3. Assembly of RNA layer

Once a left and right section of RNA platforms have been assembled as described in subsection 7.3.1, they can be stacked horizontally on each side of the central connection section that was described in subsection 7.3.2. This horizontal stack is performed by placing the central connection section on a jack and then lifting left and right RNA sections next to it. As one can recall from subsection 7.3.2 the diagonal elements are out of plane with respect to the vertical members of the central connection section and of the RNA sections as well. This allows workers to bolt these three substructures together to form a structure similar to what is shown in Figure 7.3b.

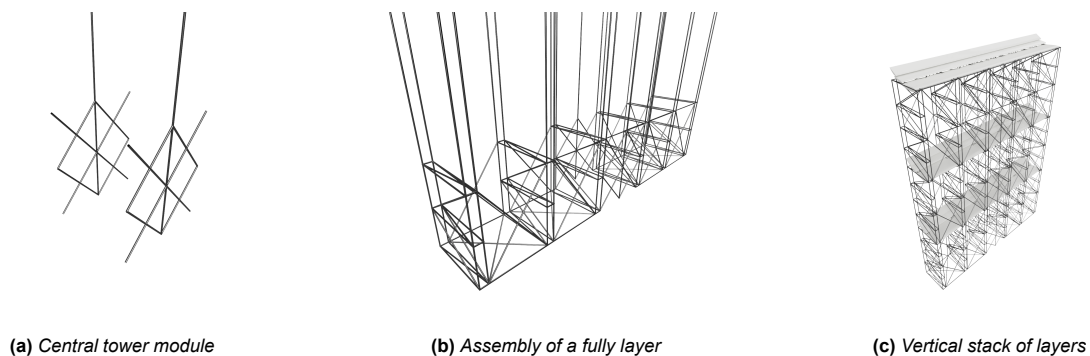


Figure 7.3: Assembly of a full superstructure

7.3.4. Complete assembly of the superstructure

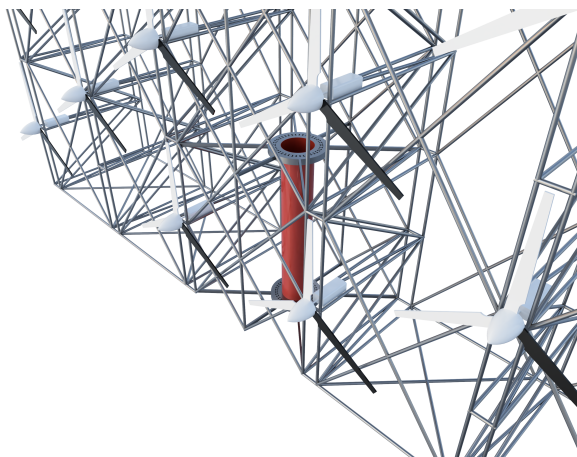
With each of the six layers created in parallel as described in subsection 7.3.3, it now becomes possible to assemble the full superstructure that will support all the RNA as well as the AFC system. This is performed by lifting new layers on top of each other and bolting them together. This will yield the superstructure shown in Figure 7.3c.

At this stage it is also worth indicating how the AFC wings will be assembled and installed within the superstructure. As one could have noticed from the render shown in Figure 15.1, the wings of the AFC system are embedded deep within the superstructure. This is done by attaching the sections of the wing to the lower layer before stacking the upper layer on top. Lastly, additional horizontal crossbars are added at the top and bottom of the structure to provide supplementary reinforcement in case of a storm where the structure is yawed parallel to the wind direction.

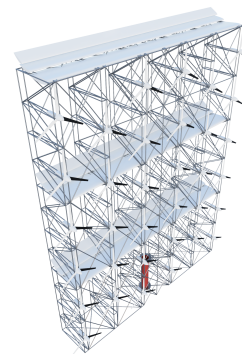
7.3.5. Integration of monopile-superstructure interface and RNA

Lastly, the now fully assembled superstructure rests on jacks, which can adjust its vertical position. However, an interface is needed between the monopile that only provides clearance from the waterline as explained in subsection 5.4.7 and the superstructure which consists of thin truss elements. To achieve a good connection and load transfer, a so-called monopile superstructure interface was designed. This structure consists of a cylindrical tower section on which two external bearings are attached. The yaw motors can then also be attached to the outside of the tower section which remains fixed when the structure yaws. A very large inner gear can be attached to the bottom of the outer bearing and much smaller

It will also allow for the transport and installation technique described in section 7.4. Once built, this junction piece can simply be assembled to the rest of the superstructure by rising the stacked the latter and sliding the connection piece in from the bottom. When placed inside the superstructure, the interface must be connected to the superstructure. This is done using 12 I-beams with a very large cross-section which are ideal designed to bear the tremendous weight and induced bending moment.



(a) Integration of the monopile-superstructure interface



(b) Full superstructure with all RNA's installed and monopile-superstructure interface

Lastly, all the RNA can be installed in the superstructure using the onshore facilities. This will help save considerable amounts of time and thus resources compared to installing them offshore. One must however be aware that the latter option is technically feasible using the internal elevator and platform systems in order to bring the drivetrains in the right place and the outside crane to attach the rotors. This last step of the assembly procedure yields a structure similar to what is displayed in Figure 7.4b.

7.4. Transport & Installation

The installation of the ReWind Turbine can be divided into two parts: the foundation installation and the fully assembled superstructure installation. The foundation installation includes driving the monopile into the ground, installing the underwater segment and lastly installing the clearance segment that will be capable of housing the tower interface.

7.4.1. Monopile & Bearing Installation

The monopile installation for the ReWind Turbine will be divided into three parts. The first part involves driving the lower straight section of the monopile into the seabed. Subsequently, the tapered underwater section that was sized in subsection 5.4.7 is installed on top of the foundations. Finally, the third portion of the monopile will be installed up to the water clearance height at 25 [m] height, where the superstructure will be positioned.

The installation process begins with the monopile being transported to the dock and loaded onto the vessel. The vessel, equipped with a powerful crane for lifting and positioning the monopile vertically, is stabilized by a dynamic positioning system. This system ensures precise positioning over the designated installation location. The lower section of the monopile is then carefully lowered into the water, with a gripper ensuring vertical alignment as it is lowered to the seabed. A hydraulic or vibratory hammer is subsequently used to drive the monopile 70.32 [m] into the seabed, securing it firmly in place. It is important to note that to ensure an optimal functioning of the hammer it will not work below sea-level. Therefore, a dummy section of equal diameter and thickness will be placed on top of the lower monopile section as to not deform the tapered part of the monopile.

For this task, the DEME Orion vessel¹³ can be used. The Orion, which is 216 [m] long and 49 [m] wide, is equipped with a crane boasting a 5000-[t] lifting capacity and can lift up to 160 [m] in height. Additionally, the vessel has a capacity of 30,000 [t], allowing it to install several monopiles in one trip, thereby speeding up the installation process.



Figure 7.5: DEME Orion Vessel for XXL monopile installation

After the lower section of the monopile is installed, the tapered underwater section of the monopile can be installed. This underwater section is carefully aligned over the foundation and slides into a male-female connection system. This will ensure a proper structural integration of the monopile.

7.4.2. Float-Over Topside Installation

The float-over installation process to lay the superstructure over the monopile consists of several consecutive stages as explained by Qin et al. [62]. Initially, in the load-out stage, the integrated topsides constructed at the quay are placed onto the transportation barge's deck using a skidway and then transported to the vicinity of the monopile foundation using tugs or self-propelled barges. In the pre-mating stage, the barge is positioned near the monopile using mooring lines and attached with lash lines, while fenders are prepared to assist in load transfer. During the mating stage, the barge approaches the monopile. Deck Support Units are used to support the topsides and absorb impact loads. The superstructure-monopile interface on the topsides is aligned with the monopile, and the topsides are transferred onto the monopile foundation using the tide-ballast system, or an active jacking system. In the post-mating stage, once the topsides' weight is fully transferred onto the monopile, the barge is further ballasted down to create sufficient clearance between the superstructure interface and the monopile before being towed away.

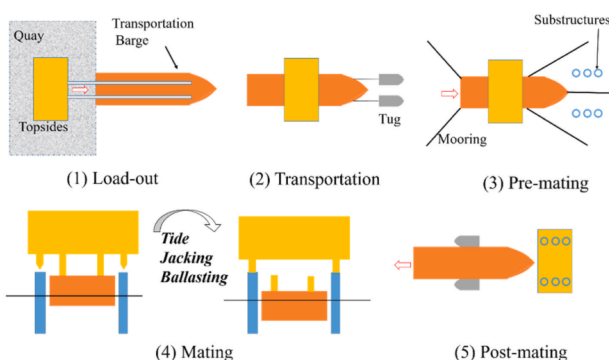


Figure 7.6: Float over phases [62]



Figure 7.7: Dual vessel float over installation [63]

In the context of float-over installation for offshore wind turbine structures, the dual vessel method becomes the necessary choice due to the substantial size of the structures involved. This approach is effectively illustrated

¹³<https://www.deme-group.com/technologies/orion> [Accessed 28-05-2024]

in Figure 7.7. To execute this method, the vessels must be equipped with a suitable transfer system

A passive transfer system relies on natural forces such as tidal movements and the ballasting system of vessels to position structures. One example is the HIDECK technology [62], which uses a non-mechanical method to transfer topsides onto substructures by increasing the draft of the barge along with the tide. In this process, the topsides and the barge move down together, maintaining constant gaps between the barge deck and the topsides. However, this approach requires a significant elevation of the topsides before mating to ensure they can span the substructure. While cost-effective, this method is highly dependent on environmental conditions, which can reduce precision and reliability.

In contrast, an active transfer system employs specialized equipment and technology to actively control the positioning and alignment of structures. This method offers higher precision and reliability, as it is less affected by environmental factors. However, it generally incurs higher costs due to the need for specialized equipment and increased operational expenses. In the active method, topsides are lifted and lowered using mechanical systems such as hydraulic jacks. The load transfer of the topsides primarily relies on these mechanical systems, sometimes assisted by ballasting and tidal movements.

In the table below a trade-off between the two methods is performed. The precision and the reliability are the most important criteria and thus are awarded respectively a weight of 0.4 while the cost has a relatively low weight of 0.2 considering they are one-off costs.

Table 7.3: Comparison of Active vs Passive transfer methods

Option \ Criteria	Precision (0.4)	Cost (0.2)	Reliability (0.4)	Total
Active	High precision control 5	Costly specialised equipment & higher operational costs 1	Less dependant on tidal conditions 4	3.8
Passive	Highly dependant on tidal conditions 2	Only ballasting system required 4	Highly dependant on tidal conditions 1	2

From the trade-off table, it can be seen that the active transfer system is preferred for this large installation. The enhanced precision and reliability offered by the active method are crucial for managing the significant size and complexity of the topside structure.

7.4.3. End of Life

Decommissioning refers to the comprehensive measures undertaken to restore a site as closely as possible to its original state, typically after a wind turbine's operational lifetime, assumed to be 25 years (REQ-MIS-01) [58]. It's imperative to consider and plan decommissioning early in the project lifecycle to mitigate potential additional costs during this phase. However, complications can arise due to various factors, such as geopolitical events or technological advancements, leading to significant variations in the Levelized Cost of Energy (LCoE), which ultimately determines whether a wind farm needs to be decommissioned [64]. These variations could necessitate major changes in the initial project plan.

Regulations regarding dismantling vary, with international and EU laws generally offering flexibility rather than stringent guidelines. However, the OSPAR convention [65], which involves several European nations including the Netherlands, sets certain standards. While European and International laws do not prescribe specific protocols for decommissioning, OSPAR dictates the removal of all added structures with a mass of over 4000 [t]. Yet, it acknowledges exceptions where removing certain structures may pose a greater environmental threat than leaving them in place. Consequently, countries and operators may make informed decisions balancing environmental conservation with decommissioning requirements.

According to Topham [66], before embarking on decommissioning, most providers explore opportunities for "repowering" or "refurbishing" turbines. Repowering entails replacing older turbines with newer, potentially more powerful models, while refurbishment involves upgrading minor components like blades, motors, or generators. Anticipating these options from the outset of the design phase is crucial to capitalize on potential efficiencies and performance enhancements. As mentioned in the requirements list [58], the blades and AFC-systems of the multi-rotor system will be designed to be replaceable [REQ-SSYS-ROT-05, REQ-SSYS-AFC-04], ensuring refurbishing remains an option.

During decommissioning, efforts are made to minimize on-water disassembly of the turbine, contingent upon technical feasibility and transportation logistics. This approach aims to reduce on-water handling operations,

which are more efficiently conducted on land, while also mitigating the risk of fluid spillage that could harm the marine environment. The decommissioning will happen onshore after the turbine is removed using a floatover deinstallation, employing the same principle as for the installation. If the foundation is in good health, repowering can occur, with a new updated model placed on top of the existing monopile using the same installation method.

Alternatively, foundation dismantling presents two primary options: partial cutting of the foundation to a certain depth, leaving it in situ, or complete removal. While the former is often preferred for reduced risk and environmental disturbance, this project prioritizes the full removal of the monopile. This decision is rooted in the project's overarching goal of optimizing the North Sea's limited space for future turbine deployments. Partial cutting could hinder future wind farms. Utilizing a pump system to apply pressure internally facilitates the full removal process with minimal environmental impact compared to traditional excavation methods [67, 68]. If feasible, cutting off the foundation base, where marine habitat has likely developed, allows for seabed preservation without impeding future constructions.

Similar methods are employed for dismantling the electrical substation, ensuring a systematic and environmentally conscious approach. However, sub-sea cable dismantling poses unique challenges due to potential seabed damage [66]. Leaving cables in situ is often deemed the best option, except in cases where they obstruct other infrastructure or vessel navigation, necessitating costly excavation or cutting procedures, with environmental impact carefully weighed against operational needs.

8. Operations

The operation phase of the wind farm is of great importance since, during this phase, the energy of the wind farm is produced. The operations involve various aspects with complex interactions that must be taken into account throughout the design. This chapter will dive into these operational aspects and scenarios encountered throughout the lifetime of the wind farm. It outlines the strategies, components and sensors necessary for effectively managing these scenarios and explores the relationship between operations and control systems.

The data sensors required for operations will be elaborated upon in section 8.1. Following, a data handling block diagram will be presented in section 8.2. Hereafter, a communication block diagram is shown in section 8.3. In section 8.4, the main phases during operation will be discussed. Afterwards, the power generation control strategy is traded off and explained in section 8.5. Lastly, the active flow control operations will be explained in section 8.6 and the operations during storm conditions will be discussed in section 8.7.

8.1. Data Sensors

For monitoring and responding to environmental changes or physical inputs during operation, sensors are needed. It is imperative also to provide a wind turbine with an array of sensors in order to identify possible problems and prevent structural failures. The different types of sensors that are mounted on the ReWind wind turbine are presented in Table 8.1, along with their respective functions. Furthermore, the specific sensor that is readily commercially available and is able to withstand the harsh offshore environment is added between brackets.

Table 8.1: Data Collection Sensors

Sensor Type	Function
Anemometers (<i>KRIWAN INT10 OF</i>)	Measure wind speed at various heights
Wind Vanes (<i>KRIWAN INT30 OF</i>)	Measure wind direction at various heights
Wind Gust Sensors (<i>Onset S-WSET-B</i>)	Detect sudden changes in wind speed
Torque Sensors (<i>FUTEK TRS605</i>)	Measure the torque exerted on the shaft of each drivetrain
Accelerometers (<i>Brüel & Kjær Vibro AS-247</i>)	Monitor vibrations within the turbine, especially for the tower
Thermometers (<i>Senmatic PTR</i>)	Monitor temperatures of various components in areas prone to overheating: power electronics, generator windings, gear-boxes, and bearings
Wave and Tide Sensors (<i>Aanderaa SEA-GUARD Wave & Tide Sensor 5218</i>)	Monitor conditions of the ocean to assess the loads the monopile has to withstand
Yaw Position Sensors (<i>Leine Linde 600 YAWMO</i>)	Monitor yawing movement at the yaw bearing
Pitch Position Sensor (<i>Leine Linde 600 YAWMO</i>)	Monitor the pitch of the blades of each rotor
Generator Voltage and Current Sensors (<i>Hangzhi AIT high precision current sensor</i>)	Measure electrical output of each generator
Rotor Speed Sensors (<i>Leine Linde MRI2850</i>)	Measure the rotational speed of the shafts for each rotor
Ice Detection Sensors (<i>New Avionics Ice*Meister</i>)	Detect ice accumulation on blades
Rain Sensors and LIDAR Scanners (<i>Vaisala WindCube</i>)	Map wind and rain characteristics
Cameras (<i>TechnoVideoCCTV</i>)	Monitor cracks and fatigue damage on the monopile and truss structure
Strain Gauges (<i>HBM Strain Gauges</i>)	Measure strain on turbine components
Oil Condition Sensors (<i>DES-CASE Oil Quality Sensor 2</i>)	Monitor the condition of oil at each gearbox
Fire Detection Sensors (<i>Hochiki ESP Fire Detection System</i>)	Detect smoke or fire in the turbine, especially near components such as the drivetrain or yaw motor

Sensor Type	Function
Humidity and Pressure Sensors (<i>Vaisala PTU307</i>)	Measure atmospheric conditions
Lightning Sensors (<i>Vaisala LS7001</i>)	Detect and improve performance in case of lightning strike
Acoustic Sensors and Microphones (<i>PAC-R61-AST</i>)	Monitor noise levels and detect mechanical malfunctions
ACFM Sensors (<i>Sensu 2 Probe</i>)	Detect surface-level cracks on conductive surfaces such as the truss structure and blades
Battery Health Sensors (<i>Efftronics Battery Health Monitoring System</i>)	Monitor the status and performance of energy storage systems
Converter and Inverter Sensors (<i>ABB PCS6000</i>)	Monitor the performance of power conversion systems

8.2. Data Handling Block Diagram / HW-SW

The efficient handling of the data from the sensors is crucial for the optimal performance and maintenance of the wind turbine. The information collected by the various sensors specified in section 8.1 must be processed and analyzed systematically. Consequently, Figure 8.1 presents a detailed data handling block diagram, illustrating the flow of data from the sensor to the location it should be implemented. By understanding this process, the turbine can operate closer to peak efficiency, anticipate maintenance needs, and adapt to changing environmental conditions. As a basis, the sensors will collect data at a rate of 20 [Hz], although this value may change for specific sensors at a later stage in the design phase. As can be seen under Figure 8.1, all the sensors indicated in yellow boxes are feeding data to their corresponding systems. Here, the health monitoring and the thermal control systems relate back to the main controller together with the data from the wind sensors, which then determines the state of the turbine. This can then deliver the necessary control inputs into the yaw, rotor and AFC systems. Next, together with data from two more sensors, these systems are able to output maximum power point tracking (MPPT) through pitch regulation to generate as much power as possible. Finally, the required outputs from the turbine can be delivered, such as the pitch angle (theta command) and the maximum power point (omega optimum). These are then fed back into the controller, which recalculates the necessary adjustments in turbine attitude to achieve the desired improved efficiency.

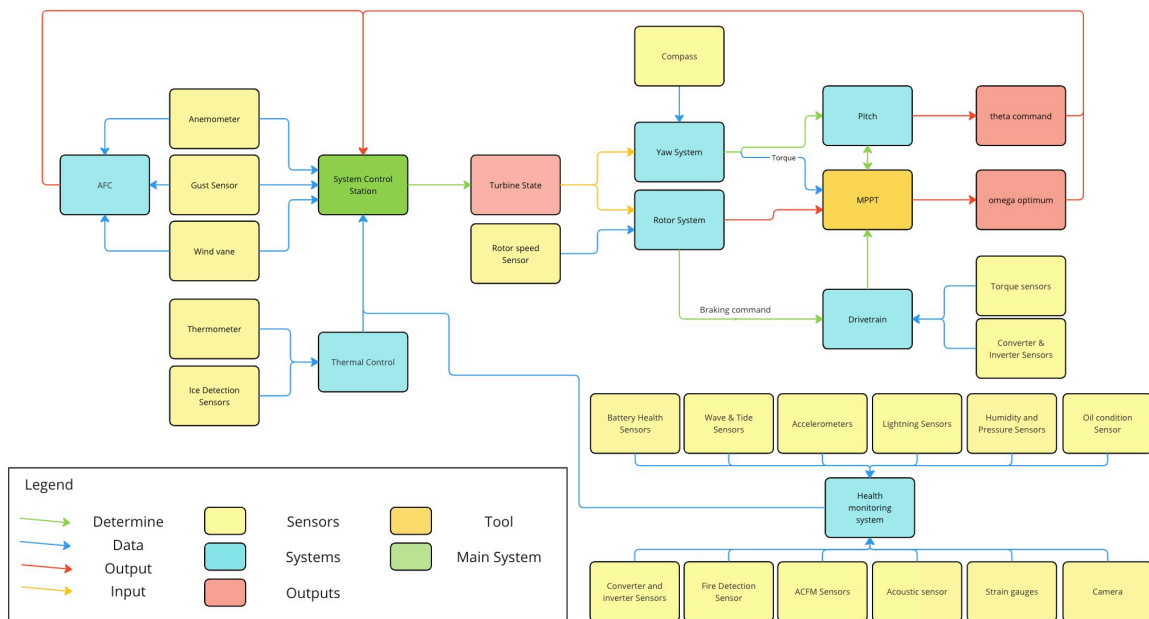


Figure 8.1: Data handling diagram.

8.3. Communication Block Diagram

The flow of communications on a wind farm level is important to ensure stable operations and seamless integration with the outside environment. A wind farm communication block diagram was made to visualise the communications. This diagram is presented in Figure 8.2. This diagram describes the flow of information from

each individual turbine to the central control system and vice versa. The data communication occurs parallel to the data acquisition processes in the wind farm. This process can be explained as follows:

- **Wind turbine unit** - at each turbine, there is a series of sensors, presented in Table 8.1, acquiring data. This data is collected and processed in the Remote Terminal Unit (RTU). To transfer this data, a fibre-optic network is used, which requires the data first to be converted into the correct format by using an Optical Network Unit (ONU). Each wind turbine unit also contains a Wind Turbine Controller (WTC), which processes control inputs to the unit and distributes them according to Figure 8.1. The fibre optic network could be replaced entirely or partially by a wireless communication network in the future if needed, but this would not change the basic architecture outlined here.
- **Tier 3: Wind farm zone** - to minimize the cable length of the wind farm, the wind turbines are connected to one another in groups. Each group is interconnected using a ring to ensure redundancy in case there is a failure in one of the cables. Each ring is then connected to the off-shore wind farm control station. This architecture allows the majority of fibre-optic cables to be routed along the power cables, simplifying the installation of the network.
- **Tier 2: Collector-Transmission zone (off-shore station)** - at the offshore station, the Supervisory Control and Data Acquisition (SCADA) system can be found. The role of the SCADA system is to integrate individual turbine units with the substation and power transmission elements of the wind farm. It allows centralised access to wind farm data, and for the distribution of centrally generated control inputs.
- **Tier 1: On-shore remote station** - the on-shore, central control station generates control inputs for wind farm operations based on data collected through the SCADA system. Additionally, the central control system is responsible for distributing data to external services and suppliers and storing data on external servers.

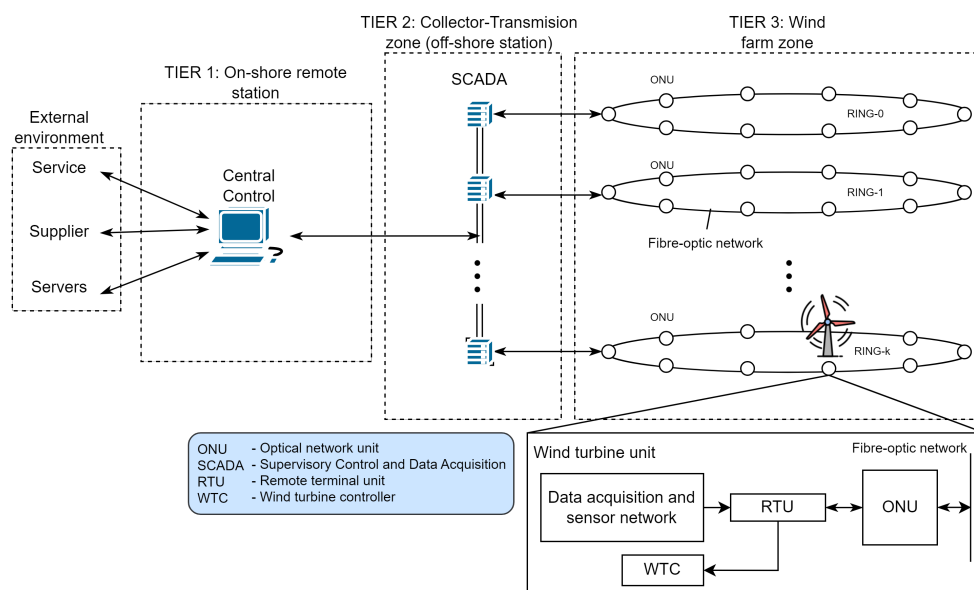


Figure 8.2: Wind farm communication block diagram for k different cascaded turbine rings.

8.4. Operation Phases

Next, the typical operation of the turbine will be explored. The main phases during normal operations of a wind turbine can be broken down into the following:

- **Parking** - During this phase, the turbine is non-operational. This may occur under several conditions, such as scheduled maintenance, extreme weather conditions (like storms), or when wind speeds fall below the cut-in speed or exceed the cut-out speed. The turbine blades are pitched to reduce wind resistance and minimise mechanical stress and then locked using the brakes. The yaw brakes are also applied in order to prevent the structure from rotating.
- **Start-up** - The start-up phase is initiated when wind speeds surpass the cut-in speed. The turbine's control system releases the brakes and adjusts the blade pitch to capture wind energy. This phase involves careful monitoring to ensure a smooth transition and prevent mechanical stress.

- **Power Generation** - This is the primary operational phase where the turbine generates electricity. The power generated by the rotors is converted to a suitable voltage and frequency for grid compatibility using a transformer and power electronics. Active control systems adjust the blades' pitch and the system yaw to optimise energy capture. During this phase, real-time data on wind conditions, turbine performance, and energy output is continuously monitored.
- **Braking** - in case the wind speed falls out of the range of operational wind speeds, or if there is a major failure of components, the yaw, pitch and drivetrain breaks are applied to stop the turbine.

Note that these are not all the possible operations the wind turbine might have to perform during its lifetime. For example, if the cable twist exceeds the maximum available value, the turbine will have to yaw to untwist the cables. This type of very specific operation cases will not be explored in further detail at this stage of the design but should be considered at a later stage.

The appropriate operational phase for the turbine at a given point in time is determined by the current conditions. These conditions can be monitored using the sensors listed in Table 8.1. To assess the desired turbine's state, a single-unit stateflow machine, as illustrated in Figure 8.3, can be utilized.

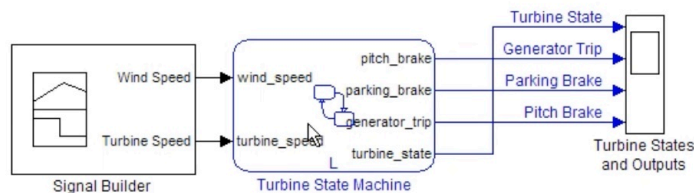


Figure 8.3: A single unit stateflow machine

In this figure, the signal builder, described in the data handling block Figure 8.1, provides the wind speed and turbine speed collected from a number of sensors. These values are then fed into the turbine state machine. The stateflow model within this machine determines the current state of the unit, manages transitions between states, and specifies which subsystems should be activated or deactivated. This then provides a series of outputs and turbine states. This is an event-based controller which is modelled using Stateflow in Simulink (MATLAB).

The turbine state machine follows a supervisory control model as shown by Figure 8.4:

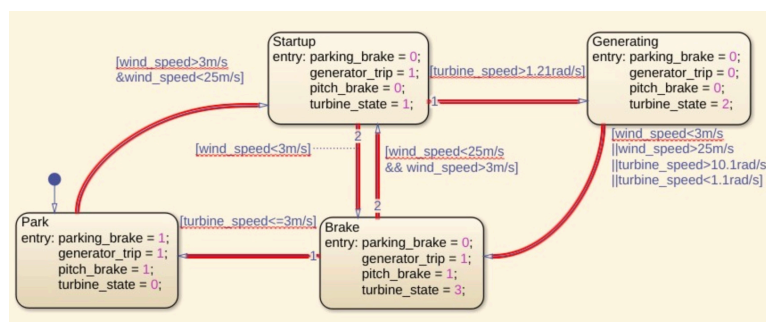


Figure 8.4: Supervisory Control Model [Simulink MATLAB]

This model demonstrates that the "park" state occurs when the wind turbine is not rotating, the park brake is engaged, the pitch brake is disengaged, and the generator is disconnected from the grid. This state is directly linked to the start-up phase, which begins once the average wind speed exceeds the cut-in wind speed (3 m/s) but remains below the cut-out speed (25 m/s). During start-up, the park brake is released, though the generator remains disconnected. When the turbine speed reaches a specified range, it enters the generating state, where the generator is activated. The turbine spends most of its time in this state. If wind speeds become excessively high or too low, or if the turbine speed varies significantly, the unit transitions to the brake state and subsequently either returns to the park state or re-initiates start-up.

8.5. Power Generation Control Strategy

In order to meet the desired power production goals for the wind farm, each individual turbine should maximise its energy generation. This can be achieved by using Maximum Power Point Tracking (MPPT). MPPT is a technique employed with variable power sources to optimize energy extraction as conditions change, namely from the cut-in to the rated wind speed. However, there are numerous methods which can be employed to do so. The trade-off shown in Table 8.2 has been performed to motivate the chosen MPPT methodology.

Table 8.2: Description of the structural trade-off results [69]

Criteria	Grid Stability (0.4)	Wind Applicability Range (0.2)	Scalability to Large Units (0.4)	Total
(1) Hill Climb Search (HCS)	2 Slow response under rapid wind change, incorrect direction detection in large/medium WTs.	5 Excellent performance under varying wind conditions, high flexibility.	2 Causes stalling in smaller WTs, less suitable for large units due to slow response.	2.6
(2) Optimum Relation Base (ORB)	3 Does not track exact maximum power point under rapid wind changes.	4 High accuracy and efficiency in maximum wind power tracking.	3 Inability to track exact maximum power point under rapid wind changes limits scalability.	3.2
(3) Incremental Conductance (INC)	4 Increased system stability, reduced costs.	2 High instability under a variable speed wind condition.	3 Easy implementation, can handle non-linearity, making it moderately scalable.	3.2
(4) Power Signal Feedback (PSF)	4 Provides robust and cost-effective control, but low efficiency under varying wind conditions.	3 Low efficiency under varying wind conditions.	4 Simple to use, fast convergence speed makes it highly scalable.	3.8
(5) Optimal Torque Control (OTC)	3 Provides robust control but lacks direct wind speed measurement.	3 Complex, high efficiency.	4 High efficiency, fast convergence speed makes it highly scalable.	3.4
(6) Tip Speed Ratio (TSR)	2 High efficiency and performance, optimal point determination is theoretical or experimental.	3 High efficiency and performance with fast convergence speed.	1 High cost of operation for small WT systems, precise wind speed measurement is impossible.	1.8

From Table 8.2, the Power Signal Feedback (PSF) method yields the highest score, making it the most suitable to maximise the power generation of the turbine between the cut-in and rated wind speed. This method outperforms the others thanks to its robust and cost-effective control, as well as its simplicity and fast convergence speed which make it highly scalable.

Electrical diagram

Next, the electrical system is addressed in further detail. The electrical power generation mechanism of the ReWind wind farm follows a complex process. The following diagram (Figure 8.5) gives a schematic overview of how the electrical system is organized on different levels, ranging from the generator to the entire wind farm.

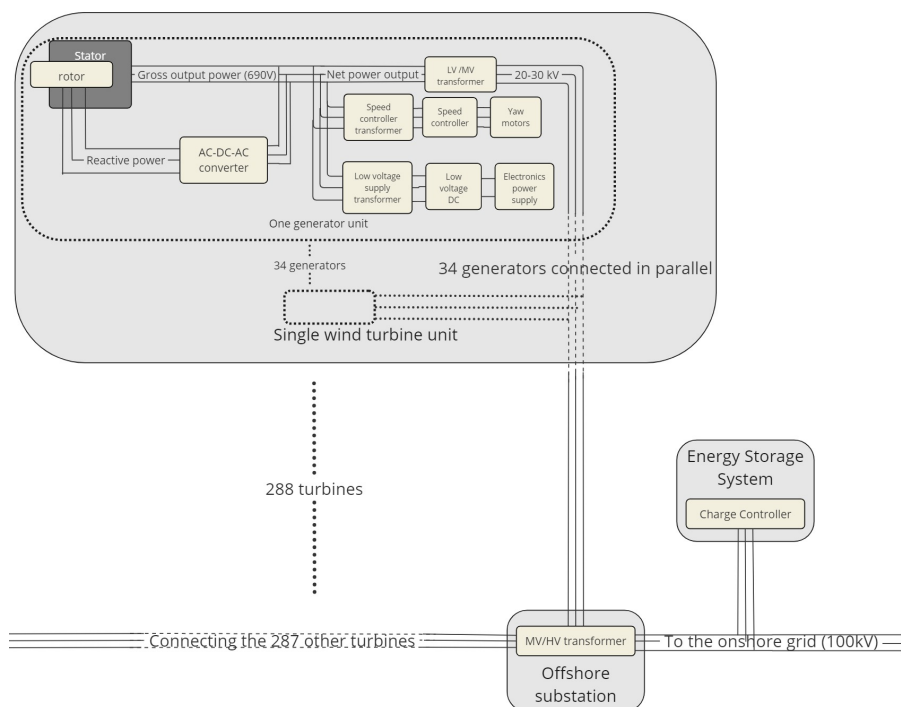


Figure 8.5: Electrical diagram of the wind farm

Firstly, on the lowest sublevel, the generator produces three phase AC power at the same frequency as the grid. However, due to the intrinsic working principle of the DFIG generator, the rotor windings need to be fed with AC current at a frequency depending on its own rotational rate. Therefore, a loop is implemented with the AC-DC-AC converter regulating the frequency fed to the rotors, in a subsynchronous case or fed from the rotor to the grid in a supersynchronous case.

Subsequently, some of the power outputted by each of the generators at a voltage of 690 [V] goes through two different transformers, providing power to the yaw motor on the one hand and to the turbine control electronics on the other. The former needs to step the voltage of the generator down from 690 [V] to 425 [V], as the independent supplies from each generator then get connected in parallel to the 6 yaw motors. The power electronics transformer steps the 690 [V] down to a much lower voltage that will have to be determined later and subsequently converts the AC current to Direct Current (DC) as to provide power to the various control subsystems.

All of the net output power of each generator then goes through a low-voltage to medium-voltage transformer, as to minimize losses when transporting the power to the offshore substation. A typical range of medium voltage values for the in-situ transportation of electricity in a wind farm is between 20 and 30 [kV] [70]. All 34 generators in a single turbine unit are connected in parallel at the bottom of the turbine before the power is sent to the offshore substation. There, all power lines from the 288 turbines come together and the current goes one last time through a medium-voltage to high-voltage (roughly 100 kV [70]) transformer before sending the power back to the shore where it can be distributed in the grid. Alternatively, the energy can also be stored in the energy storage system if the production exceeds the instantaneous demand of the grid. The choice was made to perform the power transportation with AC current instead of High Voltage Direct Current (HVDC), as a distance of 50 [km] barely reaches the cost break-even point for HVDC. However, converting AC to HVDC would add a lot of unnecessary complexity to the system.

8.6. Active Flow Control Operations

A distinctive feature of ReWind's turbine is the implementation of Active Flow Control (AFC) devices. These devices are essentially wings positioned behind the rotors that re-energize the airflow. Each wing consists of three sections that can move relative to each other using actuators, altering the amount of lift and drag they generate. These relative motions are based on specific inputs collected by anemometers, wind vanes and wind gust sensors distributed along the span of the turbine, as specified in Table 8.1. The movement of these sections is adjusted differently depending on the wind conditions to optimize performance.

Firstly, during low to moderate wind conditions, the retractable elements can be extended to enhance the lift-to-drag ratio. This will increase the amount of vortex generation and thus increase the power output of the turbines in the turbine's wake. As wind speeds increase to high levels where structural loads might become a concern, the elements can be retracted to reduce potential stress and avoid over-speed conditions. Subsequently, the deployment of these elements can be coordinated by adjusting the blade pitch. At lower wind speeds, the pitch angle can be decreased to capture more wind energy and extend the elements to maximize lift. As wind speeds escalate, the pitch angle can be increased and the elements retracted to maintain optimal turbine performance and minimize load.

For future design development, a program can be implemented to automatically retract the elements in response to sensors detecting extreme wind speeds or vibrations. This automated control system will help safeguard the turbine structure from potential damage.

8.7. Storm Condition

The most extreme conditions the wind turbines will be subject to will be during storms. Here, the system must be appropriately designed and prepared for the expected higher wind speeds. As seen in Figure 8.6, the power output of a turbine varies with the wind speed. At the turbine's rated wind speed, the turbine has achieved the rated power and is therefore producing at its maximum efficiency. The power being generated remains constant until the cut-out speed by adjusting the thrust the rotors generate. After the cut-out speed of 25 [m/s], all systems are shut off in order to prevent unnecessary strains on the generator and rotors¹.

Consequently, during storms, the turbine must be prepared for the varying winds. Where, both wind speed and direction are expected to rapidly fluctuate. Thus, different aspects are modified to adapt to this scenario. During normal operation, the turbine's yawing movement is performed using the motor system and the differential pitching option up to the cut-out speed. Once this velocity has been achieved, the yaw system is shut down and the blades can be feathered, i.e. turn into the wind to reduce their surface area and reduce unnecessary

¹<https://www.energy.gov/eere/articles/how-do-wind-turbines-survive-severe-storms> [Accessed 28-05-2024]

loads footnote 1. The structure will be oriented to minimise its frontal area with respect to the wind, meaning it will be yawed before the storm so that it is parallel to the prevailing wind direction. This will protect the turbine from unnecessary damage and extend its operational lifespan.

Secondly, to enhance turbine performance in storm situations, weather forecasts are analyzed to determine the optimal positioning of the turbine in advance. By anticipating the direction of the incoming wind, the yaw system can be activated to preemptively orient the turbine accordingly. This proactive adjustment ensures that the turbine is optimally positioned, minimizing the yawing required just before the storm hits. This strategic approach helps reduce damage on the turbine by reducing the need for frequent adjustments during rapidly changing weather conditions.

To effectively manage storm conditions, the placement of multiple anemometers at different heights on the wind turbine is recommended. Given the variation in wind speeds across different rotor levels, these anemometers provide important data for adjusting turbine operations accordingly. During storm events, turbines should employ a curtailed shutdown strategy where upper rotor levels are deactivated first, followed by lower levels. This staggered approach minimizes sudden load changes and ensures smoother transitions during shutdown phases. Given the size of the wind farm, a coordinated approach is essential. Each turbine's shutdown sequence should be carefully orchestrated to avoid grid instability. Considering that each turbine can generate up to 30 MW, the cumulative effect on the grid must be managed through phased shutdowns across the wind farm. This strategy mitigates potential disruptions to power transmission and distribution systems.

Lastly, the AFC system offers additional capabilities during storm conditions. AFC systems can reduce their pitch angle to lower their flow regeneration capabilities, effectively slowing down wind speeds and thereby reducing the need for complete turbine shutdowns. By moderating wind flow rather than halting energy generation entirely, turbines positioned in the middle of a wind farm can continue operating longer, contributing to sustained energy production during adverse weather.

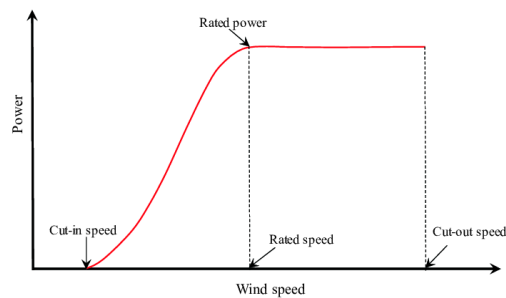


Figure 8.6: Change in wind turbine power production with varying wind speed [71]

9. Reliability, Availability, Maintainability and Safety

To assess the feasibility of ReWind’s design, the Reliability, Availability, Maintenance and Safety (RAMS) of this project has to be examined. These aspects are critical for the success of the project, as Operations and Maintenance (O&M) costs (maintenance + downtime) account for up to 34% of total LCoE over a turbine lifetime [2].

The approach which will be taken in this chapter links the reliability and maintainability to give the theoretical availability. This can then be combined with the accessibility of the site, the maintenance strategy and the safety aspects to give the actual availability of the wind farm. This can be visualized in Figure 9.1, with the basic elements of RAMS being displayed in red.

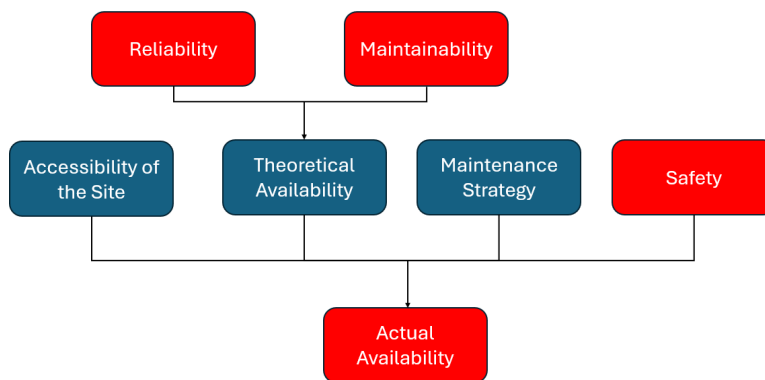


Figure 9.1: RAMS Strategy

9.1. Reliability

Reliability can be defined as: "Reliability is the probability that an item will meet its required function under the stated conditions for a specified period of time" [2]. In this case, reliability will therefore depend on the failure rate of the system. Failures need to be repaired, as they pose a major risk into the operations of the wind farm. The failure rate can be expressed as seen in Equation 9.1:

$$\lambda = \frac{\frac{\text{Total Number of Failures}}{\text{Turbine Population}}}{\text{Operating Period}} = \frac{1}{MTBF}, \quad (9.1)$$

where MTBF is the mean time between failures.

Different types of failures can be identified for ReWind’s project, namely: Major Replacement Failure, Major Repair Failure, Minor Repair Failure and Miscellaneous. The miscellaneous group includes failures in auxiliary components that support the functionality of other systems, such as lifts, ladders, hatches, door seals, and nacelle seals. A study carried out by Carroll et al. analysed and collected failure rates of components for over 350 offshore wind turbines over a five year period [72]. These turbines primarily consisted of single rotor 3 [MW] turbines [73]. This data is presented in Table 9.1.

Table 9.1: Failure Rate of Different Subsystems, in Failure/Unit/Year (original) [72]

Component	Major Replacement	Major Repair	Minor Repair	Miscellaneous	Total
Pitch Hydraulic	0.001	0.179	0.824	0.072	1.076
Other Components	0.001	0.042	0.812	0.15	1.005
Generator	0.095	0.321	0.485	0.098	0.999
Gearbox	0.154	0.038	0.395	0.046	0.633
Blades	0.001	0.01	0.456	0.053	0.52
Grease/Oil/Cooling Liquid	0	0.006	0.407	0.058	0.471
Electrical Components	0.002	0.016	0.358	0.059	0.435
Contactors/Circuit Breaker	0.002	0.054	0.326	0.048	0.43
Controls	0.001	0.054	0.355	0.018	0.428
Safety	0	0.004	0.373	0.015	0.392
Sensors	0	0.07	0.247	0.029	0.346
Pumps/Motors	0	0.043	0.278	0.025	0.346
Hub	0.001	0.038	0.182	0.014	0.235
Heaters/Coolers	0	0.007	0.19	0.016	0.213
Yaw System	0.001	0.006	0.162	0.02	0.189
Tower/Foundation	0	0.089	0.092	0.004	0.185
Power Supply / Converter	0.005	0.081	0.076	0.018	0.18
Service Items	0	0.001	0.108	0.016	0.125
Transformer	0.001	0.003	0.052	0.009	0.065
Total	0.265	1.062	6.178	0.768	8.273

Table 9.1 shows that minor repairs account for over 70% of all necessary repairs. This type of repair often requires less technicians and is of lower complexity, meaning that they can be carried out on a more frequent basis. When analysing specific components with the highest failure rates, it is easy to identify the most critical ones, namely: the pitch hydraulic system, generator and gearbox. These components should be addressed in further detail because they significantly impact the turbine's operational efficiency. For instance, the generator and gearbox alone account for 97% of all major replacements.

Firstly, the gearbox failure rate will vary from that of the reference 3 [MW] turbines. Gearbox failure rate is directly proportional on the gearbox ratio, GBR , as larger ratios require more sophisticated gearboxes. The necessary gearbox ratio for a rotor can be calculated based on the rated wind speed, V_{rated} , and tip speed ratio, TSR, and the rotor radius, R , while assuming an optimal rotational rate for a DFIG of 1500 [rpm] [74]. This relationship is expressed through Equation 9.2:

$$GBR = \frac{\omega_{DFIG}}{\omega_{rotor}} = \omega_{DFIG} \cdot \frac{R}{V_{rated} \cdot TSR} \quad (9.2)$$

For ReWind's rotors, the required gear box ratio is 54. For a reference 3 [MW] turbine, such as the Vestas V90-3.0, the required gearbox ratio is 83¹. This constitutes a reduction in gearbox ratio of 35%, which in turn reduces the failure rate of the gearbox by 35%, from 0.633 failures per year to 0.411 failures per year.

However, it should also be noted that the data was collected from the reference wind turbines over a decade ago. In recent years there have been great advancements regarding DFIGs, which has seen their reliability increase considerably. Therefore, the total failure rate of the generator subsystem was reduced by 30%, to account for these improvements, going from 0.999 failures per year to 0.699 failures per year.

Finally, the pitch system in ReWind's multi-rotor system not only regulates the amount of power which is produced, but is also responsible for the yawing of the structure through differential pitching. As a result, the pitch system is in use for a considerably higher amount of time than for conventional turbines, which will ultimately lead to higher failure rates. Based on the proposed operation, the structure will be yawed if the misalignment of the wind with the face of the turbine exceeds 5 [deg]. Based on the wind speed data presented in chapter 4, it has been calculated that wind speed changes by more than 5 [deg] for consecutive measurements approximately 25% of the time. Based on this data, it can be assumed that the failure rate of the pitch hydraulic system will increase by 50% as a first estimate, as compared to its use for conventional turbines.

¹<https://en.wind-turbine-models.com/turbines/603-vestas-v90-3.0> [Accessed 07-06-2024]

As mentioned previously, the turbines analysed by Carroll et al. primarily consisted of single rotor 3 [MW] turbines [73], meaning that the failure rates should be adapted for multi rotor systems. McMorland et al. present a procedure to convert these failure rates from a single rotor turbine to a multi rotor turbine [75], following the relationship in Equation 9.3.

$$F_{SR} = F_{MRS} = n \cdot F, \quad (9.3)$$

where F_{SR} represents the failure rate of the rotor nacelle assembly for a scaled-up single rotor turbine, such as a 30 [MW] turbine. In contrast, F_{MRS} denotes the failure rate of a 30 [MW] multi-rotor wind turbine. Using the turbines referenced by Carroll [72] as a baseline, F , each turbine is rated at 3 [MW]. Consequently, n is set to 10, indicating the number of 3 [MW] turbines needed to reach the total capacity of 30 [MW].

The scaled failure rates of the different subsystems are presented in Table 9.2. This also includes the relevant changes in failure rates to the generator, gearbox and pitch hydraulic system. Note that only the failure rates for the components which change for multi-rotor systems have been modified.

Table 9.2: Failure Rate of Different Subsystems, in Failure/Unit/Year (modified) [72]

Component	Major Replacement	Major Repair	Minor Repair	Miscellaneous	Total	Modified
Pitch Hydraulic	0.015	2.685	12.36	1.08	16.14	✓
Other Components	0.001	0.042	0.812	0.150	1.005	
Generator	0.655	2.212	3.342	0.675	6.883	✓
Gearbox	1.001	0.247	2.568	0.299	4.115	✓
Blades	0.010	0.100	4.560	0.530	5.200	✓
Grease/Oil/Cooling Liquid	0.000	0.060	4.070	0.580	4.710	✓
Electrical Components	0.020	0.160	3.580	0.590	4.350	✓
Contactors/Circuit Breaker	0.020	0.540	3.260	0.480	4.300	✓
Controls	0.001	0.054	0.355	0.018	0.428	
Safety	0.000	0.004	0.373	0.015	0.392	
Sensors	0.000	0.700	2.470	0.290	3.460	✓
Pumps/Motors	0.000	0.430	2.780	0.250	3.460	✓
Hub	0.010	0.380	1.820	0.140	2.350	✓
Heaters/Coolers	0.000	0.070	1.900	0.160	2.130	✓
Yaw System	0.001	0.006	0.162	0.020	0.189	
Tower/Foundation	0.000	0.089	0.092	0.004	0.185	
Power Supply / Converter	0.005	0.081	0.076	0.018	0.180	
Service Items	0.000	0.001	0.108	0.016	0.125	
Transformer	0.001	0.003	0.052	0.009	0.065	
Total	2.569	8.100	43.510	5.430	59.609	

The repair times for each component, also summarised by Carroll et al, are presented in Table 9.3. It can be seen that some repairs take a great amount of time, such as the replacement of blades, or the hub. These represent the repair times for each failure type, but of course do not consider how often the components fail.

Table 9.3: Average Repair Times for each subsystem failure type, in hours/failure, [72]

Component	Major Replacement	Major Repair	Minor Repair	Miscellaneous
Pitch Hydraulic	25	19	9	17
Other Components	36	21	5	8
Generator	81	24	7	13
Gearbox	231	22	8	7
Blades	288	21	9	28
Grease/Oil/Cooling Liquid	0	18	4	3
Electrical Components	18	14	5	7
Contactors/Circuit Breaker	150	19	4	5
Controls	12	14	8	17
Safety	0	7	2	2
Sensors	0	6	8	8
Pumps/Motors	0	10	4	7
Hub	298	40	10	8
Heaters/Coolers	0	14	5	5
Yaw System	49	20	5	9
Tower/Foundation	0	2	5	6
Power Supply / Converter	57	14	7	10
Service Items	0	0	7	9
Transformer	1	26	7	19

The repair rate can be expressed as seen in Equation 9.4:

$$\mu = \frac{\text{Number of Failures}}{\text{Repair Time}} = \frac{1}{\text{MTTR}}, \quad (9.4)$$

where MTTR is the mean time to repair.

Therefore, from Table 9.2 and Table 9.3, the theoretical availability, denoted by A_{TH} , can be obtained. This is equivalent to the hours per year the turbine is operating. This is presented in Equation 9.5

$$A_{TH} = 1 - \frac{\lambda}{\mu} \quad (9.5)$$

Therefore, to obtain the repair hours per year for each failure type, the values from Table 9.2 can be multiplied by those in Table 9.3. Then, summing all failure types, and dividing by 8760 hours in a year, the repair percentage can be obtained, and then the theoretical availability. For one single multi-rotor unit, the theoretical availability was estimated at 90.63%, meaning that it should be operational 90.63% of the time.

However, this approach assumes that every time there is a failure, a repair is made. While this is valid for conventional wind turbines, one of the main advantages of multi-rotor systems is their ability to continue producing close to full power even if some rotors fail. As one may expect, this will reduce the availability of the turbine slightly as it will not be working at full capacity at all times. However, thanks to the high number of rotors, this reduction in power generation is heavily offset by the benefits obtained by reducing the maintenance frequency.

To minimize maintenance needs, repairs will only be carried out if the power production of a single turbine unit drops below 90% of its full capacity due to component failures. For ReWind's design, this threshold is reached when 4 rotors fail out of 34. This strategy will substantially reduce the personnel and resources needed for wind farm maintenance, leading to significant cost savings and lower carbon emissions. To determine how long it will take for 4 rotors to fail, a statistical approach can be taken to model the failure rate, as described in subsection 9.1.1.

9.1.1. Failure Rate Modeling

Since ReWind's multi-rotor system does not require immediate repair when a single Rotor Nacelle Assembly (RNA) fails, condition-based maintenance is a viable strategy. This essentially means that maintenance interventions are planned only when the operational capacity falls below the threshold of 4 rotors. However, in order to determine the number of vessels and crew which must be employed at a given time, the time it takes for a RNA system to degrade to the specified capacity limit must first be estimated.

The failure rate of RNAs can be modelled using a Poisson distribution. This approach is suitable for modelling the number of failures occurring within a fixed interval of time, given a known constant mean failure rate and the independence of failures over time. Although this method does not account for the potential increase in failure rate due to wear and tear, it provides an initial estimate for planning purposes. Furthermore, when maintenance is performed to repair faulty components, the other RNAs in the turbine can also be checked to ensure they have not deteriorated over time. This approach combines condition-based and predictive maintenance, enhancing the overall reliability and longevity of the system. The Poisson distribution is described as:

$$P(X = k) = \frac{\lambda^k e^{-\lambda}}{k!}, \quad (9.6)$$

where λ represents the average failure rate.

It was assumed that the RNA fails when any one of its components fails, as this would stop the RNA from producing electricity. Consequently, the average failure rate for an RNA is the sum of the failure rates of its individual components. Furthermore, it is worth noting that, as shown in Table 9.2, the failure rates of components outside the RNA system are almost negligible, accounting for only 4% of total failures. Therefore, at this stage of the design, these failure rates were also included during the RNA failure analysis as a conservative assumption. Mathematically, if the failure rates of the individual components are $\lambda_1, \lambda_2, \dots, \lambda_n$, then the total failure rate λ_{RNA} is given by:

$$\lambda_{\text{RNA}} = \sum_{i=1}^n \lambda_i \quad (9.7)$$

Given the total failure rate, it is crucial to determine the time t at which the probability of a specified number of RNA failures exceeds 0.99. For instance, with 34 RNAs and a failure rate of $\lambda = 0.2011$, the goal is to find the time t at which the probability of at least 4 RNAs failing is greater than 0.99

Using the Cumulative Distribution Function (CDF) for the Poisson distribution, the following condition was set up to determine t :

$$P(X \geq 4) > 0.99 \implies P(X < 4) < 0.01 \quad (9.8)$$

The cumulative probability $P(X < 4)$ is given by:

$$P(X < 4) = P(X = 0) + P(X = 1) + P(X = 2) + P(X = 3), \quad (9.9)$$

where each term is computed using the Poisson Probability Mass Function (PMF):

$$P(X = k) = \frac{e^{-\mu} \mu^k}{k!}, \quad (9.10)$$

with $\mu = 34\lambda t$. Solving Equation 9.10 for t yields to $t = 2.02$ months. This translates into having to perform maintenance on each turbine unit every 61 days. Therefore in order to keep the nominal capacity for the farm always greater than 90%, the number of turbines to be maintained every day is $\lceil \frac{288}{61} \rceil \approx 5$. Assuming each boat performs a single maintenance a day and including contingencies for 20% of the time due to storm conditions or logistical issues, this leads to 6 vessels being required each day.

Furthermore, another strategy which could be implemented to further reduce the maintenance frequency is to over-dimension components. If the system was to be oversized through the use of larger, more resistant components, the following number of vessels which should be employed is the following:

Table 9.4: Number of maintenance and time between two maintenance for different failure rates

Failure rate of RNA per month	Days between maintenance	# maintenance on farm per day
Baseline = 0.14	60	4.8
0.9 * Baseline	70	4.10
0.8 * Baseline	76	3.79
0.5 * Baseline	127	2.26

From this table, it can be concluded that over sizing the system's components can positively impact maintainability and consequently costs. A decrease of the failure rate of 20% leads to around 15% less number of interventions. This effect is further enhanced as failure rates continue to decrease.

Consequently, based on this failure rate analysis, a new theoretical availability can be calculated assuming no repairs are done if at least 31 of the 34 rotors are still functioning. Based on this maintenance strategy, the new theoretical availability is 87.8%. It should be noted however, that with ease of accessibility and effective safety standards, this number can be increased as will be explored in section 9.2.

9.2. Accessibility of the Site

Performing any sort of maintenance on the wind turbine requires a series of accessibility options that allow the workers to perform their work safely and effectively. Thus, the wind turbine is built with a system of horizontal platforms that reach all the rotors present in the turbine. Furthermore, an elevator is installed running along the center tower to provide vertical accessibility, as well as a ladder as a backup option. At each row, the platforms extend outwards at the level of the rotors until the last turbine, simulating the shape of a tree and its branches. In addition, a visual representation is shown under Figure 9.3 to depict the platforms set up in the multi-rotor wind turbine.

Furthermore, an electric hoist pulley system is installed at the top of the truss structure that can move along its width such that it is able to deliver all the necessary parts to their required place. This is installed during the assembly process of the turbine and is used as a way of lifting heavy objects. In effect, this tool can be applied during the installation of the rotors and for any maintenance job that requires a replacement of a blade, turbine or any other heavier object. Furthermore, it is also used to lift and descend the elevator that runs up the truss structure as depicted in Figure 9.4.

During any maintenance work, the crew must be able to reach the wind farm site in an effective and quick manner. To do so, a selection of the transportation methods is performed. Firstly, the town of Den Helder in the province of North Holland is chosen as the center of operations due to its port. In effect, this port is the closest to the selected wind farm site of Lagelander at around 45 [km] (24,3 [nm]) from the closest point and 86.5 [km] (46,7 [nm]) from the furthest point of the site. These values can be used for the selection of the maintenance strategies in relation to the chosen vessel used to transport the workers.

In the current industry, different kinds of vessels are used to perform maintenance in offshore wind farms, these include: helicopter, Crew Transfer Vessel (CTV), Service Operation Vessel (SOV) and Jack Up Vessel (JUV). CTVs are small boats that travel to the site, perform maintenance tasks, and then return to port in a single trip. Thus, they are restricted to a maximum of 50 [nm] from the shore [76]. Furthermore, they are usually able to transport up to 12 passengers². However, certain major replacement jobs would require more passengers in the vessel than its limit. Even though, these vessels are the cheapest in the industry according to Figure 9.2 they need to be supported by other transportation methods during these major replacements scenarios. However, this project's design would not allow for aerial vehicles to be flying near the wind turbines due to the active flow control subsystem. The air that is moved upward can influence the helicopter's path and be dangerous for the safe deployment of the workers. Thus, this project will be using a fleet of only CTVs in order to perform all of its repairs and replacement of parts.

In effect, the capability of these vessels to transport large loads while remaining highly cost-effective and versatile makes them the most desirable option. Consequently, CTVs are the ideal option for the Lagelander wind farm site. In addition, according to McMorland et. al. these vessels are able to withstand wave heights of 1.5 [m] (Hs limit) [73]. Therefore, once more the CTV is proved to be ideal as the average wave height expected at the Lagelander is 1.34 [m] as seen under Figure 4.4.

Furthermore, these vessels are expected to cost £2,000,000 to £3,000,000/yr for a 500 [MW] wind farm [76]. Thus, for this offshore site which is able to produce up to 8 [GW], around €50,831,000/yr must be invested in workboats for the maintenance of the farm. In addition, the logistics necessary onshore can amount to £400,000 to £700,000/yr for a 500 [MW] wind farm, amounting to €12,200,000/yr [76].

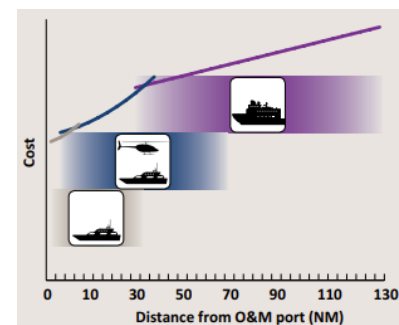


Figure 9.2: Lowest cost O&M strategies as a function of the distance from the port [76].

²<https://www.4coffshore.com/support/an-introduction-to-crew-transfer-vessels-aid2.html> [Accessed 07-06-2024]

Therefore, as was explained in subsection 9.1.1, for the daily maintenance of the wind turbine 6 vessels are required. Assuming these are CTVs, a total of 72 technicians will be working on the wind farm on a daily basis.

9.3. Safety

During maintenance the turbine will strive to remain operative during the process while ensuring the safety of the workers. In order to do so, different strategies are applied depending on the situation. In effect, in the case of a defective RNA, that does not need replacement of any major parts, then the adjacent rotors will be turned off as well as the ones that are directly in front of the platform that leads to said defective rotor. This is depicted in Figure 9.4 where the defective rotor is indicated in bold.

Here, the red case represents the scenario where the furthestmost rotor is defective. Thus, the 4 adjacent rotors are turned off as well as the one placed directly in front of the platform used to reach the faulty rotor. Finally, a total of 6 rotors must be turned off in this case.

In addition, the figure also depicts in green the case where the defective rotor is located in the middle columns. Here, the rotors placed adjacent to this one are also turned off during the maintenance process. Accounting for a total of 7 rotors being turned off during the course of the repairs.

Finally, the blue scenario is also demonstrated where the faulty rotor is located in the column closest to the monopile. Here, the total number of rotors deactivated amounts to 8. This is due to the fact that the column on the side of the tower is mirrored and accounts for three rotors that are dangerously close to the defective one and must therefore be turned off. This is the worst-case scenario in which 8 out of the 34 rotors are deactivated during the maintenance process.

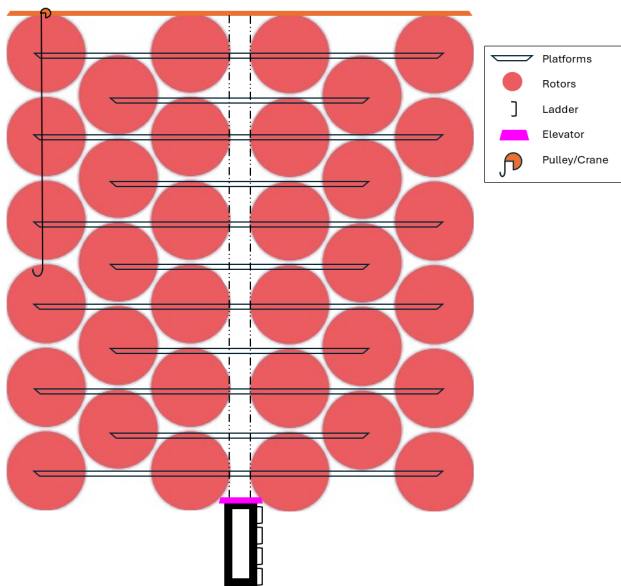


Figure 9.3: Accessibility strategies in wind turbine

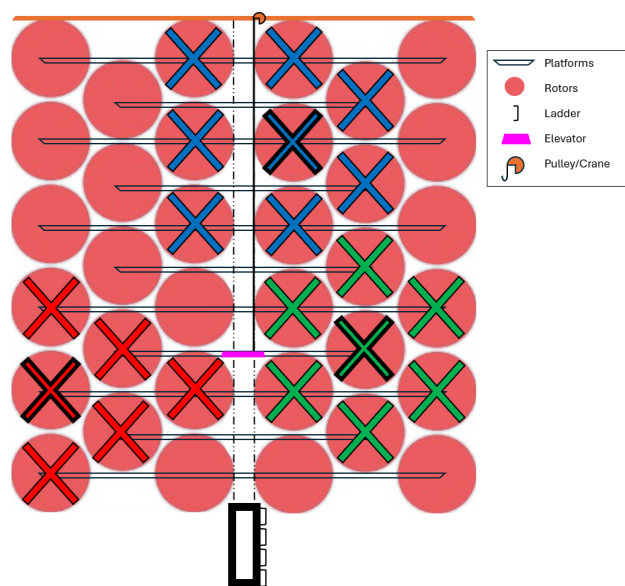


Figure 9.4: Different strategies applied during maintenance of rotors/nacelle.

It must be noted that in case a replacement of a major component is necessary, then the entire turbine must be deactivated. This is due to the fact that the proper functioning of the pulley system and the safety of the workers performing this high-risk job can only be ensured if the entire system is shut-off.

9.4. Maintenance Strategy

Offshore wind turbines are subject to great internal and external factors which compromise their correct functioning. Thus, maintenance of the turbine is of high importance to ensure the constant delivery of energy. However, throughout its lifetime this service accounts for a quarter of the total costs of the wind turbine³. Maintenance of a wind turbine is performed by applying multiple monitoring techniques to inspect all its components. These methods are summarized in Table 9.5.

³<https://www.tno.nl/en/sustainable/renewable-electricity/offshore-wind-farms/maintenance-offshore-windturbines/> [Accessed 16-05-2024]

Table 9.5: Monitoring and analysis methods for different components [77].

	Nacelle	Tower	Blade	Bearings	Shaft	Gearbox	Generator
Vibration analysis	✓		✓	✓	✓	✓	✓
Torsional vibration					✓	✓	
Acoustics Emission		✓	✓	✓	✓	✓	
Oil analysis				✓		✓	✓
Strain measurement		✓	✓				
Optical fiber monitoring			✓				
Electrical effects				✓			✓
Temperature	✓			✓		✓	✓
Ultrasonic testing techniques		✓	✓				
Thermography	✓		✓	✓	✓	✓	✓
Visual inspection	✓		✓	✓		✓	✓
Radiographic inspection		✓	✓				
Generator power output							✓

Operation During Maintenance

In the event that one of the higher-level wind turbines fails, the most critical scenario involves seven inoperative rotors, leading to a significant yaw moment that needs to be counteracted to prevent unintentional yawing of the unit. This scenario, which produces the highest yaw moment, is marked in blue. Another scenario involves a similar setup but at a single lower level, where the wind speeds are lower (green).

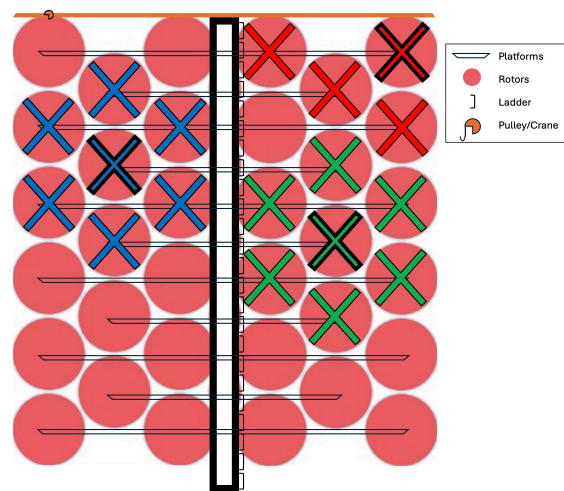


Figure 9.5: Different scenarios of maintenance

There are two potential strategies to avoid unintentional yawing to counteract the yaw along with aiming for most power within maintenance window:

- Pitch the blades on one side to produce less thrust.
- Turn off the mirrored layout of the inoperative rotors.

To address the yawing moment caused by the inoperative rotors, the change in thrust coefficient (C_t) was computed. Based on the centroid of the inactive rotor combination, the required thrust reduction was determined. By pitching the blades on the opposing side, the thrust was reduced sufficiently to counteract the yawing moment. This approach proved feasible for achieving the necessary yawing moments during maintenance, which were 48 MNm (red), 68 MNm (green), and 70 MNm (blue), respectively.

Using the Blade Element Momentum (BEM) model, it was calculated that, in all three cases, adjusting the pitch on the opposing side to reduce thrust would be beneficial. This adjustment would still result in generating at least three orders of magnitude more power in total.

9.5. Actual Accessibility

As stated previously, the theoretical accessibility was concluded to be 87.8%. However, thanks to the accessibility and safety of the site, as seen in Figure 9.4, only certain rotors are stopped when one breaks down, not the entire unit. Then, the average amount of rotors that are not operating when one is faulty is 6.29 rotors, which accounts for 18.5% of them. This means, that in the event of major, or minor failures, which do not need replacement, only 18.5% of the power is decreased. This gave an actual availability of 92.34%.

10. Cost Breakdown and Analysis

Within the competitive landscape of offshore wind energy, it is crucial for this new and potentially disruptive design to be economically attractive in order to find footing and get adopted in the market. This chapter aims to quantify the complete life cycle cost of the ReWind project and compares it to the North Sea program as proposed by the Dutch government. section 10.1 presents the methodology used to assess the cost of the wind farm. Subsequently, the results are presented in section 10.2. The expected return on investment will be computed in section 10.3. Hereafter, a sensitivity analysis will be performed on the results in chapter 11 followed by the conclusions drawn in section 11.3.

10.1. Methodology

From the market analysis done in chapter 2, it follows that this project, ReWind, aims to achieve the Dutch energy transition goals by proposing an alternative wind farm and turbine design to the current Dutch-suggested design for the North Sea program. For this project to be considered, it needs to be economically advantageous to the the Dutch North Sea program. This cost analysis aims to quantify the cost of both programs and compare them.

In order to accurately compare the cost between wind farms, each cost is normalised to [€/MWh] by calculating the Levelized Cost of Energy (LCoE) in a certain Fiscal Year (FY). This is the same metric as described in chapter 2 and is given by Equation 10.1 [78].

$$LCoE = \frac{\frac{CapEx + DecEx(1+r)^{-n}}{a} + OpEx}{AEP} \quad (10.1)$$

Where $CapEx$ are the capital expenditures per installed [MW], $DecEx$ the decommissioning expenses in [€/MW], $OpEx$ the yearly operational expenditure per [MW], n the number of years the wind farm is operative, r the real discount rate and a the annuity in years. The economic assumptions to get the discount rate and annuity are tabulated below in Table 10.1.

Table 10.1: Economic Assumptions for the calculation of the LCoE [78]

Component	Assumption
Nominal discount rate (R)	4.4%
Inflation rate (i)	2.0%
Real discount rate $\left(r = \frac{1+R}{1+i} - 1\right)$	2.35%
Operating years (n)	25 [yr]
Annuity $\left(a = \frac{1 - (1+r)^{-n}}{r}\right)$	18.74 [yr]

The LCoE encapsulates not only the initial capital expenditures for a wind farm but also considers the operational expenditures as well as the decommissioning expenditures and lifespan of the project. This metric does, therefore, allow investors and industry players to assess the commercial viability of a project and compare new projects with already established ones. Therefore, comparing the LCoE of wind farms will give a clear understanding of which project is more economically attractive and, therefore, will be used as the relevant metric of comparison throughout this cost analysis.

Starting from the Catapult cost model [3] for a general 10 [MW]-turbine wind farm, certain adjustments can be made to obtain a cost model for the proposed 30 [MW]-turbine Dutch North Sea program and the 30 [MW]-turbine ReWind wind farm. The Catapult cost model divides the life-cycle cost for the complete farm into several elements: Development and project management, wind turbine, balance of plant, installation and commissioning, operations maintenance service and decommissioning. Each of these elements are further split into all relevant components. The cost for each element is given and together form the complete life-cycle cost. After

normalizing, this model will be used to estimate the life-cycle LCoE of the North Sea program and ReWind wind farm.

The wind farm used for the Catapult model [3] differs significantly from the North Sea program and ReWind in several aspects. These discrepancies will lead to a different LCoE of the programs. To account for these differences, certain modifications are proposed that will drive the LCoE from the Catapult wind farm to the North Sea program and ReWind wind farm. The main cost-driving modifications are presented below; each step is identified with the Cost Analysis (CA) identifier.

- **CA-01** Rated power: The Catapult wind farm model [3] considers turbines with a rated power of 10 [MW]. This step will account for the change in LCoE after scaling the rated power to 30 [MW], which is the targeted rated power for the North Sea program and ReWind.
- **CA-02** Power density and location: This step will account for the change in LCoE for the doubling in power density from 5 to 10 [MW/km²]. Furthermore, the ReWind wind farm will be located closer to shore than the Catapult wind farm and the wind farm water depth is reduced from 30 [m] to 15 [m]. Thus, this step will also adjust the LCoE for the aforementioned changes.
- **CA-03** Wake losses: The higher energy density will cause significant wake losses, affecting the LCoE of the wind farm. The wake losses will be included in this step.
- **CA-04** Storage: As the amount of energy produced by wind farms grows, the need for energy storage does as well. The cost of storage will be estimated in this step. This point marks the estimate for the Dutch North Sea programme as well.
- **CA-05** Multi-rotor: The multi-rotor turbine design provides improvements in LCoE of regular wind turbines [79]. The new LCoE due to the multi-rotor design will be estimated with this step.
- **CA-06** Wake Re-energization: The AFC system will re-energize the flow and reduce the wake losses, improving the capacity factor of the wind farm and LCoE. This will be accounted for in this step. This point also marks the proposed design and LCoE estimate for the ReWind wind farm.

These steps are the main modifications considered for assessing the LCoE change from the Catapult wind farm to the North Sea program and Rewind wind farm and will be elaborated in the subsections below.

10.1.1. Rated Power

The baseline Catapult wind farm cost model is created for turbines with a rated power of 10 [MW]. The North Sea program and Rewind wind farm are both using 30 [MW] turbines. This difference will have an effect on the LCoE. As the rated power of the turbine scales by a factor of 3, using the squared-cube law, the turbine cost will increase by a factor of $3\sqrt{3}$ and the turbine costs per [MW] increase by $\sqrt{3}$. Furthermore, assuming the same energy production for the different wind farms allows the North Sea program and Rewind to install a third of the turbines of the Catapult wind farm. Accounting for a rough high-end estimate of the doubling of transportation and commissioning cost results in a decrease in installation and (de)commissioning LCoE by a factor of 2/3. Thus, having scaled the initial LCoE of the Catapult wind farm to what it would be if it had 30 [MW] turbines results in a proper starting point to apply the subsequent changes.

10.1.2. Power Density and Location

This step involves first accounting for the change in location of the Catapult and Rewind wind farms and subsequently calculating the effect of increasing the power density.

The Catapult wind farm is located 60 [km] from shore at an average depth of 30 [m], whereas the Lagelander wind farm site, selected for ReWind and assumed for the North Sea program, is only 45 [km] from shore at an average depth of 15 [m]. This difference will alter the cost for everything going from and to shore, such as cables, installation and maintenance as well as the costs for fixing the turbines to the seabed. The LCoE changes and new LCoE are presented in Table 10.2. For this and all subsequent tables, only the relevant values are shown that differ due to the current step.

The doubling of the power density from 5 [MW/km²] for the Catapult wind farm to 10 [MW/km²] for the North Sea program and Rewind wind farm reduces costs related to the area of the wind farm. Costs such as the cables within the wind farm and installation will be reduced. Furthermore, maintenance will be simplified due to less travel distance between turbines and transportation required as well and the area needed for the wind farm will decrease. This will positively impact the environment and marine life. The resulting LCoE after step CA-02 is tabulated below in Table 10.3. It was chosen to present these changes in a separate table for clarity and conciseness.

Table 10.2: LCoE CA-02 (Turbine Location)

Category	LCoE CA-01 [€/MWh] (FY 2024)	Change	LCoE CA-01.5 [€/MWh] (FY 2024)	Rationale
Surveys	€ 0.21	0.80	€ 0.17	Less travel time, closer to shore
Resource and metocean assessment	€ 0.06	0.81	€ 0.05	Shallower waters
Export cable	€ 2.41	0.75	€ 1.81	Closer to shore thus shorter cable
Cable protection	€ 0.04	0.75	€ 0.03	Closer to shore thus shorter cable
Monopile	€ 2.79	0.5	€ 1.39	Shallower waters thus shorter monopile
Corrosion protection	€ 0.37	0.5	€ 0.19	Shallower waters thus shorter monopile
Scour protection	€ 0.19	0.5	€ 0.09	Shallower waters thus shorter monopile
Facilities	€ 0.37	0.85	€ 0.32	Closer to shore
Turbine foundation structure	€ 1.11	0.75	€ 0.84	Shallower waters
Foundation installation	€ 1.23	0.6	€ 0.74	Shallower waters and closer to shore
Offshore substation installation	€ 0.43	0.75	€ 0.32	Shallower waters and closer to shore
Offshore cable installation	€ 2.70	0.75	€ 2.02	Short distance to shore thus shorter cables
Turbine installation	€ 0.61	0.66	€ 0.40	Closer to shore
Sea-based support	€ 0.03	0.75	€ 0.02	Closer to shore
Marine coordination	€ 0.01	0.9	€ 0.01	Closer to shore
Training	€ 0.11	0.9	€ 0.10	Closer to shore
Offshore logistics	€ 0.37	0.85	€ 0.31	Closer to shore
Turbine maintenance and service	€ 7.58	0.875	€ 6.63	Closer to shore
Balance of plant maintenance and service	€ 4.13	0.9	€ 3.72	Closer to shore
Turbine decommissioning	€ 0.27	0.75	€ 0.21	Closer to shore
Foundation decommissioning	€ 0.48	0.7	€ 0.34	Closer to shore and shallower waters
Cable decommissioning	€ 0.96	0.75	€ 0.72	Closer to shore thus shorter cables
Substation decommissioning	€ 0.34	0.75	€ 0.26	Closer to shore and shallower waters
Total	€ 54.68	0.89	€ 48.56	

Table 10.3: LCoE CA-02 (Power Density)

Category	LCoE CA-01.5 [€/MWh] (FY 2024)	Change	LCoE CA-02 [€/MWh] (FY 2024)	Rationale
Surveys	€ 0.17	0.87	€ 0.15	Less area to inspect

Category	LCoE CA-01.5 [€/MWh] (FY 2024)	Change	LCoE CA-02 [€/MWh] (FY 2024)	Rationale
Resource and metocean assessment	€ 0.05	0.9	€ 0.05	Less area to inspect
Array cable	€ 0.65	0.6	€ 0.39	Shorter distance between turbines
Cable protection	€ 0.03	0.9	€ 0.03	Less cable length used
Offshore substation electrical system	€ 0.84	0.9	€ 0.75	Closer to borders of wind farm
Offshore substation facilities	€ 0.32	0.9	€ 0.28	Closer to border of wind farm
Foundation installation	€ 0.74	0.8	€ 0.59	Less distance to travel between turbines
Offshore cable installation	€ 2.02	0.75	€ 1.52	Less cable used
Turbine installation	€ 0.40	0.8	€ 0.32	Less distance between turbines
Sea-based support	€ 0.02	0.9	€ 0.02	Less area to support
Marine coordination	€ 0.01	0.8	€ 0.01	Less area to coordinate
Weather forecasting and metocean data	€ 0.00	0.9	€ 0.00	Less area to coordinate
Offshore logistics	€ 0.31	0.9	€ 0.28	Less area
Turbine maintenance and service	€ 6.63	0.8	€ 5.31	Shorter distance between turbines
Balance of plant maintenance and service	€ 3.72	0.9	€ 3.35	Shorter distances
Turbine decommissioning	€ 0.21	0.8	€ 0.16	Shorter distances
Foundation decommissioning	€ 0.34	0.8	€ 0.27	Shorter distances
Cable decommissioning	€ 0.72	0.8	€ 0.58	Less cable used
Total	€ 48.56	0.94	€ 45.43	

10.1.3. Wake Losses

Following steps CA-01 and CA-02, The LCoE is evaluated for a hypothetical 30 [MW]-turbine wind farm located closer to shore and in shallower water. Furthermore, the power density increased to 10 [MW/km²] by effectively placing the turbines closer to each other. This scenario is unrealistic, as it neglects the negative impact of increasing the wind farm density. Higher density will cause increased wake losses for the wind farm [1]. These losses can reduce the capacity factor to around 35% [1], reducing the total power production of the wind farm significantly. The newly computed LCoE for the changed Annual Energy Production (AEP) is shown below in Table 10.4.

Table 10.4: LCoE CA-03.

Category	LCoE CA-02 [€/MWh] (FY 2024)	Change	LCoE CA-03 [€/MWh] (FY 2024)	Rationale
Total	€ 45.43	1.46	€ 66.25	Decreased energy production will increase the LCoE of all components by the same amount.

10.1.4. Energy Storage

In a society with wind energy accounting for a large share of energy production, energy storage will become inevitable for a stable power grid [80]. To account for potential future expenses, energy storage is included in

the design of the ReWind project and for a fair comparison, it will also be assumed to be included in the Dutch North Sea program. Note that the cost of the transformers are not included, the inclusion of the transformers will increase the difference between the North Sea Program and the ReWind project due to increased power of the North Sea Program. Because of an increase of capacity factor from the standard 35% to ReWind's 47.5%, explained in section 5.3, a standard farm would have more installed power so that the delivered power and total energy are the same. Indeed, a standard farm would have installed 285.714 % of the power demanded installed, while ReWind would only have 210.526%. Also, as seen in Figure 2.6, the power outputted increases with increasing capacity factor, and the effect is mostly present at low speeds.

Then, Figure 10.1 shows the distribution of the power outputted throughout the year, depending on the capacity factor, for both the Dutch North Sea program and ReWind's farm. In green, the average demand is shown. Both curves contain the same amount of power, but the maximums are scaled depending on the capacity factor. The slope of the curve is assumed to be cubical, as it is proportional to the wind speed.

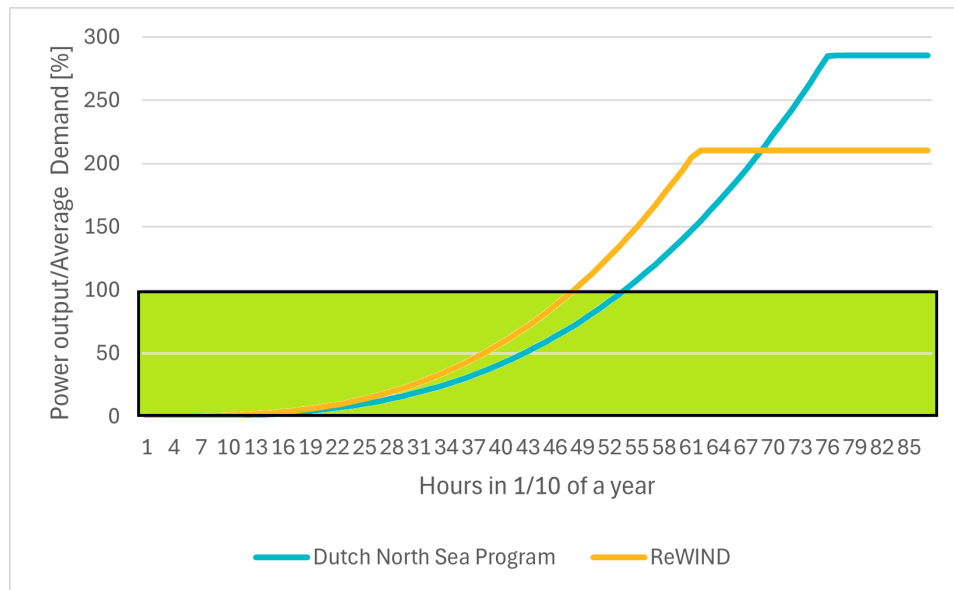


Figure 10.1: Power Curve vs Capacity factor

As can be seen, the green area is better covered by ReWind's power curve than the Dutch North Sea Program. This means that the rest of the energy has to be stored when the power outputted is greater than the demand. In turn, this means that the size of the storage system that needs to make up for the low output power periods needs to be larger for the North Sea Program scenario.

Indeed, assuming a storage time of 48h, ReWind's necessary storage system is 279.3 [MWh] and the competitor's farm storage system necessary would be 312.2 [MWh] for every unit of 30 [MW]. This is a difference of 11%.

It is also assumed a storage in Lithium-Ion batteries at a cost of 479.6 [€/kWh] (FY 2024)[81].

Although different solutions exist for the storage of energy, batteries were chosen due to their widespread availability and efficiency. Other options may be more economical, but since the different wind farms will use the same storage system it will not significantly impact for the comparison.

The limitations of the chosen method to estimate the cost of energy storage is the neglecting of efficiencies and operational costs. Including these cost will change the absolute results, but the relative results are expected to be similar since the same methodology was used for all cases.

The updated LCoE for the addition of energy storage is shown in Table 10.5.

Table 10.5: LCoE CA-04.

Category	LCoE CA-03 [€/MWh] (FY 2024)	Change	LCoE CA-04 [€/MWh] (FY 2024)	Rationale
Energy storage system	€ 0.00		€ 86.88	Energy storage system is added
Total	€ 66.25	2.31	€ 153.13	

This point in the design marks the LCoE estimation of the Dutch proposed North Sea program. Namely, all the changes that significantly affect the LCoE from the Catapult wind farm model have been accounted for. This LCoE will be used for future comparison with this project's ReWind wind farm.

10.1.5. Multi-rotor

To move from the North Sea program to the ReWind wind farm, two more changes need to be made. First of all, the wind farm needs to be altered from single-rotor turbines to multi-rotor turbines. This step, CA-05, encapsulates the appropriate change in LCoE. A Multi Rotor System (MRS) provides significant improvements over regular wind turbines in terms of cost for the rotor nacelle assembly [79]. The reduced cost for multi-rotor systems is computed using the cost formulas from INNWIND [44] from which the LCoE can be computed. These formulas require the mass per component and power per rotor as inputs, and the mass per component was obtained from the structural analysis done in section 5.4 and, if unknown, estimated using statistical relationships from NREL [82]. The results of these formulas must be corrected for inflation from the period of 2012 to 2024; during this period, the inflation was 30%¹. Furthermore, a multi-rotor system allows for a relatively smaller generator, gearbox and blade sizing, reducing the LCoE of these components. Additionally, LCoE benefits can be found in the maintenance due to the increased reliability of the smaller components. But, these benefits have to compete with the increased structural weight and complexity. The relevant LCoE breakdown is shown in Table 10.6.

Table 10.6: LCoE CA-05.

Category	LCoE CA-04 [€/MWh] (FY 2024)	Change	LCoE CA-05 [€/MWh] (FY 2024)	Rationale
Development and consenting services	€ 1.35	1.25	€ 1.96	Increased complexity of design
Engineering and consultancy	€ 0.11	1.25	€ 0.14	Increased complexity of design
Bedplate	€ 0.94	0.18	€ 0.17	Based on INNWIND [44] MRS cost relations
Main Bearing	€ 0.94	0.19	€ 0.18	Based on INNWIND [44] MRS cost relations
Main Shaft	€ 0.94	0.19	€ 0.17	Based on INNWIND [44] MRS cost relations
Gearbox	€ 3.28	0.46	€ 1.53	Based on INNWIND [44] MRS cost relations
Generator	€ 4.69	0.13	€ 0.60	Based on INNWIND [44] MRS cost relations
Power take-off	€ 3.28	0.56	€ 1.86	Based on INNWIND [44] MRS cost relations
Yaw system	€ 0.80	1.93	€ 1.54	Based on INNWIND [44] MRS cost relations
Yaw bearing	€ 0.33	1.56	€ 0.51	Based on INNWIND [44] MRS cost relations
Nacelle auxiliary systems	€ 0.33	0.50	€ 0.16	

¹<https://www.in2013dollars.com/europe/inflation/2012?amount=1> [Accessed 11-06-2024]

Category	LCoE [€/MWh] CA-04 (FY 2024)	Change	LCoE [€/MWh] CA-05 (FY 2024)	Rationale
Nacelle cover	€ 0.47	0.26	€ 0.12	Based on INNWIND [44] MRS cost relations
Small engineering components	€ 1.17	1.10	€ 1.29	Higher component count
Structural fasteners	€ 0.33	1.50	€ 0.49	Higher component count
Blades	€ 6.10	0.34	€ 2.08	Based on INNWIND [44] MRS cost relations
Hub Casting	€ 0.70	1.47	€ 1.03	Based on INNWIND [44] MRS cost relations
Blade bearings	€ 0.94	2.00	€ 1.88	
Pitch system	€ 0.47	1.37	€ 0.64	Based on INNWIND [44] MRS cost relations
Rotor auxiliary systems	€ 0.19	1.20	€ 0.23	More rotors
Fabricated steel components	€ 0.38	0.66	€ 0.25	Higher component count
Structure steel	€ 4.69	1.63	€ 7.63	Based on structural analysis
Tower internals	€ 0.33	1.20	€ 0.39	Larger tower
Monopile	€ 2.03		€ 3.05	Heavier turbine
Corrosion protection	€ 0.27	1.50	€ 0.41	Increased monopile size
Scour protection	€ 0.14	1.25	€ 0.17	Increased monopile size
Foundation installation	€ 0.86	1.5	€ 1.29	Increased monopile size
Turbine installation	€ 0.47	0.8	€ 0.38	Onshore construction and assembly possible
Onshore logistics	€ 0.15	0.80	€ 0.12	Localized production chain
Offshore logistics	€ 0.41	0.80	€ 0.33	Only installation, no assembly required
Turbine maintenance and service	€ 7.74	0.65	€ 5.03	Based on maintenance analysis in section 9.4
Balance of plant maintenance and service	€ 4.88	0.65	€ 3.17	Based on maintenance analysis in section 9.4
Turbine decommissioning	€ 0.24	0.8	€ 0.19	Easier decommissioning due to simplicity of structure
Total	€ 153.13	0.93	€ 141.89	

10.1.6. Wake Re-energization

Finally, the last change to arrive at the LCoE of this project's proposed ReWind wind farm is the addition of active flow control (AFC) devices, as explained in subsection 5.2.1. The AFC devices will re-energize the flow and improve wake recovery, resulting in a higher capacity factor and AEP. The capacity factor is determined in section 5.3 to increase from 35% to 47.5%. The new LCoE values are shown in Table 10.7. This increase in capacity factor will result in a decrease of all components' LCoE of 0.26%. Therefore, the constant factor of 0.74 will be applied to all the components. This will be taken as a baseline for all components. A relative increase in this factor shows a less steep decrease in LCoE due to the additional cost of the AFC or other components to enable the wake re-energization.

Table 10.7: LCoE CA-06.

Category	LCoE [€/MWh] CA-05 (FY 2024)	Change	LCoE [€/MWh] CA-06 (FY 2024)	Rationale
Engineering and consultancy	€ 0.14	0.79	€ 0.11	Additional costs due to high lift devices design
Fabricated steel components	€ 0.25	0.76	€ 0.19	Additional material for high lift devices
Structure	€ 7.63	0.76	€ 5.78	Additional structure due to high lift devices
Energy storage system	€ 86.88	0.66	€ 57.27	More batteries used since more power produced
Other Components	€ 46.99	0.74	€ 34.63	Change with increase in energy production
Total	141.89	0.69	97.97	

This final point marks the LCoE for this project's proposed alternative design, ReWind, for the Dutch North Sea program. As all the major LCoE driving changes have been made, this LCoE is the best estimate for the ReWind wind farm and will, therefore, be used for comparison.

10.2. Results

With the LCoE for the Dutch North Sea program and this project's ReWind wind farm estimated, a comparison can be made to assess commercial viability. Two possible scenarios will be compared. First of all, the ReWind wind farm will be evaluated against the North Sea program without energy storage. As current wind farms do not use energy storage systems, this comparison serves as a benchmark for ReWind's economic performance in the current wind energy market. The results of this comparison are presented in Table 10.8.

Table 10.8: LCoE comparison ReWind wind farm and North Sea program [3]

	LCoE
ReWind (no-storage)	€ 40.70
North-Sea (no-storage)	€ 66.25
Change	39%

From this table, it can be observed that with an LCoE of 40.70 [€/MWh], ReWind is 39% lower than the North Sea wind farm LCoE. This shows significant improvement in the economic and energy production aspects of the ReWind project and proves the commercial feasibility.

Note that, according to the market analysis presented in chapter 2, the Levelized Cost of Energy (LCoE) for a fixed-bottom turbine is between 50-65 [€/MWh]. This value was derived by averaging data from a range of wind farms, including smaller installations that have a very low density and, consequently, have lower costs. When compared to the Rewind program, this estimation would indicate an improvement of 18.6-37.4%. Although this represents a decent enhancement, using this comparison could result in an overly conservative assessment of the project's performance. Therefore, it was decided that a comparison with the North Sea model would be more appropriate. This model considers a larger wind farm with higher installed power densities, providing a more accurate benchmark.

Finally, the Rewind wind farm will be compared with the North Sea program as proposed by the Dutch government, assuming both farms will have the need for energy storage. The results are presented in Table 10.9.

Table 10.9: LCoE comparison ReWind wind farm and North Sea program

	LCoE
ReWind (Storage)	€ 97.97
North-Sea (Storage)	€ 153.13
Change	36%

As can be observed from this table, the LCoE for the ReWind wind farm, including storage, is 36% lower than the predicted LCoE for the North Sea program. This strongly indicates that the ReWind project might be better suited to achieve the Dutch energy transition plans and shows strong economic grounds to consider this design over the traditional single-rotor turbine wind farms. Furthermore, the overall high LCoE of the North Sea program points out that this program might struggle economically due to wind farm wake losses and associated increases in energy storage.

The cost breakdown of each step is presented in Figure 10.2 and Figure 10.3, for the case without storage considered and with storage considered, respectively.

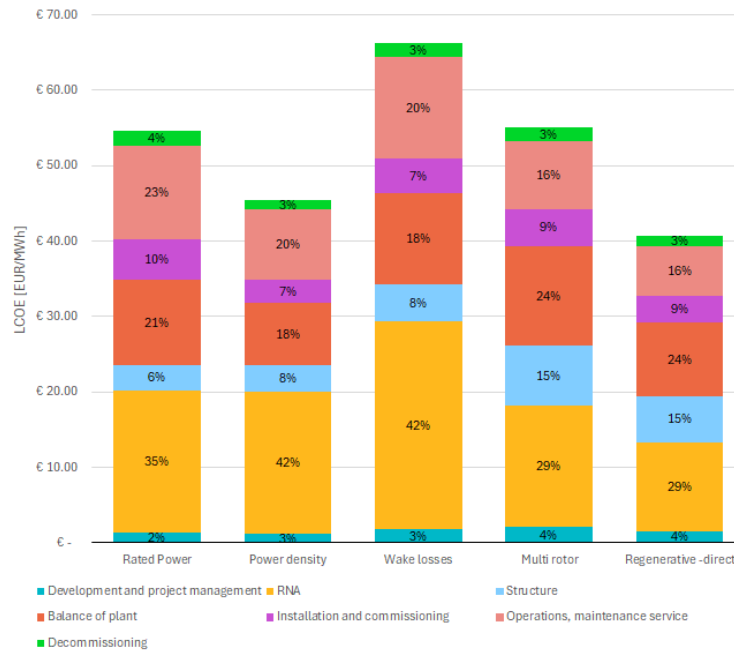


Figure 10.2: LCoE breakdown of the steps in the model excluding storage

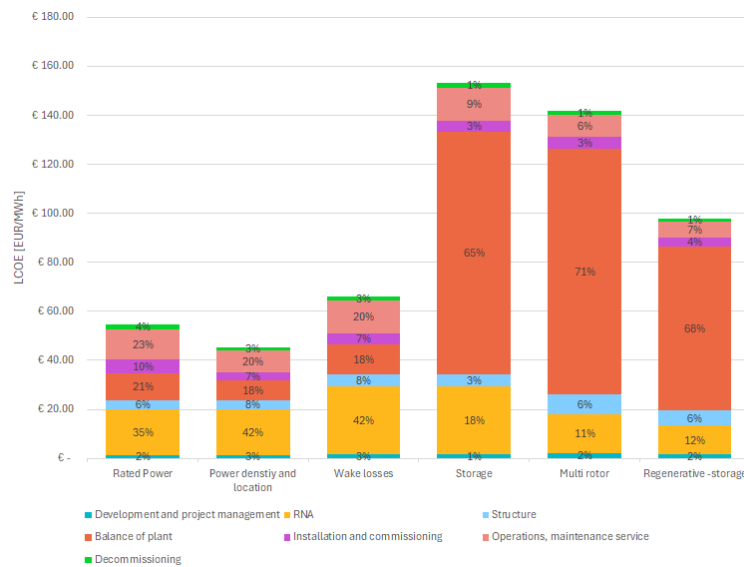


Figure 10.3: LCoE breakdown of the steps in the model including storage

Finally, the capital-, operational- and decommissioning expenditures provide valuable insights into the distribution of costs over time. The expenditures per MW of installed power are given in Table 10.10 below.

Table 10.10: Expenditures ReWind wind farm

	ReWind including Storage	ReWind excluding Storage
CapEx [€/MW] (FY 2024)	7 021 500	2 556 400
OpEx [€/MW/yr] (FY 2024)	27 402	27 402
DecEx [€/MW] (FY 2024)	184 760	184 760

10.3. Return on Investment

In the previous sections, the LCoE of the ReWind wind farm has been determined. In this section, the actual financial profitability of the ReWind project will be evaluated. As mentioned in section 2.3, the capital costs of this project are relatively high, which may require a strategic approach to attract potential investors. Therefore, showing that this project is profitable as well as reduces cost per [MWh] is crucial. This section will cover both the Return On Investment (ROI) and the Net Present Value (NPV).

ROI

The Return On Investment (ROI) is a key financial metric used to evaluate the efficiency and profitability of an investment. It measures the gain or loss generated by an investment relative to its initial cost. This metric helps investors assess the potential return they can expect from their investment and compare the profitability of different investment opportunities. Using the costs estimate in section 11.3, the ROI can be calculated using Equation 10.2.

$$\text{ROI} = \frac{\text{Return} - \text{Investment}}{\text{Investment}} \quad (10.2)$$

Naturally, the ROI revenues depend on the assumed price at which the electricity is sold. During the past 12 months (June 2023-May 2024), the average cost of electricity per MWh in the Netherlands was 78.4 €². Electricity prices can vary significantly due to seasonal changes, geopolitical events, and technological advancements in other energy sources. Consequently, the ROI of the ReWind project was calculated for three different electricity price scenarios. The calculated ROI for each scenario, along with a comparative value for single rotor turbine wind farms, is shown in Table 10.11. Clearly, the ReWind scores better than the Catapult 10 MW reference wind turbine [3]. This improved performance can be attributed to the promising implementation of the active flow control and the multi-rotor system.

Table 10.11: Return on Investment of ReWind Concept at Different Electricity Prices

Average electricity price	64 [€/MWh]	74 [€/MWh]	84 [€/MWh]
ROI ReWind concept	7.77%	8.99%	10.20%
ROI Catapult 10 MW reference	5.65%	6.53%	7.42%

NPV

While ROI provides a snapshot of the profitability of an investment, it does not account for the timing of revenues and costs. Revenue received in the future does not hold the same value as revenue received today due to factors like inflation and opportunity cost. To address this, the Net Present Value (NPV) is calculated. NPV is a financial metric that evaluates the value of an investment by considering the present value of expected future cash flows, discounted back to their value today. A positive NPV indicates that the projected earnings exceed the anticipated costs, making the investment profitable. Similar to the ROI, the NPV is determined for three price scenarios and is shown Table 10.12. Again, the ReWind concept shows a significantly higher NPV than the Catapult reference turbine [3].

Table 10.12: Net Present Value of ReWind Concept at Different Electricity Prices, in millions €

Average electricity price	64 [€/MWh]	74 [€/MWh]	84 [€/MWh]
NPV ReWind concept	M€ 15.697	M€ 22.434	M€ 29.171
NPV Catapult 10 MW reference	M€ 6.745	M€ 13.983	M€ 21.221

²<https://www.statista.com/statistics/1314549/netherlands-monthly-wholesale-electricity-price/> [Accessed 13-06-2024]

Limitations

While these metrics do provide a good indication of the profitability of the ReWind project, they nevertheless simplify the situation very much. Several aspects of the energy market are omitted in these computations. For example, long term price variations are not taken into account, only an average price is assumed. Even if the average is correct, decennial variations could skew the net present value. Furthermore, as the share of renewable energy sources on the grid increases, many expect Dutch regulators and energy suppliers to start employing constantly varying energy prices³. This would imply that energy prices will immediately depend on the available energy on the grid, further enhancing the importance for wind turbines to continue producing electricity, especially at low speeds and reduce production variability. The ReWind concept scores especially well on low wind speed production compared to current single rotor designs, and therefore, the ROI and NPV compared to these designs is very conservative.

³<https://www.ad.nl/wonen/verdwijnt-het-daltarief-door-het-prijsplafond-heeft-z-n-beste-tijd-gehad-a2eb726c/?>
[Accessed[13-06-2024]]

11. Sensitivity Analysis

Having converged to a final concept, a sensitivity analysis will be performed to assess the impact of key parameters on the performance of the design. To measure changes in the final design, the LCoE was determined to be a suitable metric since it contains contributions by all relevant aspects of the farm design and operation and reflects a primary objective of the project to increase competitiveness with respect to conventional Single Rotor Turbine (SRT) wind farms. Thus, the LCoE will respond to any changes made to requirements or assumptions at the system and subsystem levels, and the result can be compared against both the nominal value and baseline LCoE values for conventional SRT wind farms.

11.1. Parameters of interest

The sensitivity study in the LCoE model is performed by measuring the response in overall LCoE to a given change in one of the model parameters or inputs. As was done in [44], the most critical parameters are assumed to be those for which the MRS differs most in terms of design relative to existing SRT wind farms. These critical parameters were determined to be [44]:

- Structural costs: Costs of structural steel for both the truss and monopile structures.
- Yaw system cost: Cost of the yaw system and yaw bearing since the required size of the yaw bearing is higher than for conventional SRT turbines.
- AEP: The annual energy production is uncertain for several reasons. Firstly, the aerodynamic performance of closely spaced co-planar rotors has not been thoroughly explored in the literature. Secondly, the extent to which the AFC regenerates the wake depends on numerous factors and assumptions, and thus, there is an uncertainty in its impact on the capacity factor and, in turn, the AEP.
- O&M: The extent to which the MRS outperforms a SRT in terms of operations and maintenance depends on numerous uncertain factors. Additionally, the applied O&M procedures differ from those of regular SRT wind farms.
- RNA costs: A major theoretical advantage of the MRS is the non-linear down-scaling of RNA costs. From this analysis, the sensitivity relative to SRT farms can be estimated.

In the analysis, each of the outlined parameters will be varied one at a time, keeping the others fixed. The sensitivity is then defined as the gradient of the LCoE response curve. This ignores any coupling between variables (e.g. increasing the RNA cost may imply an increased RNA mass, which in turn impacts the structure). However, since the changes introduced mainly reflect isolated uncertainties in the cost model, an isolated sensitivity analysis is also deemed sufficient. Moreover, changes in the cost contributors (e.g. an increase in structural mass), reflect coupled changes in various design-level parameters (e.g. an increase in thrust, causing an increase in lift and weight), and thus cost coupling is merely a consequence of technical parameter coupling. Thus, to analyse these coupling effects, a more detailed design-level sensitivity analysis would be necessary at a later stage. To this end, the cost sensitivity analysis can provide an insight into what subsystem technical parameters influence the design most on the system level.

11.2. Results

The analysis is visualised in Figure 11.1 (without energy storage) and in Figure 11.2 (with energy storage). In Figure 11.1, the MRS LCoE is compared against the Catapult wind farm (see section 10.1) as a baseline. In Figure 11.1, the MRS LCoE with storage included is compared against the LCoE of the North Sea program as estimated in subsection 10.1.4. The LCoE of each parameter of interest has been varied constantly through +100% and -50%. This range was chosen for two reasons. Firstly, the goal is primarily to determine the sensitivity (cost gradient) of key parameters, and since the LCoE is a weighted sum, these sensitivities are in most cases linear (with exception to the AEP, which varies inversely). Thus, in most cases the same information is gathered regardless of the interval chosen. Secondly, a larger positive range is taken since (with the exception of AEP) costs increase as a parameter increases. Thus, a scenario of interest is that wherein the costs of the MRS exceed those of the baseline SRT comparison. The point at which this loss of economical advantage occurs becomes clearer by using the relatively large and positively skewed range proposed here.

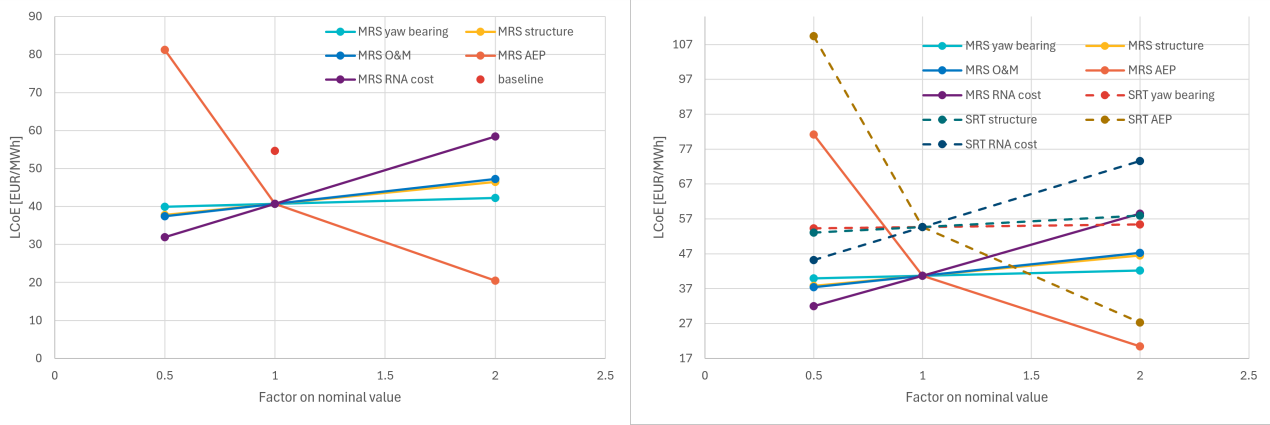


Figure 11.1: Sensitivity to changes in key parameters. Left: MRS without storage and baseline LCoE for the Catapult farm (CA-00). Right: MRS without storage and sensitivity of CA-00 LCoE overlaid.

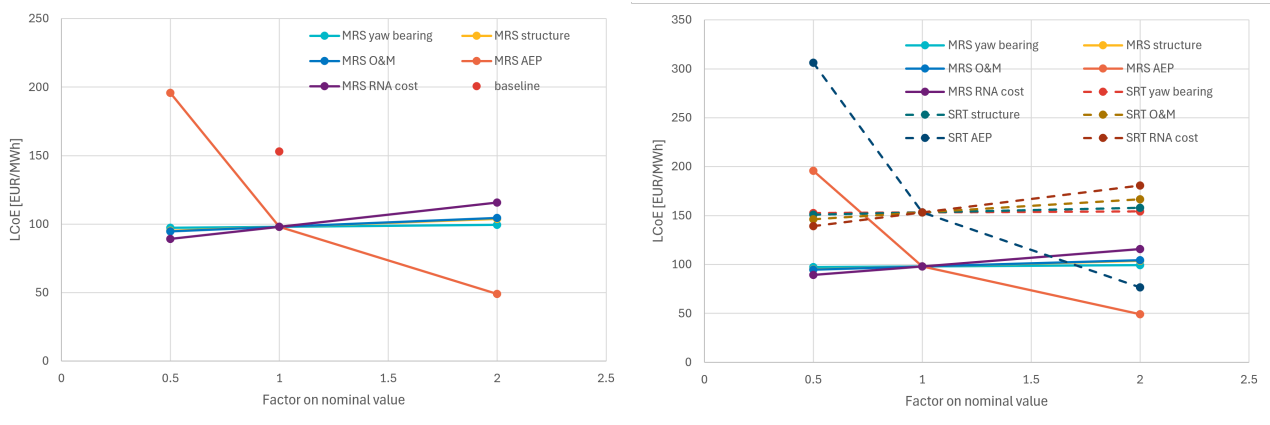


Figure 11.2: Sensitivity to changes in key parameters. Left: MRS with energy storage and estimated baseline LCoE for the North Sea program (CA-04). Right: Overlaid sensitivities of the SRT and MRS wind farms with energy storage.

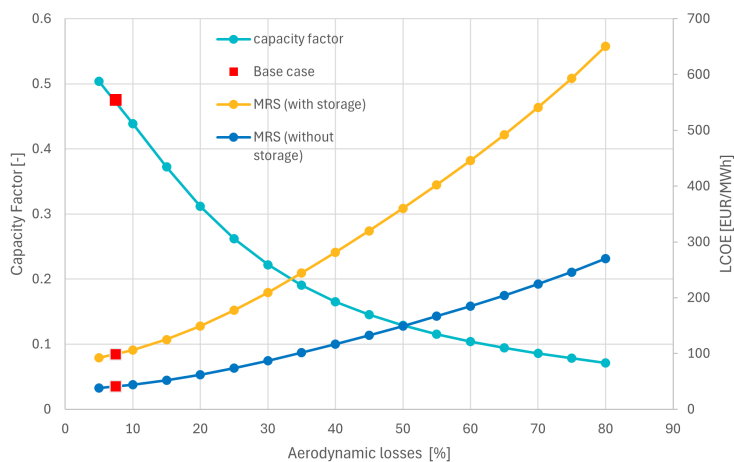


Figure 11.3: Effect of aerodynamic losses on the capacity factor and LCoE

Additionally, Figure 11.3, the LCoE and capacity factor are plotted as a function of the aerodynamic loss. To quantify the aerodynamic losses, a normalised velocity decrement is defined in terms of the recovery of cubed velocity (power) as given in [23]:

$$losses = \left(1 - \sum_i \frac{u_i^3}{U_\infty^3} \right) \cdot 100\% \quad (11.1)$$

where U_∞ is the free-stream velocity, and u_i is the velocity behind the i^{th} rotor.

Figure 11.3 shows that the capacity factor is highly sensitive for the aerodynamic losses experienced by the ReWind MRS wind farm. This is also apparent from Figure 11.1, which indicates that LCoE is most sensitive to the AEP, followed by the RNA cost. In this case, a reduction of 34% in AEP would cause the MRS to lose its competitive advantage relative to the SRT wind farm, which corresponds to a 26% decrease in capacity factor. According to the graph shown in section 5.3 [23], distributing the same lift force over two wings, corresponding to an aerodynamic loss of $\approx 15\%$ and a corresponding capacity factor of $\approx 37\%$, would already result in such a LCoE increase rendering the project unfeasible. Thus, the design is, in this sense, sensitive to the decision to implement three AFC wings. However, this number was already determined to be the lower bound (see section 5.2), and thus, only an increase in the number of wings would be a logical future modification, which would, in turn, be beneficial in terms of cost. A similar sensitivity to AEP can be observed in Figure 11.2 for the case of the MRS farm with energy storage, but here the sensitivity is higher due to the higher nominal LCoE. Besides the number of wings, other uncertainties exist in the performance analysis of the AFC devices, such as in the determination of the free-stream velocity, lift coefficients, and interaction effects. Thus, since the AFC lift also influences AEP through the capacity factor, this sensitivity analysis reveals the need for a more thorough aerodynamic analysis in the next phase of design, such that the current results can be verified. As mentioned before, this key cost sensitivity can now be traced back to design-level parameters, for which a more detailed technical sensitivity analysis could be performed in the future. In this case, these parameters could include the wing geometry, assumed operational speeds, and turbine spacing, all of which contain significant uncertainty at this stage of the design.

In both Figure 11.1 and Figure 11.2, the structure and O&M have a similar LCoE sensitivity. Similarly, in both cases, the yaw bearing has the lowest LCoE sensitivity. An increase in yaw bearing and structure costs reflects increases in the carried loads and, thus, also, size. However, this analysis does not account for external constraints, such as maximum loads on the bearing or manufacturability limits, and thus, the yaw bearing is likely to constrain the mass increase of the structure as its loading is increased. In the case without energy storage, the steel cost, and thus the structural mass, would have to be increased by a factor 3.4 for the MRS wind farm to lose its advantage over the baseline LCoE. On its own, this increase in structural mass seems unrealistic. However, in [44], the inclusion of fatigue analysis in the design of a similar structure increased structural mass by a factor of 2.7. Thus, a fatigue analysis will have to be performed before the complete contribution of the structural mass to LCoE can be determined. The cost sensitivity of the MRS yaw bearing is likely to be higher than what is shown here since an unconventional bearing must be applied. Thus, a small change in its design requirements may lead to unforeseen complications or design challenges, which potentially increase its contribution to LCoE. However, the sensitivity of LCoE to RNA, O&M, yaw bearing and structure costs are low in comparison to the sensitivity to AEP, and thus these are less critical. Thus, as with the AFC, the cost sensitivities suggests it is necessary to perform a technical sensitivity analysis of the structure, in addition to the fatigue analysis. Since the sizing of the structure is coupled to all other subsystems, fundamental design parameters such as rated power or rated wind speed would provide an indication of the bounds on the structural mass.

Although the cost sensitivity analysis has revealed technical design aspects which need further consideration, the analysis itself also has its limitations. Firstly, the coupling of different cost drivers or the simultaneous variation of different parameters is not considered. This means that cases also exist where the baseline LCoE has been overestimated and the MRS LCoE has been underestimated, in which case the sensitivities analysed here would become more critical. Moreover, there likely exists a point between the baseline and MRS nominal LCoE values where the MRS wind farm is less expensive but not by a sufficient margin to incentivise an industry shift from SRT to MRS systems. Moreover, it is necessary to perform more detailed technical sensitivity analyses for the relevant parameters in the future. However before this is possible, it is necessary to establish proper uncertainties for the baseline SRT values, as well as the cost model applied here.

11.3. Conclusions

From the sensitivity analysis, it follows that more design effort is required to establish with greater certainty the aerodynamic characteristics of the AFC devices since these greatly influence the capacity factor and AEP. Similarly, a fatigue analysis of the structure is necessary to determine whether this will increase the mass to an unacceptable extent. Additionally, a more detailed analysis of constraints on the yaw-bearing feasibility is required. However, once certainty in these aspects has been confirmed. The sensitivity analysis shows that only in cases where multiple costs are underestimated at the same time it is possible for the MRS to lose its LCoE advantage relative to the SRT wind farm.

12. Budget Breakdown

With the final design in place, a more detailed mass and cost budget can be constructed. Based on the relatively limited set of customer requirements, these two parameters were determined to be the most relevant metrics to evaluate for a final budget. This budget can be used to determine if the final ReWind turbine design meets the requirements and will be reflected in chapter 16.

The mass estimates are, where possible, taken from their sizing procedure and otherwise from statistical scaling relations provided by NREL [82]. These relations require the rotor radius as well as the power per rotor as an input and can determine all the relevant rotor and nacelle element masses. In section 5.1, the radius of each rotor was found to be 28.93 [m] and the rotor power 880 [kW]. From this, estimates of the component masses at this stage of the design can be made. The structural mass, as well as the tower mass, are determined in section 5.4. The mass of the active flow control devices follows from section 5.2. With the masses of all the relevant components determined, the final mass budget can be constructed.

In order to account for uncertainties in determining the mass of each element, a margin of 10% is applied. This value is chosen arbitrarily but reflects the estimated confidence in each calculated mass. For the mass of the tower and truss structure, as well as the mass of the AFC, which are calculated in section 5.2 and section 5.4, respectively, a margin of 5% is applied to reflect the increase in confidence in these particular values.

The cost budget follows directly from the cost analysis, done in chapter 10. In this case, it was decided to present the cost in [€] instead of the LCoE in [€/MWh] to facilitate a better intuitive understanding of the cost per element. Furthermore, only the structural cost for the wind turbine is displayed in this table. Again, each cost will have a margin of 10% applied based on the associated uncertainty with these estimates.

The final table with the appropriate cost and mass budget is presented in Table 12.1. As can be observed from this table, the total turbine cost adjusted for inflation is 52,400,000 [€] with a margin of $\pm 4,114,000$ [€]. This is in line with the predicted value from the Baseline report [58] of 40,800,000 [€]. The increase in cost can be attributed to the slight increase in structural weight compared to the estimation performed in the Baseline report as well as the inclusion of the monopile. Furthermore, Table 12.1 shows that the total turbine mass is estimated to be 11,000,000 $\pm 662,000$ [kg]. This, again, is roughly in line with the prediction of the Baseline report of 6,170,000 [kg]. Where an increase can be attributed to the inclusion of the monopile and the increase of the tower mass.

The mass of the RNA is 50 tonnes per assembly, this is in line with the masses of RNA of existing 1 [MW] turbines which range from 65 tonnes for the AN Bonus 1000/54¹ and the Bonus B54/1000² to 81 tonnes for the BWU 57-1000³. These masses are higher than the estimated masses of the ReWind turbine, this is due to the higher rated power of the reference turbines as well as the older age of these reference turbines. The CSIC H52-850, which has a rated power of 850 [kW] and uses a DFIG and is thus more comparable to the ReWind turbine, has a mass of 52 tonnes⁴. This brief analysis and comparison increases the confidence in the validity of the results.

The breakdown by mass and cost are also presented in Figure 12.1 and Figure 12.2 respectively, in the form of pie charts corresponding to each component category in Table 12.1.

¹<https://en.wind-turbine-models.com/turbines/396-an-bonus-1000-54> [Accessed 24-06-2024]

²<https://en.wind-turbine-models.com/turbines/697-bonus-b54-1000> [Accessed 24-06-2024]

³<https://en.wind-turbine-models.com/turbines/352-bwu-bwu-57-1000> [Accessed 24-06-2024]

⁴<https://en.wind-turbine-models.com/turbines/2069-csic-h52-850> [Accessed 24-06-2024]

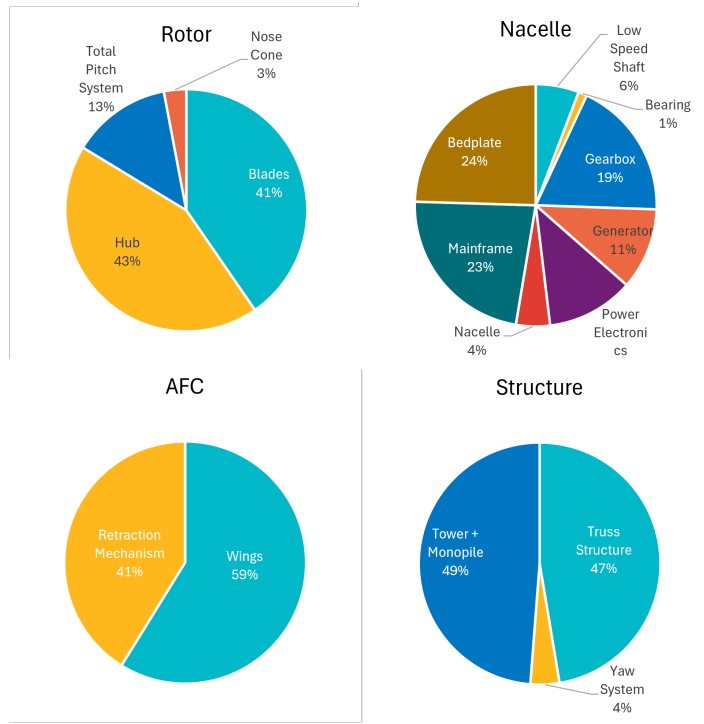


Figure 12.1: Mass breakdown by component category.

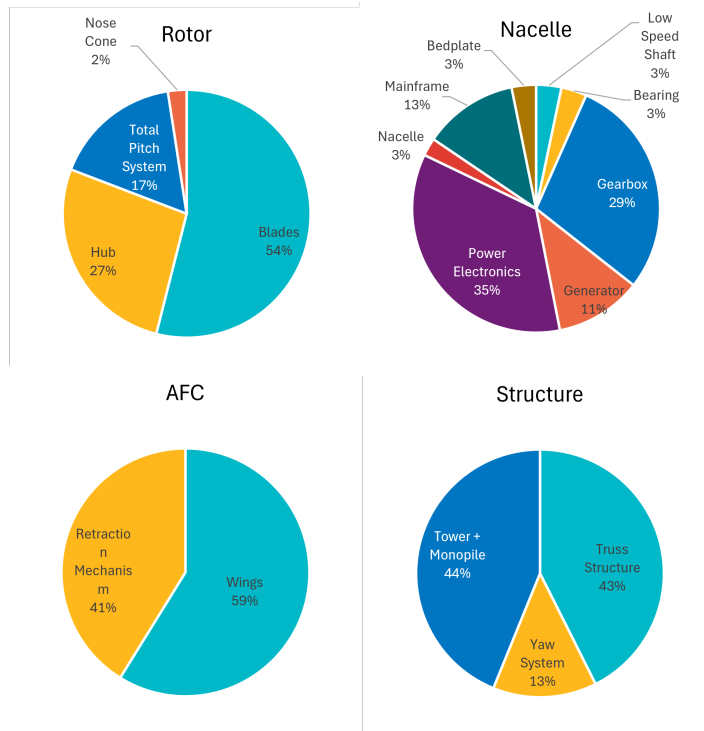


Figure 12.2: Cost breakdown by component category.

Table 12.1: Mass and cost of ReWind turbine by component

Component		Mass [kg]	Mass Margin [kg]	Mass Percentage	Cost [€] (FY 2024)	Cost Margin [€] (FY 2024)	Cost Percentage
Rotor	Blades	256 000	± 25 600	40.4%	€ 3,580,000	± € 358,000	39.9%
	Hub	275 000	± 27 500	43.3%	€ 1,780,000	± € 178,000	19.9%
	Total Pitch System	84 600	± 8460	13.3%	€ 1,110,000	± € 111,000	12.4%
	Nose Cone	19 000	± 1900	3.0%	€ 161,000	± € 16,100	1.8%
	Other	-	-	-	€ 2,340,000	± € 234,000	26.1%
	Total	635 000	± 63 500	5.8%	€ 8,970,000	± € 897,000	20.4%
Nacelle	Low Speed Shaft	60 700	± 6070	6.0%	€ 300,000	± € 30,000	2.1%
	Bearing	12 100	± 1210	1.2%	€ 302,000	± € 30,200	2.1%
	Gearbox	165 000	± 16 500	16.2%	€ 2,630,000	± € 263,000	18.2%
	Generator	196 000	± 19 600	11.2%	€ 1,030,000	± € 103,000	7.1%
	Power Electronics	122 000	± 12 200	12.0%	€ 3,200,000	± € 320,000	22.1%
	Nacelle	47 700	± 4770	4.7%	€ 212,000	± € 21,200	1.5%
	Mainframe	240 000	± 24 000	23.5%	€ 1,120,000	± € 112,000	7.8%
	Bedplate	258 000	± 25 800	25.3%	€ 289,000	± € 28,900	2.0%
	Other	-	-	-	€ 5,380,000	± € 538,000	37.2%
		Total	1 020 000	± 105 000	9.5%	€ 12,200,000	± € 1,220,000
AFC	Wings	121 000	± 12 100	58.8%	€ 236,000	± € 23,600	58.8%
	Retraction Mechanism	84 700	± 8470	41.2%	€ 165,000	± € 16,500	41.2%
	Total	206 000	± 20 600	1.9%	€ 401,000	± € 40,100	1.0%
Structure	Truss Structure	4 320 000	± 216 000	47.4%	€ 11,100,000	± € 555,000	41.5%
	Yaw System	353 000	± 35 300	3.9%	€ 3,530,000	± € 353,000	13.2%
	Tower + Monopile	4 440 000	± 222 000	48.8%	€ 11,400,000	± € 571,000	42.7%
	Other	-	-	-	€ 679,000	± € 67,900	2.5%
	Total	9 110 000	± 473 000	82.8%	€ 26,700,000	± € 1,550,000	51.0%
Total	11 000 000	± 662 000	100.0%	€ 52,400,000	± € 4,110,000	100.0%	

13. Sustainable Development Strategy

This chapter addresses the sustainable development strategy for offshore wind farms, a crucial aspect of their design and operational lifecycle. Currently, operating offshore wind farms are already fundamentally sustainable, especially compared to other energy sources. However, their development is not devoid of environmental challenges [83, 84]. These include pollutant generation during manufacturing, transportation and operation, impacts on bird and marine life, interference with marine navigation, and potential disruptions to local ecosystems. These issues require thorough consideration and strategic planning to mitigate adverse effects.

Renewable energy sources, especially wind farms, suffer from a lack of variability, as they depend on environmental and weather conditions to deliver electricity. In a future society that only depends on renewables, the lack of variability will need to be compensated by an energy storage system, as explained in chapter 10. However, as explained in section 2.3, an increase in capacity factor due to the addition of the AFC will reduce the need for storage systems and their carbon footprint.

In the following sections, a comparison between ReWind and an industry-standard wind farm will be presented, backed up with a life cycle analysis. Then, strategies to avoid disruptions to the local ecosystem will be introduced in order to polish the sustainability aspects of the farm.

13.1. Life Cycle Analysis

According to Dolan et al., the carbon footprint of wind farms is relatively low when compared to other energy sources. The life cycle greenhouse gas emissions for offshore wind power account for approximately 11 grams CO₂-equivalent per kilowatt-hour [gCO₂-eq/kWh] [85]. In effect, the life cycle measurements account for the manufacturing, installation, maintenance, and decommissioning phases of wind turbines [86].

From the previously defined requirement REQ-STK-CUS-06, ReWind intends to achieve a much lower carbon footprint, with the objective of reducing CO₂ emissions down by 40%. This will be accomplished by approaching the main pollutant parts of the current technologies on different fronts.

Firstly, the multi-rotor wind turbine will be composed of numerous smaller rotors. This goes against current technology trends, which are increasingly expanding the rotors in order to achieve turbines with higher power ratings. However, by opting for smaller ones, the manufacturing of these important parts is highly simplified, reducing its carbon footprint. In addition, certain rare Earth metals necessary for wind turbine production are increasingly scarce as the demand is expected to exceed the supply by 250% by 2030¹. Also, the implementation of DFIGs severely minimizes the use of rare earth metals.

Secondly, the re-energization of the wake is able to increase the energy density and capacity factor of the wind farm. Consequently, this will allow for higher efficiency and thus increase its delivered power, decreasing the grams CO₂-equivalent per kilowatt-hour and improving the turbine's carbon footprint. subsection 13.1.7 will expand on the benefits of the capacity factor increase.

The following section explains the Life Cycle Analysis (LCA). The goal of this analysis is to estimate the CO₂ emissions and energy consumed throughout all phases of the project, from cradle to grave. The impact assessment of this analysis also contains the inventory analysis, especially in subsection 13.1.1 and subsection 13.1.2. This analysis will start with material extraction, followed by production and transportation, the operation phase, and concluding with the decommissioning of the wind farm. As will be seen, this analysis will not be indefinitely detailed, with the limits set at every operation performed in relation to the wind farm, assuming workers and ship builders would operate despite ReWind's existence and are thus not included in this LCA.

13.1.1. Extracting materials

The initial phase of the project involves extracting the materials required for the entire farm. The masses of each component used in the 34-rotor units are summarized in Table 13.1, along with the materials used for each component. For the generator, gearbox, and blades, the material specifications are sourced from [87]. The rest of the components' materials are mentioned throughout this report.

¹<https://news.climate.columbia.edu/2023/04/05/the-energy-transition-will-need-more-rare-earth-elements-can-w-e-secure-them-sustainably> [Accessed 29-05-2024]

Table 13.1: Component Mass and Materials Used

Component	Component Mass [tons]	Steel Mass [tons]	Glass Fiber Mass [tons]	Aluminium Mass [tons]	Copper Mass [tons]
Blades and Hub	255 [88]	12.75	242.25	0	0
Generators	115.6	75.14	0	0	40.46
AFC	205.7	205.7	0	0	0
Gearbox	195.5 ²	187.68	0	3.91	3.91
Monopile	4798	4798	0	0	0
Lattice	4315	4315	0	0	0

Each material has an estimate on CO_2 and energy consumed. Copper emits $4.1 \left[\frac{tCO_2}{t}\right]^3$, steel emits $2.21 \left[\frac{tCO_2}{t}\right]^4$, glass fibre emit $2.3 \left[\frac{tCO_2}{t}\right]^5$, and aluminium emits $4 \left[\frac{tCO_2}{t}\right]^6$. These are summarised in Table 13.2.

Table 13.2: CO_2 emissions and energy consumed to extract materials

Material	Copper	Steel	Glass Fiber	Aluminium
CO2 emissions [tons per ton of material]	4.1	2.21	2.3	4
Energy Consumed [GJ per ton of material]	33[89]	22.9	32 [90]	211 [89]

Accounting for all 288 turbines in the wind farm, it was found that for material extraction, 6.3 [megatons] of CO_2 are emitted and 18.3e06 [MWh] of energy are consumed.

13.1.2. Production

The manufacturing phase of wind turbine components involves various processes that significantly contribute to CO_2 emissions. Here, the emissions for key components are evaluated by considering their weights and the specific manufacturing techniques used.

The truss structure consists of 1,353 individual truss members, all made of s355 steel. The manufacturing process involves several key stages: cutting, forming (primarily roll bending), and assembly (welding). Steel is extensively used in the construction of wind turbines, including in the blades, generator, Active Flow Control (AFC), gearbox, monopile, lattice tower, and yaw system. The manufacturing processes for steel components involve forging and hot rolling, emitting $0.879 \text{ [kg } CO_2/\text{kg}]$ [91] and $2.1 \text{ [kg } CO_2/\text{kg}]$ [92], respectively. For instance, the steel used in the blades weighs 12.75 [tonnes], leading to great emissions during both forging and rolling processes. Similarly, the generator (75.14 tonnes), AFC (205.7 tonnes), gearbox (187.68 tonnes), monopile (4798 tonnes), and lattice (4315 tonnes) contribute to a cumulative total of 9593.57 tonnes of steel. The overall CO_2 emissions from these processes are substantial, reflecting the intensive energy requirements of steel manufacturing.

On the other hand, the companies highlighted in the production plan are notable for their commitment to sustainable practices. Tata Steel is transitioning to hydrogen-based steelmaking and Direct Reduced Iron (DRI) technology, moving away from traditional blast furnace methods. This transition is expected to significantly reduce CO_2 emissions associated with steel production by 40% in the Netherlands by 2030⁷. Kersten specializes in roll bending with a focus on reducing waste and improving energy efficiency. The use of advanced roll bending techniques minimizes material wastage and energy consumption⁸. Additionally, Sif, the company responsible for producing the monopiles for ReWind's design, integrates sustainability into both the production and design phases of their operations. They have significantly minimized the use of natural and propane gas for preheating weldings by adopting induction heating for all circumferential welds. Additionally, Sif prioritizes the reduction of consumables and emphasizes the reuse and recycling of manufacturing materials. With an impressive 97% of residual materials being recycled, including steel, minerals, wood, and other wastes, Sif ensures that the byproducts of their production process are repurposed effectively. Moreover, Sif's environmental management systems adhere to the ISO 14001 standards, and their facilities in Roermond comply with the EU

³<https://internationalcopper.org/wp-content/uploads/2021/07/ICA-EnvironmentalProfileHESD-201803-FINAL-LOWRES-1.pdf> [Accessed 13-06-2024]

⁴<https://www.tatasteel.com/media/environment-performance-at-a-glance.pdf> [Accessed 13-06-2024]

⁵<https://renewable-carbon.eu/news/natural-fibres-show-outstandingly-low-co2-footprint-compared-to-glass-and-mineral-fibres/> [Accessed 13-06-2024]

⁶<https://www.climateaction.org/news/carbon-footprint-of-recycled-aluminium> [Accessed 13-06-2024]

⁷<https://www.tatasteleurope.com/nl/home> [Accessed 13-06-2024]

⁸<https://www.kerstengroup.com/en> [Accessed 13-06-2024]

Directive 2010/75/EU on industrial emissions. This initiative not only supports their production needs but also aligns with their goal of achieving CO_2 neutrality, which they accomplished in 2021⁹.

Furthermore, for the AFC system, which mainly uses s355 steel, similar manufacturing processes are applied as above. The main sections involve forming and roll bending, with additional complexity for the leading edge formed by 3D Metal Forming. These specialized 3D welding processes can contribute approximately 10 to 15 [kg CO_2 /kg] of material, further adding to the environmental impact [93] that has been taken into account along with the steel manufacturing emissions.

The rotor blades for the ReWind project, manufactured using the VARTM method, will have a significant carbon footprint due to the energy-intensive nature of resin infusion and curing. Glass fibre is predominantly used in the turbine blades, with a weight of 242.25 [tonnes]. The manufacturing process for these components emits 1.83 [kg CO_2 /kg]¹⁰.

Aluminium components include elements in the gearbox and yaw system, weighing 3.91 and 176.5 [tonnes], respectively, with a total aluminium usage of 180.4 [tonnes]. These components undergo forging and rolling processes, contributing to their CO_2 footprint. Given the emission factors of 0.879 [kg CO_2 /kg] for forging and 2.1 [kg CO_2 /kg] for rolling, the production of aluminium parts results in notable emissions. Copper is primarily used in the generator and gearbox, with weights of 40.46 and 3.91 [tonnes], respectively, totalling 44.37 [tonnes]. The manufacturing processes for copper, mainly forging and rolling, result in emissions of 0.879 and 2.1 [kg CO_2 /kg], respectively.

Adding all of the different manufacturing techniques as well as the associated factor leads to 4.26e06 [CO_2 tonnes] for the whole farm, with 20.68e06 [MWh] consumed. These emission estimates highlight the importance of optimizing manufacturing processes and materials to reduce the carbon footprint of wind turbine components. To mitigate these emissions, companies like Vestas and others in the industry are increasingly focusing on sustainability practices such as refurbishing components, which can save up to 45% of CO_2 emissions compared to producing new parts. This involves reusing up to 70% of the materials, significantly reducing the overall carbon footprint of the wind turbine components¹¹.

13.1.3. Transportation

The transportation phase of wind turbine components from the port of Rotterdam to the offshore installation site involves significant logistical efforts and associated CO_2 emissions. To estimate these emissions, the use of two 345-foot deck-size barges is considered, chosen based on their deadweight capacity suitable for carrying the wind turbine components. Each barge operates at a maximum power output of 1470 [kW], and the fuel consumption rate is 191 [g/kWh]¹².

The total round-trip distance from Rotterdam to the installation site and back is 300 [km]. Assuming the barges operate continuously at maximum power, the operational time for each round trip is approximately 9.55 hours. Given this, the fuel consumption for one barge over the entire journey is 2.682 [tonnes] of heavy marine oil. For two barges, the total fuel consumption is doubled. Using the emission factor of 3.15 tonnes of CO_2 per tonne of marine heavy oil fuel consumed [94], the total CO_2 emissions for one round trip with both barges are 33.8 tonnes of CO_2 . Multiplying this by the number of units transported, 288 units, the total CO_2 emissions is 9734.3 tonnes of CO_2 .

In this first-order estimate, the difference in CO_2 emissions for the return journey was neglected, where the ships would be lighter after unloading the components. This simplification assumes that the ships emit the same amount of CO_2 regardless of their load, focusing on the maximum operational capacity for the entire round trip. This analysis underscores the significant carbon footprint associated with the transportation phase of wind turbine deployment, highlighting the need for efficient and optimized logistical strategies to mitigate environmental impact.

13.1.4. Operations

In the operation phase of the project, the main contributor to CO_2 emissions and energy consumption are the crew transfer vessels. As mentioned in section 9.2, 12 vessels are used, with an assumed speed of 24 knots and a maximum range of 48 nautical miles. This means that each back-and-forth trip takes 2 hours, which accounts for 4 hours of operation per day. As was assumed by ORE Catapult [95], a crew transfer vessel

⁹<https://sif-group.com/en/esg/environmental/> [Accessed 13-06-2024]

¹⁰<https://www.ptonline.com/news/calculating-an-injection-molding-machines-carbon-footprint> [Accessed 13-06-2024]

¹¹<https://www.vestas.com/en/media/blog/sustainability/refurbishing-components-for-wind-turbines> [Accessed 13-06-2024]

¹²<https://www.seaboats.net/10000t-1ct-deck-barge-1508423> [Accessed 13-06-2024]

consumes 320 litres of Marine Fuel Oil per hour, which emits 999.1 kg of CO_2 per hour. The fuel used has an energy density of 40.9 MJ per liter [96]. Thus, assuming the 12 boats are operating 4 hours a day and have an operating lifetime of 25 years, 0.437 Megatons of $[CO_2]$ are emitted, with 1.59e6 [MWh] consumed.

13.1.5. End Of Life

During end-of-life and decommissioning, as a conservative approach, it was assumed that the same emissions for transportation are emitted to retire the wind farm. Then, it was assumed that only the steel can be recycled, which led to a recyclability of 97%, similar to the industry's standard. Then, it is estimated that recycling steel saves 1.67 tonnes of CO_2 per ton of steel¹³. This means 4.60 megatons of CO_2 and 13.27e6 [MWh] of energy are saved.

13.1.6. LCA conclusion

From this analysis, the CO_2 emissions per phase can be seen in Figure 13.1, along with the energy consumed per phase in the whole process.

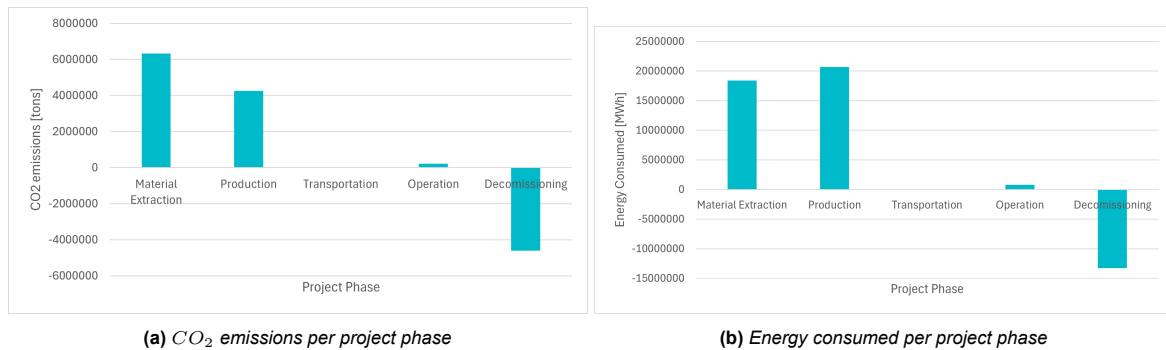


Figure 13.1: Life Cycle Analysis of the different project phases

It is clear that transportation has a negligible effect on both, and the main components for emissions are material extraction and operation. However, thanks to the proper recycling of the majority of the mass of the system (steel), decommissioning greatly reduces the emissions by 41.7%. The result of this analysis is an estimate of the emissions of $7.49 \left[\frac{kgCO_2}{MWh} \right]$ and $0.032 \left[\frac{MWh_{consumed}}{MWh_{produced}} \right]$. This, compared to the industry's standard of $11 \left[\frac{kgCO_2}{MWh} \right]$, is a reduction of 32%. It was found that 21 % of this reduction can be accounted to the higher capacity factor thanks to the addition of the AFC, and 11 % due to the MRS concept.

13.1.7. Storage system

As explained in chapter 10, energy storage will become inevitable for a stable power grid. Therefore, based on the same assumptions and using the same storage capacities, the CO_2 emissions and energy consumed to produce the batteries can be estimated assuming 27500 [kg CO_2] emitted [4] and 42.5 [MWh] consumed [5] per [MWh] of storage. Then, the resulting emissions and energy consumed during the lifetime of the farm (due to the storage system) per [MWh] produced are $19.44 \left[\frac{kgCO_2}{MWh} \right]$ and $0.03 \left[\frac{MWh_{consumed}}{MWh_{produced}} \right]$.

This yields overall farm emissions of $26.92 \left[\frac{kgCO_2}{MWh} \right]$ and an energy consumption of $0.062 \left[\frac{MWh_{consumed}}{MWh_{produced}} \right]$.

If the same calculation is performed for a typical wind farm and its respective necessary storage, it would emit $32.9 \left[\frac{kgCO_2}{MWh} \right]$.

13.2. Materials used over the lifetime

Another measure to estimate the environmental impact of the wind farm, is by taking a look at the materials and land used per MWh produced. Table 13.3 summarises the material used compared to an industry standard wind farm:

¹³<https://www.stenarecycling.com/news-insights/insights-inspiration/guides-articles/the-value-of-recycling-metals/>

Table 13.3: *Materials used per MWh for the wind farms' lifetime*

Material	Rare Earth Metals	Glass Fibres	Steel
ReWind's Material used [g] per [MWh]	<0.01	81.2	3216.3
Standard Wind Farm Material used [kg] per MWh	1.8	193.04	1683.55

As can be depicted, ReWind's farm trades the use of non-recyclable, complex and scarce materials for steel.

Also, ReWind's farm produces 41202.1344 [MWh] of energy for every $[\text{km}^2]$ of land used every year, compared to the 30660 [MWh] per $[\text{km}^2]$ per year. The impact of this 34% increase is the possibility of not using areas reserved for natural habitats, or other protected regions of the ocean.

13.3. Measures to Improve the environmental impact

Now that the Life Cycle Analysis is completed, measures to improve the environmental impact of the wind farm will be addressed.

13.4. Bird Fatalities

Bird fatalities due to offshore wind farms can occur through electrocution and collision mortality, as well as alteration of migration habits.

The following measures are implemented:

1. **Reducing the wind farm area** This aligns with the mission objective of increasing the power density.
2. **Enhanced turbine visibility:** Implement measures to make turbines more recognizable to birds, such as contrasting colours and bird deterrent devices. Painting a single blade in black was found to be a suitable measure to reduce motion smear and thus avian collision [97].
3. **Informed curtailment:** Shut down turbines whenever a bird formation is detected in a high collision risk area [98]. Alternatively, the turbines can be yawed to ensure that the blades are positioned parallel to the wind, minimizing the likelihood of bird strikes¹⁴.

Bats, much like birds, face risks from wind turbine collisions, particularly during their migration seasons. Research indicates that bats are attracted to turbines due to several factors, including the potential for roosting and the abundance of insects. To mitigate these risks, turbines will be programmed to stop and yaw during periods of high bat activity, particularly at night when bats are most active in the migration periods. Furthermore, it is necessary to implement ultrasonic deterrent devices, which help in dissuading bats from approaching the turbines to reinforce biodiversity conservation as much as possible [99].

13.5. Reduced Sea Routes and Fishing Areas

Great complexity in the navigation of offshore vessels arises due to the infrastructure of a wind farm¹⁵ [100]. This reduces the availability of sea routes, which increases the risks of collision between ships and the wind turbines. This threatens maritime safety, possibly resulting in accidents in areas with high maritime traffic. The following mitigation strategies can be implemented to minimize the associated adverse environmental effects.

1. **Signage and lighting:** Install suitable lighting and signage, enhancing visibility and reducing the likelihood of collisions of vessels with wind farm infrastructure. This includes making turbines with high-visibility paints and installing radar reflectors.
2. **Maritime traffic control** Through studying maritime traffic in a specific area, speed restrictions can be established.

13.6. Marine Biodiversity

Offshore wind turbines disrupt marine ecosystems and habitats, affecting the biodiversity of the installed area. Installation activities such as pile driving and cable laying could potentially disturb the seabed and marine life, leading to habitat loss [101, 102]. The following mitigation strategies can be implemented to minimise the associated adverse environmental effects:

1. **Impact assessment:** Identify sensitive habitats, species and ecological processes. This can inform the selection of sites and minimize these adverse impacts.

¹⁴<https://www.noordzeeloket.nl/en/functions-and-use/offshore-wind-energy/start-stop/start-stop-wind-farm-site-decision/> [Accessed 22-05-2024]

¹⁵<https://www.fisheries.noaa.gov/topic/offshore-wind-energy/fishing-community-impacts> [Accessed 22-05-2024]

2. **Habitat protection** Implement habitat protection measures to conserve critical marine habitat affected by offshore wind development.

13.7. Thermal Pollution and Corrosion

Offshore wind farms can potentially impact the marine environment by changing water temperatures. This occurs when operational machinery or electrical transmission cables dissipate heat into the surrounding seawater, potentially leading to thermal pollution. Elevated water temperatures can result in increased algal blooms, which can be detrimental to marine ecosystems by reducing oxygen levels and harming marine wildlife. On the other hand, the marine atmosphere, characterized by high humidity and salinity, can accelerate corrosion in metallic components of wind turbines, including towers and blades. This not only reduces the structural integrity of the wind turbines but also increases maintenance costs (increasing downtime) and reduces their lifespan. The following mitigation strategies can be implemented to minimise the associated adverse environmental effects:

1. **Corrosion-Resistant Materials:** Use materials with high resistance to corrosion for all components exposed to marine atmosphere, such as advanced alloys, protective coatings, or composite materials designed for marine environments.
2. **Electrical design limitation:** Include sealed internal environments for critical electrical components.
3. **Regular Maintenance:** Regular maintenance and inspections are required for timely repairs and replacement of corroded parts.

Furthermore, the wind farm may significantly affect the surface temperature of the air. This is caused by the redistribution of heat caused by the mixing of the boundary layer. It was found that if all U.S. electricity demand was produced by wind farming, the surface temperature would increase by 0.24 [° C] [103]. However, it should be noted that due to the inclusion of the AFC device, colder air may replace the atmospheric boundary layer.

13.8. Acoustic Pollution

The noise generated during the construction and operation of offshore wind turbines can disrupt marine life, particularly cetaceans like whales and dolphins that rely on echolocation. Possible mitigations include implementing bubble curtains and acoustic barriers to reduce underwater noise. Specifically in addressing acoustic pollution, the innovative silent installation technology developed by GBM Works presents a significant advancement¹⁶. This technology dramatically reduces noise during pile driving; a typically loud process in offshore wind turbine construction, by employing a vibrating flange that silently attaches the pile to the seabed. This method not only protects marine life, particularly echolocation-dependent species like cetaceans, from noise disturbances but also complies with marine noise regulations. When used alongside other measures, such as bubble curtains, this technology ensures a strategy to minimize underwater noise during construction.

13.9. Magnetism Effects

The magnetism generated by the sub-sea cables can have adverse effects on marine life. Studies have shown that the swimming activities of haddock larvae reduce in areas with high voltage direct current cables [104]. Another study showed that the speed of migrating eels reduced significantly in regions with wind turbine cables [105]. Studies performed in the North Sea also show reduced fish populations near power cables [106].

To reduce the impact of the magnetism of the cable, its magnetism must be reduced. Core twisting of the cable can be used to reduce the magnetic field and its negative effects on fish [107].

¹⁶<https://www.tudelftcampus.nl/gbm-works-to-support-wind-farm-developer-ecowende-with-innovative-silent-installation-technology/> [Accessed 22-05-2024]

14. Risk Assessment

Effective risk management is essential for a successful design outcome. This chapter provides an in-depth review of the potential technical risks associated with the ReWind project, as outlined in section 14.1, along with strategies to mitigate their impact. The severity of each identified risk is illustrated in a risk map in section 14.2, which can then be used to support resource allocation decisions.

14.1. Risk Management Table

This section provides a detailed analysis of the system's inherent technical risks. Each risk is evaluated based on its likelihood and potential impact, with specific mitigation strategies outlined to reduce these risks. Additionally, a contingency plan is included as a last resort in case a mitigation strategy fails. The effectiveness of each mitigation strategy on various risks is discussed, explaining how the likelihood and/or severity of each risk can be reduced.

The expected reduction in risk from mitigation strategies is supported by relevant sources, justifying the reduction in scores. Not all risks require mitigation strategies, as some already fall within the green region of the risk map (Table 14.6) and are deemed acceptable. Mitigating these acceptable risks would be an unnecessary use of resources.

To ensure compliance with key risk mitigation strategies, system and subsystem requirements were developed to address each new risk which was determined during the detailed design phase. The primary risks outlined in the Baseline Report [58] are reiterated in Table 14.3, as well as the most important risks outlined in the Midterm Report [16] which are presented in Table 14.4. Additional risks identified in the final design are detailed in Table 14.5. Consequently, the Risk Manager must closely monitor the design to ensure that ongoing risk mitigation measures are implemented as needed.

The prefix TR denotes a technical risk related to the design and operation of the wind farm, followed by a unique identifier between 1 and 31 to facilitate their inclusion in the risk maps (see section 14.2). A three-letter acronym at the end indicates the specific subsystem addressed. To quantify and compare these risks, the metrics in Table 14.1 are introduced. These metrics describe the likelihood and severity scores that can be attributed to each risk. For every identified technical risk, potential mitigation and contingency strategies are proposed. Additionally, for each risk, the responsible team member is indicated by a symbol. These abbreviations are detailed in Table 14.2.

Table 14.1: Likelihood and severity metrics.

Score	Likelihood (L)	Severity (S)	Description (L)	Description (S)
1	Very low	Negligible	Likelihood less than 20%: Rare event, minimal expected frequency.	Negligible impact: No effect on turbine operations, production, or safety.
2	Low	Marginal	Likelihood 20%-40%: Uncommon event, anticipated under certain conditions.	Marginal impact: Minor repairs, minimal disruptions to operations, acceptable safety risks.
3	Moderate	Moderate	Likelihood 40%-60%: Significant possibility, demands consideration and action	Moderate impact: Repairs needed, manageable damage, timely interference required.
4	High	Critical	Likelihood 60% - 80%: High probability, immediate action needed	Critical impact: Significant repairs, substantial damage, urgent action required.
5	Very high	Catastrophic	Likelihood >80%: Severe threat, needs immediate action.	Catastrophic impact: Severe damage or destruction, extensive losses, emergency response needed.

Table 14.2: Role Abbreviations

Role	Symbol	Role	Symbol
Project Manager	PM	Responsible Aerodynamics Engineer	RAE
Risk Manager	RM	Responsible Control Engineer	RCE
Sustainability Manager	SM	Responsible Structures Engineer	RSE
Quality Control Manager	QCM	Responsible Electrical Engineer	REE

Each risk with its accompanying mitigation plan and effect, as well as the contingency management, is provided in Table 14.3, Table 14.4 and Table 14.5.

Table 14.3: Risk Management Table 1

ID	Name	Description	BEFORE MITIGATION			Potential Impact	Mitigation action (preventing risks)	Effect of mitigation	Contingency plan (responding effectively if risks occur)	AFTER MITIGATION			Responsible Member
			Like-lihood	Severity	Risk					Like-lihood	Severity	Risk	
TR-1-ELC	Unavailability of a generator	A generator becomes inoperative because of a technical failure	2	4	8	Lower energy production capability, higher LCOE	Implement higher grade thermal winding insulation, perform preventive and predicative maintenance adequately.(ref)	This will ensure that the likelihood of a generator failing will be reduced by roughly a factor 2	Send a maintenance team offshore to replace the faulty generator	1	4	4	REE
TR-2-DRT	Gearbox failure	The gearbox transforming the high torque and low rotational rate of the wind turbine into low torque and high angular rate fails and impedes the production of electricity	2	4	8	Shutdown of the generator or very low energy production.	Perform regular maintenance and quality checks to ensure a minimal likelihood of occurrence (ref).	This will reduce the likelihood of a gearbox failure by roughly a factor 2	Send a maintenance team offshore to replace the faulty gearbox	1	4	4	RCE
TR-3-OCS	Excessive wind speeds	Because of evolving climate, more extreme conditions might be encountered (especially in terms of windspeed) over the lifetime of the wind farm.	1	4	4	Major structural failures, depending on the failure sequence	During design, account for extremely harsh weather conditions predicted by the most pessimistic climate models and apply safety factors on top of that (TBD) [108]	Mitigation could be possible for this risk however, implementing it would only have a limited result. Therefore, it was decided not to implement it in order to minimize the use of resources.	Based on the damage on the wind turbines, components will have to be replaced accordingly	1	4	4	RSE
TR-4-ELC	Electrical system overload	Occurrence of voltage fluctuations due to high speed winds and grid instabilities	2	4	8	Equipment damage, power outage, fire and loss of productivity	Install reactive power compensation systems [109]	This will reduce the severity and likelihood of an electrical system overload by adequately reacting to voltage fluctuations. The likelihood and severity will be reduced by a factor of 2	Backup power supply systems to reduce the stress on electrical systems during peak demands.	1	2	2	REE
TR-5-SYS	Fatigue	Fatigue failure due to repeated loading cycles.	3	4	12	Resulting in possible delamination, crack and stress accumulation leading to catastrophic failures.	Employ advanced materials and manufacturing techniques to enhance component durability and fatigue resistance. Monitoring systems to inspect early signs of fatigue [110].	These measures will reduce the likelihood of occurrence by a factor 35% roughly because of better quality control and tracking. Furthermore, the use of adapted materials will reduce crack propagation and decrease the severity by roughly 25%.	Non-destructive testing methods along with regular inspection and maintenance.	2	3	6	RSE
TR-6-OCS	Brake failure	The brake ensuring that the maximum operational rotational rate is not exceeded fails	2	4	8	Potentially exceeding maximum rotational rate and catastrophic damage	Provide a second brake system in the design or create a fail-safe system that will brake automatically if the system is powered off [111].	This will reduce the likelihood of a brake failure by a factor 2 by introducing extra redundancy in the system that can take over if the primary system fails.	Adjust the blade pitch such that the torque on the drivetrain is minimized	1	4	4	RSE
TR-7-SYS	Structural Resonance	Resonance in wind turbine components induced by wind loading and turbulence	2	5	10	Potentially catastrophic structural damage	Implement damping systems to mitigate resonance effects and sensors to trace vibrations in the structure [112].	This will reduce the likelihood of resonance occurring by a factor of 2 by damping vibrations in the system. Furthermore, damping will also reduce the severity of a resonance by 40%.	Assess structural integrity of the structure after a resonant event.	1	3	3	RSE
TR-8-OCS	Control system failure	Issues with field devices or Input/output modules causes control system to fail	2	3	6	Loss of power production due to incorrect pitch and yaw, potentially increased load on the structure	Implement a redundant control system and perform regular maintenance [113].	Mitigation could be possible for this risk however, implementing it would only have a limited result. Therefore, it was decided not to implement it in order to minimize the use of resources This will result in a reduction in greenhouse gas emissions promoting sustainability. The likelihood of pollution related incidents will decrease by approximately 40%, and the severity of the environmental impact will decrease by 33%.	Send a maintenance team offshore to repair faulty devices and/or damages	2	3	6	RCE
TR-9-SUS	Manufacturing Pollution	Construction and operation associated with offshore wind farms may generate pollutants during manufacturing, assembly, and end-of-life treatment processes	5	3	15	Air quality degradation and emission of CO2	Implement sustainable manufacturing approaches, including pollution control measures and use of eco-friendly materials [86].	The likelihood of pollution related incidents will decrease by approximately 40%, and the severity of the environmental impact will decrease by 33%.	Develop remediation strategies and restoration plans for mitigating environmental impact and restoring affected ecosystems	2	3	6	SM
TR-10-SUS	Navigation and impact on maritime traffic	Restricted sea routes and vessel traffic congestion due to wind farm infrastructure	3	1	3	Increased collision risk and navigation complexity	Spatial planning to avoid siting turbines in high-traffic areas [114].	Mitigation could be possible for this risk however, implementing it would only have a limited result. Therefore, it was decided not to implement it in order to minimize the use of resources	In order to reduce the risk of collision and guarantee safe navigation, emergency protocols for vessel traffic management and coordination should be established.	3	1	3	SM

Table 14.4: Risk Management Table 2

ID	Name	Description	BEFORE MITIGATION			Potential Impact	Mitigation action (preventing risks)	Effect of mitigation	Contingency plan (responding effectively if risks occur)	AFTER MITIGATION			Responsible Member
			Like-likelihood	Severity	Risk					Like-likelihood	Severity	Risk	
TR-11-MAN	Non-redundant Supply Chain	If a component can only be manufactured by one single supplier, the system becomes vulnerable to shortages, delays and price increases	2	4	8	a of operations because of lack of spare parts.	Choose off-the-shelf parts that can be easily replaced by others, have multiple suppliers for one part.	Choosing off-the-shelf parts will increase the ability to handle a supply chain disruption, reducing the likelihood of shortages by a factor of 2.	Contact alternative suppliers and implement new logistics chains.	1	4	4	PM
TR-12-MAN	Misalignment of Components	During the assembly process the different components could be aligned inaccurately, compromising their functionality	2	4	8	Inaccurate alignments, for instance between the elements of the drivetrain, can lead to vibrations and a reduction of the component lifetime.	Implement precision assembly techniques and enhanced quality control during assembly [115].	By increasing the alignment accuracy, the average magnitude of the vibrations will be reduced, leading to roughly a halving of the vibrations severity	If excessive vibrations are detected, the alignment of the components shall be inspected and adjusted.	2	2	4	QCM
TR-13-MAN	Unavailability of Materials	Some critical materials such as rare earth metals or composites can only be sourced in certain countries. The system then becomes reliant on these primary sources of materials.	1	5	5	A shortage of primary raw materials and resources will ultimately lead to a shortage of spare components, jeopardizing the operations.	Diversify material sourcing and invest in alternative materials research, increase the storage capacity for spare parts.	The choice of alternatives to rare earth metals, a more diversified supply chain and the increased storage will help reduce the severity by roughly 40%. Mitigation could be possible for this risk however, implementing it would only have a limited result.	If materials were to become unavailable, other suppliers shall be contracted if possible, even at an increased cost.	1	3	3	PM
TR-14-ROT	Blade Failure Cascade Effect	A blade fails in a rotor lattice structure	1	4	4	The detached blade might damage and lead to failure of other blades, generating a chain reaction of failures.	Proper spacing shall be ensured, safety factors shall be included	Mitigation could be possible for this risk however, implementing it would only have a limited result. Therefore, it was decided not to implement it in order to minimize the use of resources.	Damage shall be assessed on-site and necessary replacements shall be carried out	1	4	4	RSE
TR-15-ROT	Thrust imbalance	Rotors on one side of the structure producing more thrust might create undesirable torque that needs to be counteracted by the yaw subsystem.	5	1	5	Increased stress on the yaw subsystem leading to potential mechanical failures.	Implementing advanced control systems to detect and correct thrust imbalances in real-time.	Enhanced monitoring, maintenance, and control systems can reduce the likelihood of thrust imbalance by roughly a factor of 25% [116]	Immediate adjustment of the yaw subsystem to counteract the imbalance.	4	1	4	RAE
TR-16-ROT	Rotor Imbalance	An imbalance in the rotors due to debris accretion or damages can cause vibrations and ultimately shorten the lifetime of the system	3	3	9	Increased vibrations leading to accelerated wear and higher maintenance costs and potential downtime.	Inspection of rotors to remove debris and detect early signs of damage [117].	Regular maintenance and monitoring can reduce the likelihood of rotor imbalance by roughly a factor of 33%	Shutdown of the affected turbine to prevent further damage.	2	3	6	RAE
TR-17-ROT	Blade Delamination	Separation of composite layers within turbine blades, compromising structural integrity and aerodynamic performance.	2	4	8	Reduced aerodynamic performance leading to decreased energy production. blade failure, resulting in costly repairs	Implement non-destructive testing methods to monitor blade [118].	Enhanced materials and regular monitoring can reduce the likelihood of blade delamination by roughly a factor of 2	Shutdown of the affected turbine to prevent further damage and repair/replacement of the blade.	1	4	4	RSE
TR-18-SUS	Aggravated Climate Change	Due to the reduced velocity and the wake produced behind the wind turbine, the temperature of the atmosphere increases and alters the local climate.	3	4	12	Increased local temperature, Altered local climate including changes in precipitation patterns, fog formation, and change in wind patterns.	Careful spatial planning of wind farm [119].	By strategically placing wind farms and continuously monitoring the local climate, the likelihood of adverse climate impacts can be reduced by roughly a factor of 3	Implement adaptive management practices to address any unexpected changes in local climate.	1	4	4	SM
TR-19-ELC	Power Converter Failure	Malfunction of electrical components converting and controlling turbine-generated electricity, causing power output disruptions and potential equipment damage.	3	4	12	Reduced energy production efficiency and possible downtime	Implement a set-up where the power through the converter is reduced, implement redundant converters in the grid [120].	Redundant converters and the lower loads through the converters can reduce the likelihood of power converter failure by roughly a factor of 3	Repair or replacement of the faulty power converter.	1	4	4	REE
TR-20-ELC	Power Cable Degradation	Deterioration of cable insulation due to environmental factors, increasing electrical resistance and risk of short circuits or fires.	2	3	6	Increased risk of short circuits or fires, downtime and costly repairs.	Use of high-quality, weather-resistant cable insulation materials [121].	Mitigation could be possible for this risk however, implementing it would only have a limited result. Therefore, it was decided not to implement it in order to minimize the use of resources.	Immediate isolation and repair or replacement of the degraded cables.	2	3	6	RSE
TR-21-CON	Malfunction of Wind Sensors	A malfunction in the detection of wind properties can compromise the accuracy and effectiveness of the pitch and yaw systems	3	3	9	Reduced efficiency in energy production due to improper alignment of the turbines. Increased mechanical stress on the turbines, leading to potential damage and higher maintenance costs.	Use of redundant wind sensors to provide backup data in case of a sensor failure [122].	Ensuring regular maintenance and having redundant systems in place can reduce the likelihood of sensor malfunctions by roughly a factor of 3	Immediate replacement or repair of faulty wind sensors.	1	3	3	QCM

Table 14.5: Risk Management Table 3

ID	Name	Description	BEFORE MITIGATION			Potential Impact	Mitigation action (preventing risks)	Effect of mitigation	Contingency plan (responding effectively if risks occur)	AFTER MITIGATION			Responsible Member
			Like- lihood	Severity	Risk					Like- lihood	Severity	Risk	
TR-22-MAN	Worker injury during installation and assembly	Injury or death of workers due to accidents during manufacturing, assembly or installation	3	5	15	Loss of public confidence in project, loss of investment or ability to procure future contracts	Establish and enforce measures which promote a safe working environment. Clearly establish and communicate what repercussions will result from a breach in protocol. Follow necessary safety regulations(ref).	The likelihood can be expected to reduce by less than 20% [123], and it is also reasonable to expect that the severity of accidents occurring reduces similarly.	emergency response plan that includes first aid, evacuation procedures, and incident reporting. Ensure all workers are aware of the procedures.	2	3	6	PM
TR-23-MAN	Unavailability of installation equipment	Installation equipment becomes unavailable due to scheduling conflicts, technical issues, or logistical delays.	2	3	6	Delayed project timelines, increased costs, and potential contract penalties.	Perform proactive scheduling and coordination with suppliers and contractors. Maintain backup agreements with equipment rental companies. Regularly check and service equipment to prevent technical failures.	Mitigation could be possible for this risk however, implementing it would only have a limited result. Therefore, it was decided not to implement it in order to minimize the use of resources	Contingency plan includes backup equipment options, prioritize critical installation tasks, and negotiate flexibility with stakeholders.	2	3	6	PM
TR-24-MAN	Schedule delays due to weather conditions	Construction or installation schedules are delayed due to adverse weather conditions such as rain, wind, or storms.	3	3	9	Increased project costs, delayed project completion, potential contract penalties.	deploy installation vessels which have the maximum versatility in adverse weather conditions(ref)	The likelihood is reduced by a factor of 3, but there still exists a residual risk since it can never be fully mitigated.	Rescheduling strategies, and communication with stakeholders.	1	3	3	PM
TR-25-MAN	Emergency event during maintenance	Unexpected emergencies, such as fires, medical emergencies, or hazardous material spills, occurring during maintenance activities.	3	3	9	Endangerment of maintenance workers, or inability to evacuate the turbine unit.	Ensure multiple escape paths are available, make sure all personnel present on the structure can evacuate within 60 [sec].	The severity is reduced if the survivability and preparedness for emergency situations increases. A decrease of 30% is estimated, since the operational impact remains high regardless.	Set up an emergency rescue and response strategy, and ensure the necessary recourses are available at all times.	2	2	4	PM
TR-26-YAW	Yaw system failure during storm	The yaw system fails to adjust the turbine position in response to a storm, leading to potential structural failure.	2	4	8	Severe structural damage, reduced energy production, high repair costs.	Perform regular maintenance, and implement storm detection and early warning systems[124].	Through adequate preparation when a storm is incoming, as well as having frequent maintenance of systems, the likelihood of suffering a malfunction in the yaw system reduces by a factor of 2.	Develop an emergency plan that includes immediate manual intervention and real-time monitoring to quickly address any issues. Mobilize a repair team to fix the yaw system as soon as conditions allow.	1	4	4	RCE
TR-27-AFC	AFC actuator failure	The actuators responsible for deploying the high-lift devices (HLDs) of the AFC system malfunction	2	3	6	If the HLDs do not retract, the structure may become overloaded as the wind speed increases. Also, the HLDs themselves may become damaged.	Ensure redundancy in the actuator system, or design the HLDs such that they are destroyed before the structural design loads are exceeded.	Mitigation could be possible for this risk however, implementing it would only have a limited result. Therefore, it was decided not to implement it in order to minimize the use of resources.	Prepare a detailed maintenance and repair plan, ensuring that spare actuators and parts are readily available. Train maintenance staff to perform rapid actuator replacements or repairs.	2	3	6	RAE
TR-28-SYS	Seismic activity	Earthquakes in the region may induce extra loads to the monopile.	1	4	4	Seismic loading will affect the loading and dynamic stability of the structure, and potentially cause damage which is hard to detect.	Implement components in the design to mitigate the effect of wind-wave-earthquake loads, such as a tuned mass damper inerter (TMDI)[125].	Mitigation could be possible for this risk however, implementing it would only have a limited result. Therefore, it was decided not to implement it in order to minimize the use of resources	Schedule additional inspection and maintenance operations. Shut down affected turbine units until it has been confirmed they are safe for operation.	1	4	4	RSE
TR-29-SYS	Cascade failure of truss members	Failure of truss members can lead to a domino effect of failures which compromise the structural integrity of the structure.	2	5	10	Failure of one or multiple truss members results in load redistribution causing more truss members to fail in a snow-ball effect.	Design the truss structure with redundant load paths, include safety factors in the design. Ensure design load cases cover all extremes of the operational envelope, and analyse how the structure fails in conditions exceeding these cases[126].	By overdimensioning and implementing redundancy in the truss structure, the likelihood reduces by a factor of 2 and the severity by 40%.	Monitor the state of the structure, and plan additional maintenance and inspection after extreme loading events such as storms.	1	3	3	RSE
TR-30-COMM	Security breach of central control and data system	Unauthorized access or attack on the central control and data system, potentially compromising system integrity and safety.	1	4	4	Security of wind farm becomes compromised, potentially threatening the security of the Dutch national grid.	Ensure data storage and communication systems are designed to industry standards, and are tested to ensure they are secure(ref).	Mitigation could be possible for this risk however, implementing it would only have a limited result. Therefore, it was decided not to implement it in order to minimize the use of resources	Identify security weaknesses, and modify data and communication systems to prevent these weaknesses from being exploited. Inform shareholders and grid operator of potential security risk.	1	4	4	RM
TR-31-COMM	Fibre-optic unit failure	Malfunction or failure of the fibre-optic unit, disrupting communication and data transmission essential for monitoring and control.	2	4	8	An entire ring of turbine units could potentially be lost from the communication network.	Implement redundancy in the communication network, and ensure components are easily accessible for maintenance. Turbine units automatically enter parked state in a control loss situation(ref).	Featuring redundancy in the communication network design reduces the severity of a malfunction by a factor of 2, as there will always be an alternative path to transfer information.	Execute a repair, and assess if any damage has been done.	2	2	4	REE

14.2. Risk Map

Table 14.6 serves as a visualization tool where the aim is to mitigate the most concerning risks such that they move from the red and yellow (high risk) regions towards the green (low risk) region, risks that are already located within the green region do not need to be mitigated since the associated risk is acceptable. The numbers indicated in Table 14.6 are representative of identifiers in Table 14.3, Table 14.4, yet for simplicity 'TR' as well as the associated subsystem acronym are not mentioned.

Table 14.6: Risk map before mitigation.

	1	2	3	4	5
5	13	7,29	22		
4	3, 14, 28, 30	1, 2, 4, 6, 11, 12, 17, 26, 31	5, 18, 19		
3		8, 20, 23, 27	16, 21, 24, 25		9
2					
1			10		15

Table 14.7: Risk map after mitigation.

	1	2	3	4	5
5					
4	1, 2, 3, 6, 11, 14, 17, 18, 19, 26, 28, 30				
3	7, 13, 21, 24, 29	5, 8, 9, 16, 20, 22, 23, 27			
2	4	12, 25, 31			
1		27	10	15	

By applying the mitigation strategies presented in Table 14.3 Table 14.4, Table 14.5, and using common engineering judgement the most critical risks can be placed in the green region as can be seen in Table 14.7. Note that in Table 14.7 the risks which have been mitigated have been displayed in bold to ease readability.

By systematically addressing the identified technical risks and implementing appropriate mitigation measures, this project aims to enhance its overall resilience and increase the likelihood of achieving its objectives within the allocated resources and timeline.

Requirements to address technical risks

Each identified technical risk that requires some sort of mitigation strategy also needs accompanying requirements. This is to make sure that the design is capable of handling and mitigating the risks. The table below gives an overview of the new requirements that arose from the technical risk analysis in Table 14.5. The associated requirements originated from Table 14.3 and Table 14.4 are dictated in Baseline [58] and Midterm [16] report.

Table 14.8: Requirements derived from risks

Risk ID	Requirement ID	Requirement
TR-24-MAN	REQ-SYS-39	The installation vessels shall be certified to Dynamic Positioning Class III
TR-25-MAN	REQ-SYS-40	The time to escape the structure with one escape route obstructed shall not exceed 5 minutes.
TR-26-YAW	REQ-SSYS-Y&P-04	The yaw system shall be able to achieve a yaw rate of 0.1 [deg/s] with 1 yaw motor inoperative.
TR-29-SYS	REQ-SSYS-TOW-05	The structure shall be designed using safety factors specified by the standard IEC 61400-1.
TR-31-COMM	REQ-SSYS-Y&P-05	The turbine unit shall automatically return to a parked state if a loss of communication is detected.

15. Final Design

This chapter aims to present the final design that resulted from the detailed design phase. For each subsystem, the most important characteristics will be highlighted to give a global overview of the Rewind system. This is presented in section 15.1. Subsequently, the performance of the system will be summarized in section 15.2. Finally, a complete overview and summary will be given in section 15.3.

15.1. Subsystem Overview

As one can see from Figure 15.1, the final system is a complex assembly of different subsystems. Each of these has gone through a detailed design phase as described previously in chapter 5. A quick summary of the most important characteristics of each subsystem will be presented below.

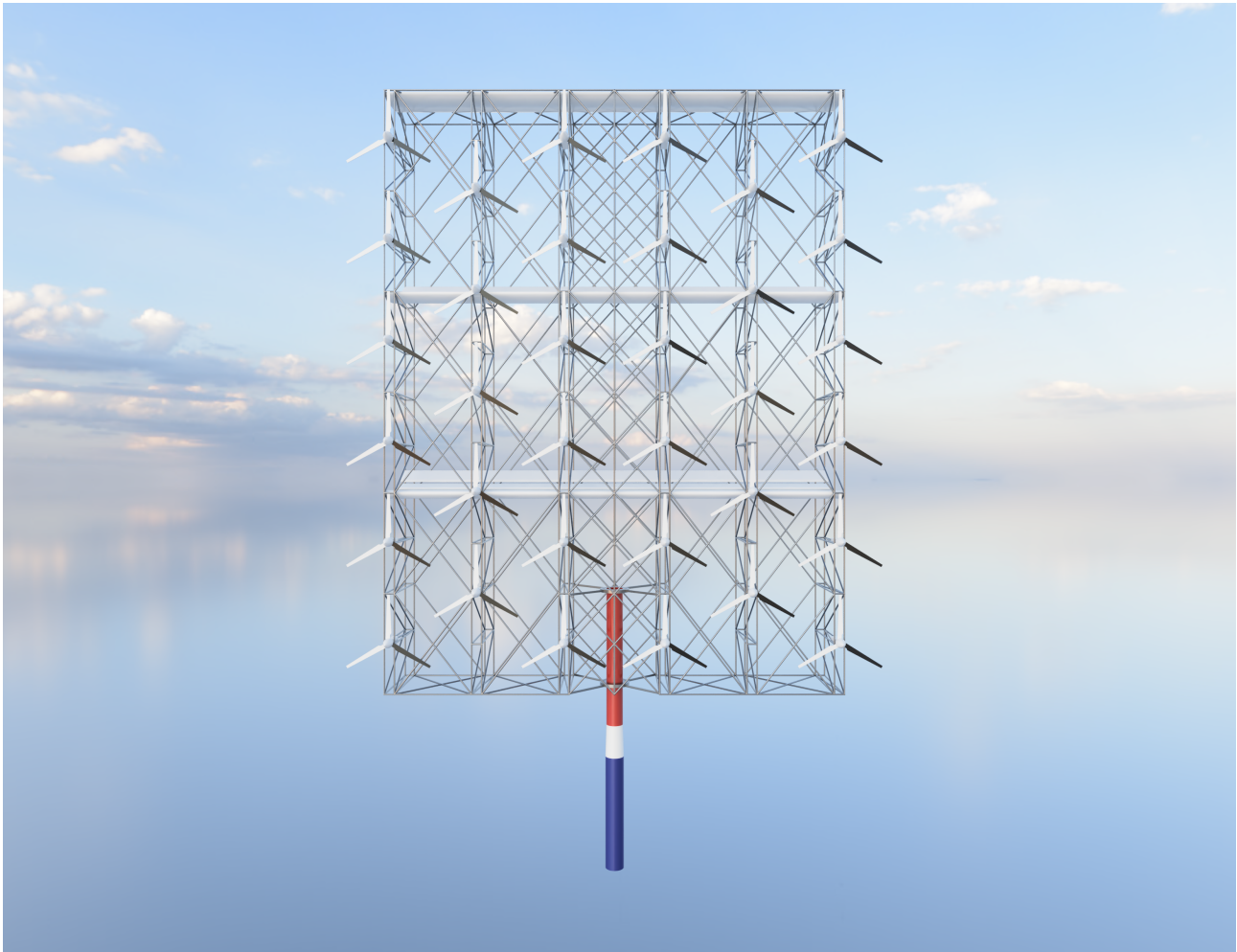


Figure 15.1: *Render of the final design*

Rotors

This design, ReWind, contains a total of 34 three-bladed rotors with a diameter of 58 [m], which coincides with the total swept area of a single rotor of equivalent rated power.

The selected airfoils in the case of ReWind's blades are S818, S816 and S817. These airfoils are developed by the U.S. National Renewable Energy Laboratory (NREL).

The exact blade radius was derived to be 28.93 [m] with a mechanical C_p of 0.49. Additionally, the maximum chord is 3.3 [m], and the root twist is -9.9° . This comes from a chosen tip speed ratio of 8 and a rated wind

speed of 10.59 [m/s]. Finally, the mechanical power outputted by each of the rotors turns out to be 937 [kW], leading to a slightly higher mechanical output power of 31.9 [MW] compared to the rated power. This was set to take into account inefficiencies in drivetrains and generators.

Active Flow Control

ReWind uses an Active Flow Control (AFC) system to reduce the penalty for placing wind turbines closer together.

The three downforce-generating triple-element wings of ReWind produce a total lift of 6.5 [MN] at the rated speed. They re-energize the flow to 95.7% of the initial available power. The wings have a cord of 50 [m] and are placed at heights of 387.4, 265, 241 [m]. The span of the wings is determined by the available space in the superstructure, which results in a span of 277 [m] for the top wing and 241 [m] for the remaining two wings.

The AFC system is able to retract its' elements during a storm to reduce its lift coefficient from 3.22 to 0.345. The total mass of the AFC system is estimated to be 205.7 [t].

Superstructure

The superstructure is the main structural element of the system. It houses all the RNAs as well as the accessibility systems for maintenance, such as walking platforms, lifts, etc. The overall dimensions of the structure are quite significant, it measures 278 [m] in width with a height of 365.56 [m]. Building such a structure was found to be an optimal application of a truss structure, using slender cylindrical truss members

The superstructure contains 1351 elements. Each truss element has a fixed thickness-to-diameter ratio of 120, with a maximum required diameter of 1.77 [m] and a minimum diameter of 0.36 [m].

Foundation

For the foundation of the ReWind turbine, a steel monopile is used. The monopile measures 20 [m] in height from its base to the waterline, in accordance with the water depth at the desired farm location. The monopile is tapered, with its diameter decreasing from 11.72 [m] at the base to 10.33 [m] at the top, where it connects to the superstructure. Additionally, the monopile's thickness tapers from 9.8 [cm] at the base to 8.8 [cm] at the top, optimizing material usage while maintaining structural integrity.

Pitch & Yaw Control

The yaw control system of the ReWind wind turbine incorporates a novel approach using differential pitching combined with secondary electric motor support. This system utilizes two bearings situated at 25 [m] and 60.68 [m] above the sealevel, designed to support both the structural weight and the dynamic loads experienced during operation.

The pitch system is equipped with a range of sensors that feed data to a central Pitch Controller, which processes this information to adjust the blade pitches accordingly. The system is designed to respond dynamically to varying operational conditions through a feedback loop. The pitch system integration within the turbine operational framework aims to maintain optimal power output and stability, even under fluctuating environmental conditions.

Drivetrain

Each rotor in ReWind's design features an asynchronous Doubly Fed Induction Generator (DFIG). Specifically, a 900 [kW] Indar DFIG has been selected, which produces electricity at 690 [V] and has a dry mass of 3.4 [t]. Complementing the DFIG is the Gamesa G5X gearbox. It has a gear ratio of 62 and an output speed of 1620 [rpm]. The gearbox has a dry mass of 5.75 [t].

Material Overview

The structure is composed of various components, each using specific materials chosen for their properties and functionalities. Steel is the predominant material used across almost all components. It makes up the entirety of the AFC, monopile, superstructure, and forms a significant part of the generators (65%) and gearbox (96%). Glass fibre is primarily used in the blades and hub, accounting for 95% of the material. Copper is another critical material, particularly in the generators (35%) and gearbox (2%). Additionally, aluminium is used in small proportions (2%) in the gearbox. The material distribution for each component is in Table 15.1, providing a precise breakdown of the materials used.

Table 15.1: Material distribution overview.

Component	Steel [%]	Glass Fiber [%]	Aluminium [%]	Copper [%]
Blades and Hub	5	95	-	-
Generators	65	-	-	35
AFC	100	-	-	-
Gearbox	96	-	2	2
Monopile	100	-	-	-
Superstructure	100	-	-	-

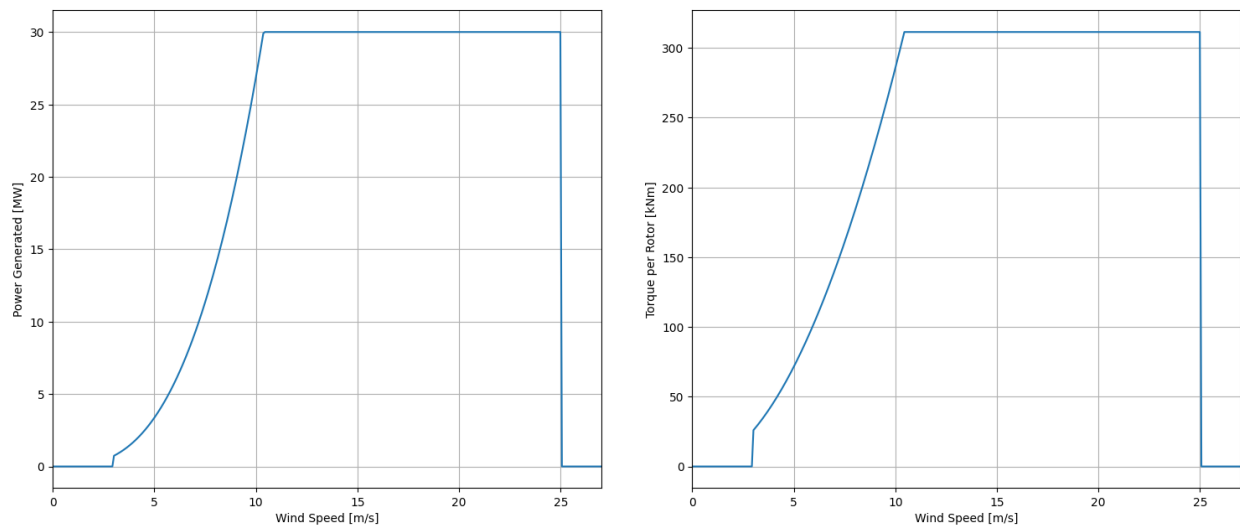
15.2. Performance Analysis

Table 15.2 summarises the main performance parameters of the wind farm:

Table 15.2: Performance Analysis of the wind farm

Parameter	Value	Units	Improvement/Reduction
Wind Farm Rated Power	8.812	[GW]	
Wind Farm Capacity Factor	47.5 %	-	+35%
Wind Farm efficiency	84.5 %	-	+47%
Power density	10.36	[MW/km ²]	
LCOE	40.7	[€/MWh]	-40%
CO2 emitted	7.48	[kgCO ₂ /MWh]	-32%
Energy Density	41202	[MWh/km ² /year]	+34%
Steel Use	3.2163	[kg/MWh]	+91%
Glass Fiber Use	0.0812	[kg/MWh]	-58%
Rare Earth Metal Use	0.01	[g/MWh]	-99%

Furthermore, the power curve and torque curve for a single Multi Rotor System (MRS) is given in Figure 15.2.

**Figure 15.2:** Power and Torque Curves

15.3. Final Design Summary

Table 15.4 summarises the key parameters of the ReWind turbine design. Furthermore, Table 15.3 breaks down the total mass of the turbine by component. The total mass of one turbine is approximately 11,003.7 [t].

Table 15.3: Overview of the mass for the major components of the system

Component	Mass	Unit
RNA	1,685,000	[kg]
Monopile + Tower + Yaw bearing	4,798,000	[kg]
Superstructure	4,315,000	[kg]
AFC	205,700	[kg]
Total	11,003,700	[kg]

Table 15.4: Key Parameters for ReWind Turbine

Parameter	Value	Parameter	Value
Rated power	30.3 [MW]	Turbine Height	365.6 [m]
Cut-in wind speed	3.0 [m/s]	Turbine Width	278 [m]
Rated wind speed	10.59 [m/s]	Diameter of Truss (min. - max.)	0.36 - 1.77 [m]
Cut-out wind speed	25.0 [m/s]	Diameter / Thickness Ratio of Truss	120
		Foundation Type	Monopile
Rotor Number	34	Monopile Diameter (min. - max.)	10.33 - 11.72 [m]
Diameter	28.93 [m]	Monopile Thickness (min. - max)	8.8 - 9.8 [cm]
Swept area	89,397 [m ²]		
Number of blades per rotor	3	Generator	Indar DFIG
Rotor speed	28 [rpm]	Generator Rated Power	900 [kW]
Tipspeed Ratio	8 [m/s]	Voltage	690 [V]
Flow Control	3 Element Wing	Gear Box	Gamesa G5X
Lift Generated	6.5 [MN]	Gear Box Type	Spur/planetary
Number of Wings	3	Gear Ratio	1:62
Span (top - middle - bottom)	277 - 241- 241 [m]	Output Speed	1620 [rpm]
Chord	50 [m]		
Airfoil Type	NACA 4418		

16. Requirement compliance

This chapter evaluates the compliance of the ReWind conceptual design with the previously established requirements. For each requirement, the performance level achieved by the ReWind concept is indicated, with a color-coded cell: green if the requirement is met, and red if it is not. Furthermore, a reference to the location in this report where the requirement compliance is designed for is also added. The chapter is structured as follows: first, the compliance of subsystems is assessed, followed by the overall system, mission, and finally, stakeholder requirements. This order is used because the lower-level requirements are more detailed specifications of the higher-level requirements. Therefore, it is necessary to satisfy lower-level requirements before moving on to higher-level ones. To maintain conciseness, only the most important and representative requirements are presented, as some requirements have not been addressed in this conceptual design phase.

16.1. Subsystem compliance

This section will detail the compliance of the ReWind concept with the subsystem requirements. These requirements are categorized according to the following subsystems: Truss Structure, Yaw and Pitch Control, Drivetrain, OCS, Rotor, and Foundation.

Truss structure:

Table 16.1: *Truss structure compliance*

ID	Requirement	ReWind performance
REQ-SSYS-TOW-01	The superstructure height of each multi-rotor unit shall not exceed 300 [m] from the MSL	The height of the superstructure is 388 [m]. (subsection 5.4.3)
REQ-SSYS-TOW-02	The superstructure width of each multi-rotor unit shall not exceed 300 [m]	The width of the superstructure is 278 [m]. (subsection 5.4.3)
REQ-SSYS-TOW-03	The structure shall withstand transverse loads generated by wind speeds up to 66 [m/s]	The structure has been designed for a constant wind of 66 [m/s]. (subsection 5.4.8)
REQ-SSYS-TOW-04	The structure shall be accessible and include safety rails for maintenance	A ladder, elevator and platforms including safety rails make the structure accessible for maintenance. (section 9.4)

Yaw & Pitch control:

Table 16.2: *Yaw & Pitch control system compliance*

ID	Requirement	ReWind performance
REQ-SSYS-Y&P-01	The multi-rotor system shall be able to yaw with a maximum offset of 5 degrees with respect to the wind direction.	(subsection 5.5.1)
REQ-SSYS-Y&P-02	The whole multi-rotor system shall yaw at a rate of 0.5 [deg/s].	The ReWind structure does not yaw at a rate of 0.5 [deg/s], depending on wind speed and yaw misalignment. (Figure 5.19)
REQ-SSYS-Y&P-03	The rotor blades shall be able to pitch in a range of -10 to 40 [deg]	(subsection 5.5.2)

Drivetrain:

Table 16.3: Drivetrain compliance

ID	Requirement	ReWind performance
REQ-SSYS-DRT-01	The gearbox shall have a gear ratio of at least 50	The gearbox has a gear ratio of 54. (Table 5.14)

Operations and Control (OCS):

Table 16.4: OCS compliance

ID	Requirement	ReWind performance
REQ-SSYS-OCS-01	Each rotor shall be able to stop rotating on command.	The pitch system combined with the brakes allow for each rotor to be stopped on command. (subsection 5.5.2)

Rotor:

Table 16.5: Rotor compliance

ID	Requirement	ReWind performance
REQ-SSYS-ROT-05	The rotor blades shall be replaceable	The pulley system at the top of the structure is capable of lifting new blades up, allowing them to be replaced. (section 9.2)
REQ-SSYS-ROT-08	Each rotor shall have a maximum rotational speed of at most 3 [rad/s]	Each rotor in the system has a maximum rotational speed of 2.93 [rad/s]. (section 5.1)

Foundation:

Table 16.6: Foundation compliance

ID	Requirement	ReWind performance
REQ-SSYS-FDT-02	The foundation shall support a weight of at least 60 [MN]	The foundation has been sized to support a weight of 64 [MN]. (subsection 5.4.7)
REQ-SSYS-FDT-03	The foundation shall transfer loads to the seabed	(subsection 5.4.6)
REQ-SSYS-FDT-04	The foundation shall withstand wave-induced loads	The foundation has been sized taking into account wave-induced loads. (subsection 5.4.7)
REQ-SSYS-FDT-05	The foundation shall be resistant to corrosion	The foundation is covered in an anti-corrosion coating. (section 7.1)

16.2. System compliance

This section will detail the compliance of the ReWind concept with the system requirements.

Table 16.7: System compliance

ID	Requirement	ReWind performance
REQ-SYS-01	90% of the wind farm components, by mass, shall be recyclable	By mass, 94 % of the ReWind system is recyclable. (subsection 13.1.1)
REQ-SYS-02	The wind farm shall comply with noise regulations value of 47 [dB] during the day	No dwellings are within 30 [km] of the development zone, so no significant noise pollution will be present. (section 4.1)

REQ-SYS-03	The wind farm shall comply with noise regulations value of 41 [dB] during the night	No dwellings are within 30 [km] of the development zone, so no significant noise pollution will be present. (section 4.1)
REQ-SYS-04	The wind farm shall comply with shadow flicker regulations of no more than 17 [days/year] for 20 [min/ day]	No dwellings are within 30 [km] of the development zone, so no shadow flicker is present. (section 4.1)
REQ-SYS-05	The wind farm area shall have a maximum water depth of 60 [m]	The wind farm area has depths within the 10-20 [m] range. (section 4.4)
REQ-SYS-06	The wind farm shall be able to withstand waves of up to 10 [m]	The monopile has been sized to withstand waves up to 10 [m]. (subsection 5.4.8)
REQ-SYS-07	The wind farm shall be able to withstand a sustained wind speed of 60 [m/s] for at least 20 [sec].	The structure has been designed for a constant wind of 66 [m/s]. (subsection 5.4.8)
REQ-SYS-08	The wind farm shall be able to withstand a gust speed of 66 [m/s]	The structure has been designed for a constant wind of 66 [m/s]. (subsection 5.4.8)
REQ-SYS-09	The wind turbines shall have a tip clearance of 25 [m] with respect to mean sea level	The tip clearance is 25 [m]. (subsection 5.4.3)
REQ-SYS-10	The maximum distance the electricity has to travel to reach the grid shall be below 450 km.	The maximum distance to shore from the Lagelander area is 73 [km]. (section 4.1)
REQ-SYS-11	The cutoff speed shall be at least 25 [m/s]	The cutoff speed is 25 [m/s]. (section 8.4)
REQ-SYS-12	The cut-in speed shall be at most 3 [m/s]	The cut-in speed is 3 [m/s]. (section 8.4)
REQ-SYS-13	The wind farm shall have the capability to interrupt operations on demand	Due to the pitch control system and brakes, each rotor can be stopped on demand. (subsection 5.5.2)
REQ-SYS-15	The power of the multi-rotor unit at low wind speeds, 6 m/s, shall reach 20% of its rated power production (6 [MW]).	At 6 [m/s], the ReWind multi-rotor produces 5.8 [MW] of power, or 18.9% of the rated power. Figure 15.2
REQ-SYS-18	The wind farm placement shall not inhibit the use of existing shipping channels	The Lagelander development zone has been determined by the Dutch government such that no shipping lines are hindered. (section 4.1)
REQ-SYS-20	Each multi-rotor unit shall be capable of re-energising the flow by producing vertical convective eddies	The upwards deflection of the wake creates large eddies, mixing the low speed flow with high speed flow. (section 5.2)
REQ-SYS-21	Each multi-rotor unit shall be capable of controlling the wake direction	The 3 active flow control wings deflect the wake upwards. (section 5.2)
REQ-SYS-23	The structure shall be accessible by a maintenance team of 10 fully equipped technicians (90 [kg], 185 [cm] tall, 70 [cm] width)	The ladder, elevator and maintenance paths allow easy access to the different systems. (section 9.2)
REQ-SYS-24	Each multi-rotor system unit shall not exceed a budget of 71.6 million €	The Capex of each Rewind turbine is 76.7 million €. (section 10.2)
REQ-SYS-26	The wind farm shall reach a total capacity factor of at least 50 %.	The ReWind wind farm achieves a farm capacity factor of 47.5 %. (section 5.3)
REQ-SYS-27	The wind farm shall prevent any harm to nature reserves as well as marine wildlife.	(chapter 13)
REQ-SYS-29	Each multi-rotor unit shall have a height less than 300 [m]	The height of the structure is at most 403 [m]. (subsection 5.4.3)
REQ-SYS-30	Each multi-rotor unit shall have a width less than 300 [m]	The maximum width of the ReWind concept is 278 [m]. (subsection 5.4.3)

REQ-SYS-31	The mass of the structure shall not exceed 4500 [tons]	The mass of the structure is estimated at 4355 [tons]. (Figure 5.4.5)
REQ-SYS-32	The wind farm shall consist of at least 200 multi-rotor units	The wind farm consists of 284 ReWind turbines. (section 4.5)
REQ-SYS-33	Each multi rotor unit shall have the ability to yaw about a fixed axis	Each ReWind unit rotates about the vertical axis located in the central tower. (subsection 5.5.1)
REQ-SYS-34	The rotor shall rotate around a horizontal axis	Each of the 34 rotors rotates around a horizontal axis. (chapter 15)
REQ-SYS-38	A single wind turbine unit shall consist of multiple rotors	Each ReWind multi rotor system is composed of 34 rotors. (subsection 5.1.1)

16.3. Mission compliance

This section will detail the compliance of the ReWind concept with the mission requirements

Table 16.8: Mission compliance

ID	Requirement	ReWind performance
REQ-MIS-01	The wind farm shall have a lifetime of at least 20 years	The wind farm operational lifetime is 25 years. (Table 10.1)
REQ-MIS-02	The wind farm shall be able to operate under wind directions varying from 0 to 360 [deg].	The yaw system allows each ReWind turbine to operate in all wind directions. (subsection 5.5.1)
REQ-MIS-03	The wind farm shall be able to operate in wind speeds in a range of 3-25 [m/s]	Cut-in speed is 3 [m/s] and Cutoff speed is 25 [m/s]. (section 8.4)
REQ-MIS-04	Each multi-rotor system unit shall have active flow control mechanism to reenergize the flow	The structure is equipped with 3 large wings, deflecting the wake upwards. (section 5.2)
REQ-MIS-05	The wind farm shall be capable of delivering generated electricity to the onshore grid	Each ReWind system sends the generated electricity to a substation, which is connected to the grid. (Figure 8.5)
REQ-MIS-06	Each multi-rotor unit shall have a bottom-fixed foundation	The ReWind concept uses a bottom fixed monopile foundation. (Table 5.9)
REQ-MIS-07	The wind farm shall be operable with a yearly OPEX of at most 30 000 [€/MW/year]	Each ReWind system is operable with an estimated OPEX of 27 400 [€/MW/year]. (section 10.2)
REQ-MIS-08	The project shall be completed with a total budget of 20 billion €	The Capex of the project is estimated at 18.4 billion €. (section 10.2)
REQ-MIS-09	The wind farm shall be operational by 2040	According to current scheduling, the wind farm is expected to be operational by 2033. (section 17.2)
REQ-MIS-10	The wind farm shall have a CO2 emission not exceeding 6.6 [g/kWh] considering the total life emissions	For each kWh produced, the ReWind system emits only 7.49 g of CO2. (subsection 13.1.6)
REQ-MIS-11	The wind farm shall monitor the properties of the produced electricity at any time	Each ReWind system continuously measures the voltage, current, frequency and phase. (Figure 8.5)
REQ-MIS-12	The wind farm shall be compliant with the Dutch Offshore Wind Energy Act	(chapter 15)
REQ-MIS-13	The wind farm shall comply with the Dutch Nature Conservation Act	(chapter 13)
REQ-MIS-14	The wind farm shall comply with the Dutch Water Decree	(chapter 15)
REQ-MIS-15	Each multi-rotor unit shall have a rated power of 30 [MW]	Each ReWind multi-rotor system has a rated power of 30.6 MW. (subsection 5.6.1)

REQ-MIS-16	The wind farm shall comply with the Dutch Activities Decree	(chapter 15)
------------	---	--------------

16.4. Stakeholder compliance

Finally, the stakeholder requirement compliance is evaluated. Naturally, these requirements are crucial as they reflect the needs and expectations of all parties involved in the project. The evaluation will consider how well the ReWind concept aligns with these diverse requirements, ensuring that the design meets the broader goals and objectives set by the stakeholders.

Table 16.9: Stakeholder requirement compliance

ID	Requirement	ReWind performance
REQ-STK-CUS-01	The farm shall have a rated power of 6 [GW]	The wind farm has a rated power of 8.69 [GW]. (section 4.5)
REQ-STK-CUS-02	The farm shall have a rated power density of 10 [MW/km ²]	The wind farm power density is 10.36 [MW/km ²]. (section 4.5)
REQ-STK-CUS-03	The wind farm efficiency of the entire wind farm shall exceed 80%	The ReWind concept achieves a wind farm efficiency of 84.5%. (section 5.3)
REQ-STK-CUS-04	The LCoE of the wind farm shall be 45% lower than current industry standards, estimated to be 68 [€/MWh] for the Netherlands	The ReWind wind farm achieves an LCoE of 40.7 [€/MWh], or 40% lower than industry standards (section 10.2)
REQ-STK-CUS-05	The wind farm shall be situated offshore within Dutch territorial waters	Wind farm is located in the Lagelander development zone, in Dutch territorial waters. (section 4.1)
REQ-STK-CUS-06	The wind farm shall have a 40% lower carbon footprint than current standards, estimated to be 11 [g/kWh]	For each kWh produced, the Rewind system emits only 7.49 g of CO ₂ , or 32% lower. (subsection 13.1.6)
REQ-STK-EZQ-07	All wind farm activities shall be compliant with Dutch regulation	(chapter 15)
REQ-STK-FIN-08	The wind farm shall have an annual ROI upwards of 8% assuming an energy price of 74 [€/MWh]	At the assumed price, the ReWind concept achieves an ROI of 8.99%. (section 10.3)
REQ-STK-GO-09	The electricity provided shall be compliant with the grid specifications (TENNET-E)	The use of the LV/MV and MV/HV along with the inherent capabilities of the chosen DFIG generator, the electricity conforms to the grid specifications. (Figure 8.5)

16.5. Future compliance

As one can notice from the compliance matrices above, a few of the requirements are not met by the current design. To address this issue, two solutions are possible: the requirement can either be renegotiated with the customer if it is really deemed to be unreachable by the design team. Conversely, the additional design steps could be taken in the future as to properly comply with the requirements in question. For each of the requirements the current design does not comply with the following strategy is proposed to mitigate the poor performance of the system:

- REQ-SSYS-TOW-01: This requirement is not satisfied because of the required rotor size. The current design already implements a so-called honeycomb packing strategy, which is a more efficient way of packing circles into a square. Even using this strategy and limiting the rotor spacing to a minimum the maximum frontal area requirement of 300 [m] by 300 [m] is exceeded. Therefore, the only way of complying with this requirement is to violate REQ-SSYS-TOW-02. As a consequence, this requirement shall be renegotiated with the customer as it seems unrealistic using current technology.
- REQ-SSYS-Y&P-02: The yaw rate could not be achieved due to the unexpectedly high mass moment of inertia about the rotational axis. This very high inertia requires huge torques in order to generate consequent angular accelerations. Therefore the problem could be tackled in two ways. The yaw rate can be increased by either increasing the yaw delivered by the yaw motors or by decreasing the mass moment of inertia of the structure. Since the latter solution seems quite hard to implement, most of the gains will come from a more detailed electrical analysis.

- REQ-SYS-15: This requirement was not met as a result of the optimal rotor sizing. It can simply be addressed by increasing the rotor size such that it captures more energy at low wind speeds. However, this will come with an added penalty in terms of frontal area, which is already an issue as stated in 16.5.
- REQ-SYS-24: The capital expenditure of a single multi-rotor was originally slightly underestimated. Firstly, the requirement can be renegotiated with the customers, showing them the long-term benefits of a slightly higher investments. Otherwise, the price of raw materials or of some standard components can be renegotiated to a lower price given the very large scale of the wind farm.
- REQ-SYS-26: Even using very powerful vortices to entrain high momentum flow and achieve low wake losses, the maximum capacity factor that could be achieved using current known technology is 47.5 % instead of the proposed 50 %. This requirement shall be renegotiated with the customer.
- REQ-SYS-29: This requirement is at the origin of requirement REQ-SSYS-TOW-01, it simply measures the total height of the system measured from the sea-level as opposed to the subsystem requirement. The plan to tackle the compliance of this requirement is already mostly outlined in 16.5, but in this case the height of the water clearance could also be reduced.
- REQ-STK-CUS-04: The LCoE could not be reduced as much as anticipated, partially due to the fact that the expected capital expenditure turned out to be higher than expected. Therefore, the procedures outlined in section 16.5. Subsequently, a more in-depth analysis of the cost could result in identifying some areas such as maintenance or decommissioning where expenses can be cut or additional revenues could potentially be generated.
- REQ-STK-CUS-06/REQ-MIS-10: The expected reduction in carbon footprint may have been estimated using the wrong models for the recycling of steel. Thus, the original estimate is below what can be achieved with current recycling technologies. Sustainability is clearly a central, and non-negotiable aspect of this design. Therefore, future research shall be focused on reducing the amount of used material as much as possible as well as trying to optimize maintenance strategies such that the very polluting CTV's don't have to be operating as often. These boats could in the future also be replaced by a new fleet of hydrogen boats. This measure could drastically cut the carbon emissions of the maintenance operations in the future.

17. Future Design

In this chapter, the future steps in the design, operation and decommissioning of the ReWind project are outlined. First, the design and development logic is presented in section 17.1, which details the necessary future operations in order of time. Then, a project Gantt chart is provided for these steps in section 17.2. The title of each section or subsection in this executive summary also contains a hyperlink to the corresponding section in the report where further explanations are given

17.1. Future Design and Development Logic

This section will detail the next steps in the design and development of the ReWind project. The future design and development logic is presented at top level in Figure 17.1

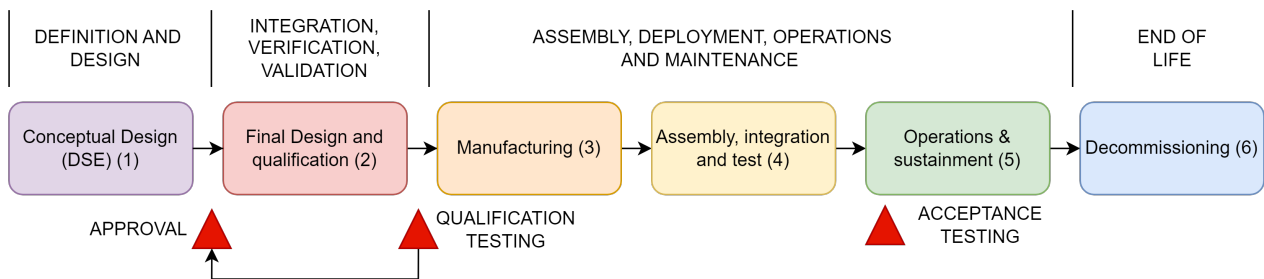


Figure 17.1: Top-level future project phases.

A more detailed break-down of Figure 17.1 is presented in the form of a flow diagram in Figure 17.2 and is assumed to start at the point where the client has approved the conceptual design. Then, the steps for the final design are outlined, including verification and validation procedures. Once qualification testing has been completed, the manufacturing and installation steps for the complete wind farm are presented, after which final customer acceptance testing is conducted. The final design and qualification phase will be detailed specifically since it follows directly from the results of this report.

17.1.1. Final Design and Qualification

The approval of the conceptual design marks the start of the final design phase, in which the design of the project will be concluded. In this final design phase, each subsystem design will be elaborated on, using the current results and limitations to identify the necessary areas for further analysis. The design will be elaborated using both analytical methods and tests on prototype models.

A more detailed analysis of the structure requires the inclusion of fatigue analysis and a consideration of dynamic effects during transient phases such as yawing, start-up and shut-down. Naturally, this will require additional design load cases to be considered and the use of more advanced analysis tools, such as a generalised finite element simulation, accounting for more degrees of freedom. The fatigue analysis can be performed either on a prototype model or by using a dynamic load model in combination with an accumulative damage model. Additionally, the final geometry of each member in the truss structure will be specified, and a more detailed analysis of the internal loading can allow the structure to be optimised for the specific load cases and resulting load paths. Aside from the truss structure, the design of the monopile transition piece will also be finalised using computational methods. The conclusion of the structural design would in turn conclude the manufacturing, assembly and installation processes, in addition to the final integration of sub-systems with the structure.

To finalize the design of the AFC devices, the aerodynamic results obtained in the conceptual design will be verified through wind tunnel tests on scale models, possibly in combination with CFD simulations, which would make aerodynamic testing of the entire system more feasible. Additionally, a detailed design of the actuator mechanism and structural design of the wings will be performed, which requires a detailed analysis of the loads acting on the wings once they are integrated into the structure. Moreover, CFD simulations will allow the effect

of the AFC devices on the wind farm capacity factor to be quantified, and a detailed analysis of wake interactions to be performed. Finalisation of the AFC design is an essential step in finalising the wind farm layout.

The detailed design of the remaining subsystems requires the sizing of subsystem-level components and assemblies, such as the drivetrain shaft, drivetrain brake system, and yaw bearing. Additionally, specific actuators for pitch and the HLDs of the AFC devices will be identified. On the turbine level, it is also necessary to identify the specific sensors which will be used, in combination with the detailed design of the turbine electrical and control systems.

Completing the detailed design on the turbine unit level, and on the wind farm aerodynamic level allows the final design of the wind farm system to be completed. This has not been treated in detail during the conceptual design since it follows the design of current wind farm technology. The wind farm design would include aspects such as a detailed design of the data electrical transmission, such as the transformer, feeder and collector stations, and the electrical cable routing. Additionally, a detailed design of the data communication and control systems will be performed, which includes the development of software, user interface logic, and external integration with servers or periphery stakeholders. Given the size of the farm, the high number of degrees of freedom resulting from the numerous rotors, and the substantial power output, tailored solutions will be required. These custom solutions are necessary to manage the complex control requirements and to prevent potential destabilising effects on the electrical grid. Additionally, the previously outlined steps are highly iterative, and thus will likely be repeated several times.

The final design phase is concluded with qualification testing, for which a qualification prototype model will be fabricated and tested. The qualification testing will conclude system integration, and verification and validation on the turbine unit level. If discrepancies are discovered in these steps, aspects of the detailed design will be revised as shown in Figure 17.1.

17.1.2. Manufacturing

Once the final design phase has been completed, and the turbine unit has passed qualification testing, the manufacturing phase starts. This involves both the manufacturing of components and sub-systems, and the finalisation of necessary software.

17.1.3. Assembly, Integration and Testing

This phase involves both the on-shore assembly of each sub-system and turbine unit, and the off-shore installation of the foundation, turbine units, and wind farm infrastructure. Once this has been completed, acceptance testing on the full system scale is performed before the project can be handed over to the client.

17.1.4. Operations and Sustainment

Following the hand-over, the initial operation phase begins, where the design team will play a supervisory and supporting role in close coordination with the client. This ensures any technical or operational issues identified during early operation by the client can be addressed or trouble-shooting can take place. This initial phase will last an estimated six months, after which the operational role of the client becomes dominating. The role of the design team then becomes limited to the provision of technical support, and the basic oversight of operations. Another aspect of sustainment is the periodic evaluation of the future life-time of the system, since this cannot be certainly estimated during the design phase.

17.1.5. Decommissioning

Once the wind-farm has reached its end-of-life, the decommissioning phase starts, which involves the dismantling of the wind farm, and assessment of material or component reuse. This is necessary because, after its complete operational life, different components of the wind farm may have degraded more or less than anticipated in the design phase.

17.2. Future Design Gantt Chart

The design and development logic outlined in section 17.1 is presented in the form of a Gantt chart in Figure 17.3 and Figure 17.4 to indicate an estimation of the timeline.

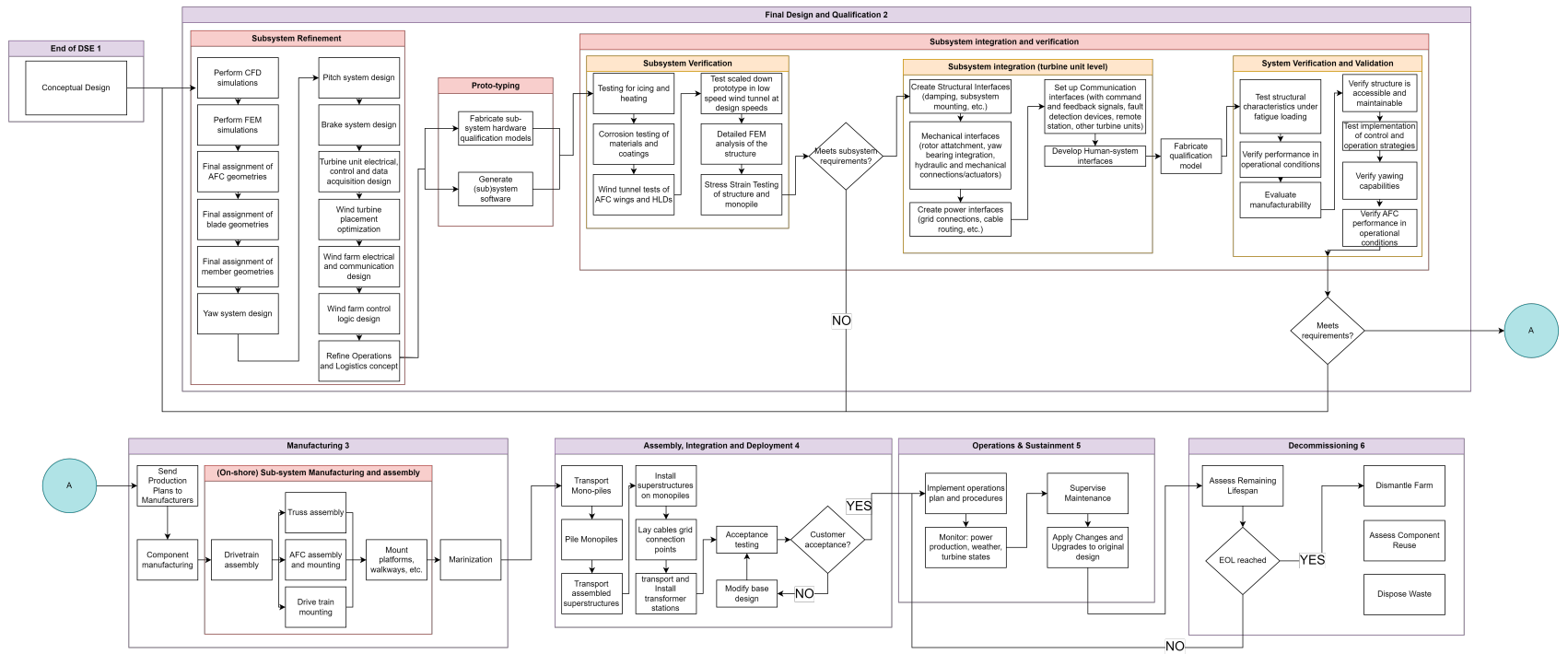


Figure 17.2: Design and development logic for the subsequent phases of the project.

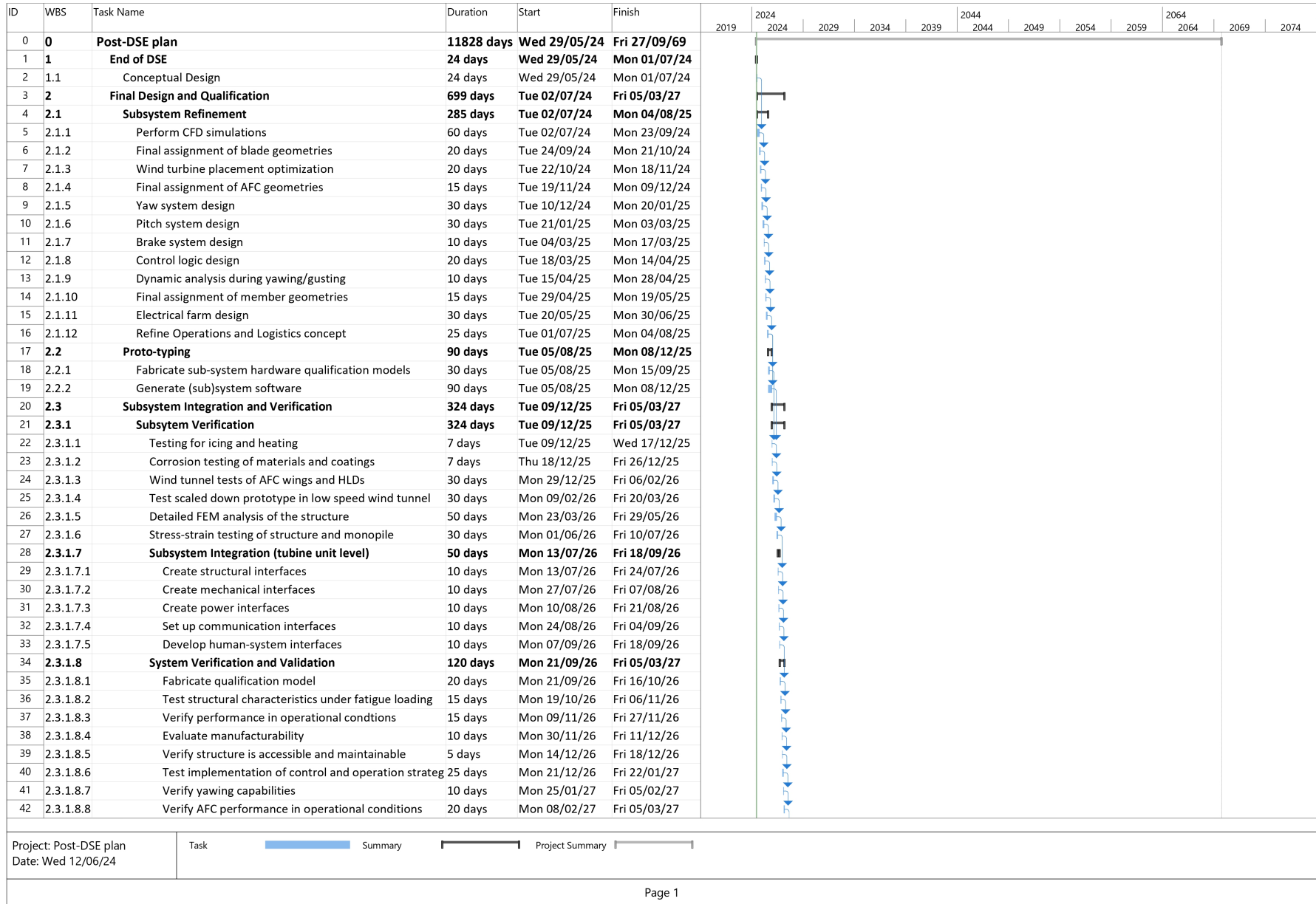


Figure 17.3: Gantt chart part 1 of 2.

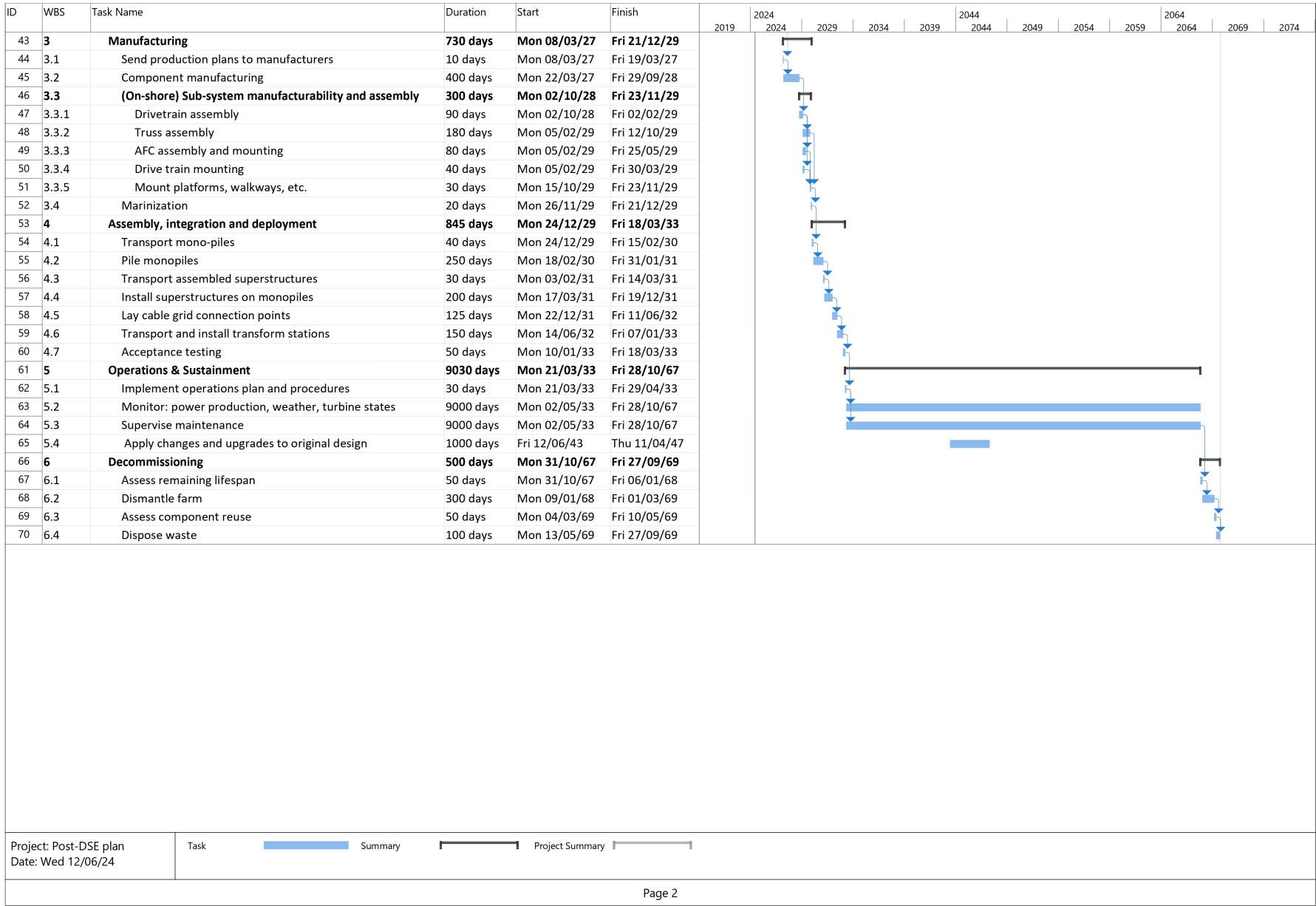


Figure 17.4: Gantt chart part 2 of 2.

18. Conclusion

This report aims to address the inherent challenges within the North Sea Programme, specifically the scalability issues of wind farms. By developing a multi-rotor wind turbine, ReWind identifies a promising solution to these problems. These innovative systems offer larger unit capacities and cost-effective alternatives. Additionally, the smaller required rotors effectively eliminate the need for rare earth metals in wind turbines. Furthermore, their simplified manufacturability allows for easier and cheaper assembly operations. A truss structure is able to support high-lift devices, which can be used to reenergize the lower atmospheric boundary layer. Thus, enabling more efficient and densely packed wind farms. Consequently, multi-rotor systems present form of overcoming the obstacles facing the North Sea Programme and advancing the sustainable development of offshore wind energy.

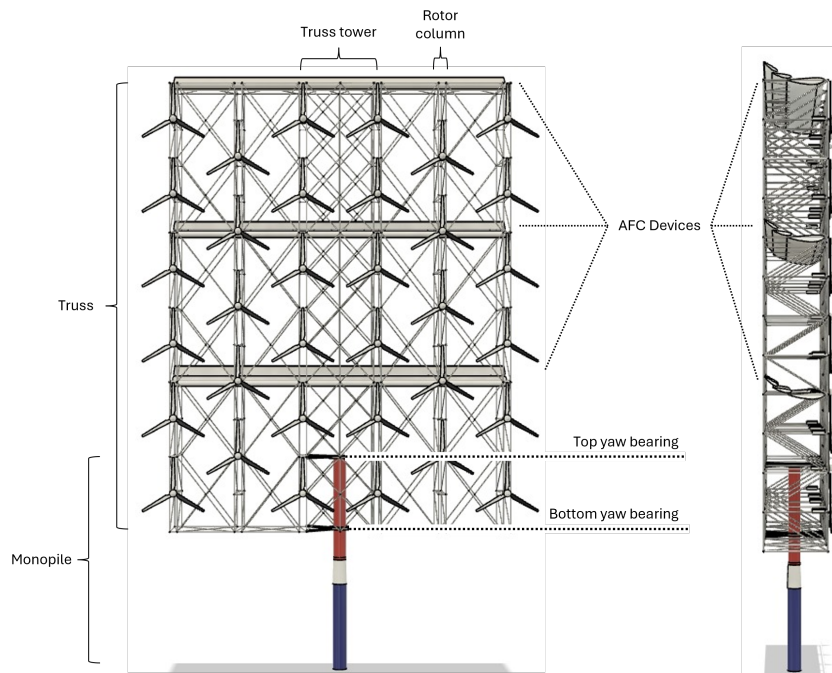


Figure 18.1: Final Design of the ReWind wind turbine.

In conclusion, the culmination of 10 weeks of work has led to the design shown in Figure 18.1. The system trade-off performed under the midterm report has been worked on and improved to produce this multi-rotor system finally. This wind turbine is capable of attaining 30.6 [MW] with its 34 rotors fit in a vertical honeycomb packing. The generators present in each rotor are able to deliver 0.9 [MW], jointly achieving the rated power of the wind turbine system. These rotors are supported by a truss structure that is attached to a monopile in a fixed-bottom foundation.

Three retractable wings are mounted on the truss structure, spanning along its width. These are used in order to provide an Active Flow Control (AFC) of the wake. Their installation is simplified by splitting them into multiple elements with a chord of 50 [m]. These wings are able to deliver up to 6.5 [MN] of lift which allows for the re-energization of the flow for the turbines situated downstream. In effect, this allows for a minimum spacing of 1.9 [km] between each turbine in the wind farm.

The Lagelander wind farm site is chosen as the location where the ReWind project will take place due to its extensive area of 850.28 [km²]. Thus, a total of 288 wind turbines are installed, attaining an energy density of 10.36 [MW/km²], satisfying REQ-STK-CUS-01, REQ-STK-CUS-02, REQ-STK-CUS-05 and REQ-STK-EZQ-07 (18.1). Additionally, the generator provides electricity at the same phase as the grid, conforming to the TENNET-E specifications and completing REQ-STK-GO-09.

A preventive and condition-based approach is used for the maintenance of the wind farm. Thus allowing for an actual availability of the wind turbine project of 95.38%. Consequently, the yearly energy production is summed up to a total of 84.5%, satisfying REQ-STK-CUS-03 (18.1). Thus, allowing for a Levelized Cost of Energy (LCoE) of 40.70 [€/MWh], which accounts for a 39% decrease from current industry standards with a return on investment of 8.99%, meeting REQ-STK-FIN-08. Even though this is an impressive and highly attractive LCoE, it does not meet the requirement REQ-STK-CUS-04. Finally, these effective maintenance strategies combined with the aforementioned innovative design choices allow for an emission rate of 7.49 kg CO₂/MWh, a reduction of 32% from current standards, completing REQ-STK-CUS-06.

Table 18.1: Stakeholder Requirements

ID	Requirement
REQ-STK-CUS-01	The farm shall have a rated power of 6 [GW].
REQ-STK-CUS-02	The farm shall have a rated power density of 10 [MW/km ²].
REQ-STK-CUS-03	The annual energy production efficiency of the entire wind farm shall exceed 80% .
REQ-STK-CUS-04	The LCoE of the wind farm shall be 45% lower than current industry standards, estimated to be 66.25 [€/MWh] for the Netherlands.
REQ-STK-CUS-05	The wind farm shall be situated offshore within Dutch territorial waters.
REQ-STK-CUS-06	The wind farm shall have a 40% lower carbon footprint than current standards, estimated to be 11 [g/kWh].
REQ-STK-EZQ-07	All wind farm activities shall be compliant with Dutch regulations.
REQ-STK-FIN-08	The wind farm shall have an annual ROI upwards of 8%, assuming an energy price of 74 [€/MWh].
REQ-STK-GO-09	The electricity provided shall be compliant with the grid specifications (TENNET-E).

In order to broaden the scope of this research, it is possible to incorporate a physical or computational experimental analysis of the wind turbine system. In effect, building a model of the final design and testing it under a wind tunnel would allow for much more precise calculations regarding the wings and the truss structure, possibly improving on the mass, stability and power output of the system.

The maintenance of the wind farm is a part in this report that inevitably comes with high imprecisions due to the scale of the project. In fact, the high number of wind turbines installed in the farm and the increased number of components per turbines leads to a high necessity of constant maintenance. However, the calculated numbers could possibly reduced if experts on wind farm maintenance could be contacted. Their expertise could estimate more precise maintenance requirements than the scaled calculations present in this report.

Finally, the assembly process of each wind turbine can be shortened in time by applying a modular assembly strategy. In effect, by restructuring the truss structure into multiple separate equal smaller modules which can be connected to form the entire wind turbine the assembly and production of the system could be streamlined.

References

- [1] Carlos Simao Ferreira. *Limits of offshore wind and how to achieve regenerative wind farming*. May 2024.
- [2] Donatella Zappala. *Lecture notes in Offshore Wind RAMS*. Nov. 2023.
- [3] BVG Associates Limited. *Guide to an offshore wind farm*. <https://www.thecrownestate.co.uk/media/2860/guide-to-offshore-wind-farm-2019.pdf>. Published on behalf of The Crown Estate. Jan. 2019.
- [4] Chengjian Xu et al. “Future greenhouse gas emissions of automotive lithium-ion battery cell production”. In: *Resources, Conservation and Recycling* 187 (2022), p. 106606. issn: 0921-3449. doi: 10.1016/j.resconrec.2022.106606.
- [5] F. Degen et al. “Energy consumption of current and future production of lithium-ion and post lithium-ion battery cells”. In: *Nature Energy* 8.11 (Sept. 2023), pp. 1284–1295. issn: 2058-7546. doi: 10.1038/s41560-023-01355-z.
- [6] Walter Musial et al. *Offshore Wind Market Report: 2023 Edition: U.S. Department of Energy (DOE), Energy Efficiency & Renewable Energy (EERE)*. American English. Other. 2023. doi: 10.2172/2001112.
- [7] Tyler Stehly, Patrick Duffy, and Daniel Mulas Hernando. *2022 Cost of Wind Energy Review*. American English. Other. 2023. doi: 10.2172/2278805.
- [8] George Bilicic and Samuel Scroggins. *2023 Levelized Cost Of Energy+*. 2023. url: <https://www.lazard.com/research-insights/2023-levelized-cost-of-energyplus/>.
- [9] Taiyang News. *High Efficiency Cell Technologies*. American English. 2019. url: <https://taiyangnews.info/high-efficiency-solar-cells-2019/>.
- [10] Misbah Abdelrahim et al. “energies-15-05412”. In: *Energies* 15 (July 2022). doi: 10.3390/en15155412.
- [11] Martin Kaltschmitt, Wolfgang Streicher, and Andreas Wiese. *Renewable energy: technology, economics and environment*. Springer Science & Business Media, 2007.
- [12] A. Sathe. “Atmospheric stability and wind profile climatology over the North Sea - Case study at Egmond aan Zee”. In: (2010).
- [13] J.P. Coelingh, A.J.M. van Wijk, and A.A.M. Holtslag. “Analysis of wind speed observations over the North Sea”. In: *Journal of Wind Engineering and Industrial Aerodynamics* 61.1 (1996), pp. 51–69. issn: 0167-6105. doi: 10.1016/0167-6105(96)00043-8.
- [14] Saskia Hommes, Suzanne Hulscher, and Ad Stolk. “Parallel Modeling Approach to Assess Morphological Impacts of Offshore Sand Extraction”. In: *Journal of Coastal Research Journal of Coastal Research* 23 (Nov. 2007), pp. 1565–1579. doi: 10.2112/06-0698.1.
- [15] Zhang Yong and Qi Shengli. “A Practical Optimization for Offshore Wind Farm Layout”. In: 2016. url: <https://api.semanticscholar.org/CorpusID:53532555>.
- [16] A. Carraro et al. *Regenerative Wind Farm Midterm Report*. Delft University of Technology, 2024.
- [17] Hai-Chau Chang and Lih-Chung Wang. *A Simple Proof of Thue’s Theorem on Circle Packing*. 2010. arXiv: 1009.4322 [math.MG].
- [18] Evan Gaertner et al. “IEA Wind TCP Task 37: Definition of the IEA 15-Megawatt Offshore Reference Wind Turbine”. In: (Mar. 2020). doi: 10.2172/1603478.
- [19] Michael Graham. *Wind Energy Handbook*. John Wiley & Sons Inc, 2021.
- [20] J L Tangler and D M Somers. “NREL airfoil families for HAWTs”. In: (Jan. 1995). doi: 10.2172/10106095.
- [21] Alois Peter Schaffarczyk. *Introduction to Wind Turbine Aerodynamics*. Springer Cham, 2024.
- [22] Thomas Broertjes. “Lift-Induced Wake Re-Energization for a VAWT-Based Multi-Rotor System”. Mentors: A. Sciacchitano, Carlos Ferreira, D.Y. Bensason. Delft, Netherlands: Delft University of Technology, Apr. 2024.
- [23] Flavio A. C. Martins, Carlos S. Ferreira, and Alexander Van Zuijlen. “Numerical Investigation of Atmospheric Boundary Layer Control in Wind Farms with Multirotor Systems”. In: *Journal of Physics: Conference Series* 2767.7 (June 2024), p. 072006. doi: 10.1088/1742-6596/2767/7/072006.

- [24] Jr. John D. Anderson. *Fundamentals of Aerodynamics*. 6th. New York: McGraw-Hill Education, 2016.
- [25] Ira H. Abbott, Albert E. Von Doenhoff, and Louis S. Stivers. *Summary of Airfoil data*. Tech. rep. Jan. 1945. url: https://digital.library.unt.edu/ark:/67531/metadc61319/m2/1/high_res_d/19930092747.pdf.
- [26] Martin Hepperle. *JavaFoil User's Guide*. Tech. rep. Dec. 2017.
- [27] Victor Igwemezie, Ali Mehmanparast, and Athanasios Kolios. "Materials selection for XL wind turbine support structures: A corrosion-fatigue perspective". In: *Marine Structures* 61 (Sept. 2018). doi: 10.1016/j.marstruc.2018.06.008.
- [28] Lars Frøyd. "Wind Turbine Design - Evaluation of Dynamic Loads on Large Offshore Wind Turbines". PhD thesis. July 2012.
- [29] Klaus-Jurgen Bathe. "Formulation of the Finite Element Method - Linear Analysis in Solid and Structural Mechanics". In: *Finite Element Procedures*. Prentice Hall, 1996, pp. 148–300.
- [30] Aslam Kassimali. *Matrix analysis of structures*. Cengage, 2022.
- [31] Daryl L. Logan. *A first course in the finite element method*. Cengage, 2023.
- [32] *Structural Standard for Antenna Supporting Structures and Antennas*. Standard. Arlington, USA: Telecommunications Industry Association, Aug. 2005.
- [33] Filip Van den Abeele and John Vande Voorde. "Stability of offshore structures in shallow water depth". In: *International Journal Sustainable Construction & Design* 2 (Nov. 2011), pp. 320–333. doi: 10.21825/scad.v2i2.20529.
- [34] Ashish Aeran et al. "A nonlinear fatigue damage model: Comparison with experimental damage evolution of S355 (SAE 1020) structural steel and application to offshore jacket structures". In: *International Journal of Fatigue* 135 (2020), p. 105568. issn: 0142-1123. doi: 10.1016/j.ijfatigue.2020.105568.
- [35] S. Störtenbecker et al. "Simplified support structure design for multi-rotor wind turbine systems". In: *Wind Energy Science* 5.3 (2020), pp. 1121–1128. doi: 10.5194/wes-5-1121-2020.
- [36] Bakhti Rachid, Baizid Benahmed, and Abdelghani Laib. "Finite Element Investigation of Offshore Wind Turbines Natural Frequency with Monopile Foundations System". In: (May 2023). doi: 10.1007/s42417-023-00989-3.
- [37] Giovanni do Amaral. "Analytical Assessment of the Mooring System Stiffness". PhD thesis. Mar. 2020. doi: 10.13140/RG.2.2.28848.38401.
- [38] Robin Maljaars. *Driving Factors in the LCOE trend of Offshore wind power*. 2021. url: https://www.worldclassmaintenance.com/wp-content/uploads/2019/12/210604-CU08813_V1_ENG8_EPE_final_research_report_Robin_Maljaars-1.pdf.
- [39] Charalampos Themistokleous. "Yaw control for floating wind turbines". MA thesis. Technical University of Denmark, 2023.
- [40] DUWIND. *OE5662, Offshore Wind Farm Design*.
- [41] TU Delft OCW. *WAVE FORCES ON SLENDER CYLINDERS*.
- [42] K.W. Hermans and J.M. Peeringa. *Future XL monopile foundation design for a 10 MW wind turbine in deep water*. Tech. rep. ECN, 2016.
- [43] Bakhti Rachid, Baizid Benahmed, and Abdelghani Laib. "Finite Element Investigation of Offshore Wind Turbines Natural Frequency with Monopile Foundations System". In: (May 2023). doi: 10.1007/s42417-023-00989-3.
- [44] P. Jamieson et al. *Innovative Turbine Concepts – Multi-Rotor Systemt*. Deliverable 1.33. Funded by the European Community's Seventh Framework Programme under grant agreement no. 308974. IN-NWIND.EU Consortium, Sept. 2015.
- [45] Markus Warner et al. "Yaw control strategies for 20 MW multi-rotor systems". In: *Journal of Physics: Conference Series* 2626 (Oct. 2023), p. 012032. doi: 10.1088/1742-6596/2626/1/012032.
- [46] Kaydon Bearings. *Catalog 390: An Engineering and Product Selection Guide*. Kaydon bearing solutions for Slewing Ring Bearings. 2860 McCracken Street, Muskegon, MI 49441: Kaydon Bearings.
- [47] *PM150DZ datasheet*. RINEHART MOTION SYSTEMS LLC. 7929 SW Burns Way, Suite B, Wilsonville, OR 97070.
- [48] European Commission. *1 MW ADAPTABLE WIND TURBINE*. Technical Report. European Union, 1999. url: https://cordis.europa.eu/docs/projects/files/JOR/JOR3950050/47698371-6_en.pdf.

- [49] Kausihan Selvam. *Individual Pitch Control for Large scale wind turbines*. Accessed: 2024-06-19. 2007. url: <https://publications.tno.nl/publication/34628827/2L7wY4/e07053.pdf>.
- [50] Francis Oyague. *Gearbox Modeling and Load Simulation of a Baseline 750-kW Wind Turbine Using State-of-the-Art Simulation Codes*. NREL, Feb. 2009. url: <https://www.nrel.gov/docs/fy09osti/41160.pdf>.
- [51] Roshan Kumar et al. "Damage detection of wind turbine system based on signal processing approach: a critical review". In: *Clean Technologies and Environmental Policy* 23 (Jan. 2021), pp. 1–20. doi: 10.1007/s10098-020-02003-w.
- [52] Michiel Zaaier. *Introduction to Wind Energy: Relevant to Offshore Wind Farm Design*. Presentation. Offshore Wind Farm Design. 2008.
- [53] Prof. Dr.-Eng. Arnaudov k. Dipl.-Eng. Giger. "High Efficiency High Torque Gearbox for Multi Megawatt Wind Turbines". In: *Scientific Proceedings VIII International Congress "Machines, Technologies, Materials" 2011* (2011). url: <https://mtmcongress.com/proceedings/2011/3/28.HIGH%20EFFICIENCY%20HIGH%20TORQUE%20GEARBOX%20FOR%20MULTI%20MEGAWATT%20WIND%20TURBINES.pdf>.
- [54] L. Jiang et al. "Analysis of wind turbine Gearbox's environmental impact considering its reliability". In: *Journal of Cleaner Production* 180 (2018), pp. 846–857. issn: 0959-6526. doi: 10.1016/j.jclepro.2018.01.078.
- [55] Umberto Boatto et al. "Assessment of a BEMT-based rotor aerodynamic model under uniform aligned steady inflow". In: *AIAA SCITECH 2023 Forum*. doi: 10.2514/6.2023-0609.
- [56] Kristen Kallstrom. "Exploring Airfoil Table Generation using XFOIL and OVERFLOW". In: *VFS Aeromechanics for Advanced Vertical Flight* (2022).
- [57] Woodward-Clyde Consultants. *Assessment of the Morison equation*. Tech. rep. Civil Engineering Laboratory (Code L44), 1980.
- [58] A. Carraro et al. *Regenerative Wind Farm Baseline Report*. Delft University of Technology, 2024.
- [59] E.K.A. Gill. *Powerpoint slides of Lecture 4 in Systems Engineering and Aerospace Design*. Feb. 2023.
- [60] M.J.L. van Tooren R.J. Hamann. *Lecture notes Systems Engineering and Technical Management Part II*. Sept. 2006.
- [61] Satya Anandavijayan, Ali Mehmanparast, and Feargal Brennan. "A numerical analysis of the effects of manufacturing processes on material pre-strain in offshore wind monopiles". In: *Procedia Structural Integrity* 13 (2018). ECF22 - Loading and Environmental effects on Structural Integrity, pp. 953–958. issn: 2452-3216. doi: 10.1016/j.prostr.2018.12.178.
- [62] Licheng Qin et al. "Review on recent research and technical challenges of floatover installation operation". In: *Ocean Engineering* 253 (2022), p. 111378. issn: 0029-8018. doi: 10.1016/j.oceaneng.2022.111378.
- [63] Xin Xu et al. "A Study of Floatover Installation onto Jacket With Two Barges". In: Feb. 2012.
- [64] Peng Hou et al. "Offshore wind farm repowering optimization". In: *Applied energy* 208 (2017), pp. 834–844.
- [65] *OSPAR Convention*. url: https://www.ospar.org/site/assets/files/1290/ospar_convention.pdf (visited on 05/16/2024).
- [66] Eva Topham and David McMillan. "Sustainable decommissioning of an offshore wind farm". In: *Renewable energy* 102 (2017), pp. 470–480.
- [67] Ahmed AbdulHameid Al Mowafy. "Investigation of decommissioning of offshore wind mono-pile foundations". In: (2023). doi: 10.48730/4ast-8a65.
- [68] *Decommissioning of Offshore Monopiles, Occuring Problems and Alternative Solutions*. Vol. Volume 9: Offshore Geotechnics; Honoring Symposium for Professor Bernard Molin on Marine and Offshore Hydrodynamics. International Conference on Offshore Mechanics and Arctic Engineering. June 2018, V009T10A020. doi: 10.1115/OMAE2018-78577.
- [69] Gbenga Apata and D.T.O Oyedokun. "An overview of control techniques for wind turbine systems". In: *Scientific African* 10 (Nov. 2020), e00566. doi: 10.1016/j.sciaf.2020.e00566.
- [70] Marcelo Molina and Pedro Mercado. "Modelling and Control Design of Pitch-Controlled Variable Speed Wind Turbines". In: Apr. 2011. isbn: 978-953-307-221-0. doi: 10.5772/15880.

- [71] Luai Alhems and Muhammad Mujahid Rafique. "Horizontal Axis Wind Turbine Blade Design Methodologies for Efficiency Enhancement—A Review". In: *Energies* 11 (Feb. 2018), p. 506. doi: 10.3390/en11030506.
- [72] James Carroll, Alasdair McDonald, and David McMillan. "Failure rate, repair time and unscheduled O&M cost analysis of offshore wind turbines". In: *Wind Energy* 19.6 (2016), pp. 1107–1119. doi: 10.1002/we.1887.
- [73] Jade McMorland et al. "A review of operations and maintenance modelling with considerations for novel wind turbine concepts". In: *Renewable and Sustainable Energy Reviews* 165 (2022), p. 112581. issn: 1364-0321. doi: 10.1016/j.rser.2022.112581.
- [74] G. Abad et al. *Doubly Fed Induction Machine: Modeling and Control for Wind Energy Generation*. IEEE Press, 2011.
- [75] Jade McMorland et al. "Multi Rotor Wind Turbine Systems: An Exploration of Failure Rates and Failure Classification". In: *Journal of Physics: Conference Series* 2626 (Oct. 2023), p. 012027. doi: 10.1088/1742-6596/2626/1/012027.
- [76] GL Garrad Hassan. *A guide to UK offshore wind operations and maintenance*. Scottish Enterprise, 2013.
- [77] Zhengru Ren et al. "Offshore wind turbine operations and maintenance: A state-of-the-art review". In: *Renewable and Sustainable Energy Reviews* 144 (2021), p. 110886. issn: 1364-0321. doi: 10.1016/j.rser.2021.110886.
- [78] *Cost Evaluation of North Sea Offshore Wind Post 2030*. Report. North Sea Wind Power Hub Consortium, 2022. url: <https://northseawindpowerhub.eu/files/media/document/Cost-Evaluation-of-North-Sea-Offshore-Wind-1.pdf>.
- [79] Peter Jamieson and Michael Branney. "Structural considerations of a 20MW multi-rotor wind energy system". In: *Journal of Physics: Conference Series*. Vol. 555. 1. IOP Publishing. 2014, p. 012013.
- [80] "Techno-Economic Analysis of On-Site Energy Storage Units to Mitigate Wind Energy Curtailment: A Case Study in Scotland". In: *Semantic Scholar* (Mar. 2021). url: <https://www.semanticscholar.org/paper/900007dbb5f3b718972dca63321dceb40c0586c8>.
- [81] Wesley Frazier et al. *Modeling the Value of Energy Storage in the U.S. Power Sector*. Tech. rep. National Renewable Energy Lab. (NREL), Golden, CO (United States), 2023. url: <https://www.nrel.gov/docs/fy23osti/85332.pdf>.
- [82] L Fingersh, Maureen Hand, and A Laxson. *Wind turbine design cost and scaling model*. Tech. rep. National Renewable Energy Lab.(NREL), Golden, CO (United States), 2006.
- [83] James Manwell, Jon MCGowan, and A. Rogers. *Wind Energy Explained: Theory, Design and Application*. Dec. 2009. isbn: 9780470015001. doi: 10.1002/9781119994367.
- [84] Shifeng Wang and Sicong Wang. "Impacts of wind energy on environment: A review". In: *Renewable and Sustainable Energy Reviews* 49 (2015), pp. 437–443. issn: 1364-0321. doi: 10.1016/j.rser.2015.04.137.
- [85] Stacey Dolan and Garvin Heath. "Life Cycle Greenhouse Gas Emissions of Utility-Scale Wind Power". In: *Journal of Industrial Ecology* 16 (Mar. 2012), S136–S154. doi: 10.1111/j.1530-9290.2012.00464.x.
- [86] Anders Arvesen, Christine Birkeland, and Edgar Hertwich. "The Importance of Ships and Spare Parts in LCAs of Offshore Wind Power". In: *Environmental science & technology* 47 (Mar. 2013). doi: 10.1021/es304509r.
- [87] Dan Ancona and Jim McVeigh. *Wind Turbine - Materials and Manufacturing Fact Sheet*. US Department of Energy, 2001.
- [88] Lars Mikkelsen. "A simplified model predicting the weight of the load carrying beam in a wind turbine blade". In: *IOP Conference Series: Materials Science and Engineering* 139 (July 2016). doi: 10.1088/1757-899X/139/1/012038.
- [89] John Rankin. *Energy Use in Metal Production*. CSIRO, Swinburne University of Technology, 2012.
- [90] Gilles Tchana Toffe et al. "A Scale-up of Energy-Cycle Analysis on Processing Non-Woven Flax/PLA Tape and Triaxial Glass Fibre Fabric for Composites". In: 3 (Nov. 2019), pp. 1–2. doi: 10.3390/jmmp3040092.
- [91] MOHIT DIGAMBER SAKORE. *Lifecycle Analysis of Forged Products*. <https://www.diva-portal.org/smash/get/diva2:1651986/FULLTEXT01.pdf>. 2022.

- [92] Julian Suer, Marzia Traverso, and Frank Ahrenhold. "Sustainable transition of the primary steel production: Carbon footprint studies of hot-rolled coil according to ISO 14067". In: *E3S Web of Conferences* 349 (May 2022), p. 07004. doi: 10.1051/e3sconf/202234907004.
- [93] Corrie Sice and Jeremy Faludi. "COMPARING ENVIRONMENTAL IMPACTS OF METAL ADDITIVE MANUFACTURING TO CONVENTIONAL MANUFACTURING". In: *Proceedings of the Design Society* 1 (Aug. 2021), pp. 671–680. doi: 10.1017/pds.2021.67.
- [94] Marine Benchmark Gothenburg. "Maritime CO² Emissions". In: *Research Brief 11/2020* (2020).
- [95] Anthony Gray. "Setting a Benchmark For Decarbonising O&M Vessels of Offshore Wind Farms". In: *Catapult Offshore Renewable Energy* (2021).
- [96] "Copyright". In: *Modern Gas Turbine Systems*. Ed. by Peter Jansohn. Woodhead Publishing Series in Energy. Woodhead Publishing, 2013. doi: 10.1016/B978-1-84569-728-0.50018-5.
- [97] Paula Garcia Rosa and John Tande. "Mitigation measures for preventing collision of birds with wind turbines". In: *Journal of Physics: Conference Series* 2626 (Oct. 2023), p. 012072. doi: 10.1088/1742-6596/2626/1/012072.
- [98] Ana Marques et al. "Understanding bird collisions at wind farms: An updated review on the causes and possible mitigation strategies". In: *Biological Conservation* 179 (Nov. 2014), pp. 40–52. doi: 10.1016/j.biocon.2014.08.017.
- [99] Martine van Oostveen et al. "Inventory and assessment of models and methods used for describing, quantifying and assessing cumulative effects of offshore wind farms". In: *Royal HaskoningDHV* (2018), pp. 20–22.
- [100] Syed Raza Ali Mehdi. "Offshore Wind Farms and Maritime Navigational Risks". Ph.D. Dissertation. World Maritime University, 2019. url: https://commons.wmu.se/all_dissertations/1234.
- [101] Laura Bray et al. "Expected Effects of Offshore Wind Farms on Mediterranean Marine Life". In: *Journal of Marine Science and Engineering* 4.1 (2016). issn: 2077-1312. doi: 10.3390/jmse4010018.
- [102] L. Leewis, A.D. Klink, and E.C. Verduin. "Benthic development in and around offshore wind farm Prinses Amalia Wind Park near the Dutch coastal zone before and after construction (2003-2017)". In: *Eurofins* (2018).
- [103] Lee M. Miller and David W. Keith. "Climatic Impacts of Wind Power". In: *Joule* 2.12 (2018), pp. 2618–2632. issn: 2542-4351. doi: 10.1016/j.joule.2018.09.009.
- [104] Alessandro Cresci et al. "Magnetic fields produced by subsea high-voltage direct current cables reduce swimming activity of haddock larvae (*Melanogrammus aeglefinus*)". In: *PNAS Nexus* 1.4 (Aug. 2022), pgac175. issn: 2752-6542. doi: 10.1093/pnasnexus/pgac175.
- [105] H Westerberg and I Lagenfelt. "Sub-sea power cables and the migration behaviour of the European eel". In: *Fisheries Management and Ecology* 15.5-6 (2008), pp. 369–375.
- [106] R.C. Snoek. *Potential effects of electromagnetic fields in the Dutch North Sea. Phase 2 – Pilot field study*. Rijkswaterstaat Dienst Weg- en Waterverkeer, 2020. url: https://www.noordzeeloket.nl/publish/pages/173407/potential_effects_of_electromagnetic_fields_in_the_dutch_north_sea_-_phase_12pilot_study_rws_wvl.pdf.
- [107] Per Petterson and Niclas Schonborg. "Reduction of power system magnetic field by configuration twist". In: *IEEE transactions on power delivery* 12.4 (1997), pp. 1678–1683.
- [108] Sara Pryor and R. Barthelmie. "A global assessment of extreme wind speeds for wind energy applications". In: *Nature Energy* 6 (Mar. 2021), pp. 1–9. doi: 10.1038/s41560-020-00773-7.
- [109] Christoph Schiel, Pedro Lind, and Philipp Maass. "Resilience of electricity grids against transmission line overloads under wind power injection at different nodes". In: *Scientific Reports* 7 (Dec. 2017). doi: 10.1038/s41598-017-11465-w.
- [110] Arturo Rodriguez Tsouroukdissian et al. "Wind Turbine Structural Damping Control for Tower Load Reduction". In: Jan. 2011.
- [111] Mani Entezami et al. "Fault detection and diagnosis within a wind turbine mechanical braking system using condition monitoring". In: *Renewable Energy* 47 (Nov. 2012), pp. 175–182. doi: 10.1016/j.renene.2012.04.031.
- [112] Wei-Hua Hu et al. "Vibration-based structural health monitoring of a wind turbine system. Part I: Resonance phenomenon". In: *Engineering Structures* 89 (Apr. 2015). doi: 10.1016/j.engstruct.2014.12.034.

- [113] Knud Kragh and Morten Hansen. "Potential of power gain with improved yaw alignment". In: *Wind Energy* 18 (Apr. 2014). doi: 10.1002/we.1739.
- [114] Engineering National Academies of Sciences and Medicine. *Wind Turbine Generator Impacts to Marine Vessel Radar*. Washington, DC: The National Academies Press, 2022. isbn: 978-0-309-27548-4. doi: 10.17226/26430.
- [115] Ziyang Xu et al. "A state-of-the-art review of the vibration and noise of wind turbine drivetrains". In: *Sustainable Energy Technologies and Assessments* 48 (2021), p. 101629. issn: 2213-1388. doi: 10.1016/j.seta.2021.101629.
- [116] A.C. Hansen. "Yaw Dynamics of Horizontal Axis Wind Turbines". In: *NREL/TP-442* (May 1992).
- [117] Jin Xu et al. "Rotor imbalance detection and quantification in wind turbines via vibration analysis". In: *Wind Engineering* 46.1 (2022), pp. 3–11. doi: 10.1177/0309524X21999841.
- [118] John Mandell et al. "Prediction of Delamination in Wind Turbine Blade Structural Details". In: *Journal of Solar Energy Engineering-transactions of The Asme - J SOL ENERGY ENG* 125 (Jan. 2003). doi: 10.1115/1.1624613.
- [119] Yonghong Liu et al. "An Observational Study on the Local Climate Effect of the Shangyi Wind Farm in Hebei Province". In: *Advances in Atmospheric Sciences* 38 (Nov. 2021), pp. 1905–1919. doi: 10.1007/s00376-021-0290-0.
- [120] Alexander Ernst et al. "Model-based Converter Control for the Emulation of a Wind Turbine Drive Train". In: *2022 24th European Conference on Power Electronics and Applications (EPE'22 ECCE Europe)*. 2022, pp. 1–10.
- [121] Baopeng Lu et al. "Insulation Degradation Mechanism and Diagnosis Methods of Offshore Wind Power Cables: An Overview". In: *Energies* 16.1 (2023). issn: 1996-1073. doi: 10.3390/en16010322.
- [122] Yang Li and Xiaojun Shen. "A Novel Wind Speed-Sensing Methodology for Wind Turbines Based on Digital Twin Technology". In: *IEEE Transactions on Instrumentation and Measurement* 71 (2022), pp. 1–13. doi: 10.1109/TIM.2021.3139698.
- [123] Xiuwen Dong et al. "Effects of safety and health training on work-related injury among construction laborers". In: *Journal of occupational and environmental medicine / American College of Occupational and Environmental Medicine* 46 (Jan. 2005), pp. 1222–8. doi: 10.1097/01.jom.0000147268.42094.de.
- [124] Shuting Wan, Lifeng Cheng, and Xiaoling Sheng. "Effects of Yaw Error on Wind Turbine Running Characteristics Based on the Equivalent Wind Speed Model". In: *Energies* 8 (July 2015), pp. 6286–6301. doi: 10.3390/en8076286.
- [125] Tianyi Zhang et al. "Vibration mitigation in offshore wind turbine under combined wind-wave-earthquake loads using the tuned mass damper inerter". In: *Renewable Energy* 216 (2023), p. 119050. issn: 0960-1481. doi: 10.1016/j.renene.2023.119050.
- [126] Z. Fang and H. Fan. "Redundancy of Structural Systems in the Context of Structural Safety". In: *Procedia Engineering* 14 (Dec. 2011), pp. 2172–2178. doi: 10.1016/j.proeng.2011.07.273.